FINAL REPORT

Electrochemical Hydrogen Storage Systems

Award Number: DE-FC36-05GO15054
Project Period: March 1, 2005 to April 30, 2010

Digby D. Macdonald, Jason McLafferty, Justin Tokash, Amr Saleh, Rezwana Sharna, Samin Sharifi-Asl, Sang-Kwon Lee, Krystaufeux Williams, Matthew Taylor

Center for Electrochemical Science and Technology
Department of Materials Science and Engineering
Pennsylvania State University
209 Steidle Bldg
University Park, PA 16802
(814)-863-7772 (Tel); (814)-863-4718 (Fax); Email: ddm2@psu.edu

Submitted to:

US Department of Energy
DOE Technology Development Manager: Grace Ordaz
202 586-8350 (Tel); 202-586-9811 (Fax); grace.ordaz@ee.doe.gov

DOE Project Officer: James Alkire
(303) 275-4795 (Tel); james.alkire@go.doe.gov

Date of Report: June 30, 2010

ABSTRACT

As the global need for energy increases, scientists and engineers have found a possible solution by using hydrogen to power our world. Although hydrogen can be combusted as a fuel, it is considered an energy carrier for use in fuel cells wherein it is consumed (oxidized) without the production of greenhouse gases and produces electrical energy with high efficiency.

Chemical storage of hydrogen involves release of hydrogen in a controlled manner from materials in which the hydrogen is covalently bound. Sodium borohydride and aminoborane are two materials given consideration as chemical hydrogen storage materials by the US Department of Energy. A very significant barrier to adoption of these materials as hydrogen carriers is their regeneration from "spent fuel," i.e., the material remaining after discharge of hydrogen.

The U.S. Department of Energy (DOE) formed a Center of Excellence for Chemical Hydrogen Storage, and this work stems from that project. The DOE has identified boron hydrides as being the main compounds of interest as hydrogen storage materials. The various boron hydrides are then oxidized to release their hydrogen, thereby forming a "spent fuel" in the form of a lower boron hydride or even a boron oxide. The ultimate goal of this project is to take the oxidized boron hydrides as the spent fuel and hydrogenate them back to their original form so they can be used again as a fuel. Thus this research is essentially a boron hydride recycling project.

In this report, research directed at regeneration of sodium borohydride and aminoborane is described. For sodium borohydride, electrochemical reduction of boric acid and sodium metaborate (representing spent fuel) in alkaline, aqueous solution has been investigated. Similarly to literature reports (primarily patents), a variety of cathode materials were tried in these experiments. Additionally, approaches directed at overcoming electrostatic repulsion of borate anion from the cathode, not described in the previous literature for electrochemical reduction of spent fuels, have been attempted. A quantitative analytical method for measuring the concentration of sodium borohydride in alkaline aqueous solution has been developed as part of this work and is described herein. Finally, findings from stability tests for sodium borohydride in aqueous solutions of several different compositions are reported.

For aminoborane, other research institutes have developed regeneration schemes involving tributyltin hydride. In this report, electrochemical reduction experiments attempting to regenerate tributyltin hydride from tributyltin chloride (a representative by-product of the regeneration scheme) are described. These experiments were performed in the non-aqueous solvents acetonitrile and 1,2-dimethoxyethane. A non-aqueous reference electrode for electrolysis experiments in acetonitrile was developed and is described.

One class of boron hydrides, called polyhedral boranes, became of interest to the DOE due to their ability to contain a sufficient amount of hydrogen to meet program goals and because of their physical and chemical safety attributes. Unfortunately, the research performed here has shown that polyhedral boranes do not react in such a way as to allow enough hydrogen to be released, nor do they appear to undergo hydrogenation from the spent fuel form back to the original hydride.

After the polyhedral boranes were investigated, the project goals remained the same but the hydrogen storage material was switched by the DOE to ammonia borane. Ammonia borane was found to undergo an irreversible hydrogen release process, so a direct hydrogenation was not able to occur. To achieve the hydrogenation of the spent ammonia borane fuel, an indirect hydrogenation reaction is possible by using compounds called organotin hydrides. In this process, the organotin hydrides will hydrogenate the spent ammonia borane fuel at the cost of their own oxidation, which forms organotin halides. To enable a closed-loop cycle, our task was then to be able to hydrogenate the organotin halides back to their hydride form.

In addition to this experimental work, a parallel project was carried out to develop a new model of electrochemical impedance spectroscopy (EIS) that could be used to define the mechanisms of the electrochemical hydrogenation reactions. The EIS technique is capable of probing complex chemical and electrochemical reactions, and our model was written into a computer code that allowed the input of experimental EIS data and the extraction of kinetic parameters based on a best-fit analysis of theoretical reaction schemes.

Finally, electrochemical methods for hydrogenating organic and metallo-organic materials have been explored. Three basic methods have been employed: (1) The production of hydrogen atoms on a palladium membrane using a Devanathan- Stachurski cell; (2) Direct cathodic hydrogenation on platinum and copper in aqueous-ionic liquid solvents; and (3) Direct cathodic hydrogenation on platinum and copper in anhydrous ionic liquid solvents with H_2 acting as a hydrogen source. The Devanathan- Stachurski cell was successfully used to hydrogenate styrene to ethyl benzene and to attempt the hydrogenation of tributyl tin chloride, $(C_4H_9)_2SnCl_2$, and "spent fuel", NH_2BH_2, to aminoborane, NH_3BH_3. Neither of these hydrogenations proved feasible. The ionic liquid work was restricted to the hydrogenation of carbon dioxide. Hydrogenation products were detected, but in very low yield, and there appear to be considerable hurdles that would need to be overcome to render the direct hydrogenation of CO_2 to CH_3OH, for example, a practical method for recycling carbon dioxide.

TABLE OF CONTENTS

Part III Hydrogenation Research

Part IV Overal Summary and Conclusions

LIST OF FIGURES

Part I

Part II

Part III

LIST OF TABLES

Part I

Part II

Part I

ELECTROCHEMICAL RESEARCH IN CHEMICAL HYDROGEN STORAGE MATERIALS: SODIUM BOROHYDRIDE AND ORGANOTIN HYDRIDES

1. Introduction

Due to concerns over limited availability of fossil fuels, the rapid increase in the cost of oil, and the specter of global warming, alternative sources or carriers of energy are being sought. In January 2003, the United States Government launched the Hydrogen Fuel Initiative, which provides funding for research and development activities for H_2 as an energy carrier. These research activities and technical barriers have been discussed by Satyapal et al [1]. The following discussion is based upon this reference.

Three barriers to commercial viability of H_2 as an on-board energy carrier have been identified, based on the currently accepted gasoline engine-powered vehicle. First, the driving range per charge of H_2 has to exceed 300 miles. Second, the cost of H_2 fuel cells has to be lowered to $30/kW.h by 2015. Third, hydrogen has to be delivered at a cost of $2.00 to $3.00 per gallon-gasoline-equivalent (untaxed) by 2015.

To address these barriers, the DOE has independent projects developing the traditional methods of high-pressure storage of H_2 gas or low temperature storage of liquid H_2 (LH_2) as well as discovery of new materials and processes for H_2 storage. Three Centers of Excellence (CoE) dedicated to metal hydrides, chemical hydrogen storage, and carbon-based materials research materials that store H_2.

High-pressure storage of H_2 is done at 5000 psi or 10 000 psi in carbon fiber-reinforced tanks. The cost of these tanks is tied to the cost of the carbon fiber, thus most research is devoted to finding lower cost carbon fiber that still has the requisite mechanical properties. To increase the capacity, two paths are being explored: cryo-compressed tanks, and conformable tanks. Cryo-compressed tanks are chilled to 77K (liquid N_2), which increase the quantity of H_2 stored in the fixed volume of the tank. However, increased weight and volume due to the insulation required to maintain cryogenic temperatures must be considered. Conformable tanks can be manufactured in different shapes to best-fit available space in a vehicle.

Liquid H_2 has a higher density than gaseous H_2 at 10 000 psi, and on this basis, storage in the liquid state appears advantageous. However, the increased bulk of thermal insulation, the energy input required for liquefying the hydrogen and the loss of hydrogen due to boil off have to be considered. Of these, the energy requirement for liquefaction is the most serious drawback, amounting to 30% of the lower heating value of hydrogen.

Hydrogen absorption materials are a class of compounds that store hydrogen by absorption – the hydrogen is incorporated into the crystal structure. Thus far, these materials suffer from high cost, low gravimetric hydrogen (based on the amount that is actually released, not the amount dictated by the chemical formula), poor volumetric density, and kinetic sluggishness in the H_2 release and uptake. Assuming that the hydrogen will be used to power a fuel cell, it is desirable to use the waste heat of the fuel cell to release H_2 from the metal hydride. However, the current technology for proton electrolyte membrane fuel cells (PEM FC) greatly limits the choices for metal hydrides, since these fuel cells operate at a relatively low temperature.

Adsorption on high surface area materials is also being investigated, for example, single wall nanotubes. The gravimetric density of these materials is controversial, however, due to lack of reproducibility in published results. In any case, the gravimetric density appears to be below 6% at this time.

The third class of materials is the metal hydrides, which are compounds between a reactive metal and hydrogen, in which the hydrogen is covalently or ionically bound to the metal. Typical examples are LiH, MgH_2, $_{AlH3}$, and SiH4, to identify but a few possible candidates. The requirement for reversible hydrogen storage is that the hydrogen must be capable of being released under convenient conditions; for example, by hydrolysis or dehydrogenation. Sodium borohydride ($NaBH_4$) is one material that releases hydrogen by hydrolysis

$$NaBH_4 + 2H_2O \rightarrow NaBO_2 + 4H_2 \tag{1.1}$$

Dehydrogenation is usually effected by heating the material. One material of great interest in this regard is aminoborane, NH_3BH_3. Many different by-products [2] are possible, but one example reaction is

$$NH_3BH_3 \rightarrow NH_2BH_2 + H_2 \tag{1.2}$$

Chemical systems are more complicated, but higher capacities can be obtained compared to the gaseous/liquid systems. Furthermore, these systems are safer, because the hydrogen is only released as needed, minimizing the quantity of free H_2 at any given time. Usually, the hydrogen release rate is good. A major drawback of the materials systems is obtaining a reliable "closed loop" approach, i.e., a method by which the hydrogen can be stored, extracted, stored, etc. with minimal loss of energy or material.

The work performed at PSU was focused on two materials systems: sodium borohydride ($NaBH_4$) and aminoborane (AB). In both cases, investigations on electrochemical regeneration of the by-products of these materials ("spent fuel") were carried out.

In the following sections, an introduction on sodium borohydride is given, followed by an overview of the electrochemical experiments performed for this material. Next, aminoborane is briefly introduced, and an overview of the electrochemical work performed relative to its regeneration is given.

1.1 Sodium Borohydride: Overview and Research Objectives

Borohydride compounds were first synthesized and studied at Professor H.I. Schlesinger's research group at the University of Chicago. Probably the first reported use of $NaBH_4$ as a hydrogen storage material was for the US Army Signal Corps for production of H_2 in field applications [3]. H.C. Brown found that $NaBH_4$ could be compressed into a pellet with $CoCl_2$; upon dissolution in H_2O, H_2 was generated. The $CoCl_2$ acted as a catalyst pre-cursor; the catalyst cobalt boride was produced in situ after dissolving in water. Later, more involved schemes for production of H_2 were designed, for example, the Hydrogen on Demand ® of Millennium Cell. In essence, this technology allows H_2 to be produced as needed, primarily to power a Proton Electrolyte Membrane Fuel Cell (PEM-FC). The reaction utilized in these methods is hydrolysis - see Equation (1.1) above. The by-product ion is often written at BO_2^- (metaborate ion) and the same convention will be used in this exposition. However, some workers in boron chemistry have found that BO_2^- does not exist in aqueous solution [4, 5, 6, 7]. Alkali metal metaborates in the crystalline state (e.g. $NaBO_2$) have been found to contain a complex anion having the empirical formula $B_3O_6^{3-}$ and having a planar, six-membered ring structure [6]. However, in aqueous solution, the "metaborate" salts give $B(OH)_4^-$ anions [4,5,6,7].

$NaBH_4$ is produced commercially by the Brown-Schlesinger process [3]:

$$B(OCH_3) + 4NaH \rightarrow NaBH_4 + 3Na(OCH_3) \qquad (1.3)$$

The reaction is carried out at elevated temperature (250°C). Note that four moles of NaH per one mole of $NaBH_4$ are required. The production of NaH is an energy-intensive process, requiring electrolysis of molten sodium salts. On this basis alone, an alternative route to $NaBH_4$ is desirable, if $NaBH_4$ is to be adopted as an H_2 storage medium. Also, it would be highly desirable to regenerate $NaBH_4$ from the $NaBO_2$ by-product.

Electrochemical regeneration of $NaBO_2$ is one method considered in the regeneration of $NaBH_4$. Ignoring the spectator Na^+ ion and considering only the cathodic process, the hypothetical reaction is:

$$BO_2^- + 6H_2O + 8e^- \rightarrow BH_4^- + 8OH^- \qquad (1.4)$$

The standard (reduction) potential for this reaction has been calculated from reversible thermodynamics to be –1.24V (vs. SHE) [8]. To the best of the authors' knowledge, this potential

has never been measured experimentally, and the reaction appears to be far from reversible on any electrode material studied thus far.

The patent literature on electrochemical production of borohydride generally suggested the use of cathodes having a high overpotential for the hydrogen evolution reaction. This is due to the fact that the standard equilibrium potential for borate reduction to borohydride is -1.24V vs. SHE whereas the standard equilibrium potential for water reduction to hydrogen gas is -0.83V vs. SHE. In order to minimize the competition between water electrolysis and borate electrolysis, a kinetic barrier in the form of a high overpotential cathode can be used to slow the rate of water reduction.

None of the patent literature surveyed at the beginning of this project discussed another problem in borate reduction. To wit, there should be electrostatic repulsion between the borate anion and the cathode. Three classes of experiments were explored to see if this problem could be overcome. The first method was the use of tetraalkylammonium hydroxides. Tetraalkylammonium cations (TAA^+) are known to be specifically adsorbable and thus modify the potential profile at the electrode – solution interface. The second method was the use of chemically- and polymer- modified cathodes, which were to electrostatically attract borate anion or chelate borate anion. The third method was the pulsed power method, in which a "square wave" current or potential pulse was applied to the cell.

The electrochemical regeneration attempts for borohydride described in this work were performed in aqueous solution. A quantitative analytical method for borohydride ion in aqueous solution was thus needed to determine the outcome of electrolysis experiments. Cyclic voltammetry (CV) at a gold working electrode was chosen for this purpose. Stability of sodium borohydride in aqueous solutions of several compositions was monitored in time with the CV method. Some of these experiments were performed with borohydride in contact with cathode materials that were used in the electrochemical regeneration experiments, whereas other experiments studied the stability of sodium borohydride in aqueous solution without cathode materials present.

The chapters that follow contain the details of the CV method experiments, the stability test experiments, and electrochemical borohydride regeneration experiments. Pertinent literature and electrochemical theory are reviewed in these chapters. Finally, conclusions for the work on sodium borohydride in aqueous solutions are presented.

1.2 Organotin Hydrides - Reagents Important to the Regeneration of Aminoborane: Overview and Objectives.

Due, in part, to the lack of positive results for electrochemical regeneration of sodium borohydride in aqueous solution, the US DoE decided to discontinue research on sodium borohydride. Instead, work is focused on aminoborane (AB), which contains 19.3% hydrogen by

mass. Other Centers have identified possible regeneration schemes [9, 10, 11]. The first step in these schemes is digestion of the spent AB fuel. Depending upon how the hydrogen was released from the AB, a variety of products result [2]. Thus, the digestion method should be able to handle a variety of spent AB products while producing one material. The product of digestion is usually a boron-sulfur or boron-halogen species. These species must be reduced to a boron hydride material. Organotin hydrides have been demonstrated as reducing agents in this capacity in some of the regeneration schemes. An example regeneration scheme is presented in Hausdorf et al [2].

The work performed at PSU and described here was regeneration of organotin hydrides from organotin halides. This process is represented schematically in the Figure 1.1. In this figure, atom X may be a halogen, sulfur, oxygen, etc. In most regeneration schemes under investigation at this time, X is sulfur or a halogen. The blue arrow represents how the work described here is to fit into the regeneration scheme. Essentially, the objective of the method is to close the loop between tributyltin hydride (Bu_3SnH) and tributyltin halide (Bu_3SnX), of course, assuming atom X is a halogen. The work of the other centers in this project is shown schematically on the right side of the figure.

Following reduction of B-X bonds to B-H bonds, the ligand L is exchanged for ammonia (NH_3). Other ligands, L, are typically incorporated from the beginning to simplify handling of the digested spent fuel, which otherwise may be a gaseous species such as BBr_3. The choice of the other ligand L is not arbitrary, for it must be displaced by NH_3 in this final step. Also, it must not diminish the reactivity of B-X bonds towards reduction. This aspect of the project, as well as the actual reduction and the digestion, is being handled by other centers.

The work described in later chapters was to confirm that organotin hydrides could be generated from the chlorides, which was described in the literature. These literature references primarily used mercury or amalgamated metals as the working electrode. Silver was examined, in addition to mercury or amalgamated metals as the cathode material, since has been demonstrated as an electrocatalyst for alkyl halide reductions [12]. Thus, it was of interest to see if it would perform in a similar capacity for alkyltin halide reductions. Furthermore, it is beneficial to avoid the use of mercury whenever possible, due to its high toxicity. For this reason, any process based upon mercury would not be adopted industrially.

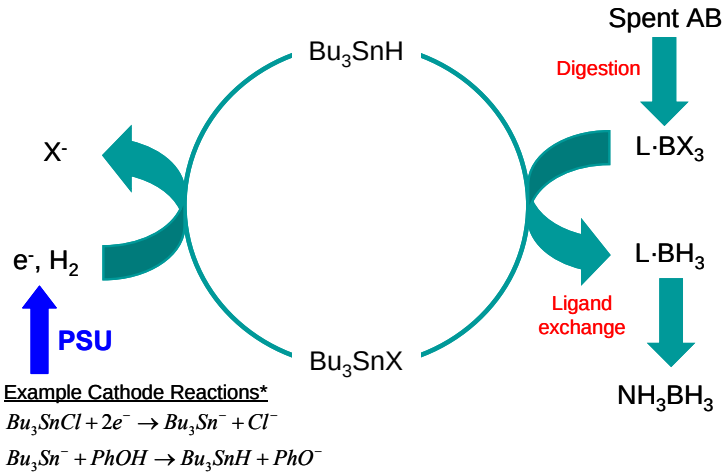

Figure 1.1: The example cathodic reactions are based upon mechanistic information contained in Mazzocchin et al [13].

1.3 References

1. S. Satyapal et al. *Catalysis Today* 120 (2007) 246.
2. S. Hausdorf et al. *International Journal of Hydrogen Energy* 33 (2008) 608.
3. H.C. Brown. *Boranes in Organic Chemistry*. Cornell University Press, Ithica, 1972.
4. R.M. Adams. *Journal of Chemical Documentation*. 4 (1964) 95.
5. J. O. Edwards, G.C. Morrison, V.F. Ross, and J.W. Schultz. *Journal of the American Chemical Society* 77 (1955) 266.
6. R.K. Momii and N.H. Nachtrieb. *Inorganic Chemistry* 6 (1967) 1189.
7. H.D. Smith and R.J. Wiersema. *Inorganic Chemistry* 11 (1972) 1152.
8. J. H. Morris, H.J. Gysling, and D. Reed. *Chemical Reviews* 85 (1985) 51
9. http://www.hydrogen.energy.gov/pdfs/progress07/iv_b_5e_sneddon.pdf. Last accessed: August 26, 2008.
10. http://www.hydrogen.energy.gov/pdfs/progress07/iv_b_5f_aardahl.pdf. Last accessed: August 26, 2008.
11. http://www.hydrogen.energy.gov/pdfs/progress07/iv_b_5g_ott.pdf. Last accessed: August 26, 2008.
12. C. A. Paddon et al. *Journal of Physical Organic Chemistry*. 20 (2007) 115.
13. G-A. Mazzocchin, R. Seeber, and G. Bontempelli. *Journal of Organometallic Chemistry*, 121 (1976) 55

2. Cyclic Voltammetry

2.1 Introduction

The first task in the electrochemical regeneration of sodium borohydride was to develop an analytical method to detect and to quantify sodium borohydride in aqueous solution.

Other analytical methods, such as the iodate back-titration, have been reviewed [1]. Voltammetry, using a gold working electrode, has also been used for quantification of sodium borohydride. Linear sweep voltammetry at a 2mm diameter gold electrode yielded linear calibration curves using peak current as the analytical signal [2]. In this work, the detection limit appeared to be at least 8.1×10^{-5} M in 0.2M NaOH. The relative standard deviation in the peak current was reported to be less than 3%. Other workers [3] investigated cyclic voltammetry and square wave voltammetry of sodium borohydride solutions in 0.5M sodium hydroxide solution at a 2mm diameter gold electrode. These studies report a limit of detection of 3×10^{-5} M using square wave voltammetry, however typical measures of precision were not reported. Au was chosen as an electrode material based on cyclic voltammetry results in the literature (for example, the work of Gyenge [4]); compared to Pt, on Au the electro-oxidation of BH_4^- is simpler.

The objective of the present report is to investigate the effect of electrode size on the dynamic range and analytical sensitivity. Also, the repeatability and reproducibility of the method were investigated. Finally, different 'matrices' for sodium borohydride are investigated: 2M NaOH, 2M NaOH + 10% $NaBO_2$, 2M NaOH + 20% $NaBO_2$, 2M NaOH + 25% w/w $NaBO_2$, and 25% w/w $NaBO_2$ in pH 12 solution (henceforth, this will be referred to as "pH 12 solution") to reveal the effect of solution composition on the calibration curve. Previous work has indicated that a ratio $[OH^-]/[BH_4^-] > 4.44$ minimizes the rate of homogeneous chemical hydrolysis of borohydride [5]. Furthermore, other research [6] indicates that the same ratio must be much greater than the stoichiometric value of eight for the oxidation kinetics to not depend upon $[OH^-]$. In this study, $[OH^-]/[BH_4^-] \geq 100$ in the matrices containing 2M NaOH; thus, both of these conditions are satisfied. The pH 12 solution was used for comparison; it was hypothesized that the stability of sodium borohydride in this medium would be lower. Also, it was of interest to see if there is any effect on the voltammetry response of $NaBH_4$ in this medium due to the lower concentration of hydroxide ion.

2.2 Experimental

2.2.1 Electrodes/Cell

For the 6mm diameter working electrode, a gold disk/gold ring RRDE was used (Pine Instruments AFMTI34DCAUT). The 1mm diameter gold disk was prepared by soldering a 1cm segment of Au wire (Alfa Aesar, 99.95%) to a piece of nickel wire. This assembly was place in a 5mm diameter PTFE heat shrink tube, and potted with epoxy (MetLab M135). At the beginning of each day, the electrode was prepared by polishing with 0.3□m and 0.05□m alumina paste on Imperial cloth (Leco brand). Following each step, the electrode was rinsed thoroughly with distilled, de-ionized (D.I.) water and then dried in a stream of air. The electrode was then conditioned by performing ten CVs over a potential range of -1V (initial potential) to +0.3V (switching potential) vs. Hg/HgO at 100mV/s in 2M NaOH + 25% w/v $NaBO_2$. The same potential range and sweep rate was used to record all CVs in this work. Prior to subsequent experiments, the working electrode was thoroughly rinsed in D.I. water, followed by drying with a stream of air.

A graphite rod (Alfa Aesar, 99%) served as the counter electrode in all experiments. The reference electrode was an Hg/HgO (Koslow Scientific, Part No. 5088) electrode filled with 2M NaOH solution. The sweep rate and potential range for all CV measurements are the same as those employed in conditioning the electrode.

It has been already demonstrated that the cyclic voltammetry (CV) of sodium borohydride at a gold electrode shows that the oxidation is irreversible [4,7]. Because of the irreversibility, the concentration of borohydride is depleted near the electrode with successive cycling in CV experiments. Therefore, the solution was agitated between duplicate measurements to restore the initial concentration profile.

In the RDE experiments for determination of the diffusion coefficient for BH_4^-, a 5mm diameter gold disk WE was used (Pine Instruments AFE6R1AU). The electrode was prepared prior to experiments in the same manner as the WE in the CV experiments. A Zeitfuchs Cross-Arm viscometer (Cole-Parmer) having a useable range of 0.6 to 3cSt was used to measure the kinematic viscosity of each solution for the RDE experiments.

2.2.2 Reagents

All solutions were prepared in D.I. water from a Millipore Milli-Q UV Plus system. Reagents used were NaOH (EMD, min. 99%), $NaBO_2.4H_2O$ (Alfa Aesar, tech. grade; Sigma Aldrich, 99% min.), and $NaBH_4$ (Rohm and Haas, Venpure AF granules). The pH 12 solution was prepared by making first the 25% w/v $NaBO_2$ solution, and then adjusting the pH to 12 by addition of 6M NaOH solution.

2.2.3 Instrumentation

All cyclic voltammograms were obtained using Pine Chem. software with a Pine Instruments AFCBP1 bi-potentiostat.

2.3 Results

Figure 2.1 shows a CV of 1mM $NaBH_4$ in 2M NaOH obtained at a 6mm diameter gold-disk working electrode. The appearance of this CV is the same as that reported by other workers [4]. It is evident that the potential corresponding to the onset of oxidation current is quite positive to the hypothetical standard potential corresponding to the eight-electron oxidation of BH_4^- (Equation 1.4); $E^0 = -1.24V$.

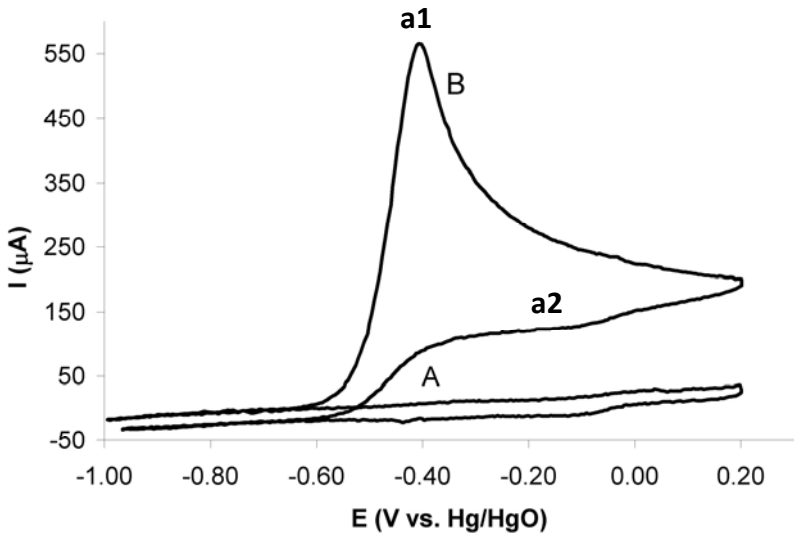

Figure 2.1: Cyclic voltammograms of 2M NaOH (A) and 1mM $NaBH_4$ in 2M NaOH (B) at 6mm Au disk working electrode. Sweep rate: 100mV/s.

The shape of the voltammogram in Figure 2.1 suggests that there is significant kinetic sluggishness in some initial step of the reaction. In fact, Rostamikia and Janik have found in their computational study that the oxidative adsorption of borohydride anion is weak below –0.2V vs. SHE; closer to –1V this adsorption is highly unfavorable [8]. Thus far, a mechanism accounting for all eight electrons of the hypothetical reaction has eluded researchers. Mirkin, Yang, and Bard were able to determine that a two-electron ECE sequence accounted for the first two electron transfer steps using a microelectrode and high sweep rates [7]. However, the following six-electron transfer could not be elucidated even using very high sweep rates up to 3×10^4V/s.

Other workers have used other methods to try to understand the mechanism of borohydride oxidation at gold. Chatenet and co-workers found that the open circuit potential of a gold electrode in Ar-sparged sodium borohydride/sodium hydroxide solution was –0.8V vs. SHE; the value of this potential indicates a probably mixed potential [6]. The oxidation of borohydride anion on gold is known to be irreversible as Figure 2.1 illustrates. A Tafel analysis of diffusion-corrected current density-overpotential data gave j_o = 7.4 x 10^{-6} A/cm^2 and b = 150mV/dec for borohydride oxidation on Au. The meaning of an exchange current density in this context is not clear; presumably the measurement is analogous to a corrosion current. The identity of the cathodic reaction is not clear; if it were water reduction, the open circuit potential would be expected to fall between –1.24V and –0.83V (SHE scale); the measured potential is just positive to this upper limit. Gyenge [4] also determined b for borohydride oxidation from the equation for the peak current for an irreversible voltammogram, choosing the same peak as that seen on the forward sweep in Figure 2.1 here. A value of 190mV was obtained, assuming that n_a = 1 (number of electrons in the rate-determining electron transfer step).

Chatenet and co-workers also used RDE voltammetry to study the reactions [6]. Voltammetry of Ar-sparged 1M NaOH showed no gold oxidation below 0.2V; thus it was concluded that borohydride oxidation occurs on gold itself. Levich analysis of the limiting current data gave n = 7 for borohydride oxidation at gold. The influence of electrolyte composition was also studied by fixing the borohydride concentration at 10^{-2} M and varying the NaOH concentration to effectively vary the ratio of $[OH^-]/[BH_4^-]$. This ratio has been shown by other workers to impact the stability of borohydride against hydrolysis [5]. Ratios in the range of 10 to 50 were investigated, which exceed the theoretical ratio of eight from Equation (2). RDE voltammograms show that the oxidation kinetics for borohydride is dependent upon this ratio; low ratios inhibit the oxidation. These workers hypothesize that this behavior is indicative of OH^- involvement in the rate-determining step of oxidation. When the hydroxide concentration was fixed at 1M and the borohydride concentration was varied, a ratio of unity gave a different voltammogram. The voltammogram at unit ratio had an onset of oxidation at a much lower potential (-1.2V, compared to about –0.5V at higher ratios). The oxidation current begins at potentials negative to the equilibrium potential for water reduction (-0.83V in 1M NaOH), thus, this current is not due to hydrogen oxidation. Chatenet and co-workers instead suggest oxidation of the postulated intermediate BH_3OH^-, formed under hydrolysis of BH_4^-. Gardner and Collat have shown for values of this ratio below 4.4, hydrolysis of BH_4^- is promoted [5].

Cheng and Scott also used RDE voltammetry with a gold electrode to obtain n and k (heterogeneous rate constant for borohydride oxidation) [9]. Unlike Chatenet, their RDE voltammograms did not have the typical appearance showing a limiting current plateau. These workers ascribed this deviation to side reactions such as water oxidation and/or adsorption of intermediates. However, we speculate that the real reason is due to their working conditions, employing ratios of $[OH^-]/[BH_4^-]$ insufficient for facile oxidation of BH_4^-. Under such conditions, the oxidation reaction would not reach mass-transport control, leading to the appearance of their voltammograms, showing only kinetic and mixed control. It appears that Cheng and Scott were using conditions closer to those expected in fuel cell operations, and they did consider the

findings of Gardiner and Collat in keeping $[OH^-]/[BH_4^-] > 4.4$. Analysis in the mixed control region was attempted with the Koutecky-Levich equation. The Koutecky-Levich plot showed that series at different overpotentials did not give parallel lines. It should be considered, as Gardner and Collat have stated, that the oxidation of BH_4^- consumes OH^-; thus, the interfacial concentration of OH^- could be less than the bulk under certain conditions. In this circumstance, hydrolysis of BH_4^- could be promoted. Indeed, in efforts to reproduce the findings of Cheng and Scott, we met with significant bubbling at the gold working electrode when it was stationary. We speculate that these bubbles are hydrogen, formed by hydrolysis at the gold electrode; as the oxidation reaction consumes OH^-, the OH^- concentration at the electrode-solution interface decreases, thereby enhancing the rate of hydrolysis. It is also notable that their voltammogram at 0rpm (corresponding to an ordinary CV) shows a peak occurring at a much more positive potential than the peak potential of the CV in Figure 2.1, or those obtained by other workers (e.g. Gyenge). This would point to oxidation of some species other than borohydride anion (perhaps hydrogen).

Based upon the findings of Chatenet and co-workers, a large excess of NaOH was used in most solutions, corresponding to a ratio $[OH^-]/[BH_4^-] \geq 100$. This choice satisfies two criteria: sufficient OH^- to satisfy requirements for borohydride oxidation, and sufficient OH- to suppress as much as possible hydrolysis of borohydride anion. The 25% w/v $NaBO_2$ solution at pH = 12 was the exception; this was used for comparison.

In previous experiments by the present authors, a 1mm diameter gold disk-working electrode was used for cyclic voltammetry experiments [10]. With the use of the larger diameter gold disk-working electrode, it was expected that the peak current would be proportionally higher for a given concentration. This is hypothesized based on the equation for the peak current for an irreversible voltammogram [11]:

$$i \propto AC^b D^{1/2} \tag{2.1}$$

In the above equation, A is the electrode area, C^b is the bulk concentration of the species undergoing reaction, and D is the diffusion coefficient of the same species [11]. Figure 2.1 shows a cyclic voltammograms of 1mM $NaBH_4$ in 2M NaOH at the 6mm diameter Au electrode as well as a CV of the blank (2M NaOH). Peak a1 occurs on the forward sweep and the current corresponding to this peak was used as the analytical signal in these experiments. The portion labeled a2 is an anodic wave appearing on the reverse sweep. Note that there is a large separation between the background current (2M NaOH) and the current for BH_4^- oxidation, in particular on the forward sweep. For the 1mm diameter electrode, the slope of the calibration curve was 0.0163mA/mM BH_4^- whereas the slope was 0.5158mA/mM BH_4^- for the 6mm electrode (Figure 2.2). It is seen that the slope of the calibration curve, indicating the sensitivity of the method, is 32 times greater when the 6mm diameter electrode is used. From Equation 2.1, it is predicted that a 6mm electrode should give an increase of 36 times in the peak current compared to a 1mm diameter electrode, in fair agreement with the experimental value.

Next, the repeatability of the CV method was evaluated for solutions in 2M NaOH. Two concentration ranges for sodium borohydride were investigated: 0.1mM to 1mM $NaBH_4$ and 1mM to 20mM $NaBH_4$. The repeatability was determined from five calibration curves measured for each concentration range on one day. Measurements were made in duplicate at each concentration. In order to quantify the precision in the regression, the following measures of indeterminate error were calculated [12]: the standard deviation of the slope (S_{b1}), the standard deviation of the intercept (S_{b0}), the standard deviation in the peak current (s), the relative standard deviation in the peak current (RSD), and the signal-to-noise ratio (SNR).

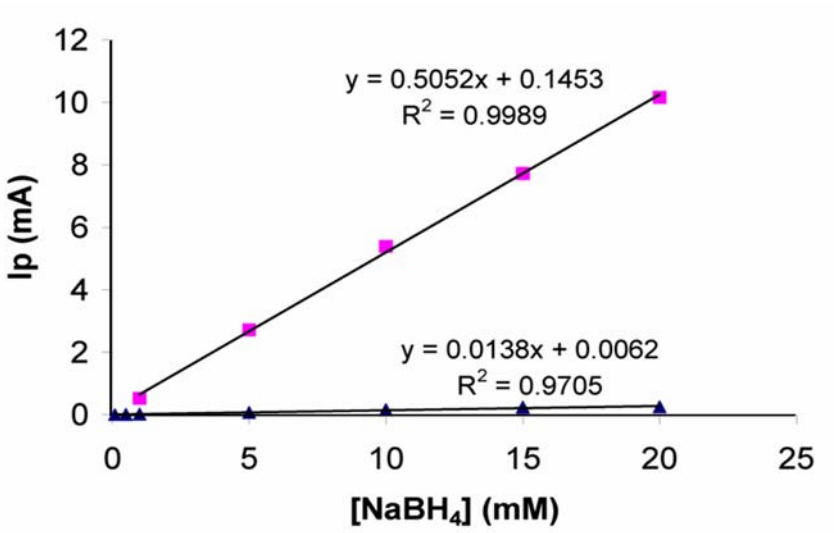

Figure 2.2: Calibration curves for sodium borohydride in 2M NaOH determined with 1mm diameter Au working electrode and with 6mm diameter Au working electrode. Sweep rate: 100mV/s.

Table 2.1 shows the regression parameters for the low concentration range (0.1mM to 1mM $NaBH_4$) calibration curve and Table 2.2 shows the regression parameters for the high concentration range (1mM to 20mM $NaBH_4$) calibration curve. These regression results were obtained from the data using Wolfram Mathematica v.6.0. Note that the slope is similar for both calibration curves. The square of the correlation coefficient is higher for the high concentration-range calibration curve, indicating greater linearity in this range. Also, the standard deviation in the slope is greater for the low concentration range, indicating less precision in the measurements in this concentration regime. However, the intercept for the high concentration-range curve is much higher. This means that extrapolation of the calibration curve to zero sodium borohydride concentration (the value of the intercept) gives a signal higher than the signal produced by 0.1mM sodium borohydride.

Table 2.1: Regression parameters (repeatability test) for low concentration range calibration curve.

Slope (b_1) (mA/mM BH_4^-)	0.5132
Intercept (b_0) (mA)	0.0198
square of the correlation coefficient (r^2)	0.9831
Standard deviation slope (S_{b1}) (mA/mM BH_4^-)	0.0158
Standard deviation Intercept (S_{b0}) (mA)	0.0090

Table 2.2: Regression parameters (repeatability test) for high concentration range calibration curve.

Slope (b_1) (mA/mM BH_4^-)	0.5025
Intercept (b_0) (mA)	0.1759
square of the correlation coefficient (r^2)	0.9969
Standard deviation slope (S_{b1}) (mA/mM BH_4^-)	0.0059
Standard deviation Intercept (S_{b0}) (mA)	0.0717

The 'blank' measurement is often taken to be the signal of a solution otherwise the same as the sample but without the analyte – the "reagent blank." In some other cases, the intercept of the calibration curve is taken to be the blank - the "calibration blank."[13]. It is more correct to use the so-called Total Youden Blank (TYB), which accounts for matrix-analyte interactions. In order to determine the TYB, the response of samples of different sizes (e.g. differing weights) diluted to a fixed volume is plotted versus the sample size and a regression line is determined. The y-intercept of the regression line is the TYB. Then the concentration of any sample C_A is:

$$C_A = \frac{I_{p,samp} - TYB}{mW_x} \tag{2.2}$$

In this equation, $I_{p,\,samp}$ is the peak current from the sample, m is the slope of the calibration curve determined from the standards, and W_x is the weight of the sample used.

Next, the residual errors in the peak current as a function of sodium borohydride concentration were calculated. For residual errors randomly distributed about an average value of zero with no clear trend towards large or small values of error, good modeling by linear regression can be assured [12]. This appears to be the case for the high concentration range data (Figure 2.4), but not for the low concentration range data (Figure 2.3). The appearance of the residual errors plot for the low concentration-range data suggests that the random errors affecting the peak current are not independent of the concentration of each standard. Therefore, a linear regression should not be strictly used on these data.

Finally, the precision in the peak current measurement itself was quantified by determining the standard deviation (s), the relative standard deviation (RSD), and the signal-to-noise ratio (SNR). To determine the SNR, the following formula was used:

$$SNR = \frac{I_{p,avg}}{s} \tag{2.3}$$

In this expression, $I_{p.avg}$ is the average peak current and s is the standard deviation of the measured signal. For the low concentration range, the RSD in the peak current is around 8 – 10% for each standard, with a SNR of 10 to 15 – see Table 2.3. For the high concentration range, there is a tendency for the RSD to decrease regularly with increasing concentration and for the SNR to increase regularly with concentration – see Table 2.4.

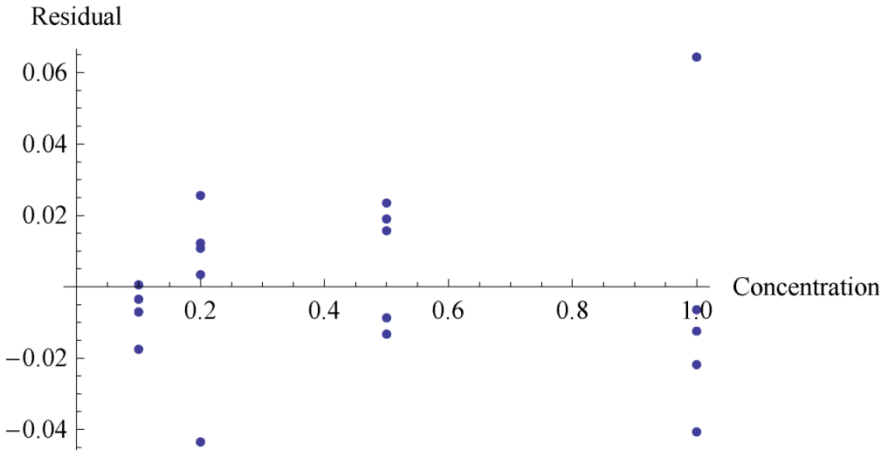

Figure 2.3: Residual errors in peak current as a function of sodium borohydride concentration for the concentration range of 0.1mM to 1mM $NaBH_4$ in 2M NaOH.

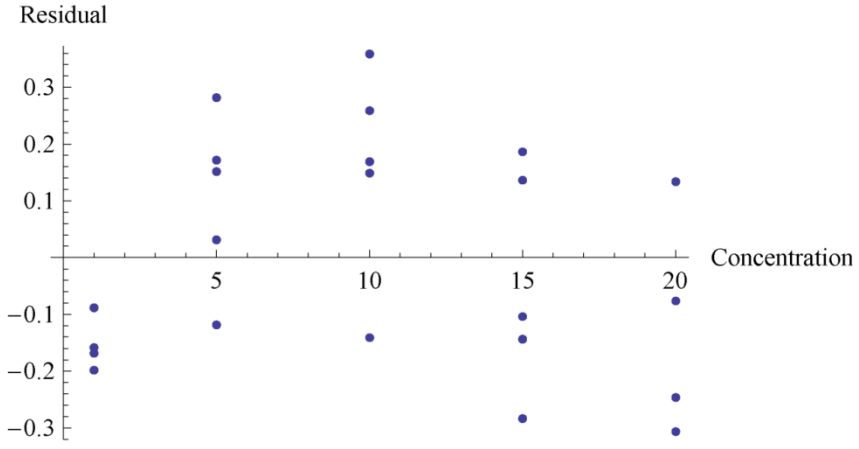

Figure 2.4: Residual errors in peak current as a function of sodium borohydride concentration for the concentration range of 1mM to 20mM $NaBH_4$ in 2M NaOH.

Table 2.3: Precision of peak current measurements (repeatability test) for low concentration range.

$[BH_4^-]$ (mM)	i_p average (mA)	S (mA)	RSD	SNR
0.1	0.065	0.007	11.20	9.97
0.2	0.134	0.01	7.56	15.06
0.5	0.284	0.027	9.36	12.39
1	0.530	0.055	10.37	11.51

Table 2.4: Precision of peak current measurements (repeatability test) for high concentration range.

$[BH_4^-]$ (mM)	i_p average (mA)	S (mA)	RSD	SNR
1	0.52	0.06	10.62	11.26
5	2.79	0.16	5.60	19.09
10	5.36	0.26	4.81	21.91
15	7.67	0.21	2.74	37.96
20	10.16	0.21	2.08	49.16

The reproducibility of the method was examined by measuring the response of the standards on five different days. Again, two concentration ranges were used (0.1mM to 1mM and 1mM to 20mM $NaBH_4$, both in 2M NaOH), and measurements were made in duplicate. Thus, five calibration curves were created for each concentration range.

The precision of the linear regressions obtained in the reproducibility tests were determined using the same figures-of-merit as were used for the repeatability tests. The slopes of the calibration curves were quite similar; however, the intercepts were significantly different, as demonstrated in Table 2.5 and Table 2.6. The standard deviation in the slope for the low concentration range is higher than that for the high concentration range. On the other hand, the standard deviation in the intercept is about ten times smaller for the low concentration range than for the high concentration range. The RSD for the peak current measurements decreases regularly in both the low concentration and high concentration range, and the SNR increases regularly for both concentration ranges as well – see Table 2.7 and Table 2.8. These trends in precision for the peak current measurements may explain the higher standard deviation in the slope for the low concentration range, but do not explain the higher standard deviation in the intercept for the high concentration range. Again, it is suggested to use the TYB in quantifying sample concentration. Finally, residual error plots, not shown here, were constructed to evaluate reproducibility data. As for the repeatability experiments, the distribution of random errors suggests that a linear regression should not be strictly applied in the low concentration range.

Table 2.5: Regression parameters for reproducibility test for low concentration range.

Slope (b_1) (mA/mM BH_4^-)	0.4983
Intercept (b_0) (mA)	0.0085
square of the correlation coefficient (r^2)	0.9883
Standard deviation slope (S_{b1}) (mA/mM BH_4^-)	0.0128
Standard deviation Intercept (S_{b0}) (mA)	0.0073

Table 2.6: Regression parameters for reproducibility test for high concentration range.

Slope (b_1) (mA/mM BH_4^-)	0.5080
Intercept (b_0) (mA)	0.1143
square of the correlation coefficient (r^2)	0.9971
Standard deviation slope (S_{b1}) (mA/mM BH_4^-)	0.0057
Standard deviation Intercept (S_{b0}) (mA)	0.0703

Table 2.7: Precision of peak current measurements (reproducibility test) for low concentration range.

[BH_4^-] (mM)	**i_p average (mA)**	**S (mA)**	**RSD**	**SNR**
0.1	0.050	0.013	26.38	5.60
0.2	0.119	0.014	12.11	9.82
0.5	0.257	0.025	9.74	12.10
1	0.506	0.043	8.44	13.52

Table 2.8: Precision of peak current measurements (reproducibility test) for high concentration range.

[BH_4^-] (mM)	**i_p average (mA)**	**S (mA)**	**RSD**	**SNR**
1	0.515	0.048	9.24	12.43
5	2.633	0.161	6.13	17.79
10	5.410	0.105	1.94	53.12
15	7.770	0.201	2.59	40.14
20	10.15	0.21	2.11	48.92

Matrix effects on the analytical response were investigated by creating calibration curves for sodium borohydride in 25% w/v $NaBO_2$ in pH 12 solution, 2M NaOH + 25% w/v $NaBO_2$, 2M NaOH + 20% w/v $NaBO_2$, and 2M NaOH + 10% w/v $NaBO_2$. Sodium borohydride concentration in these solutions ranged from 0.1mM to 15mM. Figure 2.5 demonstrates that the calibration curves vary with electrolyte composition. The slope is greatest for 2M NaOH at 0.5151mA/mM BH_4^- and lowest for 25% $NaBO_2$ in pH 12 solution, at 0.2267mA/mM BH_4^-. With addition of $NaBO_2$ to 2M NaOH, the slope decreases; at 10% $NaBO_2$ the slope is 0.4353mA/mM

BH_4^- and at 25% $NaBO_2$ the slope is 0.4013mA/mM BH_4^-. The slope for 20% $NaBO_2$ was similar to 25% $NaBO_2$ at 0.3916mA/mM BH_4^-. Other workers [13] have studied the influence of NaOH concentration on the diffusion coefficient of borohydride ion; as [NaOH] increased, D decreased, as predicted by the Stokes-Einstein relation. As described by Equation (2.1), the peak current depends upon the diffusion coefficient for the electroactive species of interest, thus the variation in the calibration curves with the matrix is most likely due to a variation of the diffusion coefficient for borohydride ion in these different media. In order to evaluate this hypothesis, some experiments were undertaken to determine the value of D in the different matrices. Rotating disk voltammetry was used to determine D for BH_4^- in the different solutions by application of the Levich Equation [14]:

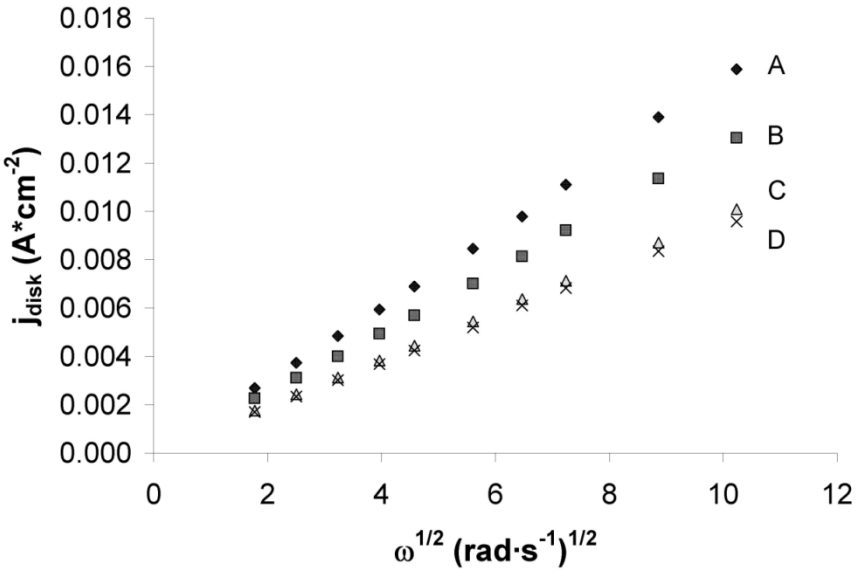

Figure 2.5: Calibration curves for 0.1mM to 20mM $NaBH_4$ in various electrolytes. Each point is an average of duplicate measurements. (A): 2M NaOH (B): 2M NaOH + 10% $NaBO_2$ (C): 2M NaOH + 20% $NaBO_2$ (D): 2M NaOH + 10% $NaBO_2$ (E): 25% $NaBO_2$, pH 12.

$$i = 0.62nFAD^{2/3}\omega^{1/2}\nu^{-1/6}C \tag{2.4}$$

where A is the electrode area (cm^2), D is the diffusion coefficient (cm^2/s), ω is the angular velocity (rad/s), ν is the kinematic viscosity (cm^2/s), and C is the bulk concentration (mol/cm^3). Linear sweeps from –700mV to +300mV at a sweep rate of 10mV/s were used; the data corresponding to a disk potential of +40mV were used to ensure mass-transfer control (as required by the Levich equation). To determine D, values for n, C, and ν had to be known or assumed. C was taken as the nominal concentration of $NaBH_4$ in the solution, which was chosen

as 3mM for all experiments. The kinematic viscosity was measured for each solution. To determine n and the value of D for $NaBH_4$ in 2M NaOH the method reported by Wang [13] was used with the Levich analysis for 2M NaOH. The value of n was assumed to be the same for BH_4^- oxidation in all solutions; this assumption is justified by the observation that no other species in these solutions is electroactive in the same potential region as BH_4^- oxidation. The voltammograms, recorded at a potential sweep rate of 10mV/s, had a similar appearance to those obtained by Chatenet and co-workers [6]. Figure 2.6 shows the Levich plots used to obtain D. Once the values of D were obtained from the Levich analyses, the ratio of (D[2M NaOH + x $NaBO_2$]/D [2M NaOH]) were evaluated, where x is the w/v percent of $NaBO_2$ in the electrolyte.

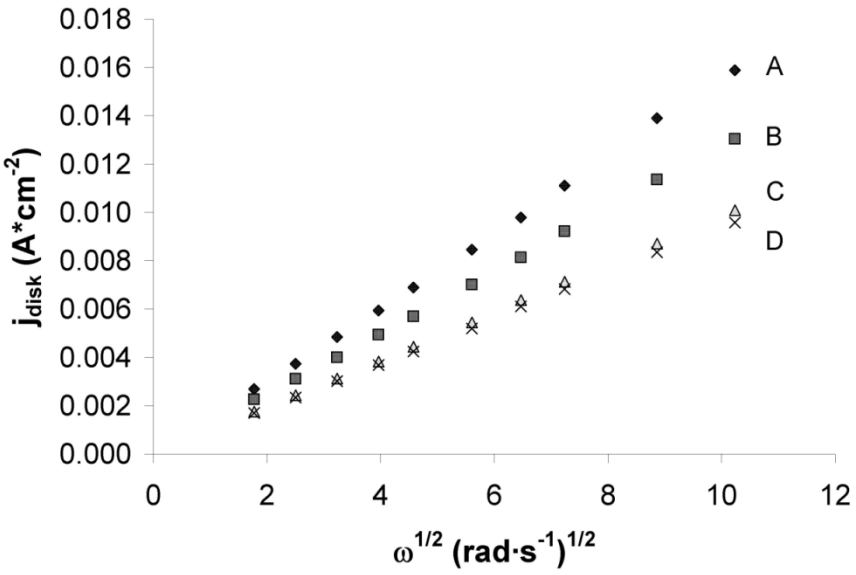

Figure 2.6: Levich plot for 3mM $NaBH_4$ in: 2M NaOH (A), 2M NaOH + 10% $NaBO_2$ (B), 2M NaOH + 20% $NaBO_2$ (C) and 2M NaOH + 25% $NaBO_2$ (D). The data are taken at a disk potential of +0.04V vs. Hg/HgO. Potential sweep rate: 10mV/s

The exponent of one-half is used, since the peak current scales with D to the one-half power in diffusion-controlled CVs. This ratio is then compared to the ratio i_p [2M NaOH + x $NaBO_2$]/i_p [2M NaOH] as shown in Table 2.9. The values for ν and D in Table 2.9 show that ν increases monotonically with the concentration of $NaBO_2$ over the concentration range studied. The diffusion coefficient D decreases with increasing ν, and hence, with increasing concentration of $NaBO_2$ in the electrolyte. Also, the two ratios in Table 2.9 (ratios of $D^{1/2}$ and i_p) show a very close correlation. Thus, it appears that the change in slope of the calibration curve with matrix is due to variations in the diffusion coefficient with the viscosity of the solution.

Although the regression for sodium borohydride in pH 12 solution shows an R^2 value of about 0.99, some curvature is evident when looking at the data. Better linearity in peak current with concentration was noted for the lower concentration range of 0.2mM to 1mM $NaBH_4$ in pH 12 solution. In pH 12 solution, the concentration of hydroxide may not be high enough that the oxidation kinetics are independent of the ratio $[OH^-]/[BH_4^-]$. This could explain the curvature in the standards response for the higher concentration range of 1mM to 20mM $NaBH_4$, where the ratio becomes smaller.

Table 2.9: Mass transport parameters and peak current ratios for $NaBH_4$ in 2M NaOH, 2M NaOH + 10% $NaBO_2$, 2M NaOH + 20% $NaBO_2$, and 2M NaOH + 25% $NaBO_2$ [10].

Solution	**ν (cm^2/s)**	**D (cm^2/s)**	**(D[2M NaOH + x$NaBO_2$]/D [2M NaOH])$^{1/2}$**	**i_p [2M NaOH+x$NaBO_2$]/ i_p [2M NaOH]**
2M NaOH	1.37×10^{-2}	*1.25×10^{-5}	-	-
2M NaOH + 10% $NaBO_2$	1.78×10^{-2}	9.73×10^{-6}	1.13	1.11
2M NaOH + 20% $NaBO_2$	2.40×10^{-2}	7.08×10^{-6}	1.33	1.33
2M NaOH + 25% $NaBO_2$	2.67×10^{-2}	6.73×10^{-6}	1.36	1.382

2.4 Conclusions

Depending upon the concentration range, the CV method as described in this chapter can serve as a semi-quantitative or quantitative method for $NaBH_4$ in aqueous alkaline solutions. The relative simplicity and low cost of this method make it ideal for the first analysis in electro-synthesis experiments for $NaBH_4$, like those described in Chapter Three.

A 6mm diameter disk working electrode was shown to offer increased sensitivity, demonstrated by the slope of the calibration curve being 32 times greater than that obtained with the 1mm electrode.

In repeatability tests and reproducibility experiments, statistical analysis shows that the signal-to-noise ratio is lower while the relative standard deviation is higher in the peak current for the concentration range of 0.1mM to1mM $NaBH_4$ in 2M NaOH. Furthermore, with consideration of residual errors, it is suggested that the technique is semi-quantitative for the low concentration regime. These same figures-of-merit suggest that for concentrations of $NaBH_4$ 1mM and above, the method is quantitative.

Finally, the effect of matrix has been investigated by using five different aqueous solutions of borohydride. The presence of sodium borate is seen to affect the slope of the calibration curves (the sensitivity); a study of mass-transport parameters in the different electrolytes demonstrates the differences in viscosity and diffusion coefficient are responsible for

this behavior. For the pH 12 solution, the dynamic range is also affected. Here, it is proposed that the concentration of hydroxide is affecting the kinetics of the oxidation at higher concentrations of borohydride. These results demonstrate that the matrix must be known and that the same matrix should be used to prepare standards.

2.5 References

1. E.L. Gyenge and C.W. Oloman, *Journal of Applied Electrochemistry*, 28 (1998) 1147.
2. M.V. Mirkin and A.J. Bard. *Analytical Chemistry*, 63 (1991) 532.
3. H. Çelikkan, H. Aydin, and M.L. Aksu, Turkish *Journal of Chemistry*, 29 (2005) 519 – 524.
4. E.Gyenge. *Electrochimica Acta*, 49 (2004) 965 – 978.
5. J.A. Gardiner, and J.W. Collat. *Inorganic Chemistry*, 4 (1965) 1208 – 1212.
6. M.F. Chatenet, F. Micoud, I. Roche, and E. Chainet. *Electrochimica Acta*, 51 (2006) 5459 – 5467.
7. M.V. Mirkin, H. Yang, and A.J. Bard. *Journal of the Electrochemical Society*, 139 (1992) 2212 – 2217.
8. G. Rostamikia and M.J. Janik. *Journal of the Electrochemical Society*, 156 (2009) B86.
9. H.Cheng and K. Scott. *Electrochimica Acta*, 51 (2006) 3429.
10. J.B. McLafferty, J.C. Tokash, Y.-C. Zhang, W.J. Coulson, and D.D. Macdonald, *ECS Transactions*, 2 (2007) 19.
11. D.D. Macdonald, Transient Techniques in Electrochemistry. Plenum Press, New York, 1977.
12. D. Harvey, Modern Analytical Chemistry. McGraw-Hill, Boston, 2000.
13. K. Wang, J. Lu, and L. Zhuang. *Journal of Electroanalytical Chemistry*, 585 (2005) 191 – 196.
14. A.J. Bard and L. R. Faulkner. Electrochemical Methods: Fundamentals and Applications, 2nd ed. John Wiley & Sons, 2004.

3. Electrochemical Reduction of Borate Anion and Stability of Sodium Borohydride in Aqueous, Alkaline Solution

3.1 Overview of Electrochemical Kinetics

When current flows through an electrochemical cell, the cell operates away from equilibrium. Thus, irreversible processes occur within the cell. Historically, the electrical potential drops corresponding to these irreversible processes have been called polarizations. The net polarization of a cell can be attributed to the following processes: charge transfer (or activation) polarization, occurring at the working and counter electrode of the cell; mass transfer

polarization, occurring at the working and counter electrode of the cell; and ohmic polarization, occurring in the electrolyte between the working and counter electrodes. The basic principles of charge transfer polarization will be described to put into proper context some of the work described in this chapter.

Charge transfer polarization is the result of a kinetic barrier to the transfer of electrons at the electrode-solution interface. The phenomenological equation that describes the current-potential relationship for charge transfer polarization is known as the Butler-Volmer equation:

$$I = I_o[\exp(-\alpha\eta F / RT) - \exp((1-\alpha))\eta F / RT)] \tag{3.1}$$

This equation is for a one-electron cathodic reaction [1].

The first characteristic quantity in this equation is the exchange current, I_o. Electrochemical, as well as chemical, equilibria are dynamic. Thus, the forward and reverse processes occur at the same rate at equilibrium. A generic electrode reaction is represented as:

$$O + e^- \underset{I_a}{\overset{I_c}{\rightleftharpoons}} R \tag{3.2}$$

In the convention used in this exposition, electrochemical reactions are written in the reduction sense, cathodic currents are negative, and anodic currents are positive. Since current is a measure of an electrochemical rate, at equilibrium $I_c = I_a = I_o$. I_o is the exchange current for this electrode reaction. Customarily, the exchange current is normalized to the electrode surface area (usually, the apparent area calculated by geometry) to give the exchange current density. The exchange current density can be used to understand a concept called polarizability (of an electrode). An ideally non-polarizable electrode can pass any amount of current without changing its potential. In this case, the electrode reaction would have an infinitely large exchange current density. An ideally polarizable electrode changes potential suddenly and to a large extent upon passage of current. This electrode would have an infinitesimally small exchange current density. A real electrode would behave between these two extremes.

A given electrode reaction may show radically different exchange current densities depending upon the electrode material. Two benefits of this observation can be used in designing an electrolytic process. The first benefit is electro-catalysis, meaning that the electrode reaction shows facile kinetics with certain electrodes; with these electrodes, the energy requirement for the process will be lowered. The second benefit is that selectivity of an electrode reaction can be enhanced or even permitted where otherwise it would not occur. This selectivity occurs if there is a kinetic barrier to the electrode reaction in competition with the desired electrode reaction. In this case, the rate of the competing process will be lowered. Polarography with the dropping mercury electrode has used this to advantage to study many cathodic processes. For example, in water, many metals cannot be reduced from their ions, for example, sodium. With a mercury

electrode, however, an amalgam (alloy with mercury) can be formed, allowing analysis of these metal ions.

The second characteristic quantity of the Butler-Volmer equation is the charge-transfer coefficient α. Two interpretations have been applied to this parameter. The first, and most widely adopted, is that this factor describes the symmetry of the energy barrier to charge transfer [1]. The second interpretation is that the charge transfer coefficient describes separation of charge in the transition state formed upon transfer of charge [2].

The third characteristic quantity of the Butler-Volmer equation is the overpotential η, which is the difference between the applied potential and the equilibrium potential (as given by the Nernst equation). The overpotential in this equation only has sense for a reaction in which a reversible equilibrium condition can be specified (for which the net current is zero) and hence an equilibrium potential as described by the Nernst equation can be determined. Some reactions, notably corrosion, occur under conditions of a mixed potential. This means that the potential at zero current is not an equilibrium potential, but rather a steady-state potential. In this case, the anodic reaction is not simply the reverse of the cathodic reaction; rather, the anodic reaction is a distinct reaction from the cathodic reaction. One example from corrosion would be an anodic current corresponding to oxidation of the metal and a cathodic current corresponding to reduction of hydronium ions (in acidic solution) to hydrogen gas. The actual steady-state potential that the electrode maintains depends upon the equilibrium potential and the charge transfer characteristics of both the anodic and cathodic reactions. The concept of the mixed potential is discussed further in the section on stability of sodium borohydride in aqueous solutions.

3.2 A Very Brief Introduction to the Hydrogen Evolution Reaction (HER)

The HER has been extensively studied primarily for two reasons: (1) this reaction has great importance in the operation of fuel cells, water electrolyzers, and for the "hydrogen economy" in general and (2) It is the simplest of electrode reactions and thus serves as a prototype for mechanistic investigations of electrode reactions. As it would be impossible to cover all of the research into this electrode reaction, only a few points of interest will be covered here.

In this chapter, all electrochemical experiments have been carried out in alkaline, aqueous solution. Electrochemical evolution of hydrogen from alkaline solution occurs by discharge of water molecules. There are three elementary reactions involved in the HER [3]. The first is the Volmer reaction; in alkaline solution it is:

$$H_2O + e^- \rightarrow H_{ads} + OH^- \tag{3.3}$$

H_{ads} represents hydrogen atoms adsorbed on the electrode surface. Another step is chemical combination of the adsorbed hydrogen atoms, the Tafel step:

$$H_{ads} + H_{ads} \rightarrow H_2 \tag{3.4}$$

Alternatively, the hydrogen may finally form by the Heyrovský step:

$$H_2O + H_{ads} + e^- \rightarrow H_2 + OH^- \tag{3.5}$$

Thus, the mechanism of hydrogen evolution will either involve a combination of the Volmer and Tafel steps or a combination of the Volmer and Heyrovský steps. In either case, the net reaction is

$$2H_2O + 2e^- \rightarrow H_2 + 2OH^- \tag{3.6}$$

The standard potential of this reaction is –0.83V vs. SHE. This reaction is of prime importance in this chapter, as it is the reaction competing with the reduction of borate, expressed as:

$$BO_2^- + 6H_2O + 8e^- \rightarrow BH_4^- + 8OH^- \tag{3.7}$$

This reaction has a standard potential of –1.24V vs. SHE [see reference (8), Chapter 1].

Thermodynamically, then, water reduction is favored to borate reduction. Approaches to overcome this difficulty are outlined below.

3.3 Borate Reduction: Literature Review

Patents have been issued in which claims are made that this reaction occurs. Typically, investigators in this field have used two approaches. Recall from the overview of electrochemical kinetics at the beginning of this chapter that electrode reactions can show very different rates depending upon the cathode material. This observation allows for enhancement of rate by electro-catalysis or increasing selectivity by lowering the rate of a competing reaction. Both approaches have been used. The first approach, use of electro-catalysis, is called indirect reduction in this work. Essentially, indirect reduction is hydrogenation by electrochemically-generated hydrogen. In this case, materials having a low overpotential for the HER (henceforth called "low overpotential" cathodes) are used, i.e., cathode materials having a high I_o. These cathodes promote water electrolysis to yield adsorbed hydrogen atoms and hydrogen gas; the adsorbed hydrogen and hydrogen gas are thought by some workers to hydrogenate borate to borohydride (more discussion below). The second approach, increasing selectivity by lowering the rate of the competing reaction, is called direct reduction in this exposition. In this case, materials having a high overpotential for the HER (henceforth called "high overpotential" cathodes) are used, i.e. materials having a low I_o. These cathodes thus inhibit water reduction (E^o = -0.83V) and therefore allow potentials to be reached where borate reduction can occur (E^o = -1.24V).

In the following discussion, the work of Gyenge and Oloman [4] in testing of early patents is discussed, and some more recent patents and publications are discussed. A comprehensive review of all patents in this field is not given; however, representative patents are discussed below.

Gyenge and Oloman [4] tested several of the patents issued previous to 1998. These workers tried three basic approaches: indirect reduction, direct reduction, and reduction of a borate ester in organic media. Reduction in organic media was attempted to eliminate competition of the Hydrogen Evolution Reaction (HER) in reduction of B-O compounds (in this case, borate esters).

For indirect reduction of borate, Gyenge and Oloman tested Ni, Raney Ni on stainless steel mesh, a Raney Ni bed, a NiB bed, Pd, and Zn as cathode materials. Varying quantities of borate, as $NaBO_2$, were used, as well as varying quantities of alkalis (NaOH, K_2CO_3). Nafion 324 or a fine porosity ceramic frit was used as the cell divider in their experiments. Different current densities, from 0.5 to 3.5 kA/m^2, and different reaction times of 1 to 3 hours were employed for the indirect reduction experiments. In these experiments, no BH_4^- could be detected. These workers note that the commonly used iodate method (a back titration) was prone to error if the acidification of the catholyte is insufficient.

For their direct reduction experiments, the following cathodes were tried: amalgamated Cu, Ni, Raney-Ni on stainless steel mesh, NiB, Pd, and Zn. Although Ni, Raney Ni, Pd, and Zn were also tried for the indirect reductions, they were used in the direct reductions because various additives were tried to increase the overpotential. These additives were tetraethylammonium hydroxide (TEAH), tetramethylammonium iodide (TMAI), cetyltrimethylammonium bromide (CTAB), and thiourea (TU). The tetraalkylammonium compounds (TEAH, TMAI, and CTAB; generically referred to as TAA+ henceforth) are thought to increase the overpotential by inhibiting the Volmer step of the HER. TU inhibits the Tafel step of the HER. The current densities in these experiments varied over a wider range (0.12 kA/m^2 up to 7.50 kA/m^2) and the reaction time was from 0.5 to 4 hours. Quite negative cathode potentials could be achieved: about -3.2V on amalgamated Cu with TEAH and about -2.7V on Zn with TU as additive. Also, for the experiment using TEAH, the composition given was 10% w/w $NaBO_2$ + 2M NaOH in 35% w/w TEAH. None of these direct reduction experiments yielded a detectable amount of BH_4^-. Finally, reduction of an organoborate compound in organic media was attempted. The organoborate compound tried was trimethylborate ($B(OCH_3)_3$). In these experiments, the most extreme direct reduction method was attempted – the so-called solvated electron reduction. In some solvents, notably liquid ammonia, simple amines, and hexamethylphosphoramide (HMPA), electrons can be 'ejected' from the cathode and stabilized by solvation. Two cathode materials were investigated: graphite and aluminum. In one experiments, a 50:50 mol % mixture of HMPA and ethanol was used with lithium perchlorate as the supporting electrolyte. The addition of ethanol to HMPA at or below 50 mol % does not inhibit the formation of solvated electrons but does provide a hydrogen source [5]. The other experiment utilized LiCl and tetrabutylammonium hexafluorophosphate ($TBAPF_6$) in ethylenediamine (EDA). Much lower current densities (0.08 and 0.09 kA/m^2) were employed in these experiments and the cathode potential was not reported

(presumably due to the difficulty in finding a suitable reference electrode for organic media). Even under the relatively extreme conditions of solvated electron reduction, no BH_4^- was detected after the electrolysis.

Amendola was issued a patent in 2002 that includes aspects on electrochemical reduction of borates in aqueous solution [6]. This patent calls for the use of high overpotential cathodes, such as Bi, Tl, Cd, Sn, Pb, Ga, In, Hg, and amalgamated materials; thus direct reduction is suggested. The anode material was suggested to be gold, iridium oxide, manganese (IV) oxide, or other materials have a low overpotential for oxygen evolution, since the anode reaction is oxidation of hydroxide ion to oxygen. No examples of operation were given in this patent.

Kawai and Ito were granted a patent in 2003 for production of alkali metal borohydrides in aqueous solution [7]. Materials suggested for the cathode include Ta, In, Zn, Pb, and C (hydrogen overpotential of more than 0.3V preferably). A hydrogen oxidation anode was suggested to minimize cell potential; thus anode materials having a low potential for hydrogen oxidation were suggested: Pd, Pt, Ru, Os, Ir, Rh, etc. When using the hydrogen oxidation anode, co-evolution of oxygen is necessary for safety reasons, so materials having a large overpotential for hydroxide oxidation should be used. Several embodiments were given. The first of these examples called for a gas diffusion anode (for hydrogen oxidation), with H_2 supplied at a pressure of 0.2MPa. The cathode was Ta and the cell divider was an anion-exchange membrane. The anolyte was 6M NaOH and the catholyte was $NaBO_2$ in 6M NaOH (concentration of $NaBO_2$ not given). A potential of 1V was applied across the cell and a current efficiency of 80% was reported. The analytical method used to establish the current efficiency was not reported. The use of an anion-exchange membrane is a mystifying choice; as such a membrane would allow any borohydride produced to eventually reach the anode where it would be destroyed.

Jianqiang et al. reported in a publication that reduction of $NaBO_2$ in aqueous, alkaline solution could be accomplished at a copper cathode [8]. Many important details were missing in this report: the size and form of the cathode, the applied current, working electrode potential and/or cell potential, and the cell divider was reported to be a "self-made" cation-exchange membrane with no details at all given as to the constitution or preparation of this membrane. The authors did state that the anolyte was 1M H_2SO_4 and the anode was Pb; the catholyte was 1M NaOH with 0.2M $NaBO_2$ and the cathode was copper. CV at a Cu working electrode (area and preparation not disclosed) at a sweep rate of 100mV/s with a lead counter electrode and an SCE reference electrode was performed. A peak occurring at –1.52V was supposed to be due to reduction of $NaBO_2$; the "drifting" of the "actual reduction potential" was supposed to occur due to adsorption and desorption of oxygen. Ion chromatography, X-Ray Diffraction (XRD), and iodometry (iodide back-titration method) were reported as analytical techniques.

The foregoing discussion reveals that much work has been devoted to electrochemical reduction of boron oxides in aqueous solutions by direct and indirect methods. Many of these patents make the process appear to be a simple electrolysis in a two-compartment cell, yet none of these processes have been adapted commercially. It became evident that the previous work

overlooked a fundamental problem: on the basis of simple electrostatics, borate anion should be repelled from the cathode, inhibiting reduction.

3.4 Electrostatic Repulsion of Borate Anion from Cathode

One important aspect of borate reduction appears to have been overlooked by other workers: electrostatic repulsion of the borate anion from the cathode. Several ideas to overcome this problem were investigated: (1) use of a cathode material having a very negative Potential of Zero Charge (PZC) (Ti); (2) use of a rectangular wave pulse, a method already known in electroplating for such use; (3) "engineering" of the Electrical Double Layer (EDL) to modify the potential profile; (4) modification of the cathode surface to promote attraction/binding of borate anions.

Essentially, the PZC is the potential at which a metal has no net charge [1]. For reduction of anions, the PZC could have important consequences, as the cathode surface will undoubtedly carry an excess negative charge, causing migration of anions away from the cathode. From this perspective, the metal having the most negative PZC would be the best cathode material. Polycrystalline Ti is supposed to have a PZC of -1.05V vs.SHE, the most negative of the metals in one table of PZC values [9]; thus Ti was used as a cathode in some experiments.

A rectangular wave potential or current form is already known in electroplating [10]. In many electroplating baths, metal ions are not present as cations, but rather as complex anions (often complexed with Cl^-, CN^-, etc.). In such cases, migration of the complex metal anions away from the cathode leads to problems in obtaining a good metal deposit. The rectangular wave current or potential solves this problem as follows. When the current or potential is stepped to a negative value, the cathode reaches a potential where reduction of the anion is favored. After holding at the negative-most potential or current for some time, the current or potential is then stepped to a more positive value, during which time the surface begins to acquire a positive charge. The electrode then attracts complex anions close to the surface by electrostatics. The potential is next switched rapidly negative, reducing anions close to the surface before they migrate away. Evidently, the period for the positive and the period for the negative portion of the waveform are important, as well as the values for the negative-most and positive-most potential or current. One can imagine that if the positive-most potential is too great or the period of the positive portion is too long, oxidation can occur, thus reversing the desired reaction.

Before discussing "engineering" of the EDL, some basics of the EDL need to be discussed. As with the HER, a large amount of theoretical and experimental work has been dedicated to understanding the EDL. Only the very most basic aspects of the EDL will be discussed in the following. Actually, there are more layers than two in the more advanced models; the term "double" is left over from the first version of the model (the Helmholtz model). For the purpose of this discussion, the Stern model will be considered [1]. The basic layers of this model are the Inner Helmholtz Plane (IHP), the Outer Helmholtz Plane (OHP), and the

diffuse layer. In the IHP and OHP, solvent molecules and ions are sufficiently close to the electrode that electric forces dominate and these layers are structured. Further away from the electrode, thermal forces become more dominate and the disarray results in the diffuse region. The IHP is populated by solvent molecules and specifically-adsorbed ions. The OHP is populated by solvated ions and solvent molecules, as is the diffuse region. The region comprising the electrode surface and the double layer (including the diffuse region) will be referred to here as the interphase region.

Specific adsorption of ions requires that at least part of the ionic solvation sphere can be removed so that the ion can directly contact the electrode surface and occupy the IHP [11]. Larger ionic radii promote this in two ways. The first is that the charge density of a large ion is lower than that of a smaller ion, and hence the solvation sphere is not so tightly bound to the larger ion. The second factor is that specific adsorption is exo-entropic: water molecules are displaced from the electrode surface when an ion specifically adsorbs. As there is more freedom for water molecules in the bulk of the solution (or at least, in the interphase region) compared to when the same molecules are adsorbed to the electrode, there is a positive gain in entropy. A larger ion will displace more water molecules, thereby favoring the process to a greater extent.

The potential profile in the interphase region changes in the presence of specific adsorption. For example, specific adsorption of cations at a cathode will make the potential between the IHP and the OHP appear positive. This should promote approach of the borate anion and if it does, this should accelerate reduction of the borate. Such effects are known in other systems, and some citations are given below in the experimental section. Figure 3.1 shows a schematic of the EDL in the absence of specific adsorption, and Figure 3.2 shows a schematic of the EDL in the presence of specific adsorption.

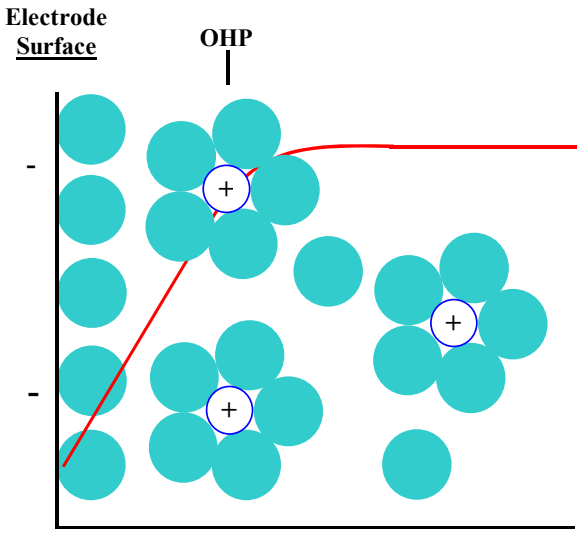

Figure 3.1: Schematic representation of the EDL in the absence of specific adsorption. The turquoise circles represent water (solvent) molecules. The red curve represents the potential profile. Note that the potential is negative at the OHP, inhibiting approach of anions.

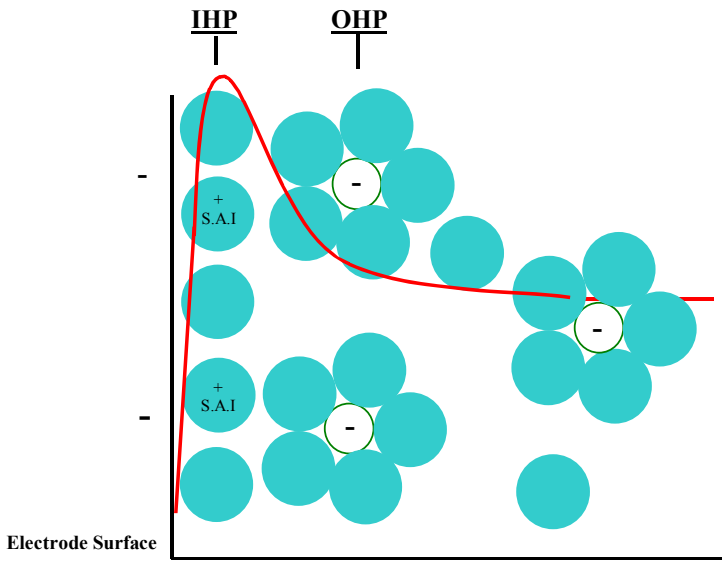

Figure 3.2: Schematic of EDL with specific adsorption. Turquoise circles represent water (solvent) molecules. +S.A.I. represents a specifically adsorbed cation. Red curve is potential profile. Note that the potential is now positive at the IHP and still positive at the OHP. Thus, repulsion of anions may be avoided in this scenario.

Two modifications to the cathode were attempted to see if these could promote borate reduction. The first of these was to try to form a self-assembled monolayer of 1-thioglycerol on a polycrystalline gold flag-working electrode. 1-thioglycerol was chosen because it contains a thiol group (-SH) allowing anchoring to the gold substrate, as well as a cis-diol functionality, which has been shown to bind borate anions [12]. The second modification tried was coating a cathode substrate with a quaternized and cross-linked poly(4-vinylpyridine) [P(4VP)]. Quaternized and cross-linked P(4VP) is a cationic polyelectrolyte, meaning that the polymer chains bear fixed positive charges – in this case, the positive charges are on nitrogen atoms of the pyridine moieties. The objective was then to use these positively charged functionalities to electrostatically-bind borate anions on the cathode.

3.5 Experimental Work

Experimental work in this chapter is divided into several areas: assessment of $NaBH_4$ stability in alkaline solutions of different compositions, reduction experiments of $NaBO_2$ or $B(OH)_3$ using high overpotential cathodes (similar to patent work reviewed above), experiments

using methods to try to overcome electrostatic repulsion of borate ion from the cathode (as described above), and stability experiments for $NaBH_4$ in aqueous solution in the presence of cathode materials.

The first task was to ensure that $NaBH_4$ would be stable in the catholyte solutions that were planned for the reduction experiments. Early work on $NaBH_4$ shows that the hydrolysis of $NaBH_4$ is subject to general acid catalysis [13]. For this reason, many of the patents for aqueous reduction to $NaBH_4$ suggest the addition of an alkali such as NaOH to the catholyte to retard loss of $NaBH_4$ by hydrolysis [4]. The following electrolytes were chosen for this study: 2M NaOH, 2M NaOH + 25% w/v $NaBO_2$, and 25% w/v $NaBO_2$ adjusted to pH 12 by addition of 6M NaOH. Three concentrations of $NaBH_4$ were used in each electrolyte: 0.1mM, 1mM, and 20mM in 2M NaOH and 2M NaOH + 25% $NaBO_2$; and 0.5mM, 1mM, and 20mM in 25% $NaBO_2$ at pH 12. The CV method was used to record the peak current for $NaBH_4$ oxidation vs. time; measurements were made in duplicate each day for each solution.

Figure 3.3 shows the peak current vs. time plot for 2M NaOH with 0.1mM $NaBH_4$. The average peak current over the 19-day test period was determined to be 0.068mA. The figure shows two different ranges enclosed by dashed lines. The range of ±1.29 s [s: standard deviation for a small sample set] corresponds to a confidence interval of 80%, which assumes that the data follow a normal distribution. The range corresponding to ±1 s corresponds to a confidence interval of 95%, again assuming a normal distribution. Almost all the data is within the 80% confidence interval about the average peak current measurement, and most of the data are within the 95% confidence interval. Thus, it would appear that $NaBH_4$ is stable in 2M NaOH over the 19-day test period.

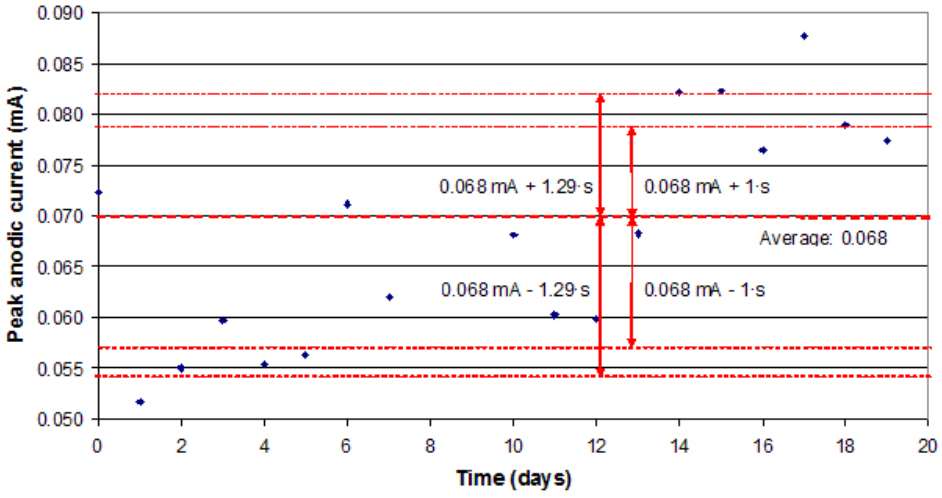

Figure 3.3: Peak current vs. time measured by CV method for 0.1mM $NaBH_4$ in 2M NaOH.

Table 3.1: Stability Data for $NaBH_4$ in 2M NaOH solution. *This "RSD" calculated using an 80% confidence limit rather than 1 standard deviation as a confidence limit. **This RSD is calculated using only the first 10 days to compare it with the stability data in 25% w/w $NaBO_2$ + 2M NaOH (see Table 3.2).

[$NaBH_4$] (mM)	**Average I_p (mA)**	**S (mA)**	**RSD (1 SD)**	**"RSD" (1.29 SD)***	**RSD (1 SD)****
0.1	0.068	0.011	16.76	21.62	12.55
1	0.511	0.044	8.57	11.06	7.61
20	9.545	0.334	3.50	4.52	3.62

Table 3.2: Stability Data for $NaBH_4$ in 2M NaOH + 25% $NaBO_2$ solution. *This "RSD" calculated using an 80% confidence limit rather than 1 standard deviation as a confidence limit.

[$NaBH_4$] (mM)	**Average I_p (mA)**	**S (mA)**	**RSD (1 SD)**	**"RSD" (1.29 SD)***
0.1	0.070	0.005	6.96	8.98
1	0.417	0.028	6.79	8.75
20	7.616	0.126	1.65	2.13

Similar plots were constructed for 1mM and 20mM $NaBH_4$ in 2M NaOH; Table 3.1 summarizes the average peak current measurements for each $NaBH_4$ concentration as well as the various measures of precision. The RSD decreases with increasing concentration since the signal increases relative to random fluctuations causing the scatter in the data. Figure 3.4 shows a plot analogous to Figure 3.3 but for 0.1mM $NaBH_4$ in 2M NaOH + 25% $NaBO_2$; Table 3.2 summarizes the data obtained in these experiments. These measurements were only carried out over 10 days; thus an extra column was added to Table 3.1. This extra column contains data within the first ten days for the 2M NaOH measurements, allowing comparison over the same time interval. Again, it appears that $NaBH_4$ is stable in 2M NaOH + 25% $NaBO_2$ over the 10 day test period.

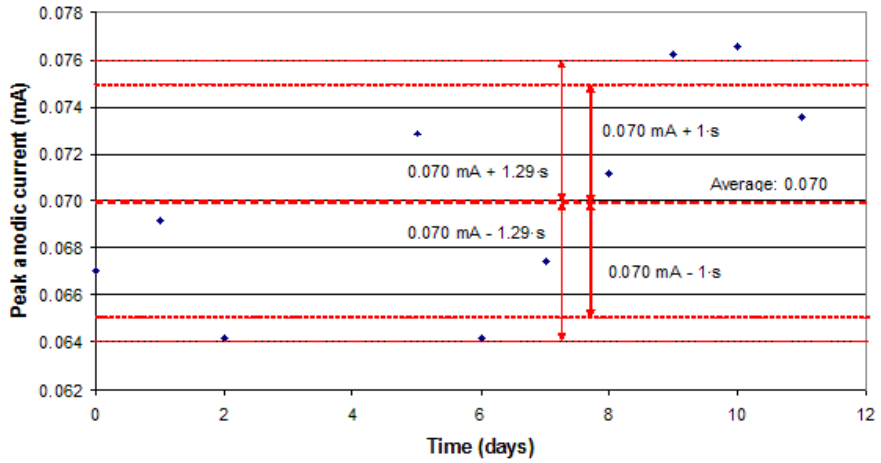

Figure 3.4: Stability of 0.1mM $NaBH_4$ in 2M NaOH + 25% $NaBO_2$ monitored for 10 days. Two different confidence limits are shown: 1s (68%) and 1.29s (80%).

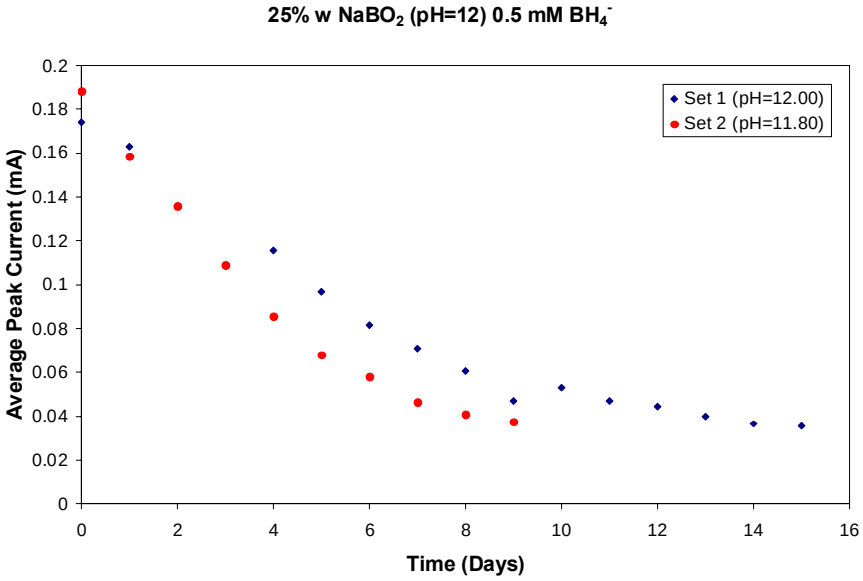

Figure 3.5: Stability of 0.1mM $NaBH_4$ in 25% w/w $NaBO_2$ (pH = 12) monitored for 9 and 15 days.

In contrast to 2M NaOH and 2M NaOH + 25% $NaBO_2$, there is a definite tendency for the peak current to decrease in time for the $NaBH_4$ in 25% $NaBO_2$ at pH 12. For this reason, the higher concentration of 0.5mM $NaBH_4$ was required for the lowest concentration so that sufficient data could be acquired. Figure 3.5 shows this data for two experiments; one started

with a slightly lower pH (11.8). In both cases, the same trend was observed, but the peak current decayed faster in the lower pH solution. This is reasonable considering that the stability of $NaBH_4$ against hydrolysis depends upon the solution pH, the reaction being subject to general acid catalysis [13]. The change in peak current over from beginning to end was found to be about 80% for all the trials and for all three concentrations of $NaBH_4$ studied. The vast majority of electrolysis experiments used a high concentration of alkali (2M OH^-) in accordance with these findings.

The first approach in the electrolysis experiments focused on direct reductions with high overpotential cathodes. The reason for this is that many of the materials used as cathodes in direct reduction also happen to be good catalysts for hydrolysis of BH_4^- [14]. As one example, Gyenge and Oloman [4] reported that the Raney Ni bed caused rapid hydrogen evolution from an alkaline $NaBH_4$ solution. Because hydrolysis of $NaBH_4$ had to be avoided, it appeared more profitable to focus on direct reductions for aqueous media.

Mercury is the quintessential high overpotential cathode material and is generally held to be the cathode material giving the most negative cathodic limit in aqueous solutions. However, and this was not appreciated early in this project, the formation of alkali metal amalgams is known to be the cathodic limit when alkali metal cations are present in solution [15]. For example, the standard potential for the deposition of sodium metal is -2.713V (SHE). On the other hand, the potential for sodium deposition at a mercury cathode in 1M NaOH has been reported to occur at -1.68V (SHE; after conversion from RHE scale) [16]. This potential is very far positive to the standard potential for sodium metal deposition. The formation of an alkali metal amalgam occurs at a potential more positive than the formation of the pure alkali metal due to the spontaneity of amalgam formation.

To see if amalgam formation could be avoided and therefore a more negative cathodic limit reached, tetraalkyammonium hydroxides (TAAH; also called quaternary ammonium hydroxides in literature) were used. Hydroxides were used because maintaining the catholyte alkaline is necessary to slow hydrolysis of any borohydride that might form. An additional benefit of using TAAH is that given by Gyenge and Oloman: increasing the overpotential of the HER. Later, it was realized that use of TAAH might be beneficial due to electrical double layer (EDL) effects. The EDL effects will be described later. Boric acid served as the oxidized boron reactant in these experiments; the composition of the electrolytes was 2M TAAH + 0.2M $B(OH)_3$. Boric acid was used in place of sodium borate ($NaBO_2$) to avoid the presence of sodium cation. Some of the experiments also had 1mM $NaBH_4$ in the catholyte initially as a positive control. Most of the experiments were performed at a constant current of 10mA in small, custom-made divided H-cells as shown in Figure 3.6. The cell divider was Nafion N-112. Nafion was used as a cell divider because it is the most easily obtained perm-selective membrane material. It is also stable at high pH, being a perfluorinated polymer. Perm-selectivity for cations is necessary to avoid any BH_4^- that might form from reaching the anode of the electrolysis cell where it would be destroyed by oxidation. Electrical contact to the mercury pool was made through a stainless steel cathode post. The counter electrode was a 6mm diameter graphite rod. Most of the experiments

used 2M TAAH + 0.2M $B(OH)_3$ as the anolyte ("symmetric electrolyte") but some later experiments used 1M H_2SO_4 as the anolyte.

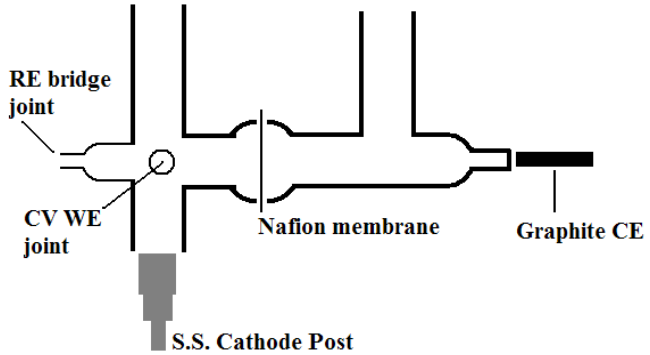

Figure 3.6: Custom H-cell used in mercury pool electrolysis experiments. The cell is made of glass. The mercury pool cathode rests on top of the stainless steel (S.S.) cathode post inside the cell. The Nafion membrane is clamped between two Goretex (expanded PTFE foam) gaskets; the clamp is not shown in this figure. A graphite rod (6mm diameter) and RE bridge are connected to the cell through No. 7 Chem Thread joints (Chem Glass). There is a joint labeled "CV WE joint" – initially, it was planned to place a 1mm diameter Au disk WE through this joint for continuous monitoring of reaction progress using the CV method. As described in the text, it was later realized that the formation of unstable amalgams lead to a dispersion of colloidal Hg in the catholyte compartment. Therefore, the Au electrode was not used during electrolysis because the colloidal Hg would quickly amalgamate it.

During the electrolysis, the volume of the catholyte increased and the volume of the anolyte decreased. This was attributed to electro-osmosis, an irreversible thermodynamic effect that occurs when charge and mass transport are coupled [17]. The Nafion membrane is assumed to transport cations primarily. However, the movement of cations also promotes transfer of water by two mechanisms: transport of water of hydration and "hydrodynamic pumping" of water [18]. Among the alkali metal and alkaline earth metal cations, as the ionic radius increases, the amount of water/ion transferred decreases, i.e. transport by water of hydration is dominant. Among the tetraalkylammonium cations, the quantity of water transported/ion increases with effective ionic radius, since hydrodynamic pumping is dominant (in fact, it is assumed that all water is transported by hydrodynamic pumping with these hydrophobic cations). This is a problem because the concentration of the catholyte decreases with increasing time of electrolysis.

An additional complication was seen: shortly after electrolysis begun, the Hg pool became quite unstable, erupting with release of tiny mercury droplets. The catholyte quickly became a cloudy grey color from the large amount of mercury droplets in suspension. The cause of this effect was identified as formation of tetraalkylammonium 'amalgams.' The reduction of tetraalkylammonium cations at a mercury pool to form an unstable amalgam is described in the

literature, but this was not known prior to beginning these experiments [19,20]. Since gold is easily amalgamated, the CV method could not be used with the catholyte until all of the mercury settled out of suspension. Thus, after the first two days of electrolysis, the current was shut off and the Hg was allowed to settle until the following day. After making the CV measurement on the catholyte, electrolysis was started again. After three more days of electrolysis, the current was shut off and the mercury was again allowed to settle until the following day. Then the final measurement was made. Thus, in these experiments, there were a total of five days of electrolysis with two days off. The electrolysis time was 4 x 10^5 to 5 x 10^5 s total for such experiments. Faraday's Law of Electrolysis may be written as

$$C = \frac{Q}{nFV} \tag{3.8}$$

In this equation, C is concentration (M), Q is charge passed during electrolysis (C), n is the number of electrons required per mole of substance electrolyzed to bring about the desired reaction, F is Faraday's constant (96485 C/mol), and V is volume of catholyte being electrolyzed (L). Consider one experiment : the catholyte volume before electrolysis was 20mL of 2M TEAH + 0.2M $B(OH)_3$, the time of electrolysis was about 406,800s, and n = 8 (from hypothetical cathode reaction). Using these values gives

$$C = \frac{(406800s)(0.01C/s)}{(8)(96485C/mol)(0.020L)} = 0.264M \tag{3.9}$$

Note that Q = I t since this is a constant-current electrolysis. The result of 264mM assumes 100% current efficiency (CE); assuming different values of CE simply inserts a linear scaling factor. For example, assuming a CE of 10% is the same as multiplying the result by 0.1; then the yield of BH_4^- would be 26.4mM. Even at 1% CE the yield would be 0.264mM, an amount detectable by the CV method (see Chapter 2). Thus, sufficient charge was passed to detect borohydride even if the experiment was working at 1% CE. Figure 3.7 shows CVs of 2M TEAH + 0.2M $B(OH)_3$ catholyte before and after electrolysis in this experiment; no evidence of BH_4^- formation is seen in these CVs.

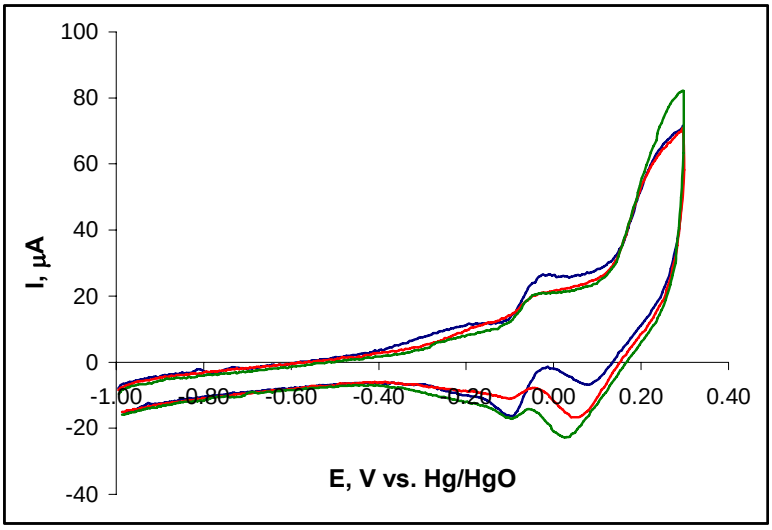

Figure 3.7: Hg pool electrolysis experiment. Blue curve: CV of 2M TEAH + 0.2M $B(OH)_3$ before electrolysis. Red curve: CV of 2M TEAH + 0.2M $B(OH)_3$ catholyte after 2 days of electrolysis at 10mA. Green curve: CV of 2M TEAH + 0.2M $B(OH)_3$ catholyte after 3 more days of electrolysis at 10mA. CV performed using a 6mm diameter disk Au WE; 100mV/s sweep rate; 6mm diameter graphite rod CE.

During the electrolyses, the cell potential was generally about 3.5 to 5V and the working electrode potential was generally –2.5V to –3V vs. Hg/HgO reference, when TMAH and TEAH-based electrolytes were used.

Positive control experiments indicated that $NaBH_4$ was not stable during electrolysis, even accounting for the volume change that occurred due to electro-osmosis. The first attempt at addressing this issue was Ar sparging of the catholyte for four hours prior to commencing electrolysis. The hypothesis was that O_2 in solution was promoting decomposition of $NaBH_4$ directly or by reduction to a more reactive species (e.g. H_2O_2). However, there was no effect in the experiments when this was performed. The next hypothesis was that the dispersion of mercury droplets in the catholyte during electrolysis could be catalyzing the decomposition of $NaBH_4$. Considering that the rate of an electrochemical reaction (e.g. borate reduction) depends upon temperature and potential, whereas the rate of a chemical reaction (e.g. hydrolysis, amalgam decomposition) depends upon temperature, low temperature electrolysis was investigated.

Water is a much more efficient cooling medium than air, but construction of a similar divided H-cell with water jackets would be very demanding. At 10mA, Joule heating of the catholyte was rather minimal, so very little heat would be generated during electrolysis. Thus, it was simpler to use a small refrigerator to cool the electrolysis cell.

A temperature of -4°C could be achieved with the temperature control on the lowest setting. The cell with electrolyte and the stirring plate were placed in the refrigerator and electrical connections were made to the cell; the refrigerator was then closed and allowed to cool to –4°C again. After attaining this temperature, electrolysis was commenced. In the positive

control experiments, decomposition of borohydride was still noted. Furthermore, the decomposition of TAA amalgams could not be prevented; the catholyte still had the same cloudy grey appearance.

Due to the intractable problems with Hg because of amalgam formation, other high overpotential materials were tried as cathodes. These included Au, Ti, Pb, Ag, and Cu. For Au, several electrolyte solutions were tried: 2M NaOH + 25% $NaBO_2$, 1M TMAH + 12.5% $NaBO_2$, and 2M TEAH + 0.2M $B(OH)_3$. The anolyte in most of these experiments was the same as the catholyte (symmetrical electrolytes) but in some experiments, 1M H_2SO_4 was used since the electro-osmosis effect was not observed with this anolyte. That electro-osmotic dilution of the catholyte did not occur with 1M H_2SO_4 anolyte was noticed when trying to repeat the experiments of Jianqiang et al [8]. It is not clear why electro-osmotic dilution of the catholyte occurred in this case, but one possible explanation is that the number of water molecules per "proton" transferred is less than the number of water molecules per sodium ion or TAA+ ion transferred. H-cells with Nafion 112 as a divider were used; usually the catholyte volume was 35 – 45 mL and the anolyte volume was typically 75 – 85mL. The cathodes were 25mm x 25mm square flags and the anodes were 25mm x 25mm square platinum flags unless otherwise indicated.

A small amount of $NaBH_4$ (1mM to 3mM) was added to the catholyte prior to electrolysis in some experiments as a positive control. Figure 3.8 shows a representative CV result obtained on catholyte from a constant-current electrolysis at 10mA using an Au cathode with 2M NaOH + 25% w/v $NaBO_2$ as catholyte (and anolyte). Figure 3.9 shows the CV result obtained in a similar experiment, using all the same conditions but with 2mM $NaBH_4$ in the catholyte as a positive control. Note the decrease in peak current vs. time for the anodic peak representing oxidation of $NaBH_4$. Figure 3.10 is also for an experiment using an Au cathode; in this case the anolyte and catholyte were 1M TMAH + 12.5% w/w $NaBO_2$. In none of the experiments could CV detect BH_4^- in the catholyte post-electrolysis. Again, Faraday's Law of Electrolysis was used to estimate how much BH_4^- could be produced at the end of electrolysis assuming 1% current efficiency. Using this estimation, it was ensured that enough electrolysis time was allowed to form a detectable quantity of BH_4^-.

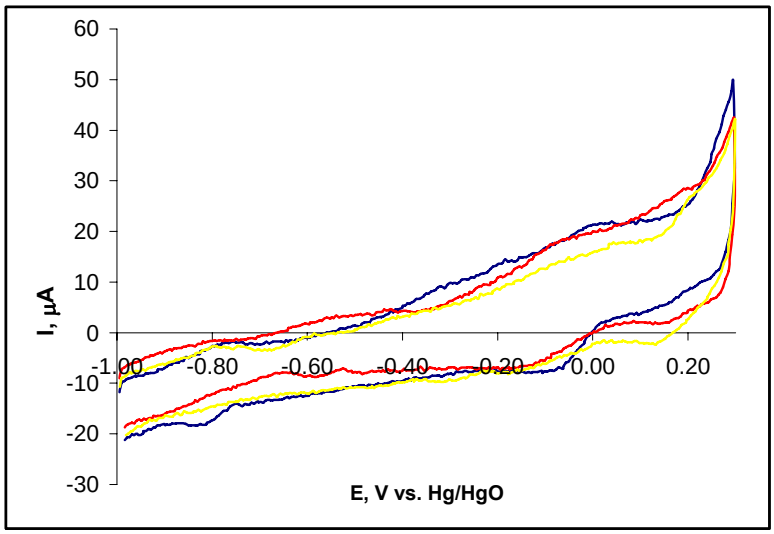

Figure 3.8: Au cathode electrolysis experiment. Blue curve: CV of 2M NaOH + 25% w/v $NaBO_2$ catholyte before electrolysis. Red curve: CV of 2M NaOH + 25% w/v $NaBO_2$ catholyte after two days of electrolysis at 10mA. Yellow curve: CV of 2M NaOH + 25% w/w $NaBO_2$ catholyte after three more days of electrolysis at 10mA. CV conditions same as with Hg pool experiment (see Figure 3.7).

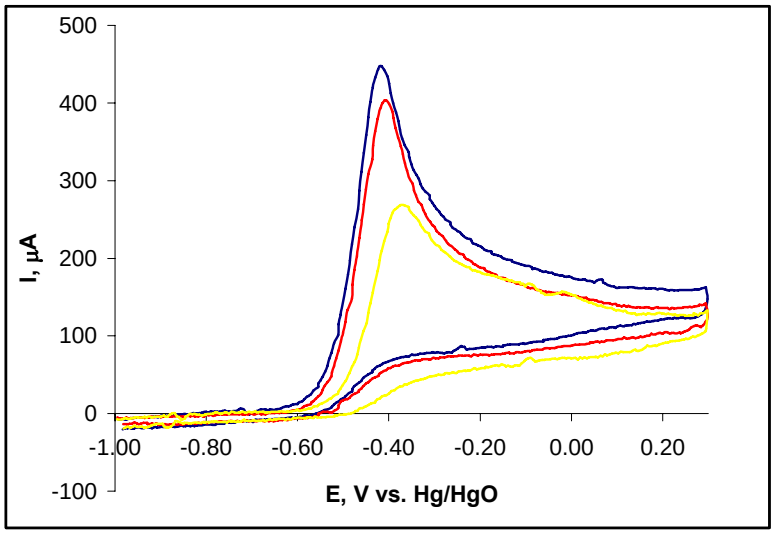

Figure 3.9: Au cathode electrolysis experiment. Blue curve: CV of 2M NaOH + 25% w/v $NaBO_2$ with 2mM $NaBH_4$ (as a positive control) catholyte before electrolysis. Red curve: CV of 2M NaOH + 25% w/v $NaBO_2$ with 2mM $NaBH_4$ catholyte after two days of electrolysis at 10mA. Yellow curve: CV of 2M NaOH + 25% w/w $NaBO_2$ with 2mM $NaBH_4$ catholyte after three more days of electrolysis at 10mA. CV conditions same as with Hg pool experiment (see Figure 3.7).

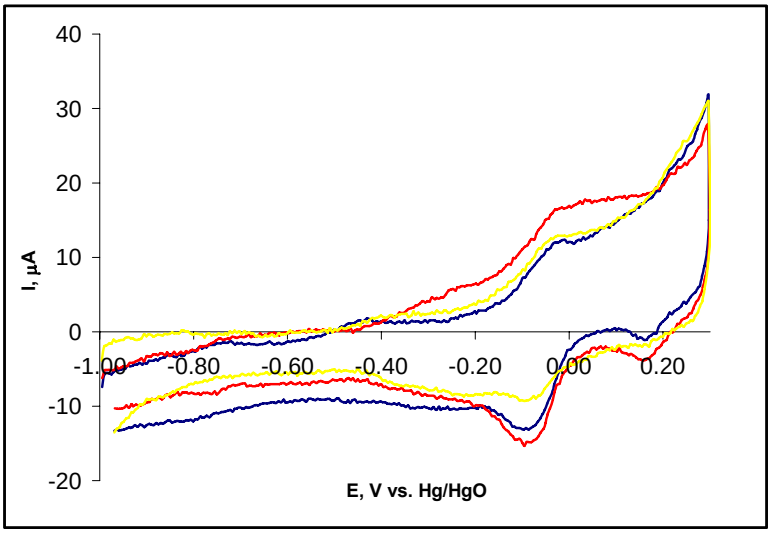

Figure 3.10: Au cathode electrolysis experiment. Blue curve: CV of 1M TMAH + 12.5% w/v $NaBO_2$ catholyte before electrolysis. Red curve: CV of 1M TMAH + 12.5% w/v $NaBO_2$ catholyte after two days of electrolysis at 10mA. Yellow curve: CV of 1M TMAH + 12.5% $NaBO_2$ catholyte after three more days of electrolysis at 10mA. CV conditions same as with Hg pool experiment (see Figure 3.7).

In some experiments, a current or potential pulse was applied. The purpose of the pulsed current or potential was to attempt to overcome electrostatic repulsion of the borate anion from the cathode. In principle, the negative-most potential or current should be such that reduction can occur. The positive-most potential or current should be chosen to attract the borate anion close enough to the electrode for reduction. The time and potential or current for the positive portion of the pulse should be chosen to avoid oxidation of any BH_4^- that may form. Also, the electrochemical cell presents a reactive load because of the capacitive behavior at the working and counter electrodes. Thus, the time it takes to charge and discharge these capacitive elements should be considered. However, while these principles are understood, characterizing the electrical behavior of the cell and choosing the appropriate values for potentials and times is a troublesome process and depends upon such parameters as the cell geometry and real electrode areas. Due to the demanding nature of this process, some times and potentials or currents were chosen for experiments to evaluate the pulse method. For the current pulse, the following parameters were tried: 150ms at 0mA and 50ms at 150mA. For the potential pulse, the following parameters were tried: 100ms at -2V and 230ms at -0.5V; 100ms at -1.6V, 100ms at 0.4V, and 200ms at -1.6V; 100ms at -3V, 10ms at -2V, 100ms at 0.4V, and 200ms at -3V; or 100ms at -2V, 100ms at -0.4V, and 200ms at -2V. Figure 3.11 shows the results obtained using an Au cathode with the following potential program: -1.6V vs. Hg/HgO for 100ms; 0.4V vs. Hg/HgO for 100ms; -1.6V vs. Hg/HgO for 200ms. The anolyte and catholyte were 2M NaOH + 25% $NaBO_2$ in this experiment. Again, there was no evidence of $NaBH_4$ production.

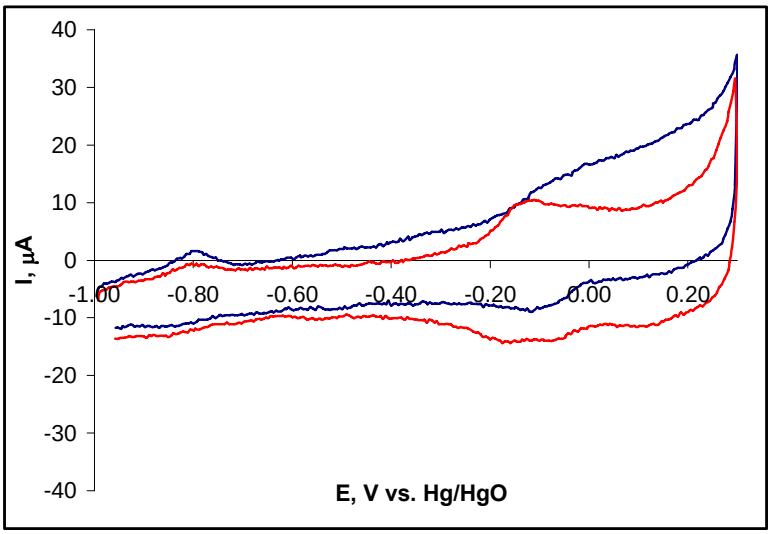

Figure 3.11: Au cathode square wave electrolysis experiment. Blue curve: CV of 2M NaOH + 25% w/v $NaBO_2$ catholyte before electrolysis. Red curve: CV of 2M NaOH + 25% w/v $NaBO_2$ catholyte after three days of electrolysis. Electrolysis parameters: 100ms at –1.6V vs. Hg/HgO; 100ms at 0.4V vs. Hg/HgO; 200ms at –1.6V vs. Hg/HgO. CV conditions same as with Hg pool experiment (see Figure 3.7).

In addition to an expected large HER overpotential, Ti was chosen for its negative PZC as discussed above. As with the Au cathodes, a constant current of 10mA was used in some experiments whereas others used a current or potential pulse. Ti is known to form hydrides in the presence of hydrogen, although this fact was not appreciated at the time that Ti was chosen to be used as a cathode [21]. The titanium hydride is more resistive than the Ti metal [21], thus, in future experiments it was necessary to abrade the electrode with SiC paper prior to use to remove the hydride layer. None of the experiments with Ti cathodes yielded a positive result for BH_4^- in the catholyte.

Ag and Pb were two other cathode materials tested under similar conditions as Au and Ti. Figure 3.12 shows results obtained with a Pb cathode for electrolysis at 10mA in 2M NaOH + 25% w/v $NaBO_2$ catholyte (and anolyte); as before, no evidence of BH_4^- formation exists. In addition to the experiments at 10mA and the pulsed current/potential experiments, another series of experiments was attempted with Pb. Pb was chosen because of its large overpotential for the HER. Other workers have found that the rate of reduction for chromate anion depends upon the concentration of the tetraalkylammonium hydroxide and the size of the carbon chains on the N atom [22]. Large carbon chains and higher concentrations of tetraalkylammonium cations inhibit reduction of oxyanions by blocking the electrode. With this in mind, lower concentrations of tetraethylammonium hydroxide (TEAH) in 1M NaOH + 0.5M $B(OH)_3$ were tried as electrolytes. Three concentrations of TEAH were used: 0.001M, 0.01M, and 0.1M. These experiments used a beaker for a cell, with a 25mm x 25mm square Pb flag WE, a graphite rod CE inside a fine

porosity fritted-bottom glass tube (as cell divider) and 60mL of solution. At first, a current of 350mA was applied, but the solution became cloudy in a short period of time. Dissolution of the lead cathode was occurring; when this was noted, the polarity of the WE was checked and it was indeed found to be the cathode. After confirming this, the current was lowered to 50mA; the working electrode did not appear to be undergoing dissolution at this current. However, with time, the counter electrode became covered with a highly resistive film, causing the required voltage to maintain 50mA to exceed that available from the potentiostat. A very dark, "burnt"-looking layer was found on the bottoms of the graphite rod counter electrodes. After cleaning with SiC paper, the cell voltage dropped but overtime the counter electrodes became fouled again. Nickel and platinum were tried next, but these also became fouled with a resistive layer in time. With no evidence from these experiments that $NaBH_4$ could be produced, work was not continued with these systems. The observation of cathode dissolution at the higher current of 350mA was quite unexpected. As with the tetraalkylammonium amalgams, a search of the literature indicated that other workers have observed this phenomenon; however, the cause of this behavior is controversial. Salzberg, for example, proposed formation of volatile PbH_2 ("plumbane") which reacts with water after being released from the electrode, yielding colloidal Pb and H_2 gas [23].

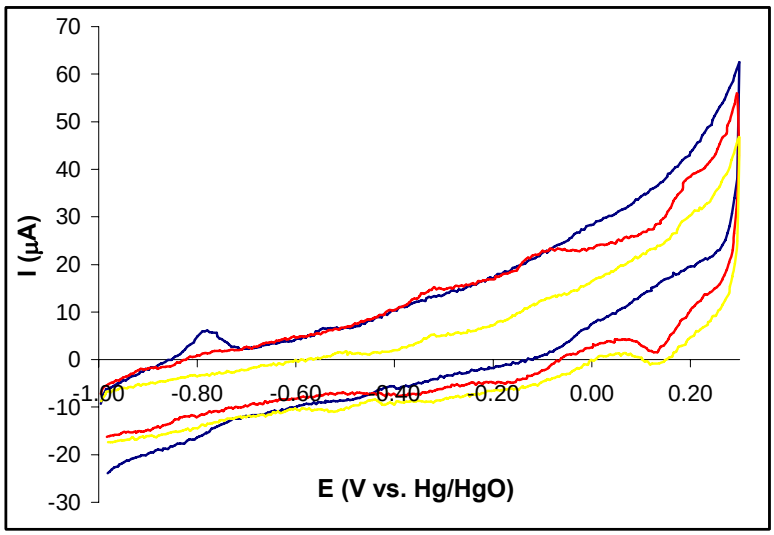

Figure 3.12: Pb cathode electrolysis experiment. Blue curve: CV of 2M NaOH + 25% w/v $NaBO_2$ catholyte before electrolysis. Red curve: CV of 2M NaOH + 25% $NaBO_2$ w/v catholyte after two days of electrolysis at 10mA. Yellow curve: CV of 2M NaOH + 25% w/v $NaBO_2$ after three more days of electrolysis at 10mA. CV conditions same as with Hg pool experiment (see Figure 3.7).

It was later found in the literature that the accelerating effect of cations is dependent upon the nature of the reaction [24]. When the reaction rate is controlled by electron transfer, the electrostatic effect of changing the potential profile to positive near the outer Helmholtz plane is

dominant. On the other hand, when the rate of reduction is controlled by electron transfer and proton transfer, the effect is more complex. In this case, water of hydration on the cation can function as a proton source. Tetraalkylammonium cations, being large and weakly hydrated, do not function as good modifiers of the electrical double layer in this case. Rather, small, highly charged cations that have strong hydration have been shown to be more effective at accelerating reduction [24]. Furthermore, another later discovery from the literature is that in aqueous solution, TAA+ ions are specifically-adsorbing near the PZC desorb at more negative potentials. Water replaces the TAA+ at these more negative potentials to act as an electron acceptor – i.e. to allow the HER to occur [25]. This could explain why TAAHs were not effective in these experiments.

Cu was tried as a cathode material following the report of Jianqiang et al [8]. These experiments were not exact reproductions of those of Jianqiang and co-workers, as they did not report the electrolysis conditions (current, current density, cell potential, working electrode potential, electrode area, etc.) were not disclosed. As with the other solid metal electrodes, an ordinary divided H-cell was used with a 25 x 25mm square flag of Cu metal as the cathode and a 25mm x 25mm square flag of Pt as the anode. Notably, Jianqiang et al. reported the use of a lead anode, rather than a Pt anode. Pt was chosen for this experiment based upon the reasoning that in a divided cell, the anode reaction should not affect the cathode reaction; thus the choice of anode would not be of great importance in such an experiment. The result shown here in Figure 3.13 was obtained with 1M NaOH + 0.2M $NaBO_2$ catholyte, 1M H_2SO_4 anolyte, and a current of 62.5mA. No peaks attributable to BH_4^- are seen after electrolysis, in Figure 20. Due to the use of 1M H_2SO_4 anolyte, it was suspected that transfer of "protons" through the membrane would decrease the alkalinity of the catholyte during electrolysis. A titration of un-electrolyzed catholyte gave $[OH^-] = 1.04M$; after electrolysis a titration yielded $[OH^-] = 0.88M$. This decrease in hydroxide concentration is undesirable as it could lead to an increased rate of BH_4^- hydrolysis.

A final approach to overcoming electrostatic repulsion consisted of preparing modified cathodes [26]. Two principle approaches were considered: anchoring a compound that could chelate the borate anion or coating the cathode with a cationic polyelectrolyte. The first approach was described in the invention disclosure. It is known in the field of ion exchange resins that borate anion can be chelated by compounds containing a diol functionality [12]. A first attempt at producing such an electrode was to use an ion-exchange resin, but unfortunately it was not appreciated that these resins are cross-linked. It thus proved to be impossible to dissolve the resin in any solvent to apply to the cathode substrate. We next decided to consider binding molecules such as N-metyl D-glucamine to the cathode substrate by covalent attachment (e.g. silane treatments) or by self-assembled monolayers (SAMs). Compounds containing thiol groups (-SH) are well known to form SAMs on Au surfaces. The molecule 1-thioglycerol contains the required diol functionalities for chelating boron and the thiol functionality to form an SAM on Au, thus this was tried. An Au electrode was treated with 1-thioglycerol (neat) by dipping for five minutes. After submersion for the defined time, the electrode was rinsed well with de-ionized water to remove free 1-thioglycerol and then used as a cathode in galvanostatic electrolysis at 10mA. During electrolysis, the cathode became progressively darker, starting at a blood red color

and finally turning black. This layer was very strongly adhered to the gold; even treatment with piranha solution (1:1 v/v 30% H_2O_2 and concentrated H_2SO_4) failed to remove this layer and mechanical polishing had to be used to remove the layer. Apparently this layer formed by reduction of the thiol.

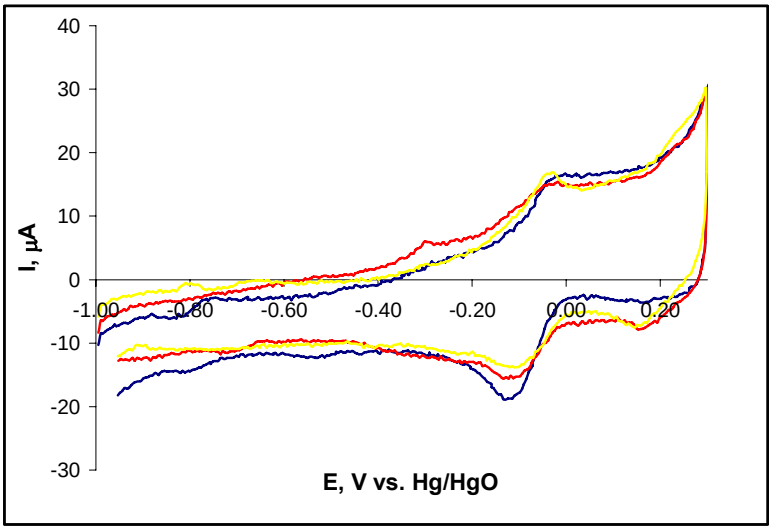

Figure 3.13: Cu cathode electrolysis experiment. Blue curve: CV of 1M TEAH + 0.2M $NaBO_2$ before electrolysis. Red curve: CV of 1M NaOH + 0.2M $NaBO_2$ catholyte after 2 days of electrolysis at 62.5mA. Green curve: CV of 1M NaOH + 0.2M $NaBO_2$ catholyte after 3 more days of electrolysis at 62.5mA. CV conditions same as with Hg pool experiment (see Figure 3.7).

The second approach was the use of a cationic polyelectrolyte. Cationic polyelectrolytes are polymer chains bearing positive charges on some regular unit of the polymer chain. Quaternized poly(4-vinylpyridine) was chosen as the cationic polyelectrolyte. Quaternization was necessary to introduce fixed positive charges on the polymer chain; otherwise at the high pH employed in the electro-reduction experiments the polymer would be neutral. The quaternization procedure was adapted from the literature [27]. The resulting polymer was dissolved in methanol and applied to carbon felt and nickel mesh squares 25 x 25mm to form the cathodes. In early experiments, softening of the coating was observed. To prevent this, cross-linking was tried. Since the cross-linked polymer would no longer dissolve, the polymer had to be applied to the cathode substrate first. Two approaches were taken in cross-linking: the quaternized polymer was applied and then cross-linked, or the unquaternized polymer was applied and crosslinked/quaternized in one step. The procedure for cross-linking was also adapted from the literature [28]. The polymer was applied to the cathode substrate from methanol solution. 1,4-diiodobutane was placed in a long glass tube 3cm in diameter sealed only at the bottom. The electrode was held in this tube while heating to ~80°C for 6 hours. Attenuated Total Reflectance Fourier Transform Infrared Spectroscopy (ATR-FTIR) was used to estimate the extent of reaction

for the quaternization and for the quaternization/crosslinking. This method was described by Sakai et al. [28]: the intensity of the IR bands at 1600cm^{-1} (unquaternized) and at 1640cm^{-1} (quaternized) were compared. For polymer quaternized with 1-iodopropane, two different reaction times were used: about 3.5 hours and about 6 hours; the ratio A(1640cm^{-1})/A(1600cm^{-1}) was higher after 6 hours of reaction [1.82 vs. 0.80 after 3.5 hours]. The polymer quaternized and then crosslinked was also examined by ATR-FTIR to see what effect the crosslinking had on the ratio. The ratio was somewhat lower after 6 hours [3.20] compared to 3 hours [3.6]. It should be mentioned that the effect of differing molar absorptivity for the two bands was not investigated. Since the phenomenon of IR absorption by chemical bonds depends upon the strength of the dipole moment, and the quaternized polymer has a larger dipole moment due to the formal positive charge on the nitrogen atom, the peak at 1640cm^{-1} might be stronger for this factor alone. Nonetheless, the IR analysis shows a correlation between reaction time and amount of quaternized polymer. The polymer that was quaternized and crosslinked in one operation with the 1,4-diiodobutane was not analyzed by ATR-FTIR.

Higher currents were employed in the experiments with these polymer-modified cathodes: 50mA, 62.5mA, and 100mA. The catholyte was 2M NaOH + 25% $NaBO_2$ and the anolyte was 1M H_2SO_4. Two experiments were performed with the polymer on carbon felt and the remainder used the polymer on nickel mesh. Positive control methodology was used in some of these experiments. Formation of sodium borohydride could not be detected, and the positive control experiments showed a loss of sodium borohydride.

After many electrolysis experiments failed to yield detectable quantities of $NaBH_4$, the issue of stability was examined again. In the new series of experiments, CV was used to track concentration with time but with cathode materials present. This was performed to determine if the presence of cathode material was influencing the stability of $NaBH_4$. Two basic types of experiments were performed: cathode materials in $NaBH_4$ solutions at open circuit (no applied current), and electrolysis with $NaBH_4$ added to the catholyte at the beginning of the experiment (positive control method).

Au, Ag, and Cu electrodes were used in open circuit tests. The electrodes were 25 x 25mm flags. The electrolyte was 3mM $NaBH_4$ in 2M NaOH + 25% $NaBO_2$. In all cases, there was a decrease in peak current with time at open circuit, with the gold and silver behaving similarly but with the copper showing a more rapid decrease in peak current with time – see Figure 3.14 and Figure 3.15.

The copper electrode was also used for electrolysis at 10mA. The catholyte was 3mM $NaBH_4$ in 2M NaOH + 25% $NaBO_2$ and the anolyte in this experiment was 1M H_2SO_4. As mentioned above for the electrolysis experiment of 0.2M $NaBO_2$ in 1M NaOH, consideration was given to decreased alkalinity of the catholyte due to crossover of "protons" from the 1M H_2SO_4 anolyte. In that experiment, a comparison of titration results for un-electrolyzed and electrolyzed catholyte showed that [OH^-] had decreased after electrolysis.

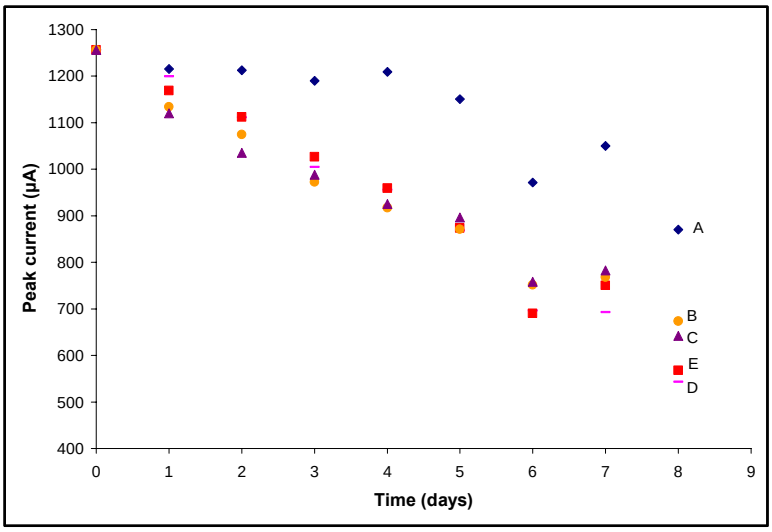

Figure 3.14: Peak current (from CV measurement) vs. time for 3mM $NaBH_4$/2M NaOH in contact with various metal electrodes. Series: A: 3mM standard, no metal; B: Ag, sample a; C: Ag, sample b; D: Au, sample a; E: Au, sample b.

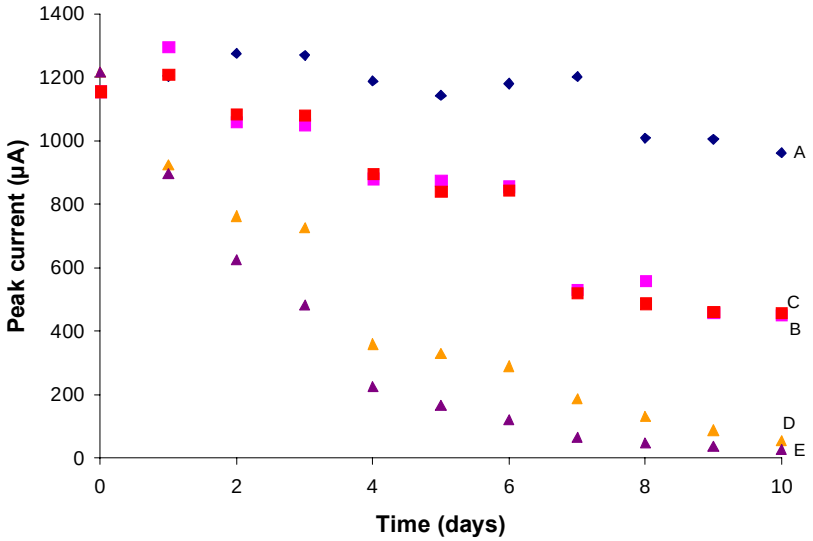

Figure 3.15: Peak current (from CV measurement) vs. time for 3mM $NaBH_4$/2M NaOH in contact with copper electrodes. Series: A: 3mM standard, no metal; B: Cu, sample a; C: Cu, sample b; D: Cu, electrolysis at 10mA a; E: Cu, electrolysis at 10mA b.

Hg pool electrodes were also used at open circuit and at cathodic polarization. In these experiments, the electrolyte was 2M TEAH (tetraethylammonium hydroxide) + 0.2M $B(OH)_3$. As with the copper experiments, the anolyte was 1M H_2SO_4. At open circuit, there was some tendency for the peak current to decrease with time, although the trend did not appear to be as pronounced as that observed with Cu or even Au and Ag. However, during electrolysis at 10mA ($j = 7.52mA/cm^2$), there was a definite trend in decreasing peak current with time – see Figure 3.16. This behavior parallels that observed with Cu; both experiments used 1M H_2SO_4 anolyte. This could suggest that the lowering of the catholyte pH is playing a role in the instability of $NaBH_4$ in these electrolyses.

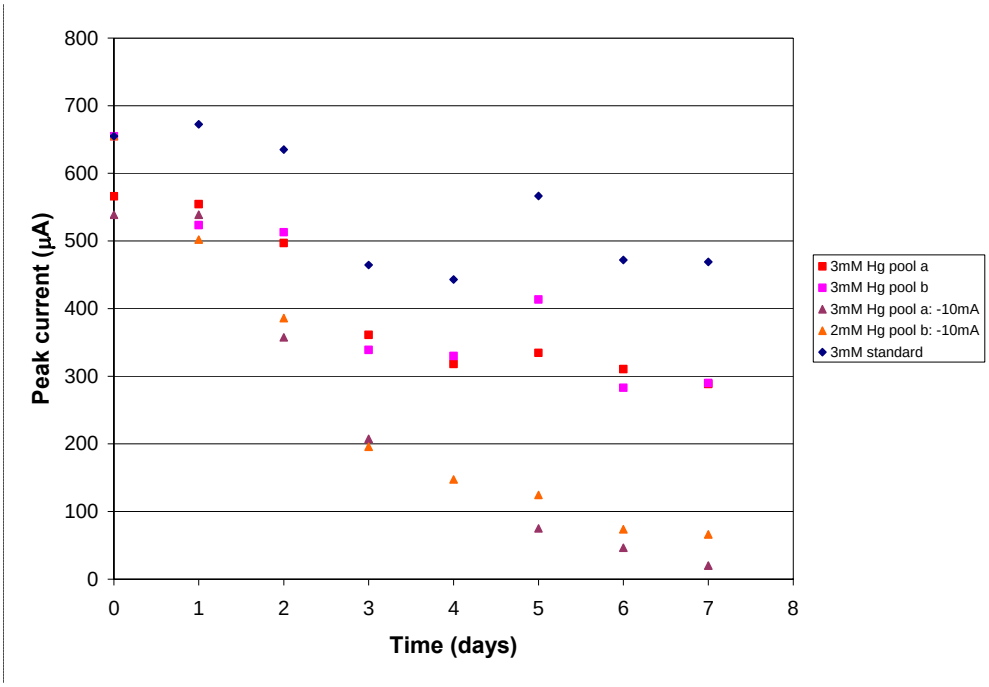

Figure 3.16: Peak current (from CV measurements) vs. time for 3mM $NaBH_4$ in 2M TEAH/0.2M $B(OH)_3$ in contact with Hg electrodes.

Why the peak current decreases with time in the open circuit potential measurements is not clear. Among the metals used, Au has been studied the most because of its potential use as an anode material in borohydride fuel cells. In none of these studies are there indications that Au is catalytic for borohydride hydrolysis.

This conclusion is reached primarily through the determination of n, the number of electrons measured during oxidation. In these studies, n was found to be near eight for BH_4^- oxidation on gold [29,30,31,32]. The other metals - Cu, Ag, and Hg - are much less studied for

$NaBH_4$ oxidation or hydrolysis. At least in the case of Au, it appears that oxidation of $NaBH_4$ is catalyzed by the presence of the metal. As a consequence of charge conservation, a reduction reaction has to be occurring at the same electrode, since at open circuit no charge can travel through an external circuit. This behavior is well known in corrosion and is called "mixed potential theory." The open circuit potential of an electrode exhibiting a mixed potential is somewhere between the equilibrium reduction potential of the anodic and the cathodic reactions depending upon the charge transfer kinetics. It has been suggested that this same effect is responsible for the inability to experimentally observe the standard potential for $NaBH_4$ in water [14]. The open circuit potential measured on gold was close to -400mV (at least near the beginning of the experiments), so this rules out the HER as the cathodic reaction. Since no effort was made to remove oxygen from these solutions, oxygen reduction is a likely candidate for the reduction reaction. The CRC Handbook gives the standard potential for two-electron reduction of oxygen in basic solution as –0.076V vs. SHE and the standard potential for four-electron reduction of oxygen under the same conditions as –0.146V [33].

3.6 Conclusions

In conclusion, none of the aqueous electrochemical reduction experiments gave convincing evidence of BH_4^- formation. In addition to the typical indirect and direct electrochemical reductions (mostly discussed in patents), attempts were made to overcome electrostatic repulsion of BO_2^- ion from the cathode. Among these were application of a current or potential pulse to the cell, the use of modified cathodes, and the used of specifically-adsorbable cations to modify the potential profile at the cathode/solution interface. As discussed earlier, the pulse method was far from optimized with regard to the amplitude of the current or potential and the on/off times. For the modified cathodes, only two modifications were tried: quaternized or quaternized and cross-linked poly (4-vinylpyridine) coating or creation of a self-assembled monolayer of 1 – thioglycerol on a gold substrate. More work could be done with modified cathodes, particularly the choice of the modifying substance. Finally, with regard to modification of the interface by specific adsorption, it seems that TAAH compounds are not optimal for the following reasons. First, at very negative cathode potentials, TAA+ cations may desorb. Admittedly, no attempts were made in this work to determine that adsorption of TAA+ ions was indeed occurring, and if so, the potential range in which adsorption occurs. This determination would require a surface-selective in situ technique. Perhaps Second Harmonic Generation (SHG) spectroscopy or an infrared spectroscopic technique such as Infrared Reflection Absorption Spectroscopy (IRRAS) could be used to assess this [21]. SHG spectroscopy relies upon the breaking of symmetry at an interface (in this case, the electrode/solution interface), which leads to the non-linear optical effect of frequency doubling (second harmonic generation), making this method inherently surface-selective. A drawback of the method is that the identity of the adsorbing species is not generally obtainable; however, coupling with another method (e.g. cyclic voltammetry) can mitigate this problem. IRRAS involves the modulation of IR radiation between p (polarized parallel to the plane of incidence) and s (polarized perpendicularly to the plane of

incidence) polarized radiation. The p-polarized radiation is surface selective, while the s-polarized radiation is absorbed by the surface and solution. The difference, then, gives a signal representing species adsorbed at the electrode surface. Second, since TAA+ cations are weakly hydrated, there may not be a suitable source of hydrogen in the interface region for BO_2^- reduction to BH_4^-, as this reaction requires the transfer of electrons and protons to occur. Third, TAA+ with A = ethyl or higher can undergo the Hofmann elimination [34]. Essentially, this means that base (in this case, OH^-) reacts with TAA+ to form an amine and an alkene. Since the HER is evidently occurring at the cathode and generating OH^- , this reaction could be promoted. Fourth, with Hg cathodes, replacing alkali metal cations by TAA+ cations still cannot prevent amalgam formation. However, other modifiers of the interfacial region may prove useful. For example, the work of Ferapontova suggests small, highly charged cations like La^{3+} could be useful for reductions involving electron and proton transfer [24]. However, before continuing work, it should be borne in mind that if the reduction experiments disclosed here produced any BH_4^-, the current efficiency was well below 1%. Thus, a spectacular improvement would have to be realized even before an aqueous, electrochemically- based process could be optimized and accepted.

3.7 References

1. J. O'M. Bockris, A.K.N. Reddy, and M. Gamboa-Aldeco. Modern Electrochemistry 2A: Fundamentals of Electrodics. 2nd ed. Kluwer Academic, NY, 2000.
2. H. Eyring, S. Glasstone, and K.J. Laidler. *Journal of Chemical Physics*, 7 (1939) 1053.
3. T.S. Lee. *Journal of the Electrochemical Society*, 118 (1971) 1278.
4. E. L. Gyenge and C.W. Oloman. *Journal of Applied Electrochemistry*, 28 (1998) 1147.
5. H. Lund. Use of the Solvated Electron. In: Organic Electrochemistry: An Introduction and a Guide. 2nd ed. M. Baizer and H. Lund, ed. Marcel Dekker, NY, 1983.
6. S. Amendola. US Patent 6,497,973 B1. Issued December 24, 2002.
7. M. Kawai and M. Ito. Japanese Patent 2003 – 247088. Issued September 5, 2003. Translated version courtesy of Rohm and Haas.
8. W. Jianqiang, S. Yanping, and L. Zhenhai. *Journal of Taiyuan University of Technology*. 37 (2006) 539. Translated version courtesy of Rohm and Haas.
9. S. Trasatti. Potentials of Zero Charge. What They Suggest About the Structure of the Interfacial Region. In: Trends in Interfacial Electrochemistry. A.F. Silva, ed. D. Reidel Publishing, 1986.
10. R.J. Duva. Pulse Plating. In: Electroplating Engineering Handbook, 4th ed. Van Nostrand Reinhold. 1984.
11. F. C. Anson. *Accounts of Chemical Research*. 8 (1975) 400.
12. C. Shao et al. *Macromolecules* 33 (2000) 19.
13. Davis, R.E., and C.G. Swain. *Journal of the American Chemical Society* 82 (1960) 5949.
14. C.P. de Leon et al. *Journal of Power Sources* 155 (2006) 172.
15. A. Frumkin, V. Korshunov, and I. Bagozkaya. *Electrochimica Acta*, 15 (1970) 289.

16. H. Kita, S. Ishikura, and A. Katayama. *Electrochimica Acta*, 20 (1975) 441.
17. J. Jörissen. Practical Aspects of Preparative Scale Electrolysis. In: Encyclopedia of Electrochemistry, Vol. 8. A.J. Bard and M. Stratmann, ed. Wiley-VCH, 2004, Weinheim.
18. X. Gie and T. Okada. *Electrochimica Acta*, 41 1996 1569.
19. B.C. Southworth, R. Osteryoung, K.D. Fleischer, F.C. Nachod. *Analytical Chemistry*, 33 (1961) 208.
20. H.N. McCoy and F. L. West *Journal of Physical Chemistry*, 16 (1912) 261
21. K. Azumi, Y. Asada, T. Ueno, M. Seo, and T. Mizuno. *Journal of the Electrochemical Society*, 149 (2002) B422.
22. A .J. Bard and L. R. Faulkner. Electrochemical Methods: Fundamentals and Applications. 2nd ed. John Wiley and Sons, 2004.
23. H. W. Salzberg. *Journal of the Electrochemical Society*, 100 (1953) 146.
24. E.E. Ferapontova and N.V.Fedorovich, *Journal of Electroanalytical Chemistry* 476 (1999) 26.
25. K. Izutsu. Electrochemistry in Nonaqueous Solutions. Wiley-VCH, 2002, Weinheim.
26. J.B. McLafferty and D.D. Macdonald "Novel Modified Electrodes for the Electrochemical Reduction of Boron-Oxygen Entities to Boron-Hydrogen Species." Invention Disclosure, Pennsylvania State University, April 20, 2006
27. N. Oyama et al. *Journal of Electroanalytical Chemistry* 112 (1980) 271.
28. Y. Sakai et al. *Journal of the Electrochemical Society* 136 (1989) 171.
29. Gyenge, E. *Electrochimica Acta* 49 (2004) 965.
30. Wang, K. J. Lu, and L. Zhuang. *Journal of Electroanalytical Chemistry* 585 (2005) 191.
31. Mirkin, M., H. Yang, and A.J. Bard. *Journal of the Electrochemical Society* 139 (1992) 2212.
32. Wang, K. J. Lu, and L. Zhuang. *Journal of Electroanalytical Chemistry* 585 (2005) 191.
33. Weast, R.C, ed. CRC Handbook of Chemistry and Physics, 59th ed. CRC Press, 1978.
34. J. McMurray. Organic Chemistry, 5th ed. Brooks/Cole, Pacific Grove, CA, 2000.

4. Electrochemistry of Tributyltin Chloride: Attempts at Tributyltin Hydride Regeneration from Tributyltin Chloride Using Silver Electrodes

4.1 Literature Review for Organotin Hydride Regeneration

Several chemical routes to organotin hydrides are available: reduction of organotin halides with metal hydrides; decarboxylation of organotin formates; and hydrolysis of stannylmetallic compounds. The brief discussion of each of these follows from the comprehensive text of Davies on organotin chemistry [1].

Organotin halides are reducible by various metal hydrides in ethereal solvents. Lithium aluminum hydride reacts with organotin halides in ethers such as dioxane at room temperature to afford the organotin hydrides, which are distilled from the reaction mixture:

$$Me_2SnCl_2 + LiAlH_4 \xrightarrow{dioxane} Me_2SnH_2 \tag{4.1}$$

In glymes, sodium borohydride can reduce organotin chlorides to the corresponding hydrides. With crown ethers as a phase-transfer catalyst, the same reactions can be accomplished in toluene.

Decarboxylation of tripropyltin formate and tributyltin formate at 170°C under reduced pressure drives off carbon dioxide, forming the corresponding hydrides:

$$Bu_3SnOCOH \xrightarrow{170^oC,1mm\ Hg,9h} Bu_3SnH + CO_2 \tag{4.2}$$

Reduced pressure is required since the reaction is reversible; again, distillation is used to isolate the hydride product.

Hydrolysis of stannylmetallic compounds in the presence of ammonium chloride is the third classic route to organotin hydrides. In this method, a ditin species such as hexaphenylditin is reacted with a metal in the THF solution:

$$Ph_3SnSnPh_3 \xrightarrow{Mg,THF} (Ph_3Sn)_2Mg \tag{4.3}$$

The stannylmetallic compound ($(Ph_3Sn)_2Mg$) is then reacted with water in the presence of ammonium chloride (the hydrolysis step) to afford to equivalents of the corresponding hydride:

$$(Ph_3Sn)_2Mg \xrightarrow{H_2O,NH_4Cl} 2Ph_3SnH \tag{4.4}$$

None of the above methods is really satisfactory for large-scale regeneration of organotin hydrides required for production of aminoborane. The requirement of metal hydrides for reduction of organotin halides is a major problem, since the production of these hydrides involves

highly irreversible processes. The decarboxylation of organotin formates was found to be an energy-intensive process [2]. Hydrolysis of a stannylmetallic compound would involve another step in addition to the two shown above: conversion of the by-product of aminoborane regeneration (e.g. tributyltin chloride) into hexabutylditin. A possible alternative to these chemical methods is electrochemical reduction of the halides.

The electrochemistry of organotin halides (in particular, triphenyltin chloride, Ph_3SnCl) has been investigated by polarography, cyclic voltammetry, and coulometry (citations below). There is agreement that Ph_3SnCl undergoes a one-electron reduction yielding a triphenyltin radical and chloride ion:

$$Ph_3SnCl + e^- \rightarrow Ph_3Sn^* + Cl^- \tag{4.5}$$

Following the production of the triphenyltin radical, another one-electron reduction may occur at a more negative potential:

$$Ph_3Sn^* + e^- \rightarrow Ph_3Sn^- \tag{4.6}$$

In addition to the two reactions above, the triphenyltin radicals may combine yielding hexaphenylditin:

$$Ph_3Sn^* + Ph_3Sn^* \rightarrow Ph_3SnSnPh_3 \tag{4.7}$$

Finally, hexaphenylditin may undergo a one electron reduction to triphenyltin anion:

$$\tfrac{1}{2}\, Ph_3SnSnPh_3 + e^- \rightarrow Ph_3Sn^- \tag{4.8}$$

The species $Ph_3SnSnPh_3$ is hexaphenylditin (Ph = benzene substituent).

There is disagreement among researchers on the last reaction, reduction of hexaphenylditin to triphenyltin anion. Dessy and co-workers studied the reaction in glyme (1,2-dimethoxyethane) with tetrabutylammonium perchlorate as supporting electrolyte, using polarography [3]. A wave appearing at -2.9V (vs. Ag/Ag+) is identical with that of hexaphenylditin. It should be mentioned that when dry HCl was added during electrochemical reduction of the hexaphenylditin, triphenyltin hydride was detected. Overnight exposure to air caused reversion to hexaphenylditin.

However, in the work of Booth and Fleet [4], hexaphenylditin was not found to be electrochemically-active. These workers used 50% v/v ethanol in water with acetic acid-ammonia buffer (pH maintained at 7.3 in most experiments). These authors did not comment on what influence the solvent may have, since they used a protic solvent in contrast to the aprotic solvent employed by Dessy et al. However, Booth and Fleet did comment on the role of the supporting electrolyte cation; Li^+, Ba^{2+}, and La^{3+} (as chloride salts) did not have any influence

upon the polarography of triphenyltin chloride. However, tetrabutylammonium chloride (Bu_4NCl) did have an influence – the wave appearing at the most negative potential disappeared upon addition of this salt at 0.1M concentration. This wave was attributed to reduction to triphenyltin anion. Since Bu_4N^+ cation specifically adsorbs, competition between adsorption of this cation and the triphenyltin radical (an intermediate in formation of triphenyltin anion) is thought to be the reason for the disappearance of the third wave.

Mazzocchin and co-workers [5] studied triphenyltin chloride electrochemistry in acetonitrile with tetrabutylammonium perchlorate as supporting electrolyte. This solvent/supporting electrolyte system is more similar to that employed by Dessy et al. These workers concluded that hexaphenylditin is electrochemically active, in agreement with the findings of Dessy et al. Additionally, these workers found that the triphenyltin anion can react with triphenyltin chloride to yield hexaphenylditin:

$$Ph_3Sn^- + Ph_3SnCl \rightarrow Ph_3SnSnPh_3 + Cl^- \qquad (4.9)$$

Coulometry in the presence of phenol, performed at a potential corresponding to the reduction of hexaphenylditin, gave triphenyltin hydride. The identity of this species was confirmed by cyclic voltammetry, using a known sample of triphenyltin hydride. The phenol acted as a source of hydrogen, protonating the triphenyltin anion. Mazzocchin suggested that electrochemical activity of hexaphenylditin was not observed in the work of Booth and Fleet because a potential sufficiently negative to reduce hexaphenylditin could not be reached in the ethanol/water solution.

Savall et al. used polarography and small-scale electrolysis to study triphenyltin chloride and tributyltin chloride in methanol with lithium chloride or lithium perchlorate as supporting electrolyte [6]. For triphenyltin chloride, electrolysis at -1.8V and -2.2V (vs. Ag/Ag+) afforded hexaphenylditin. For tributyltin chloride, electrolysis at -1.7V gave hexabutyldistannane. However, electrolysis at -2.2V gave by-products, proposed to be the polymeric $(Bu_2Sn)_x$ as well as Bu_4Sn.

Taken together, it would seem that these results suggest that hexaphenylditin is not electrochemically active in protic media with simple supporting electrolytes (lithium salts or pH buffers). In contrast, aprotic media with tetrabutylammonium supporting electrolytes seem to promote electrochemical activity of hexaphenylditin. The reason for this behavior is most likely that suggested by Mazzocchin, since the cathodic limit obtained in aprotic solvents is significantly more negative than that attainable in protic solvents. Since the dimerization of triphenyltin radicals is a rapid, irreversible process, any conditions where this species is not electrochemically-active must be avoided for successful production of triphenyltin hydride.

Tanaka and co-workers examined the electrochemical activity of triphenyltin chloride at a gold disk working electrode by cyclic voltammetry [7]. THF was used as the solvent with tetrabutylammonium tetrafluoroborate as the supporting electrolyte. A cathodic peak at -2.48V vs. SCE was described as a two-electron reduction of the triphenyltin chloride:

$$Ph_3SnCl + 2e^- \rightarrow Ph_3Sn^- + Cl^- \quad (4.10)$$

Similarly to Mazzocchin et al, Tanaka and co-workers found that the triphenyltin anion reacts with triphenyltin chloride to give hexaphenylditin. Tanaka found that the oxidation of the thus formed triphenyltin anion was not seen at low sweep rates (200mV/s) but was evident at higher sweep rates (2V/s). This is evidence of a fast follow-up chemical step, this step being the reaction between triphenyltin anion and triphenyltin chloride. The hexaphenylditin was found to be electrochemically active at nearly the same potential as the triphenyltin chloride, the potential of the hexaphenylditin reduction being -2.47V. Constant current electrolysis was performed at a lead cathode in N, N-dimethylformamide (DMF) with tetraethylammonium tosylate supporting electrolyte, until 1.5F/mol of charge passed. Extraction of the catholyte to organic solvent (1:1 hexane:dichloromethane) followed by recrystallization from hexane afforded 43% yield of hexaphenylditin.

Contrarily to Mazzocchin's results, Tanaka's group did not find a reduction peak attributable to the one electron reduction of triphenyltin chloride to triphenyltin radical. However, the difference in working electrodes must be considered; Mazzocchin used a gold microsphere coated with Hg (essentially a mercury WE) whereas Tanaka used a gold disk WE. An electro-catalytic effect could explain the difference in the electrochemistry found by these two groups, using two different working electrode materials.

Tanaka's group did not study the influence of added hydrogen sources upon the electrochemical reduction of triphenyltin chloride.

Triphenyltin compounds appear to be the most investigated in electrochemistry experiments among the organotin compounds. However, as indicated above, tributyltin chloride was studied by Savall et al. Fleet and Fouzder studied bis (tributyltin oxide) (TBTO) and found reactions analogous to those described above [8]. Additional side reactions were found with this material, however, many yielding hexabutylditin. Thus it would appear that a range of organotin compounds could be used as starting reagents. Again, conditions promoting the electrochemical-activity of the hexa-akylditin compounds are necessary for high yields of the hydride.

Silver was chosen as the working electrode material for these experiments for two reasons. First, to the present author's knowledge, the electrochemistry of tributyltin chloride has not been investigated at a silver working electrode. Second, silver has been shown to act as an electrocatalyst in the reduction of *alkyl* halides [see, for example, 9]. It was then of interest to see if silver exhibits the same electrocatalytic activity for *trialkyltin* halides.

The objective of the new work, in relation to AB regeneration, is to confirm that organotin hydrides can indeed be generated as suggested in the above literature. Although voltammetric evidence is given for generation of the hydrides, no attempt at producing the hydrides on any sort of preparative scale by these methods is evident. Thus, small-scale electrolyses experiments are planned to determine the feasibility of this method. The literature indicates that a source of hydrogen is needed to form the hydride; in the work of Dessy et al., HCl

was used; Mazzocchin and co-workers used phenol; and Fleet et al. used the protic medium ethanol/water. Each of these has drawbacks for electrolytic production of the hydride. HCl is a toxic and corrosive gas, making handling difficult. Phenol is also toxic and corrosive. Furthermore, phenol may be oxidized at the anode of the electrolysis cell, yielding "tar" like by-products. Protic solvents such as ethanol/water seem to inhibit the electrochemical activity of the hexa-alkylditin species. Therefore, it is suggested to use hydrogen gas as the hydrogen source. Hydrogen gas can be oxidized at platinized-platinum in organic media to yield protons [10]. An additional benefit of using hydrogen is that it can act as an anodic depolarizer. An anodic depolarizer is sacrificially oxidized at the anode, thus avoiding oxidation of the solvent, supporting electrolyte, reagents, or products. Thus, formation of by-products such as "tars" can be avoided. Savéant and co-workers reported the use of such a hydrogen anode for electrochemical hydrogenations in organic media [11,12]. If the reduction product is not more easily oxidized than hydrogen gas, and if the reactant is not hydrogenated at the anode surface, the use of a divided cell can be avoided. This offers a tremendous advantage in cell construction, since an appropriate membrane does not have to be found and the cell design is much simpler. Also, the power requirements of an undivided cell are typically substantially less than for a divided cell, since the ohmic losses are reduced in the absence of a membrane. Savéant and co-workers reported successful pinacol coupling of acetophenone yielding a few percent of an alcohol (1-phenylethanol), which was said to be produced by hydrogenation of acetophenone (the reactant) at the anode of the cell. The hydrocyclization of 1,3-dibenzoylpropane to a cyclic pinacol was also examined and found to give a yield of near 80% for the desired pinacol product. These electrolyses were performed in acetonitrile with tetraethylammonium perchlorate supporting electrolyte. An important observation in these electrolyses was that the solution did not change color, which typically occurs in organic media when some component (e.g. solvent, supporting electrolyte) is electrochemically destroyed. This observation indicates that hydrogen is acting as an efficient anodic depolarizer, preventing oxidative destruction of the electrolyte solution. To the present author's knowledge, the use of such a hydrogen anode has not been reported for the reduction of organic or organometallic halides. Finally, observations from these experiments will be used to conjecture whether silver is acting as a catalyst in the electrochemical reduction of tributyltin chloride.

Characterization of the products is expected to entail the same methods suggested in the literature: comparison of CVs with those of known samples, NMR spectroscopy (^{1}H and ^{119}Sn), and IR spectroscopy.

4.2 Analysis/Characterization

Fourier Transform Infrared Spectroscopy was tried to see if tributyltin chloride (reagent), hexabutylditin (intermediate or product), and tributyltin hydride (target product) could be identified. Since all three of these materials are liquids, Attenuated Total Reflectance (ATR) was used to acquire the spectra. In this method, the neat liquid is placed upon a crystal; in this case, zinc selenide was used. The beam of IR radiation enters the crystal, and when the angle of

incidence exceeds the critical angle of the crystal + sample, the beam is reflected internally to the IR detector. Where the wave reflects from the crystal, an evanescent wave is emitted normal to the crystal surface. This evanescent wave interacts with the sample and some of the IR energy is absorbed. Thus, the IR beam reaching the detector is not the same as that incident upon the crystal; the difference in energy is characteristic of the function groups present in the sample. It is critical that the conditions for attenuated total reflectance are satisfied; this is governed by the index of refraction of the crystal, the index of refraction of the sample, and the angle of incidence. The user of the system may select the sample material and the angle of incidence, thus allowing many materials having different indices of refraction to be examined. [13].

For acquiring the spectra, a Bruker IFS 66/S FT-IR with a mercury cadmium telluride detector was used, with assistance provided by Dr. Joshua Stapleton of Materials Research Institute. Opus 6.0 software was used to acquire data and to process spectra.
Figure 4.1 compares the spectra obtained for tributyltin chloride, hexabutylditin, and tributyltin hydride, each as neat liquids. Some negative absorbances are noted for tributyltin chloride. In each case, a "blank" spectrum of the crystal with ambient air as the sample was obtained. A spectrum of the sample on the crystal was then taken; the spectrum of the sample was calculated from these two measurements. Both water and carbon dioxide have IR-active modes, so the spectra for these compounds are superimposed on all spectra. Thus, if the quantity of water or carbon dioxide differs between when the blank spectrum was acquired and when the sample spectrum was acquired, calculation of the sample spectrum can show negative absorbances for water and/or carbon dioxide. Absorbance due to free water in the air occurs around 1470 – 1900 cm^{-1} and 3500 – 4000 cm^{-1} in these spectra; carbon dioxide absorbance occurs around 2270 – 2370 cm^{-1} in these spectra.

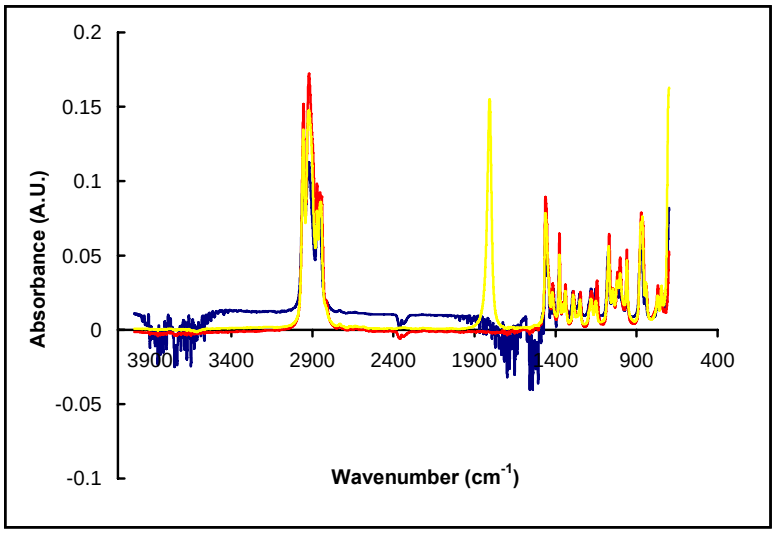

Figure 4.1: ATR FT-IR spectra for tributyltin chloride (blue), hexabutylditin (red), and tributyltin hydride (yellow), all as neat liquids, as received. Spectra acquired using a zinc selenide crystal and a 45° angle of incidence.

A very clear identifier of tributyltin hydride is evident in the absorbance near 1800 cm^{-1}. This absorbance is attributed to the vibration of the Sn-H bond [1]. No distinguishing absorbances are seen for tributyltin chloride or hexabutylditin. The vibration of the Sn-Cl bond is supposed to occur around 318 – 336 cm^{-1}, and the vibration of the Sn-Sn bond in hexabutylditin is supposed to occur much lower, below 200 cm^{-1} [1]. The reason for this is that the vibration frequency is dependent upon the mass of the atoms constituting the functionality of interest; higher mass results in a lower frequency. Thus, Sn-Cl and Sn-Sn bonds are not observable by IR spectroscopy, but may be observed by Raman spectroscopy [1].

Note that similar absorbances are seen for all three materials: the group of absorbances centered near 2900 cm^{-1} and the group of absorbances with wavenumbers less than 1400 cm^{-1}. The absorbances centered at 2900 cm^{-1} are due to alkyl groups, in this case, butyl groups, which are present on all three substances. The region below 1400 cm^{-1} is commonly called the "fingerprint" region, and these absorbances are not often used to determine what functionalities a molecule contains. Based on the similarities in the fingerprint region for all three substances seems to indicate that these absorbances too are arising from the butyl groups.

Farina suggested separation of organotin compounds by reversed-phase chromatography [14]. The mobile phase was a mixture of dichloromethane (CH_2Cl_2) and acetonitrile (CH_3CN). Hexabutylditin was one compound tested by Farina for separation by this chromatographic procedure, but the other two compounds of interest in this study, tributyltin chloride and tributyltin hydride, were not studied. The present author tried various proportions of dichloromethane and acetonitrile to see if hexabutylditin, tributyltin chloride, and tributyltin hydride (all applied neat, as received) could be resolved on C-18 reversed-phase Thin Layer Chromatography (TLC) plates (Whatman MKC18F Silica Gel 60A, 200□m thickness). Dichloromethane and acetonitrile mixtures did not work well. Various other solvents and mixtures were tried. A mixture of 75% acetonitrile, 25% toluene (v/v) could show differences between the three materials. However, the procedure is not optimized – the hexabutylditin showed streaking, and the tributyltin chloride and tributyltin hydride gave fainter spots with some distortion – the spots were more crescent-shaped than dot-shaped.

4.3 Development of a Reference Electrode for Organic Solvents

For aqueous electrochemical experiments, a number of stable and well-characterized reference electrodes are available commercially or may be easily prepared in the laboratory. These reference electrodes generally have a thermodynamically established potential referenced to the standard hydrogen electrode scale. Unfortunately, this is not the case for non-aqueous systems. Often, so-called pseudo-reference electrodes are employed. In some cases, these amount to a silver or platinum wire immersed directly into the test solution. In other cases, a redox pair is employed. Example redox pair electrodes include ferrocene/ferrocenium [15] and polypyrrole/polypyrrole cation [16]. Alternatively, one member of a redox couple, e.g. ferrocene, can be added to a solution and a characteristic voltammetry potential (e.g. peak potential) can be

used to standardize the potential of a pseudo-reference electrode in the test solution. Significant drawbacks attend these methods. First of all, interactions between the standard and the test solution have to be considered - the oxidation and reduction peaks of the standard can not overlap any of those due to the sample itself. Furthermore, as the composition of the solution varies, the potential of the pseudo-reference can vary. Thus, if the standard is added at the end of series of voltammetry experiments, no assurance is made that the potential measured against the standard is the same throughout all of the measurements. Finally, even if the redox couple is fabricated as an electrode, instability is a significant problem. Ferrocenium cation is quite unstable towards molecular oxygen, and therefore any electrode prepared using the ferrocene/ferrocenium couple will have to be prepared often. Even the polymeric polypyrrole/polypyrrole cation electrode of Ghilane et al. can have its potential upset by exposure to strongly oxidizing or reducing agents. Probably the most condemning aspect of these quasi-reference electrodes is their unsuitability for bulk electrolyses. This stems from their inherent instability as well as fluctuations in potential occurring as the solution composition changes over the course of the electrolysis.

Aqueous reference electrodes, in particular saturated calomel electrode (SCE), have been used by many workers. These electrodes have to be place in a salt bridge containing the electrolyte and solvent used in the experiment. Thus, liquid junction potentials result, which are not generally reproducible. Also, the potassium chloride electrolyte used in most of these electrodes is quite insoluble in organic solvents, even those having high dielectric constants (e.g. acetonitrile), meaning that precipitation of this salt in the junction(s) will lead to a very large increase in the impedance of the reference electrode circuit. Replacement of the electrode filling solution by an organic solvent is also unsatisfactory in many cases for SCE or Ag/AgCl. Dipolar aprotic solvents, like acetonitrile, promote disproportionation of calomel in the presence of chloride ion or dissolution of silver chloride in the presence of chloride ion, due to stabilization of complex anions containing these metals. Drift in the potential then occurs as these side reactions proceed.

The silver/silver(I) ion system has been used extensively, particularly for acetonitrile, in which it has been found to function reversibly. This electrode suffers from two significant drawbacks: the electrode must be prepared often due to instability associated with the silver(I) ion, and contamination of the working solution often results.

For the purpose of these experiments, then, it is clear that pseudo-reference system will be unsatisfactory. In searching for a suitable reference electrode, two factors were decided to be of paramount importance: stability and avoidance of contamination of the working solution. Two systems were found in the literature that were described as being stable. The first was the cadmium amalgam electrode in DMF [17], and the second was a modified silver/silver chloride electrode in acetonitrile [18]. The modified silver-silver chloride electrode was chosen for further investigation in this work.

As described above, for dipolar aprotic solvents, the ordinary silver/silver chloride reference electrode consisting of a silver chloride-coated silver wire in a solution of potassium chloride is unsuitable. Popov and Geske addressed the problem of the dissolution of silver

chloride in chloride containing aprotic solvents by using a filling solution consisting of acetonitrile/supporting electrolyte saturated with silver chloride and trimethylethylammonium chloride [18]. The addition of the silver chloride and trimethylethylammonium chloride established equilibrium in the filling solution for the reaction of silver chloride with free chloride ion:

$$AgCl + Cl^- \rightarrow AgCl_2^- \tag{4.11}$$

Two practical problems had to be addressed in preparing this electrode in our laboratory. The first was that trimethylethylammonium chloride is not commercially available. However, tetramethylammonium chloride is commercially available in high purity (electrochemical grade); this was substituted for the trimethylethylammonium chloride. The second problem was the selection of and preparation of a suitable junction. Aqueous reference electrodes often use porous glass (glass frits or unsintered Vycor ®) or porous ceramic frits as the junction. These materials were tried but the leak rate was unacceptably high. While leading to a low impedance junction, high leak rates are unsuitable due to contamination of the working solution and due to the need to continuously refill the reference electrode.

To address the junction problem, a zirconia frit was modified by coating it with a layer of cross-linked poly (4-vinylpyridine). Poly (4-vinylpyridine) undergoes a cross-linking reaction with α, ω-dihaloalkanes to produce a cationic polyelectrolyte, meaning the polymer chain contains fixed positive charges [19]. The cross-linked polymer then acts as an anion exchange polymer. The modified frit junction was prepared as follows. A 25% w/w solution of poly (4-vinylpyridine) (Sigma Aldrich, average molecular weight 60,000) in methanol was prepared. Two grams of this solution, containing 0.5 grams of poly (4-vinylpyridine) were stirred with 0.026g of 1,4-dichlorobutane for one hour in a closed glass vial. A 4mm diameter zirconia frit was attached to a 5mm outer diameter glass tube with PTFE heat shrink tubing. The mixture of poly (4-vinylpyridine), methanol, and 1,4-dichlorobutane was applied over the frit using a Pasteur pipet; the thickness of the layer was about 5 – 6mm. The tube was left open overnight on the bench top, to evaporate the methanol. The next day, the above assembly was heated at 110°C in an oven for 5 hours, 20 minutes. After cooling, acetonitrile was placed in the tube and the open end of the tube was closed with parafilm to check for leaks. After leaving overnight, no leaks were found, and the tube was emptied of the acetonitrile. The assembly was then filled with a solution of 0.1M $TBAPF_6$ in acetonitrile saturated with silver chloride and tetramethylammonium chloride. The silver chloride was prepared by metathesis between aqueous silver nitrate and potassium chloride, followed by drying the silver chloride precipitate in the oven. A 0.5mm diameter silver wire was soldered to a 0.5mm diameter nickel wire. The solder joint was enclosed in a PEEK tube just under 4mm in outer diameter. Devcon 5 minute epoxy was used to fill the PEEK tube to insulate the solder joint. After curing the epoxy, the silver wire was anodized in saturated aqueous potassium chloride to form a light khaki-colored layer of silver chloride. The silver chloride-covered silver wire assembly was inserted to complete the reference electrode assembly; the PEEK tube fit snugly and a layer of parafilm was applied over the top to prevent evaporation of the acetonitrile from the filling solution.

The stability of this electrode was assessed by using it as a reference electrode in obtaining the cyclic voltammogram of ferrocene. A solution of 10mM ferrocene (Alfa Aesar Avocado brand, 100%) in 10mL of 0.1M $TBAPF_6$/acetonitrile was prepared and de-aerated in the CV cell for 5 minutes with Ultra High Purity (UHP) Ar bubbled through a Pasteur pipet. A 1mm Pt disk, polished with 5□m Al_2O_3 paste on Leco Imperial cloth, followed by rinsing thoroughly with de-ionized water and drying, was used as the working electrode. A platinum wire was used as the counter electrode. A sweep rate of 250mV/s over a potential range of –1V to 1V vs. the Ag/AgCl reference electrode was employed. The peak potential for the oxidation of ferrocene under these conditions was chosen as the figure for assessing the stability. The same ferrocene solution was used on several days to check the repeatability of the peak anodic potential. It should be noted here that before settling on the polymer-modified zirconia frit described above for the junction, other junctions were tried. These were the cracked-glass junction described by Moe, the same cracked-glass junction with a plug of Pyrex wool over it as a diffusion barrier, and a zirconia frit with a plug of Pyrex wool as an additional diffusion layer. Each of these electrodes used filling solution from the same batch, prepared as described above. Excellent repeatability and reproducibility were obtained using this non-aqueous silver/silver chloride electrode with different junctions but the same filling solution over several days. The polymer-modified zirconia frit junction had the lowest leak rate combined with the most ruggedness of the junctions tried, so it was chosen for use in the organotin electrochemistry experiments.

4.4 Tributyltin Chloride Electrochemical Experiments

Tributyltin chloride was used as received from Sigma Aldrich for all experiments. The stated purity was 96% (technical grade); the method of analysis was not stated. Davies, in his comprehensive text on organotin chemistry, states that tributyltin chloride is prepared commercially by the Kocheshkov reaction (sometimes called Kocheshkov redistribution reaction):

$$3Bu_4Sn + SnCl_4 \rightarrow 4R_3SnCl \qquad (4.12)$$

As indicated, the required stoichiometry is 3:1 mole ratio tetrabutyltin (Bu_4Sn):tin (IV) chloride ($SnCl_4$). The Kocheshkov reaction can be used to produce other types of organotin halides if this mole ratio is changed. Luijten and van der Kerk gave a synthesis procedure using the Kocheshkov reaction; the product was removed from the reaction mixture by distillation under reduced pressure [20]. The yield was given (the present author was unable to calculate the same percentage based on their figures) and an analysis based upon the chlorine content was provided. The authors state that halogen directly attached to tin is ionized in aqueous solutions, allowing its determination by gravimetric analysis or potentiometric titration with silver nitrate. The amount of chlorine determined was in excess of the theoretical amount; this might suggest that a major impurity was the tin (IV) chloride. The present author tried a few experiments with Thin Layer Chromatography (TLC) on reversed-phase C-18 plates, following the suggestion of

Farina to see if a separation could be achieved, but these experiments failed to yield a visible separation [14]. Thus, all experiments used the as-received reagent.

Two solvents were chosen for electrochemical studies of tributyltin chloride: glyme (1,2-dimethoxyethane) and acetonitrile. Anhydrous solvents were used due to the importance of maximizing the cathodic potential limit. The glyme and acetonitrile were purchased from Sigma Aldrich in septum-sealed bottles packed under an inert gas atmosphere. Sigma Aldrich Chem-flex ® transfer lines, dedicated for each solvent, were used to transfer the solvents to the cyclic voltammetry cell under flow of UHP Ar. This standard method for handling of anhydrous or moisture-sensitive reagents is known as a cannula technique. Electrochemical-grade tetrabutylammonium hexafluorophosphate ($TBAPF_6$) or tetrabutylammonium perchlorate (TBAP), both from Sigma Aldrich, were used as received. A custom-made cyclic voltammetry cell, made from a 100mL roundbottom flask with four size 7 Chem-Thread joints (Chemglass P/N CG-350), was used for all CV experiments. Prior to each experiment, the working, counter, and reference electrodes were fitted through three of the Chem-Thread joints. The counter electrode consisted of a small loop of 0.5mm diameter Pt wire cemented in a 6mm outer diameter glass tube with MetLab epoxy. The working electrode was a 1mm diameter silver wire cemented in MetLab epoxy. Another working electrode was prepared by "sealing" a 1mm diameter silver wire in a 6mm outer diameter Pyrex glass tube. However, in some experiments, an unacceptably high background current was found in CV of 0.1M $TBAPF_6/CH_3CN$. This was traced to the working electrode. Undoubtedly, the glass-to-metal seal was imperfect, with a crevice that trapped water during the polishing procedure. Thus, only by potting the silver wire in epoxy was a serviceable working electrode obtained. The working electrode was prepared by polishing with 5□m Al_2O_3 paste on Leco Imperial cloth, followed by thorough rinsing with tap water, then de-ionized water, and then finally drying with a stream of compressed air or by keeping under vacuum in the antechamber of a glovebox. The reference electrode was a Pt wire pseudo-reference in the early experiments or a silver/silver chloride non-aqueous reference electrode in later experiments. The fourth Chem-Thread joint was fitted with a septum; two needles were inserted through this septum to allow UHP Ar flow through the cell. A septum was also fitted to the 24/40 ground glass neck of the flask after placing a magnetic stir bar into the cell. Ar was flowed through the cell for at least five minutes to flush out air. The Ar syringes were then removed. The Chem Flex transfer line was inserted into the septum of the solvent bottle; the other end was clamped upright. The UHP Ar needle was inserted into the septum and the Chem Flex transfer needle was kept above the solvent line in the bottle so as to purge the Chem-Flex line with UHP Ar for at least four minutes. After this time, the Ar outlet syringe re-attached to the cell, and the Chem-Flex line outlet needle was inserted into the septum of the 24/40 joint. The Chem-Flex needle in the solvent bottle was pushed below the solvent line in the bottle and solvent was transferred until 50mL was in the cell (a line on the cell indicated the 50mL fill line). The Ar needle was removed from the solvent bottle and placed in the CV cell to ensure a positive pressure of Ar within the cell. The proper quantity of supporting electrolyte was added through the 24/40 joint by quickly removing the septum, quickly adding the electrolyte from a weighing boat, and quickly replacing the septum. Ar was continually flowed during this time, and magnetic stirring was used to help dissolve the electrolyte. After obtaining blank measurements,

the proper quantity of the tributyltin chloride was weighed into a glass vial. A syringe was used to withdraw a bit of solvent/supporting electrolyte from the cell. This was ejected into the vial with the tributyltin chloride; after swirling, the syringe was used to pull up this solution and it was ejected into the cell through the large septum. This procedure was repeated two to three times to transfer all of the tributyltin chloride; magnetic stirring and bubbling of Ar through the solution was used throughout.

After each experiment, the cell was rinsed well with acetonitrile. After evaporating the remaining acetonitrile, the cell was kept with either 1:1 v/v nitric acid/de-ionized water or concentrated nitric acid for one hour to overnight; the use of concentrated nitric acid accelerated the procedure. In early experiments, only acetonitrile followed by water rinses were used, but after drying, the characteristic spicy/earthy smell of tributyltin chloride was still noticeable in the cell. After the nitric acid wash, the cell was rinsed thoroughly with tap water, de-ionized water, and then a small amount of ethanol or methanol to speed drying. The cell was dried in an oven at 80^{o}C or under vacuum in the antechamber of a glovebox. With this procedure, no smell of tributyltin chloride was noticeable after drying.

Many cyclic voltammetry experiments were performed in glyme with 0.1M $TBAPF_6$ as the supporting electrolyte. Figure 4.2 shows a representative CV for 10mM Bu_3SnCl in this solvent/supporting electrolyte system at a silver disk working electrode using a sweep rate of 300mV/s. This system was of interest due to the number of peaks, compared to 10mM Bu_3SnCl in 0.1M $TBAPF_6/CH_3CN$ (Figure 4.4). Cyclic voltammetry experiments were performed to determining the electrochemical reactions corresponding to the peaks seen for Bu_3SnCl in 0.1M $TBAPF_6$/glyme. The first hypothesis involved the following peak assignments: A2 – oxidation of solvent, supporting electrolyte, or the silver working electrode surface; C1 – conjugate peak of A2, i.e. reduction of oxidized solvent, supporting electrolyte, or the silver surface; C2, C3 – reduction of tributyltin chloride to tributyltin radical (analogous to findings of Mazzocchin and co-workers, described above), C4 – reduction of hexabutylditin (formed by coupling of tributyltin radicals formed at C2/C3). It is important to note here that the shapes and peak current of the cathodic peaks, particularly C2 and C3 were not very repeatable, and seemed to be highly dependent upon the sweep direction and "history" of the working electrode. Figure 4.3 shows a typical result of the difference in CV when the initial sweep direction was up compared to when the initial sweep direction was down.

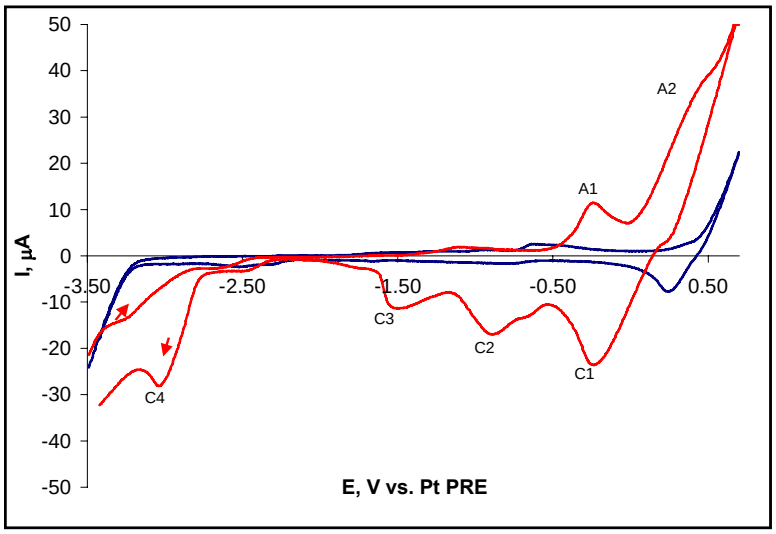

Figure 4.2: CV at 1mm Ag disk WE of 0.1M $TBAPF_6$ in glyme (blue curve) and of 10mM Bu_3SnCl in 0.1M $TBAPF_6$/glyme (red curve). Sweep rate: 300mV/s. Initial sweep: up. CE: Pt wire.

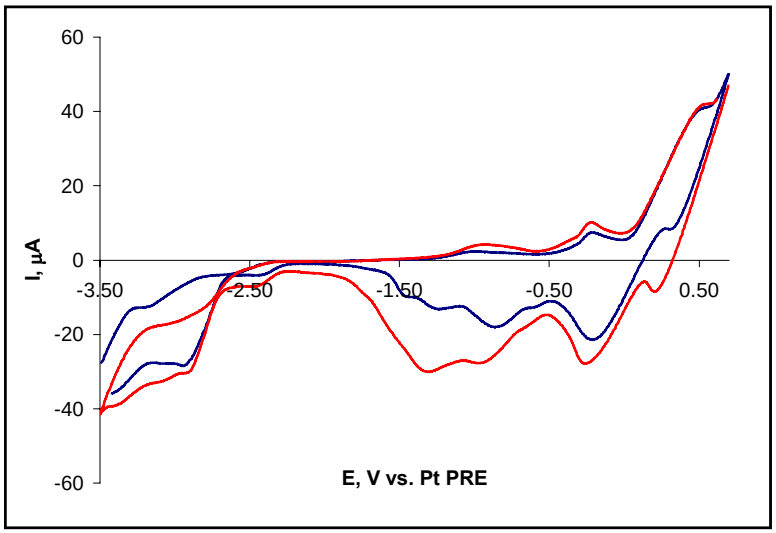

Figure 4.3: CV of 10mM Bu_3SnCl in 0.1M $TBAPF_6$/glyme at 1mm diameter Ag disk working electrode. Blue curve is for initial sweep direction up and red curve is for initial sweep direction down. Sweep rate is 300mV/s. CE: platinum wire.

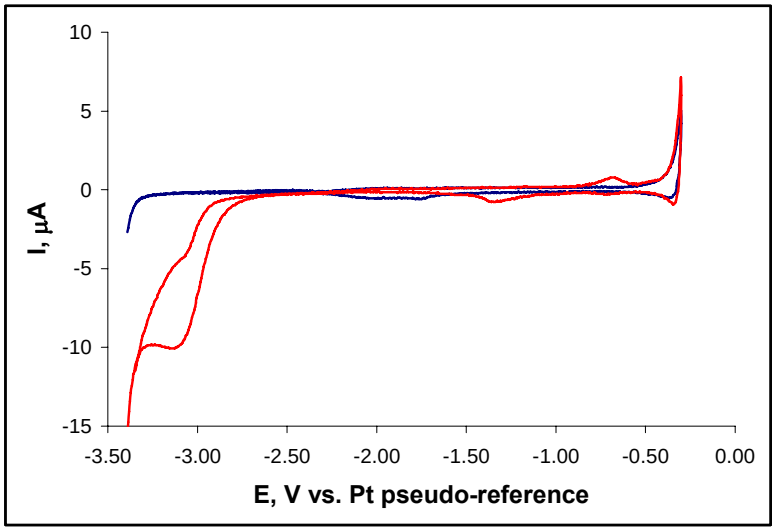

Figure 4.4: CV of 0.1M $TBAPF_6$ in CH_3CN (blue curve) and 10mM Bu_3SnCl in 0.1M $TBAPF_6/CH_3CN$ (red curve) at 1mm diameter Ag disk working electrode. Sweep rate: 100mV/s. Initial sweep up. CE: platinum wire.

The first step in examining this peak assignment was to start the potential sweep at -2V vs. the Pt pseudo-reference electrode. At this potential, the current was near zero, and this potential was beyond the peak potential of peaks C2 and C3. Thus, by starting at this potential, no intermediate tributyltin radicals should exist, if it is true that these radicals are formed at peaks C2 and/or C3. Figure 4.5 shows the result from this experiment. The cathodic peak C4 is seen on the first sweep from -2V to -3.5V, as well as on the final sweep from +0.3V to -3.5V; the peak current is almost the same in both cases. This is evidence that peak C4 is not due to electrochemical activity of any intermediate species, thus implying that it is due to reduction of tributyltin chloride itself.

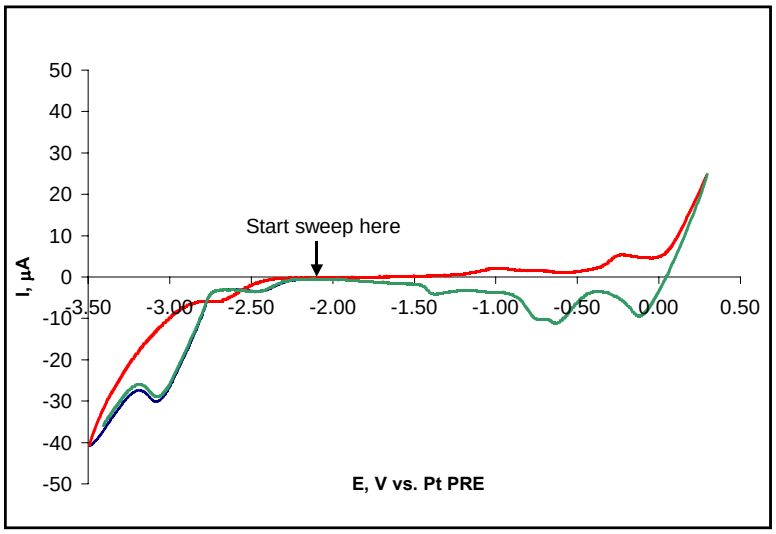

Figure 4.5: CV of 10mM Bu_3SnCl in 0.1M $TBAPF_6$/glyme at 1mm diameter Ag disk working electrode. Potential program: start sweep at -2V, sweep down to -3.5V (blue, solid), sweep up to +0.3V (red, dashed), sweep back to -3.5V (green, dashed). Sweep rate: 300mV/s. CE: platinum wire.

As an independent test of whether peak C4 is due to reduction of tributyltin chloride or to hexabutylditin (formed by coupling of hypothetical intermediate radicals), the cyclic voltammogram of hexabutylditin was obtained at the silver disk working electrode in 0.1M TBAPF6/glyme. Figure 4.6 shows that peak C4 is absent in the CV of hexabutylditin, providing further evidence that peak C4 is due to the reduction of tributyltin chloride itself.

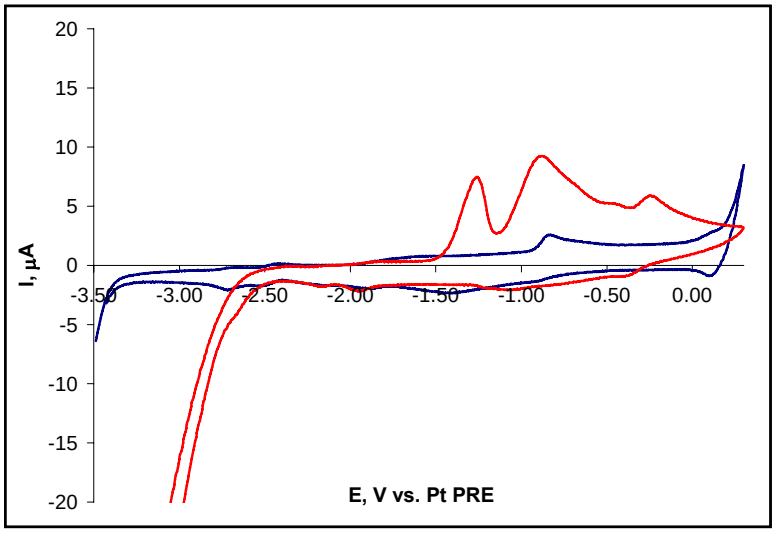

Figure 4.6: CV of 0.1M TBAPF6/glyme (blue curve) and 10mM Bu3SnSnBu3 in 0.1M TBAPF6/glyme (red curve) at 1mm diameter Ag disk working electrode. Initial sweep up. Sweep rate: 300mV/s. CE: platinum wire.

Peaks C2 and C3 thus do not appear to be related to any electrochemical activity of tributyltin chloride. At first, the role of the silver working electrode in the origin of these peaks was not considered, since the peaks were absent in the blank measurement (0.1M TBAPF6 in glyme). However, taking another look at Figure 5.2 shows that the anodic limit at the silver working electrode has shifted in the negative direction upon addition of the tributyltin chloride. The current at the anodic limit has also increased. Thus, it appears that some oxidation reaction is favored when tributyltin chloride is added. Aurbach et al. stated that the anodic limit in aprotic solvents at a silver working electrode was set by silver dissolution [21]. Upon addition of the tributyltin chloride, the anodic limit could shift in the negative direction due to the influence of chlorine in the tributyltin chloride. That silver dissolution sets the anodic limit in aprotic media could explain the significant differences in peak current and shape for the cathodic peaks between when the initial sweep is down compared to when the initial sweep is up. When the initial sweep is down, the sweep is started in a region of anodic current – silver dissolution – so peaks C2 and C3 would be higher in current if they correspond to reformation of the silver surface. This behavior would also explain the lack of reproducibility and history effects, since dissolution and reformation of the silver during potential cycling would be accompanied by morphological changes of the surface.

Based upon these findings, as well as the single observed reduction peak for tributyltin chloride at silver in 0.1M $TBAPF_6/CH_3CN$ seems to indicate that the reduction of tributyltin chloride in aprotic media at silver follows a similar mechanism as proposed by Tanaka et al for triphenyltin chloride at gold in THF.

Because there is no real difference in electrochemical activity of tributyltin chloride at silver in glyme compared to acetonitrile, acetonitrile was chosen for electrochemical reduction experiments. A very important practical reason exists for this choice also – the dielectric constant of glyme is very low (3.5), compared to the dielectric constant of acetonitrile (37) [22]. Performing electrolysis in glyme would be nearly impossible as the cell impedance would be very large, leading to very high ohmic losses in the electrolyte solution. Contrarily, while the impedance in acetonitrile is greater than aqueous solutions, bulk electrolysis in this solvent is practicable.

An undivided cell having cylindrical geometry was settled upon for the electrolysis/coulometry cell. This cylindrical design maximizes the cathode surface area to electrolyte volume (A/V) ratio, has a short anode/cathode gap, and the anode/cathode gap is symmetrical. The short anode/cathode distance minimizes ohmic losses and the symmetry minimizes variations in the current and potential distributions over the cathode surface. The reference electrode (silver/silver chloride non-aqueous as described above) was placed between the anode and the cathode just below the surface of the solution. This placement of the reference electrode minimizes current distribution problems resulting from shielding of the cathode. The cell was prepared from a Pyrex glass tube closed at one end and having the nominal dimensions of seven centimeters tall, three centimeters outer diameter, and 2.8 centimeters inner diameter. A

piece of silver foil (Alfa Aesar, 0.025mm thickness, 99.95% purity) four centimeters tall was cemented to the inside of this glass tube using Devcon 5 minute epoxy. A bead of the same epoxy was applied at the junction of the silver foil and glass at the top and the bottom of the cylinder constituted by the foil, in order to close any crevice between the foil and glass that could trap solution. After this epoxy cured (overnight), a segment of silver wire (Alfa Aesar, 0.64mm diameter, 99.9% purity) was attached near the top of the silver foil using silver epoxy (SPI Supplies part number 05067-AB). The anode of the cell was prepared from a 6mm diameter coarse porosity gas dispersion tube (Chemglass part number CG-207-03) to bubble 10% H_2 in Ar or 100% UHP H_2 over a spiral of platinized platinum wire. The anode, reference electrode, and gas outlet tube were held in a number six black rubber stopper. The stopper was drilled to receive these tubes with an ordinary electric drill after freezing in liquid nitrogen; this method was quick and resulted in clean holes. Figure 4.7 shows a diagram of this cell.

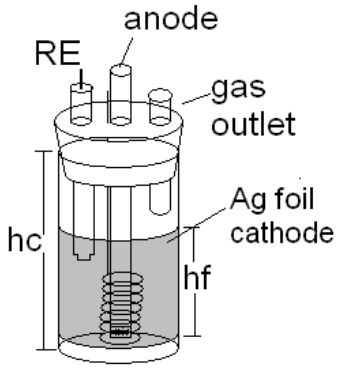

Figure 4.7: Cylindrical cell design for electrolysis of tributyltin chloride in acetonitrile solution. The overall height of the cell, hc, is 7cm. The height of the silver foil cathode, hf, is 4cm. The anode consists of a fritted bubbler concentric with a spiral of platinized platinum wire. 10% H_2 in Ar is bubbled through the fritted bubbler during operation. The stopper is a number 6 black rubber stopper drilled to receive the reference electrode (RE), the gas outlet tube, and the anode assembly. The nominal outer diameter of the glass cell is 30mm and the nominal inner diameter is 28mm. Electrical connection to the cathode was made by 0.5mm diameter Ag wire connected to the silver foil with silver epoxy; this connection was not shown for clarity.

Several methods were tried in preparing the platinized platinum anode, but the best method was adapted from that of Marrese [23]. It should be noted that since several methods were tried with the same electrode, it started with some platinum black on it already when this method was developed. This method, however, was found to give a layer of platinum black that appeared to be more uniform and better adhering than the previous methods. This method called for ultrasonic agitation of the plating bath and was adapted as follows. Instead of cementing the plating cell directly to the ultrasonic bath, a 50mL beaker was cemented to a steel bar with

Devcon 5 minute epoxy. The steel bar served as an anchor for the beaker, and the assembly could be removed from the ultrasonic bath after plating. The plating bath composition follows that recommended by Feltham and Spiro: 0.07M hexachloroplatinic acid (H_2PtCl_6) and $1x10^{-4}$M lead (II) acetate in de-ionized water [24]. This bath was prepared from 1.476g of hexachloroplatinic acid (Aldrich, purity > 99.9%) dissolved in 50mL of de-ionized water. A 1.3×10^{-4}M lead (II) acetate trihydrate (Aldrich, 99.999% purity) solution was then made by dissolving 0.05g of the lead (II) acetate trihydrate in 10mL of de-ionized water. From this solution, 0.5mL was placed in a 50mL volumetric flask, and diluted to the mark with the 0.07M hexachloroplatinic acid solution, finally giving a solution 0.07M in hexachloroplatinic acid and 1.3×10^{-4}M in lead (II) acetate.

Two 25 x 25mm square platinum flag electrodes served as counter electrodes; the platinum wire spiral placed mid-way between these. All electrodes were held by three-pronged clamps attached to a ring stand. An EG&G 366A bi-potentiostat was used to apply a constant current of -100mA for seven minutes, during which time the cell potential was close to two volts. After plating, the electrode was uniformly black and slightly shiny. The electrode was rinsed well with tap water and then de-ionized water, until the de-ionized water rinse showed a pH near five on pH indicator paper. This process was used as a check of thorough rinsing of the plating solution from the electrode; the pH of the plating solution was near zero whereas the pH of de-ionized water was near five. The electrode was dried on a paper towel, or when it was needed immediately for an experiment, it was rinsed with acetone, and then dried under vacuum in an antechamber of a glove box.

After each experiment, the platinum anode was cleaned by immersion in concentrated nitric acid for a few minutes to overnight, followed by thorough rinsing with tap water, and then de-ionized water. It was then re-plated according to the above procedure.
A Pine AFCBP1 bi-potentiostat controlled by Pine Chem software was used to perform constant-potential electrolyses experiments. The Pine Chem software was set up to record the current vs. time for the electrolysis. In some experiments, an EG&G 279A digital coulometer was connected in the working electrode circuit to record the total charge passed. In other experiments, the current-time data was imported into MS Excel and integrated numerically using the trapezoid rule to obtain the total charge passed.

The hydrogen flow was metered through a rotameter, and then passed through a gas wash bottle filled with acetonitrile to saturate the hydrogen with acetonitrile before being bubbled over the anode in the cell. A two-stage regulator was used on the hydrogen tank as this was found to maintain a more constant flow of the gas than a single-stage regulator.

The experiments with the silver foil cathode were plagued by many problems. In some cases, the solution was found to change color from clear to orange or yellow over the course of the electrolysis. This occurred primarily when 10% H_2 in Ar was used. Such color changes are typical of electrolysis in organic solvents when the electrolyte or solvent undergoes oxidation at the anode [11, 12]. In these experiments, then, this color change was taken to indicate inefficient depolarization of the anode by hydrogen, such that oxidation of the solution instead occurred. To

circumvent this, 100% UHP H_2 was substituted. In these experiments, the solution did not turn orange or yellow over the course of the electrolysis. However, the solutions were slightly straw colored at the end of several experiments. This is most likely due to reaction between the solution and the epoxy used to cement the silver foil cathode to the glass cell. Support for this comes in the additional observation that the solutions smelled of epoxy resin after these experiments.

CVs were performed with a silver working electrode on the electrolyte solution before and after electrolysis. Before the electrolysis, the solution in the CV cell was de-aerated with UHP Ar and one CV was performed. The solution was then placed in the electrolysis cell and sparged with UHP H_2 for 15 minutes. Some of this solution was transferred to the CV cell and another CV was performed. The solution was transferred back to the electrolysis cell, sparged five minutes more with UHP H_2, and then electrolysis was begun. After terminating electrolysis, the volume of remaining solution was measured, and then a CV was performed on some of this solution. Finally, the solution in the CV cell was sparged with UHP Ar for 10 minutes and a final CV was performed.

This first important observation in comparing the CV of the electrolyte solution before and after electrolysis (Figure 4.9) is that the cathodic peak (near –2.5V) postulated to be reduction of tributyltin chloride is a significant fraction of its initial value (the current in the voltammogram of the same solution before electrolysis). If tributyltin chloride was reduced during the electrolysis, the current for this cathodic peak should be greatly diminished. This would suggest more facile reduction of some other species. Protons formed by anodic oxidation of hydrogen would be an obvious possibility, for as long as hydrogen is oxidized at the anode, a supply of protons would be available.

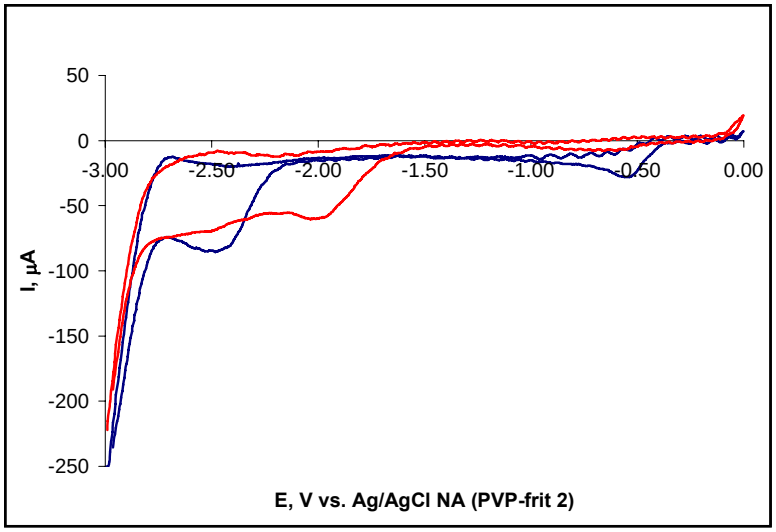

Figure 4.8: CV of 50mM (nominal) Bu3SnCl in 0.1M TBAPF6/CH3CN at Ag WE. Blue curve: solution before electrolysis after sparging with UHP Ar for 10 minutes. Red curve: solution before electrolysis after sparging with UHP H2 for 15 minutes. Sweep rate: 300mV/s. Counter electrode: Pt wire.

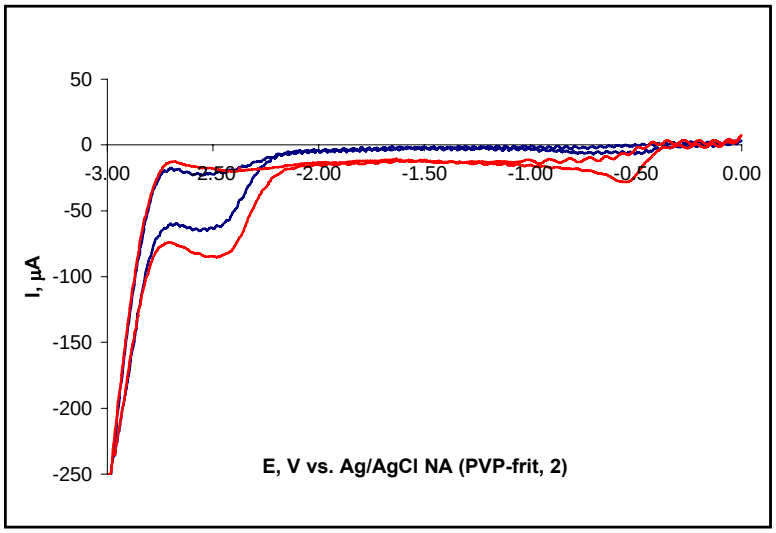

Figure 4.9: CV of 50mM (nominal) Bu_3SnCl in 0.1M $TBAPF_6/CH_3CN$ at Ag WE. Blue curve: solution before electrolysis after sparging with UHP H_2 for 15 minutes. Red curve: solution immediately after electrolysis. Sweep rate: 300mV/s. Counter electrode: Pt wire.

The current-time curves for the electrolyses performed at -2.5V vs. the Ag/AgCl non-aqueous reference did not exhibit reproducible shapes. For electrolysis performed at constant potential in the absence of chemical complications (i.e. only involving electron transfer), the current-time curve is a simple exponential decay [25]. Such behavior was not seen in these experiments. Faraday's Law of Electrolysis was used to estimate the quantity of tributyltin chloride that should have been reduced assuming 100% current efficiency. Faraday's Law of Electrolysis may be written as

$$Q = CnFv \tag{4.13}$$

where Q is the charge (Coulombs), C is the concentration of the species being reduced (here, tributyltin chloride, in molarity), F is Faraday's constant (96,485C/mol), and v is the volume of solution (liters). The volume of solution decreased over the course of the electrolysis, as acetonitrile evaporated due to hydrogen bubbling. Tributyltin chloride is a very non-volatile liquid (vapor pressure less than 0.01mm Hg at 20°C; vapor pressure of acetonitrile at same temperature is 72.8 mm Hg, both according to Sigma Aldrich). Thus, it is assumed that the tributyltin chloride is not significantly displaced by hydrogen bubbling. The nominal concentration of tributyltin chloride was 50mM; real concentration was 51.4mM calculated from the quantity of tributyltin chloride used in preparing the solution. Using Faraday's Law of Electrolysis as outlined above gives a charge Q ~ 139 C required to electrolyze the tributyltin chloride assuming n = 2; the initial volume of the solution in this experiment was 14mL. Integration of the current-time curve gives a total charge of about 279 C. This is further evidence of a lack of selectivity for reduction of tributyltin chloride under these conditions. As the current-

time curve shows (Figure 4.10), the current was substantial when the electrolysis was terminated, indicating a still substantial supply of a reducible species.

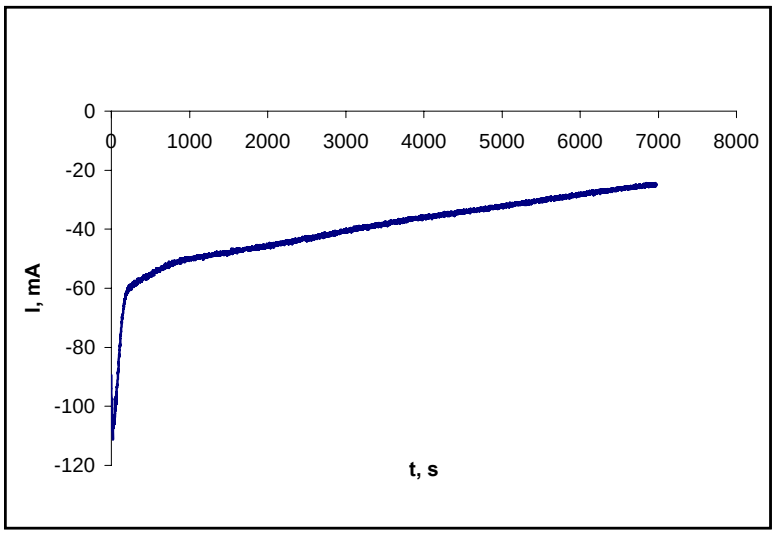

Figure 4.10: Current-time curve for electrolysis at -2.5V vs. Ag/AgCl non-aqueous reference electrode for 50mM (nominal) Bu_3SnCl in 0.1M $TBAPF_6/CH_3CN$.

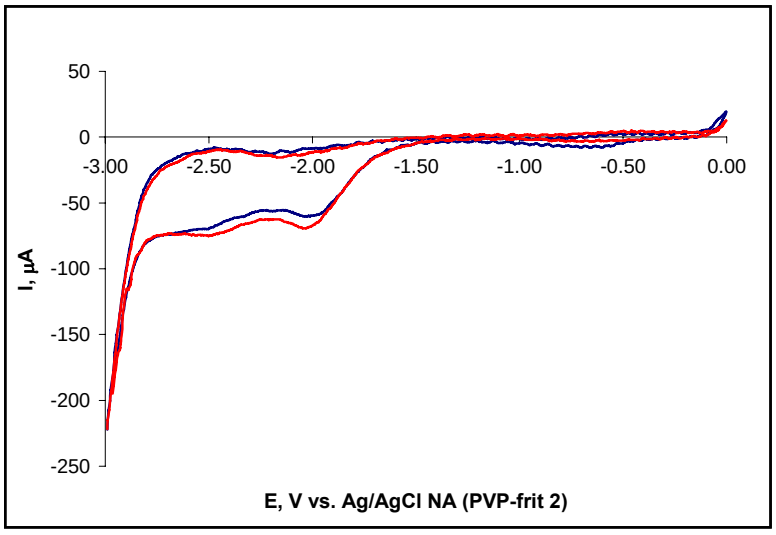

Figure 4.11: CV of 50mM (nominal) Bu_3SnCl in 0.1M $TBAPF_6/CH_3CN$ at Ag WE. Blue curve: solution immediately after electrolysis. Red curve: solution after electrolysis after sparging with UHP Ar for 10 minutes. Sweep rate: 300mV/s. Counter electrode: Pt wire.

Looking at Figure 4.11, it is evident that a new peak occurs around -2V after the electrolysis. UHP Ar was bubbled through the electrolyte solution in the CV cell after electrolysis; this did not diminish the current of the new peak. Therefore, this peak was not due to a volatile (gaseous) species dissolved in the electrolyte. Two non-volatile products were expected from the electrolysis: hexabutylditin and/or tributyltin hydride. Attempts were made to prepare solutions of these two materials in 0.1M $TBAPF_6/CH_3CN$; however, both were found to be immiscible in acetonitrile. CVs of the acetonitrile phase were attempted anyway, but the CVs did not look much different than those of blank solution (0.1M $TBAPF_6/CH_3CN$). This test ruled out these two compounds. Although the identity of the peak near -2V in the CVs after electrolysis could not be identified from these tests, there is strong evidence that tributyltin hydride was not generated in these experiments.

Evidently, some parasitic reaction is occurring, causing the current efficiency to be lower than 100%. Also, as the above analyses show, the expected products hexabutylditin and tributyltin chloride are not obtained. Organotin halides can be cleaved by HCl [26]. In these experiments, HCl can be formed as a product by interaction of the cathodic and anodic electrode reactions: Cl^- is liberated at the cathode (see Equation 4.10) and H^+ is liberated at the anode. The cleavage of Bu_3SnCl proceeds as

$$Bu_3SnCl + HCl \rightarrow Bu_2SnCl_2 + BuH \tag{4.13}$$

In this reaction, BuH is butane (C_4H_{10}). Similar reactions on Bu_2SnCl_2 and $BuSnCl_3$ can also occur. Future experiments should include cyclic voltammetry of Bu_2SnCl_2 and $BuSnCl_3$ in acetonitrile/0.1M $TBAPF_6$ to determine if the new peak near –2V is due to one of these products.

4.5 Suggestions for Future Work

The results obtained for electrolysis at constant potential with a silver cathode do not appear to be promising. The experiments discussed showed a current efficiency for tributyltin chloride electrolysis to be less than 100%, even electrolyzing at a potential corresponding to the cathodic peak corresponding to Bu_3SnCl reduction observed in CV. This observation likely means that parasitic reactions are occurring. Two candidates for parasitic reactions are reduction of H^+ at the silver cathode, or cleavage of tributyltin chloride by HCl generated in coupling of the anode and cathode reactions. If H^+ reduction is the interfering cathodic reaction, using a different cathode material may solve this problem. As discussed in the chapter on borate reduction, it is well known in aqueous systems that the overpotential for the HER is highly dependent upon the cathode material. Thus, cathode materials having a higher overpotential for H^+ reduction should be tested. Notably, Savéant and co-workers used an Hg cathode in their experiments involving the use of a hydrogen oxidation anode [11, 12]. As already discussed, Hg has a higher overpotential for H^+ reduction, at least in aqueous systems.

Furthermore, much of the literature for triphenyltin chloride electrochemistry has involved the use of an Hg working electrode [references in literature review section]. Lead would also be worth studying, and has been used by Tanaka et al. as a cathode material for electrolysis [7].

As hexabutylditin and tributyltin hydride are not soluble in acetonitrile, direct analysis of the electrolyte solution after electrolysis by CV cannot be used to detect these products. Therefore, optimization of the TLC procedure as a spot test for hexabutylditin and tributyltin hydride would be very beneficial to save the time and expense of analysis by FT-IR. The objectives of the optimization procedure would be to get darker, more defined spots for tributyltin chloride and tributyltin hydride, and to eliminate or minimize streaking for the hexabutylditin.

Finally, the non-aqueous Ag/AgCl featuring a cross-linked polymer junction was developed for this work. The stability of this reference with time seemed to be quite good, based upon comparison of peak potentials for the anodic peak of ferrocene on platinum from day-to-day. This reference electrode has the potential to fulfill a very important need for non-aqueous electrochemistry: a stable electrode that does not need to be prepared daily and does not contaminate the test or electrolysis solution. More work should be done to assess the longer-term stability of the potential, using several different electrodes prepared by the same method to assess the reproducibility in potential.

In the broader view of chemical hydrogen storage, the regeneration scheme in Figure 1.1 actually suffers from a pretty significant problem, namely, that one kg of H_2 gas requires 218.3kg of tributyltin hydride based upon the conversion of 1.5 mol of tributyltin hydride per mol of H_2 [27]:

$$1000g\ H_2\left(\frac{1\,mol}{2\,g}\right)\left(\frac{1.5\,mol\,Bu_3SnH}{1\,mol\,H_2}\right)\left(\frac{291.06g}{1\,mol}\right)=218.3kg\ Bu_3SnH \tag{4.14}$$

This equation is true independent of how the tributyltin hydride is produced and imposes a fundamental limitation on the regeneration scheme in Figure 1.1. As with sodium borohydride, regeneration of aminoborane is the foremost challenge to its adoption as a hydrogen storage material.

4.6 References

1. A.G. Davies. Organotin Chemistry, 2nd ed. Wiley-VCH, 2004, Weinheim.
2. Private communication with Argonne National Laboratory.
3. R.E. Dessy, W. Kitching, and T. Chivers. *Journal of the American Chemical Society*, 88 (1966) 453.
4. M.D.Booth and B. Fleet. *Analytical Chemistry* 42 (1970) 825.

5. G.-A. Mazzocchin, R. Seeber, and G. Bontempelli. *Journal of Organometallic Chemistry*, 121 (1976) 55.
6. A. Savall, G. Lacoste, and P. Mazerolles. *Journal of Applied Electrochemistry*, 11 (1981) 61.
7. H. Tanaka et al. *Journal of Organic Chemistry*, 61 (1996) 9402.
8. B.Fleet and N.B. Fouzder. *Journal of Electroanalytical Chemistry*, 63 (1975) 59.
9. C.A. Paddon, F.L. Bhatti, T.J. Donohoe, R.G. Compton. *Journal of Physical Organic Chemistry*, 20 (2007) 115.
10. K. Izutsu, Electrochemistry in Nonaqueous Solutions, Wiley-VCH, 2002, Weinheim.
11. J.M. Savéant and S.K. Binh. *Electroanalytical Chemistry and Interfacial Electrochemistry*, 50 (1974) 417
12. C.P. Andrieux, J.M. Dumas-Bouchiai, and J.M. Savéant. *Journal of Electroanalytical Chemistry*, 83 (1977) 355.
13. ATR – *Theory and Applications*. Application Note, Pike Technologies, 2005.
14. V.Farina. *Journal of Organic Chemistry*, 56 (1991), 4985.
15. C.A. Paddon and R.G. Compton. *Electroanalysis*, 17 (2005) 1919.
16. J. Ghilane, P. Hapiot, and A.J. Bard. *Analytical Chemistry*, 78 (2006) 6868.
17. J.L. Hall and P.W. Jennings. *Analytical Chemistry*, 48 (1976) 2026.
18. A.I. Popov and D.H. Geske. *Journal of the American Chemical Society*, 79 (1957) 2074.
19. Y. Sakai, Y. Sadaoka, and M. Matsuguchi. *Journal of the Electrochemical Society*, 136 (1989) 171.
20. J.G.A. Luijten and G.J.M. van der Kerk. Investigations in the Field of Organotin Chemistry. Tin Research Institute, Middlesex, 1955.
21. D. Aurbach, M. Daroux, P. Faguy, and E. Yeager. *Journal of Electroanalytical Chemistry,* 297 (1991) 225.
22. C.K. Mann. Nonaqueous Solvents for Electrochemical Use. In: Electroanalytical Chemistry, A Series of Advances, Vol. 3. A.J. Bard, ed. Marcel Dekker, 1969, New York.
23. C.A. Marrese. *Analytical Chemistry*, 59 (1987) 217.
24. A.M. Feltham and M. Spiro. *Chemical Reviews*, 71 (1971) 177.
25. A.J. Bard and L.R. Faulkner. Electrochemical Methods: Fundamentals and Applications, 2nd ed. Wiley, New York, 2000.
26. R.K. Ingham, S.D. Rosenberg, and H. Gilman. *Chemical Reviews*, 60 (1960) 459.
27. Arthur Chin, Rohm and Haas, Philadelphia, PA. Personal communication, July 2008

PART II

A GENERAL MODEL OF ELECTROCHEMICAL IMPEDANCE SPECTROSCOPY AND ITS APPLICATION TO HYDROGEN STORAGE MATERIALS

1. Introduction

It is all too clear that the demand for energy on a global scale is an ever-growing problem. One of the most promising solutions to this problem is to utilize hydrogen as an energy carrier. The benefits of harnessing hydrogen to carry energy are many; however, the main points are: a reduction in the use of fossil fuels, a corresponding reduction in the production of greenhouse gases, and an increased economic benefit by making other sources of energy available for consumers. However, the present limitation on this technology is a safe and effective method to store enough hydrogen for individual applications (these may vary in scale from powering a cellular phone or a laptop computer to powering an automobile or a standalone power unit as a primary or secondary source of electricity).

There are four primary areas of research that are required in order to make hydrogen a part of our daily lives: production, storage, transportation, and utilization. Typically, hydrogen is produced by the steam reforming of fossil fuels, although other methods are being developed in order to eliminate fossil fuels from the overall energy cycle; some of these methods include: algae bioreactors, fermentation of organic materials by anaerobic bacteria and enzymes, electrolysis of water (using non-carbon cycle power such as hydroelectric, solar, or nuclear power), and thermal decomposition of water (for example using solar power). The transportation of hydrogen is a separate task that will depend on the final form (solid, liquid, or gas) in which it will be consumed; as such this will not be discussed further. The utilization of hydrogen is assumed here to be in a fuel cell where the only reaction product is water.

The most obvious method of storing hydrogen is in compressed gas or liquefied hydrogen tanks; nevertheless, the primary drawback of these methods is the limited quantity that is able to be stored. In recent years, the storage of hydrogen as a compressed gas entailed the use of large and heavy containers. For example, in a common steel tank only about 1% of the total weight was that of the hydrogen gas when it was fully compressed (14 MPa). Additionally, storing

liquid hydrogen presents serious safety problems due to its extreme volatility if discharged and because of the temperatures required to maintain it as a liquid (20 K).

In order to address these problems, compressed hydrogen tanks are now being operated at extremely high pressures; most are in the range of 35 – 70 MPa. And although modern tanks are being designed for liquefied hydrogen storage, the major problem that still exists is boil-off. As a result, these hydrogen storage methods still present serious safety and engineering issues; this topic is discussed further in [1].

To overcome these downfalls, a vast quantity of research has been performed on various alternative mediums for hydrogen storage. These mediums include, but are not limited to: metal and chemical hydrides [2, 3], physisorption-based techniques [4, 5], and alloys such as Ti-Zr-Cr-V or lanthanum-rich intermetallic nickel alloys [6, 7]; some reviews of the recent research on hydrogen storage mediums can be found in [8, 9].

This dissertation stems from a five year research project through the Center of Excellence for Chemical Hydrogen Storage within the U.S. Department of Energy (DOE) to study various hydrogen storage materials that are based upon boron hydrides. The idea of this research is to limit or eliminate fossil fuels to power our everyday needs.

Boron hydrides were chosen for this project in order to eliminate carbon from the overall lifecycle of the chemical hydrogen storage materials, and doing so would automatically reduce or do away with the production of greenhouse gases. One thing to note immediately about boron hydrides is the general trend that they are more reactive (less stable) in the more simple molecules, whereas the larger, more complex molecules of boron hydrides are more stable and less reactive.

To give the reader an idea of what is meant by stable and reactive, consider two such boron hydrides, namely borane (BH_3) and dodecahydrododecaborate ($B_{12}H_{12}$). Borane is a simple molecule (Figure 1.1) that is in the gaseous phase at ambient temperature and pressure and readily dimerizes to form diborane, B_2H_6 (Figure 1.2), which when released into an environment that contains oxygen and water vapor will spontaneously combust to form hydrogen (H_2) and boric acid, $B(OH)_3$.

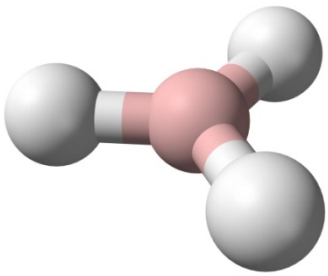

Figure 1.1: The borane molecule, BH_3.

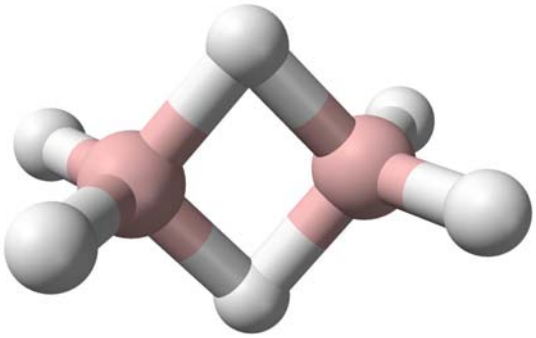

Figure 1.2: The diborane molecule, B_2H_6.

On the other hand, the $B_{12}H_{12}$ cluster molecule, often called a polyhedral borane or more simply a polyborane, is a complex icosahedral shape (Figure 1.3) and is found as an anion of various salts, for example potassium dodecahydrododecaborate ($K_2B_{12}H_{12}$).

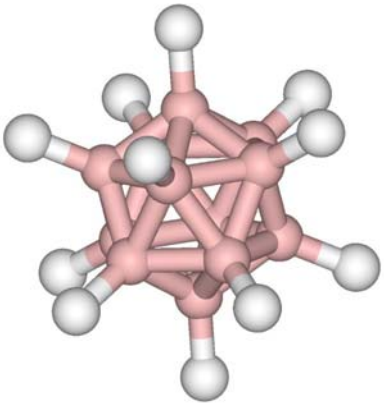

Figure 1.3: The dodecahydrododecaborate cluster, $B_{12}H_{12}$.

The physical properties of dodecahydrododecaborate salts are such that they are found as powders at room temperature and pressure that are thermally stable up to a few hundred degrees Celsius. In addition, the chemical stability of these salts is such that they do not decompose unless they are in strongly acidic or caustic solutions. Figure 1.4 shows various polyhedral boranes ranging from four to twelve boron atoms in the polyborane; as mentioned before, the relative reactivity decreases as the number of boron atoms within the cluster increases.

The immediate solution to the needs of chemical hydrogen storage would seem to be that borane, or more appropriately, diborane, is the most likely candidate due to its ease of reaction, i.e. we could simply have a container of diborane and expose it in a controlled manner to water, for example, in order to produce hydrogen spontaneously. Although this could be done, it is not in use due to safety issues of accidental release, which could cause catastrophic fires or explosions.

To address the requirements of the DOE, the original proposal made by Dr. Digby D. Macdonald was to use the salts of dodecahydrododecaborate as the first molecules to examine based on their safety qualities and ability to contain a sufficient amount of hydrogen (theoretically 8.2%, actual 6.2%). In addition, the proposal to use polyboranes as hydrogen storage materials is not only because they contain a sufficient quantity of hydrogen to meet the DOE goals, but also because virtually no work has been done to determine whether electrochemical transformations exist for these materials and if they do exist whether they are reversible as would be necessary to form a hydrogen storage system. Therefore, because this has not been investigated in the past I must emphasize that this work is primarily exploratory at the onset.

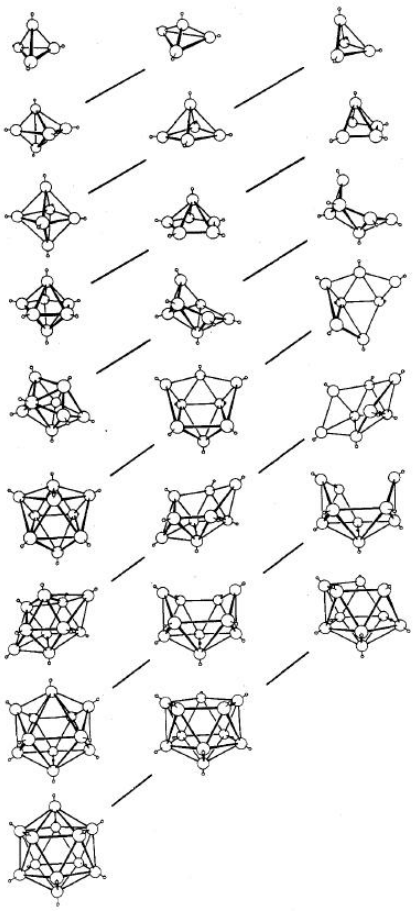

Figure 1.4: The family of polyborane clusters from B_4H_4 up to $B_{12}H_{12}$. The terminal hydrogen atoms are omitted for clarity. Image from [10].

The results of this research are presented in Chapter 2 below, the goal of which is to identify whether the hydrogen release and uptake steps can be identified by electrochemical techniques.

Over time, the results of our research came to conclusions that spurred the DOE to stop investigating polyboranes as chemical hydrogen storage materials. The next material of interest to the Department of Energy was ammonia borane, H_3BNH_3, (Figure 1.5) and it is the subject of Chapter 3 below.

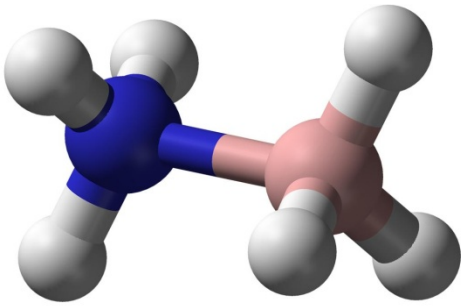

Figure 1.5: The ammonia borane molecule, H_3BNH_3.

The ammonia borane molecule follows a stepwise release of hydrogen from H_3BNH_3 to H_2BNH_2, then from H_2BNH_2 to HBNH, and finally from HBNH to BN. In traversing these reactions, the original ammonia borane fuel is capable of releasing 19.3% hydrogen by mass. My goal in this case was to determine whether the lower hydrides could be hydrogenated to the higher hydrides in a "refueling phase." The process of hydrogenation was looked at in two different ways: a direct electrochemical hydrogenation, and an indirect hydrogenation. The indirect hydrogenation method results in the use of organotin halides (Figure 1.6) as intermediate hydrogenation materials (i.e., they hydrogenate the spent ammonia borane fuel at the cost of their own oxidation) that need to be recycled (hydrogenated) back to the hydride form; this is discussed in Chapter 3 below.

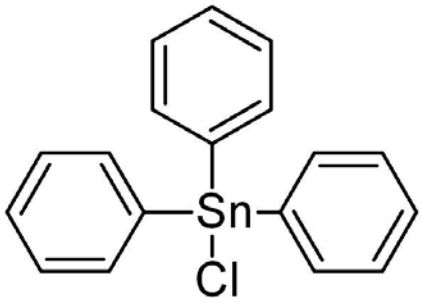

Figure 1.6: The triphenyltin chloride compound, an example of an organotin halide compound. The regeneration of organotin chloride removes the chlorine and replaces it with a hydrogen atom to form the organotin hydride compound.

Finally, the ultimate goal of this research is to identify the reaction mechanisms that take place during hydrogen release and uptake reactions, therefore a novel model of electrochemical impedance spectroscopy (EIS) was developed. The EIS technique is able to probe reactions at time scales spanning approximately ten orders of magnitude, which makes it a very powerful tool for electrochemical analysis. The new model of EIS is presented below in Chapter 4.

1.1 References

1. F. Schüth, B. Bogdanović, and M. Felderhoff, *Chem. Commun.*, 2249 (2004).
2. S. Orimo, Y. Nakamori, and A. Züttel, *Mater. Sci. Eng. B*, **108**, 51 (2004).
3. J. J. Vajo, F. Mertens, C. C. Ahn, R. C. Bowman, Jr., and B. Fultz, *J. Phys. Chem. B*, **108**, 13977 (2004).
4. Y. L. Zhao, R. Q. Zhang, and R. S. Wang, *Chem. Phys. Lett.*, **398**, 62 (2004).
5. W.-K. Hu, Y.-S. Zhang, D.-Y. Song, and P.-W. Shen, *Int. J. Hydrogen Energ.*, **21**, 651 (1996).
6. S. E. Hsu, V. M. Beibutian, and M. T. Yeh, *J. Alloys Compd.*, **330–332**, 882 (2002).
7. Y. Fukumoto, M. Miyamoto, M. Matsuoka, and C. Iwakura, *Electrochim. Acta*, **40**, 845 (1995).
8. E. Fakioğlu, Y. Yürüm, and T. N. Veziroğlu, *Int. J. Hydrogen Energ.*, **29**, 1371 (2004).
9. A. Züttel, *Naturwissenschaften*, **91**, 157 (2004).
10. R. W. Rudolph, *Acc. Chem. Res.*, **9**, 446 (1976).

2. Polyhedral Boranes

2.1 Introduction

In order to overcome the hydrogen storage problems associated with many chemical hydrides and to achieve DOE goals for weight percent (9 wt. % by 2015) and volumetric density (80 g/L by 2015) of stored hydrogen, we began to explore the electrochemistry of complex polyhedral boranes (polyboranes) to assess their capabilities for the controlled release and uptake of hydrogen.

A literature review reveals that very little work has been reported on this topic [1-6] with virtually no work published since the mid-1970s. Due to a lack of knowledge about the electrochemical behavior of the polyboranes, we performed fundamental studies on these materials in an exploratory manner.

Neutral polyboranes and polyborane anion salts appear to be promising materials for hydrogen storage based on preliminary data. In order to determine if the polyborane anion salts would function as hydrogen-storage materials, we began to investigate whether electrochemically-mediated and reversible transitions between anions of different oxidation states could be achieved with an accompanied change in hydrogen content.

It was proposed that polyhedral borane (polyborane) anions and neutral species of the general formula $B_xH_x^{y-}$ (where x > 6 and y = 0 – 4) are suitable in order to achieve sufficient gravimetric and volumetric hydrogen storage densities if electrochemically-mediated and reversible transitions between polyboranes of different oxidation states could be achieved. Obtaining a suitable polyborane for this task was not a problem, although the selection process was more challenging because nearly 50,000 boron cluster compounds have been synthesized in the past half-century [7].

Because this was a new research project, we began by studying the electrochemistry of the dodecahydrododecaborate dianion, $B_{12}H_{12}^{2-}$, as well as decahydrodecaborate dianion, $B_{10}H_{10}^{2-}$, in nonaqueous solutions with acetonitrile as the solvent. We have noticed interesting differences in the cyclic voltammograms for various solutions that depend on: (1) the cation that is part of the polyborane salt, (2) the sweep rate of the electrode potential, and (3) the material of the working electrode. Also of interest is the effect of various concentrations of the polyboranes. For instance, a solution of triethylamine dodecahydrododecaborate, $[(CH_3CH_2)_3NH]_2B_{12}H_{12}$, at a concentration of 1 mM exhibits an oxidation wave whose potential value is dependent on the cycle number in a cyclic voltammogram. Additionally, by varying the polyborane concentration in a solution of tetra-*n*-butylammonium dodecahydrododecaborate, $[(CH_3CH_2CH_2CH_2)_4N]_2B_{12}H_{12}$, from 1 to 10 mM, we noticed additional oxidation features occuring at the higher concentrations.

The initial data leads us to suspect that an ECE reaction mechanism is involved, i.e. a reaction where a chemical reaction is coupled in between preceding and following electrochemical reaction steps [8].

2.2 Experimental Approach

The first experiments were designed to study the complex electrochemical behavior of polyhedral borane anions as supplied by Dr. M. Frederick Hawthorne from his lab at The University of California at Los Angeles (currently at The University of Missouri). As such, the supplied polyboranes were in limited quantities because they were synthesized only when they were needed. This led me to design a small-volume electrochemical cell (V = 2.5 mL) in order to limit the need for large quantities of working materials.

The cell was built in our department's glass shop by joining together four threaded glass joints (Chemglass, Inc.) with 7 mm internal diameter. The geometry of the electrochemical cell is a "cross shape" such that the working electrode and the counter electrode are facing one another and the reference electrode was able to be placed perpendicularly between the working and counter electrodes. The fourth glass joint is used as a septum port, while all other joints are sealed with o-rings to provide an airtight seal.

The chemical oxidation of polyboranes has been studied and reported in the literature [9-12], yet there is a limited quantity of open literature available on the electrochemistry of polyboranes [1,2,4,6]. Based upon the literature that was found, we decided to perform our initial experiments in an anhydrous, aprotic solvent. Acetonitrile was chosen because of its use in previous electrochemical studies, its wide, available potential range, and its ability to dissolve many inorganic salts.

All work has been conducted in a continuously purified argon glovebox with < 1 ppm H_2O and < 1 ppm O_2. The acetonitrile used throughout was HPLC grade (EMD Scientific, OmniSolv, 99.99%) and has been degassed by sparging with ultra-pure grade argon that was passed through a gas purifier (NuPure Corp., < 10 ppb impurities). The supporting electrolyte dissolved in all solutions was tetra-*n*-butylammonium hexafluorophosphate, $(CH_3CH_2CH_2CH_2)_4N(PF_6)$, (Sigma Aldrich, electrochemical grade, 99.0%) at a concentration of 0.100 M; this forms the blank solution. Note that tetra-*n*-butylammonium hexafluorophosphate is referred to as TBA-PF_6 throughout the text.

We used the silver/silver ion couple in my reference electrode because it is nonaqueous and thus more compatible with our solutions than a customary aqueous reference electrode. The silver/silver ion couple has an equilibrium potential in this system that is +0.637 V vs. SHE (standard hydrogen electrode). The reference electrode was designed and built in-house. A 10 cm length of 6 mm outer diameter glass tube was fused at one end to a small length of 4 mm outer diameter glass tube and it was also fused at the other end to a threaded glass joint (Chemglass, Inc.) to form the electrode body.

A silver wire (Alfa Aesar, 99.9985%) runs coaxially inside the glass body where it was sealed at the threaded end allowing for electrical contact to be made. Inside the electrode body, the silver wire contacts a solution of 0.010 M $AgNO_3$ (Sigma Aldrich, 99.9995%), which was made by dissolving silver nitrate in a portion of the blank solution. The reference electrode has a small porous glass (Corning, Inc., Vycor #7930) frit as the liquid junction; it was cut to 3 mm in length and attached to the glass body onto the tip of the 4 mm glass tube by PTFE heat-shrink tubing.

The working electrode and the counter electrode were made from short lengths of platinum wire (Alfa Aesar, 99.99%) that are 1 mm and 2 mm in diameter, respectively. The platinum wires were soldered to longer lengths of copper wire and each was potted into chemically inert epoxy. The electrodes were removed from the epoxy molds and the platinum wire was polished flush to the end of the electrode making a disk-geometry for each electrode; the final polish used a 0.05 micron alumina suspension. External electrical contact was made via the copper wire extending from the opposite end of each electrode. The geometric surface area of the platinum working electrode is 0.00785 cm^2 and all electrochemical current measurements have been converted to apparent current density (A/cm^2) for ease of comparison with other electrode dimensions. In addition, all potential values are automatically converted to the standard hydrogen scale by the data acquisition software (CorrWare, Scribner Associates Inc.).

Also of interest is the solubility of the polyborane salts in acetonitrile. We attempted to dissolve the potassium dodecahydrododecaborate methanolate salt, $K_2B_{12}H_{12}•CH_3OH$ (BASF Corp., 95%), however we discovered that its solubility was quite low and also that particles were visible in solution. In order to increase the solubility, we exchanged the potassium cations for tetra-*n*-butylammonium, which has a different surface charge density and allows for more complete solvation. After performing the cation exchange, the solubility was determined to be well over 0.3 M in acetonitrile. This was determined by adding a sufficient amount of the salt to acetonitrile in order to form a saturated solution, then a known volume of the solution was collected and added to a different container whose mass had already been measured, finally after the solvent had evaporated the mass of the salt was found, which allowed for a simple calculation to be made to yield the maximum soluble concentration in that solvent.

The cation exchange procedure was performed by mixing one equivalent of $K_2B_{12}H_{12}•CH_3OH$ in water (taking into account the methanol content) with slightly more than two equivalents of tetra-*n*-butylammonium bromide in water (in order to maintain this reactant in excess of the initial potassium polyborane salt). Upon mixing the two solutions, a white, paste-like slurry immediately precipitates. The precipitate was rinsed with Milli-Q deionized water (Millipore Corp.) and was then vacuum filtered with one-micron filter paper. The precipitate was collected from the filter paper in almost quantitative yield and it was allowed to air dry. After drying in air, the salt was further dried under vacuum to remove any remaining water. Once the sample was completely dry, it was transferred into the argon glovebox where it was recrystallized from pure acetonitrile several times. During this process, the methanol content is removed from

the polyborane salt, and the identity of the final product was determined for this procedure by chemists at BASF [13].

2.3 Results and Discussion

In order to establish a starting point, a cyclic voltammogram (CV) was recorded for the blank solution (0.100 M TBA-PF_6 in acetonitrile). The 10-cycle CV for the blank solution is shown in Figure 2.1 where it can be seen that this combination of solvent and supporting electrolyte provides a wide available potential range with little background signal. Note that the arrows in Figure 2.1 indicate the directions of the potential sweeps; all Figures follow this pattern by beginning at the cathodic limit and progressing toward the anodic limit on the forward sweep.

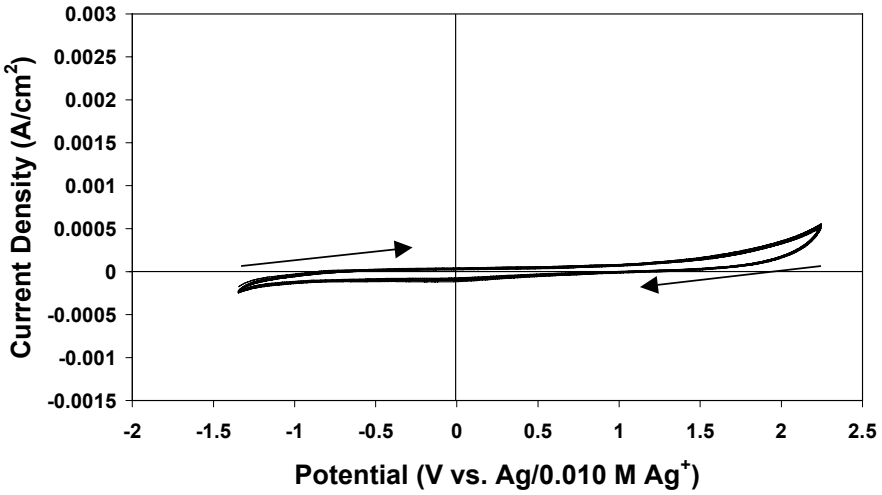

Figure 2.1: Cyclic voltammogram over 10 cycles for a blank solution containing only the supporting electrolyte (0.100 M tetra-n-butylammonium hexafluorophosphate) dissolved in acetonitrile. The arrows indicate the direction of the potential sweeps; each cycle begins at the cathodic limit. The working electrode was a 1 mm Pt disk, the counter electrode was a 2 mm Pt disk, and the reference electrode was Ag/0.010 M Ag^+. The scan rate was 100 mV/s.

After verifying that the blank solution was suitable for electrochemical studies, we recorded a cyclic voltammogram for a sample of 1 mM triethylamine dodecahydrododecaborate, $[(CH_3CH_2)_3NH]_2B_{12}H_{12}$, which was dissolved in the blank solution. The 10-cycle CV for this sample is shown in Figure 2.2, where now the arrow indicates that the location of the oxidation wave is progressing to higher potential and current density values with successive cycles. The cause of this behavior is unknown at this point, however the change in the oxidation wave appears to have no effect on the reduction wave located at –1.05 volts.

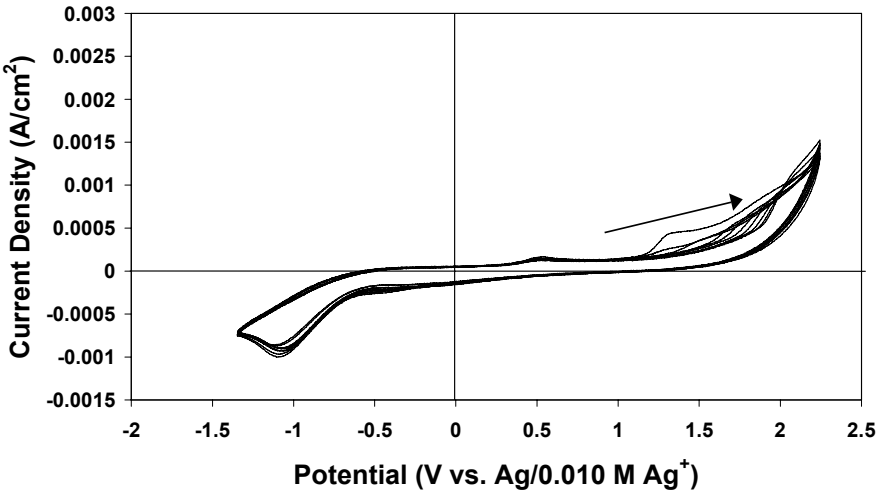

Figure 2.2: Cyclic voltammogram over 10 cycles for a sample of 1 mM triethylamine dodecahydrododecaborate ($[(CH_3CH_2)_3NH]_2B_{12}H_{12}$) dissolved in the blank solution (0.100 M tetra-n-butylammonium hexafluorophosphate in acetonitrile). The working electrode was a 1 mm Pt disk, the counter electrode was a 2 mm Pt disk, and the reference electrode was Ag/0.010 M Ag^+. The scan rate was 100 mV/s. The arrow indicates the progression of the oxidation wave with successive cycles toward higher potential and current values. The oxidation wave moves from 1.35 to 2.00 volts, and it becomes smaller with respect to the background on each additional cycle. The reduction wave is at –1.05 volts.

The next sample to be studied was 1 mM tetra-*n*-butylammonium dodecahydrododecaborate, $[(CH_3CH_2CH_2CH_2)_4N]_2B_{12}H_{12}$, also written as $TBA_2B_{12}H_{12}$. This polyborane is the product of the cation exchange reaction discussed earlier. Figure 2.3 shows the 10-cycle voltammogram of 1 mM $TBA_2B_{12}H_{12}$ under the same experimental conditions as before. The oxidation peak at 1.25 V appears only on the first cycle with a broad shoulder that appears to contain a very small oxidation wave near 1.52 V. A small reduction wave can be seen at –0.55 V; the small nature of this wave should not be completely unexpected based upon the lack of oxidation features other than the small oxidation wave on the first cycle.

The third solution studied was 10 mM tetra-*n*-butylammonium dodecahydrododecaborate ($[(CH_3CH_2CH_2CH_2)_4N]_2B_{12}H_{12}$). This solution was made with the same recrystallized polyborane salt as used for the 1 mM solution, so the results are not due to any other factor than increased polyborane concentration. As shown in Figure 2.4, the increase in polyborane concentration has a profound impact on the oxidation features, however the reduction wave was virtually unchanged. A sharp oxidation peak is seen in Figure 2.4 at 1.25 volts; this is at the same potential value as that of the 1 mM solution.

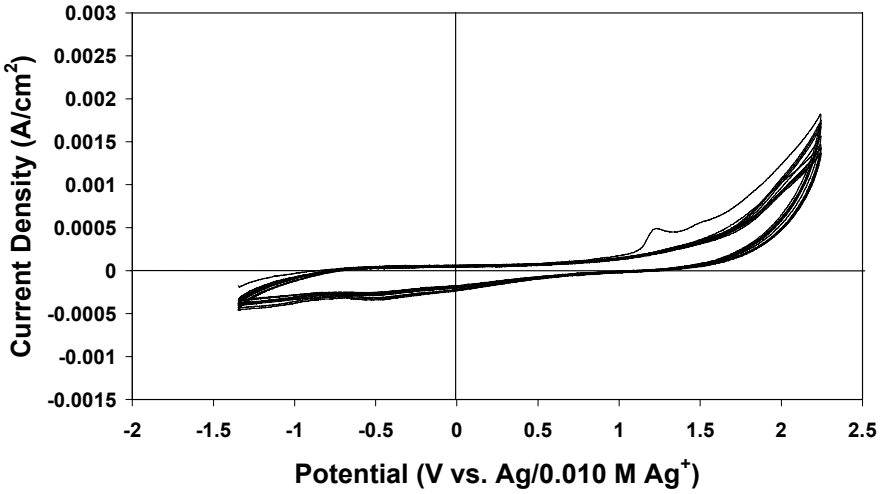

Figure 2.3: Cyclic voltammogram over 10 cycles for a sample of 1 mM tetra-n-butylammonium dodecahydrododecaborate ($[(CH_3CH_2CH_2CH_2)_4N]_2B_{12}H_{12}$) dissolved in the blank solution (0.100 M tetra-n-butylammonium hexafluorophosphate in acetonitrile). The working electrode was a 1 mm Pt disk, the counter electrode was a 2 mm Pt disk, and the reference electrode was Ag/0.010 M Ag^+. The scan rate was 100 mV/s. On the first cycle, an oxidation wave is seen at 1.25 V with a broad shoulder that appears to contain another small oxidation wave near 1.52 V. The small reduction wave is located at –0.55 V.

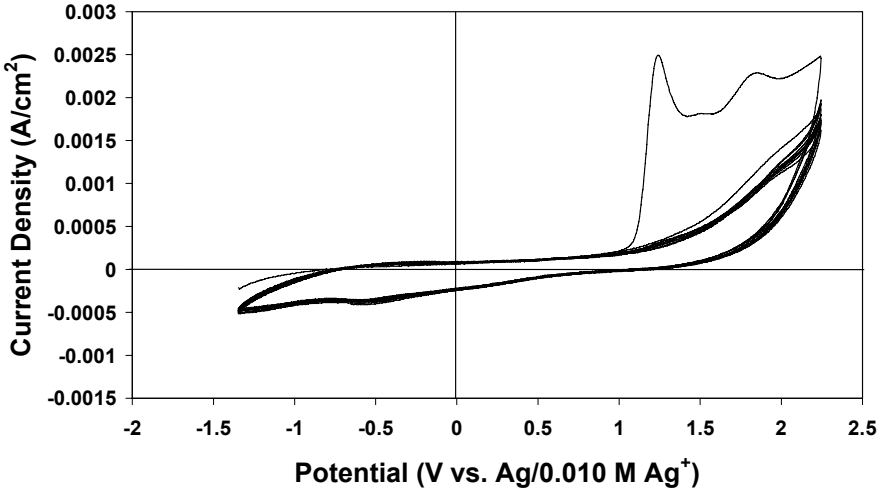

Figure 2.4: Cyclic voltammogram over 10 cycles for a sample of 10 mM tetra-n-butylammonium dodecahydrododecaborate ($[(CH_3CH_2CH_2CH_2)_4N]_2B_{12}H_{12}$) dissolved in the blank solution (0.100 M tetra-n-butylammonium hexafluorophosphate in acetonitrile). The working electrode was a 1 mm Pt disk, the counter electrode was a 2 mm Pt disk, and the reference electrode was Ag/0.010 M Ag^+. The scan rate was 100 mV/s. A sharp oxidation peak is seen on the first cycle at 1.25 V with another small oxidation wave at 1.53 V and a third oxidation wave at 1.86 V. The small reduction wave is located at –0.57 V.

Additionally in Figure 2.4, we notice that the small oxidation wave at 1.53 volts on the anodic shoulder of the first peak is more visible now as compared to that of Figure 2.3. Finally, we now see in Figure 2.4 that a new oxidation peak is present at 1.86 volts. We believe this is evidence of an ECE coupled reaction mechanism, and we investigated this further by adjusting the CV parameters as will be discussed below. Similar to Figure 2.3, the small reduction wave observed in Figure 2.4 is located at –0.57 volts.

An interesting observation for Figure 2.4 is the lack of oxidation peaks in the 1 – 2 V region at cycles beyond the first. Thus, the entities that are oxidized within this potential region are either removed irreversibly (and quantitatively) or their oxidation is inhibited on further cycling. Given the relatively high potential sweep rate, the time spent in the 1 – 2 V window is short (10 s) and noting that the current density is approximately 0.0025 A/cm^2 the total charge passed in the 1 – 2 V region on the first cycle is ~ $2 \cdot 10^{-4}$ C. Assuming a one-electron reaction, the number of moles removed is about $2 \cdot 10^{-9}$. This may be compared with $(2.5/1000) \cdot 0.01 = 2.5 \cdot 10^{-5}$ moles of the polyborane in the system; thus, only 0.008% of the polyborane is consumed on the first, forward potential sweep. If the reaction involves multiple electrons, the amount removed is even less. Thus, we conclude that the lack of oxidation peaks on the second and higher sweeps is not due to depletion of the reactant, leaving passivation of the surface by an adsorbed, inert oxidation product as being the most likely cause.

Our examination of the electrochemical properties of the decahydrodecaborate dianion ($B_{10}H_{10}^{2-}$) in anhydrous acetonitrile began as we collected CV data on triethylamine decahydrodecaborate, $[(CH_3CH_2)_3NH]_2B_{10}H_{10}$, as shown in Figure 2.5.

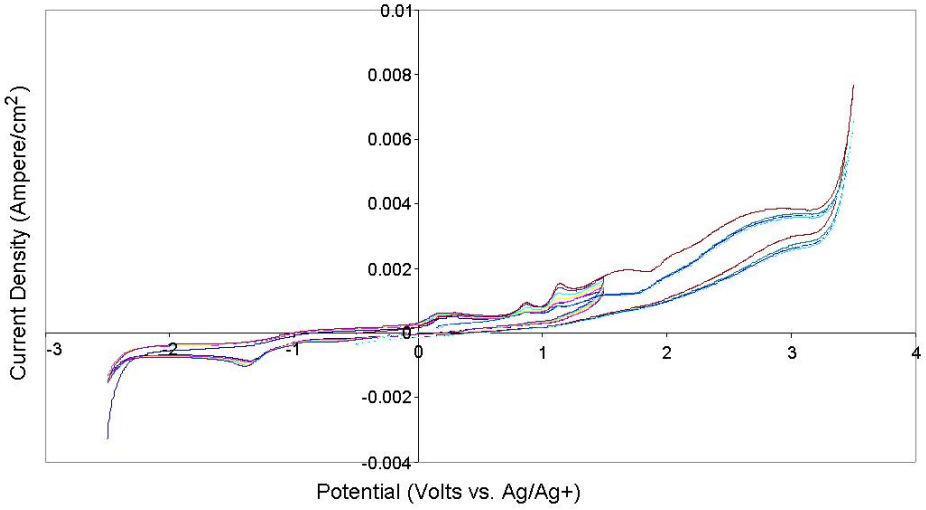

Figure 2.5: Cyclic voltammogram of 1 mM triethylamine decahydrodecaborate, $[(CH_3CH_2)_3NH]_2B_{10}H_{10}$, in anhydrous acetonitrile with 0.05 M TBA-PF_6 supporting electrolyte. WE = 0.5 mm Pt disk (area = 0.00196 cm_2), CE = 2 mm Pt disk, RE = anhydrous Ag/Ag+ (+0.637 V vs. NHE). Scan rate = 100 mV/s.

The two oxidation peaks just below and above +1 volt form as hydrogen [1,4,6] is released, and we would expect to see a conjugate reduction peak for the hydrogenation reaction. The reduction peak near -1.3 volts was suspected to be the conjugate to one of the oxidation peaks, so further experiments were performed by changing the initial and switching potentials of the cyclic voltammograms.

Beginning with a fresh solution of triethylamine decahydrodecaborate, we collected CV data in the region of the reduction peak alone to determine if this peak is absent before the oxidation peaks are reached, see Figure 2.6.

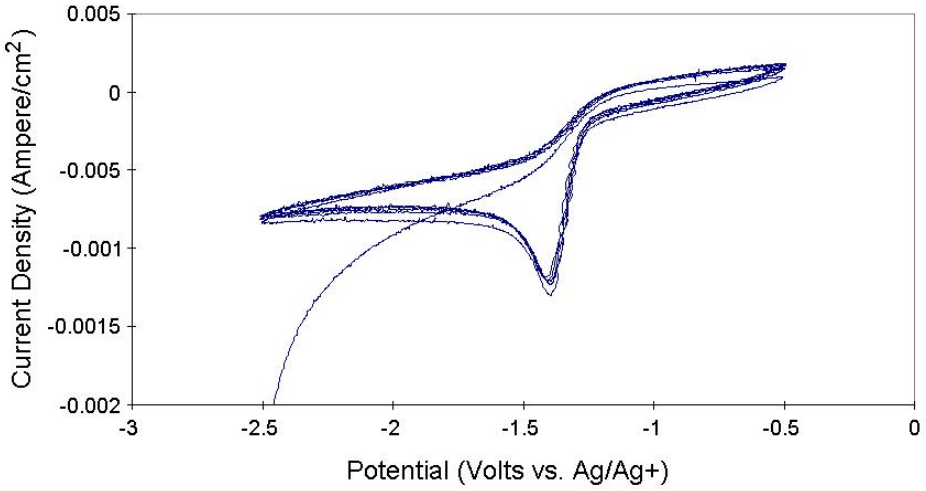

Figure 2.6: Cyclic voltammogram of 1 mM triethylamine decahydrodecaborate, $[(CH_3CH_2)_3NH]_2B_{10}H_{10}$, in anhydrous acetonitrile with 0.05 M $TBAPF_6$ supporting electrolyte. WE = 0.5 mm Pt disk (area = 0.00196 cm_2), CE = 2 mm Pt disk, RE = anhydrous Ag/Ag+ (+0.637 V vs. NHE). Scan rate = 100 mV/s.

We discovered that the reduction peak was in fact present after cycling the potential only in the region of the reduction peak; therefore, we conclude that the supplied polyborane salt contains some impurity that is able to be reduced electrochemically.

The study of the two oxidation peaks was more straightforward because there are no conjugate reduction peaks near to the potential region of the oxidation peaks – this indicates that the oxidation of the decahydrodecaborate dianion is irreversible. By starting the cyclic voltammogram at a potential value that is between the two oxidation peaks and then sweeping the potential higher to the anodic limit, we found that the more anodic peak (more positive potential)

is not present, which indicates that the more anodic peak is due to a species that is formed by the lower potential value oxidation peak.

As indicated in References 1 and 2, the behavior of decahydrodecaborate dianion ($B_{10}H_{10}^{2-}$) is paralleled by that of the dodecahydrododecaborate dianion ($B_{12}H_{12}^{2-}$), so that it was decided to examine the $B_{12}H_{12}$ salts again in more detail.

By switching from the silver/silver ion reference electrode to a plain silver wire pseudo reference electrode we were able to collect cyclic voltammogram data at higher potential sweep rates. When using the silver/silver ion reference electrode, the internal impedance of the reference electrode was sufficiently high to limit the potential sweep rate to no more than 100 mV/s, however the sweep rate was able to reach 2500 mV/s when using the silver wire pseudo reference electrode. The only drawback of using a pseudo reference electrode is that potential values recorded are not able to be directly corrected to any standard potential scale, such as the standard hydrogen electrode scale. Therefore, each set of data then needs to be collected twice – the first set is collected as usual, but the second set has a small amount of a known redox couple added to the test solution. Such redox couples are then used as an internal standard to adjust the potential scale after the data has been collected. In this work, ferrocene and ferrocenemethanol were used with the choice of which one to use depending on the solubility of the compound in the solvent being used for the sample under study.

In Figure 2.7 we see the CV of triethylamine dodecahydrododecaborate, $[(CH_3CH_2)_3NH]_2B_{12}H_{12}$, in which the more anodic oxidation peak is now slightly suppressed.

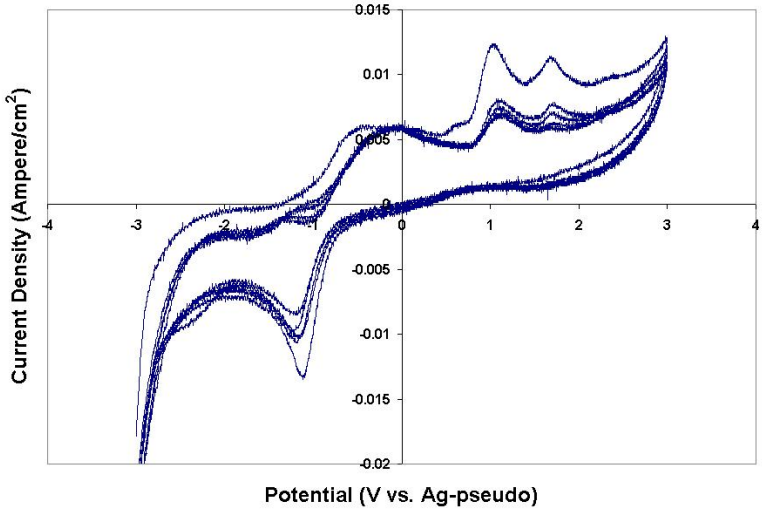

Figure 2.7: Cyclic voltammogram of 9.49mM $[Et_3NH]_2B_{12}H_{12}$ cyclic voltammetry in acetonitrile with 0.1 M $TBAPF_6$ as a supporting electrolyte. WE = 1 mm Pt disk, CE = 2 mm Pt disk, RE = Ag (pseudo). Sweep rate = 1000 mV/sec.

The reason for the lowering of the second oxidation peak current is because as the potential is scanned very quickly past the lower potential value oxidation peak there is not sufficient time to form as much of the reaction product that is then oxidized a second time at the higher potential valued peak. This indicated that the chemical step that is coupled between the two electrochemical steps has a small reaction rate constant.

In addition to the triethylamine dodecahydrododecaborate, we also studied the potassium salt, $K_2B_{12}H_{12}$, in the same manner. This time, however, the results were drastically different as seen in Figure 2.8.

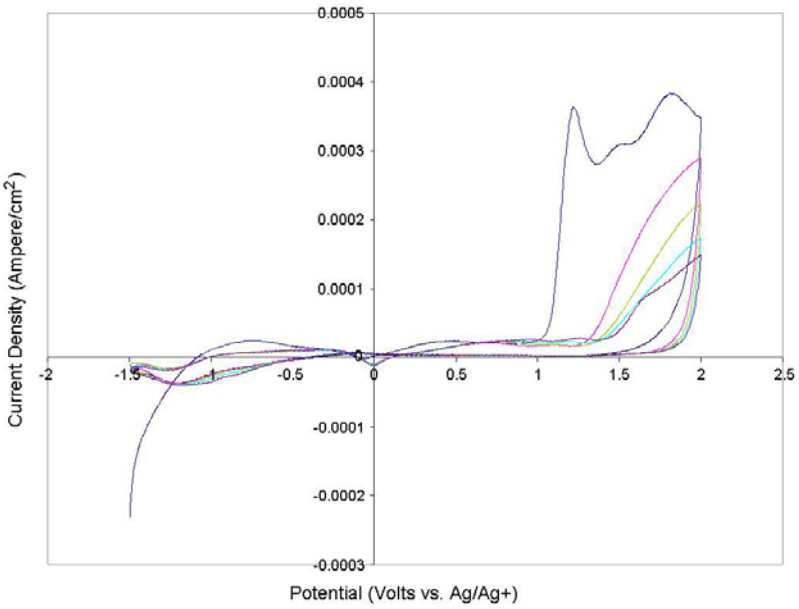

Figure 2.8: Cyclic voltammogram of 1 mM $K_2B_{12}H_{12}$ in anhydrous acetonitrile without supporting electrolyte. The background current density was subtracted. Scan rate = 50 mV/s, WE = 0.5 mm Pt disk, CE = 2 mm Pt disk, RE = anhydrous Ag/Ag+ (+0.637 V vs. NHE).

We can see in Figure 2.8 that the first sweep of potential in the cyclic voltammogram results in the usual oxidation peaks, but we notice that the current decreases for each subsequent cycle. This demonstrates the importance of the cation type that is used for the polyborane salts because in this case, for the potassium cation, the working electrode was being coated with a film as the experiments were taking place. We expect this is a similar problem as that shown above in Figure 2.4.

2.4 Effect of Working Electrode Material and Potential Sweep Rate

One problem that was present throughout the study of the polyboranes was the fact that the data looked different when collected on different working electrode materials. Although this is to be expected to a certain degree, the two materials used here were either platinum or gold – both of which are used extensively in the field of electrochemistry for being inert, i.e. they do not take part in electrochemical reactions as a general rule but rather they are simply the source/sink of electrons at the electrode surface.

In Figures 2.9 through 2.14 we see the cyclic voltammograms of 1 mM $[Et_3NH]_2B_{12}H_{12}$ in acetonitrile with 0.1 M TBA-PF_6 supporting electrolyte as the potential sweep rate is varied. For these Figures, the working electrode is a 0.5 mm platinum disk, the counter electrode is a 2 mm platinum disk, and the reference electrode is a silver wire pseudo reference electrode. Note that in Figures 2.9 through 2.14 the current density axis scale and the potential axis scale are the same for each Figure so that the effect of sweep rate is more obvious.

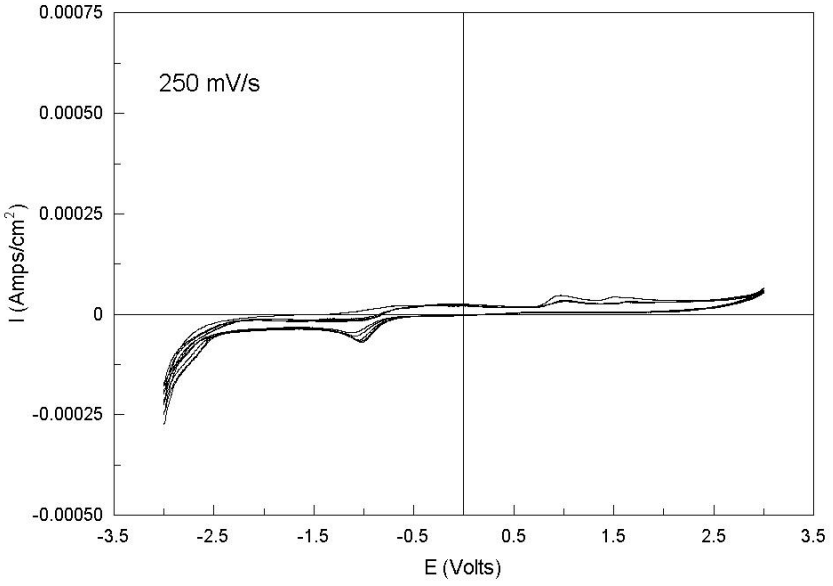

Figure 2.9: Cyclic voltammogram of 1 mM $[Et_3NH]_2B_{12}H_{12}$ in anhydrous acetonitrile with 0.1 M TBA-PF_6 supporting electrolyte. Scan rate = 250 mV/s, WE = 0.5 mm Pt disk, CE = 2 mm Pt disk, RE = silver wire pseudo reference electrode.

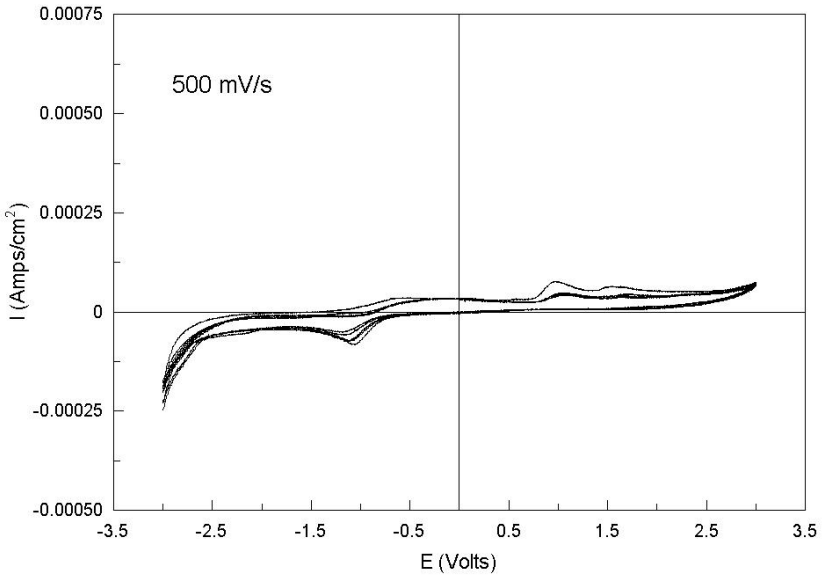

Figure 2.10: Cyclic voltammogram of 1 mM $[Et_3NH]_2B_{12}H_{12}$ in anhydrous acetonitrile with 0.1 M TBA-PF_6 supporting electrolyte. Scan rate = 500 mV/s, WE = 0.5 mm Pt disk, CE = 2 mm Pt disk, RE = silver wire pseudo reference electrode.

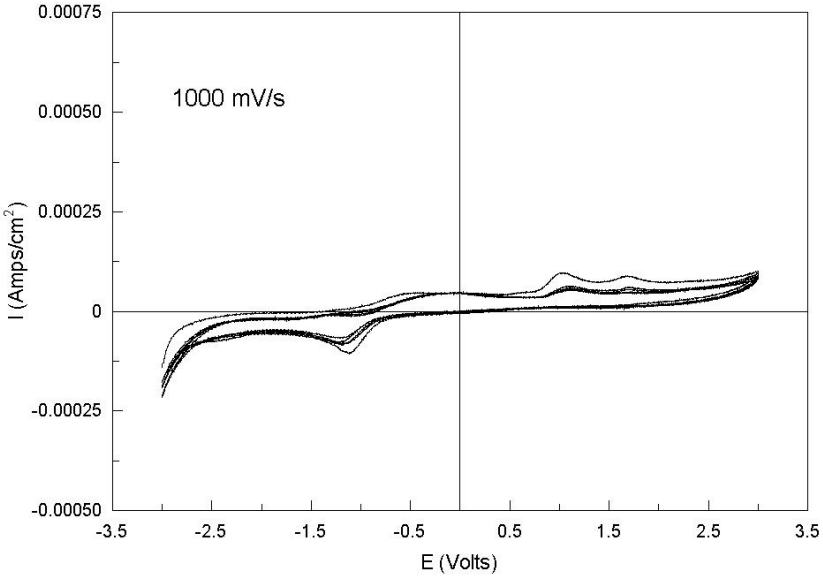

Figure 2.11: Cyclic voltammogram of 1 mM $[Et_3NH]_2B_{12}H_{12}$ in anhydrous acetonitrile with 0.1 M TBA-PF_6 supporting electrolyte. Scan rate = 1000 mV/s, WE = 0.5 mm Pt disk, CE = 2 mm Pt disk, RE = silver wire pseudo reference electrode.

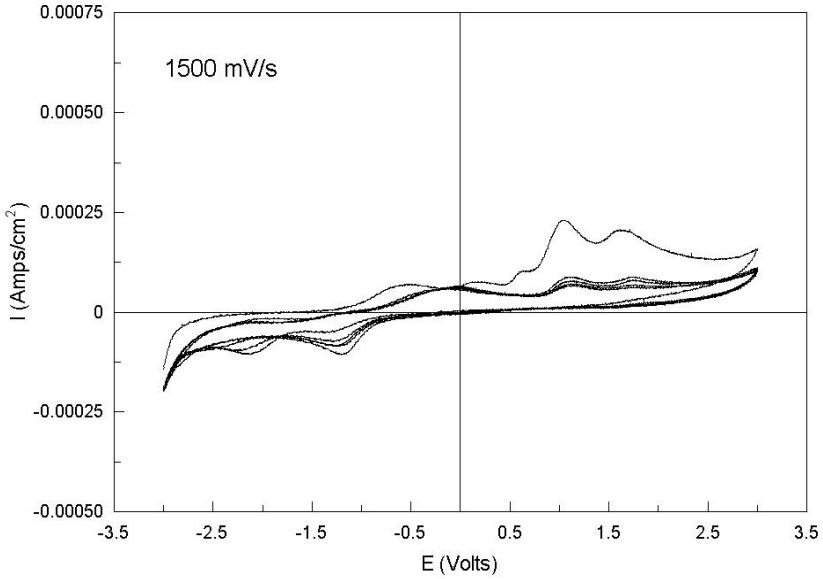

Figure 2.12: Cyclic voltammogram of 1 mM $[Et_3NH]_2B_{12}H_{12}$ in anhydrous acetonitrile with 0.1 M TBA-PF_6 supporting electrolyte. Scan rate = 1500 mV/s, WE = 0.5 mm Pt disk, CE = 2 mm Pt disk, RE = silver wire pseudo reference electrode.

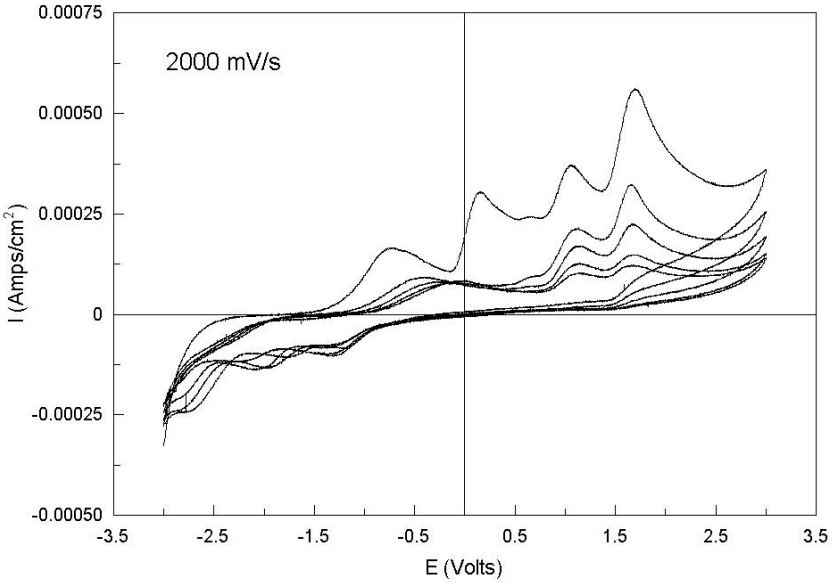

Figure 2.13: Cyclic voltammogram of 1 mM $[Et_3NH]_2B_{12}H_{12}$ in anhydrous acetonitrile with 0.1 M TBA-PF_6 supporting electrolyte. Scan rate = 2000 mV/s, WE = 0.5 mm Pt disk, CE = 2 mm Pt disk, RE = silver wire pseudo reference electrode.

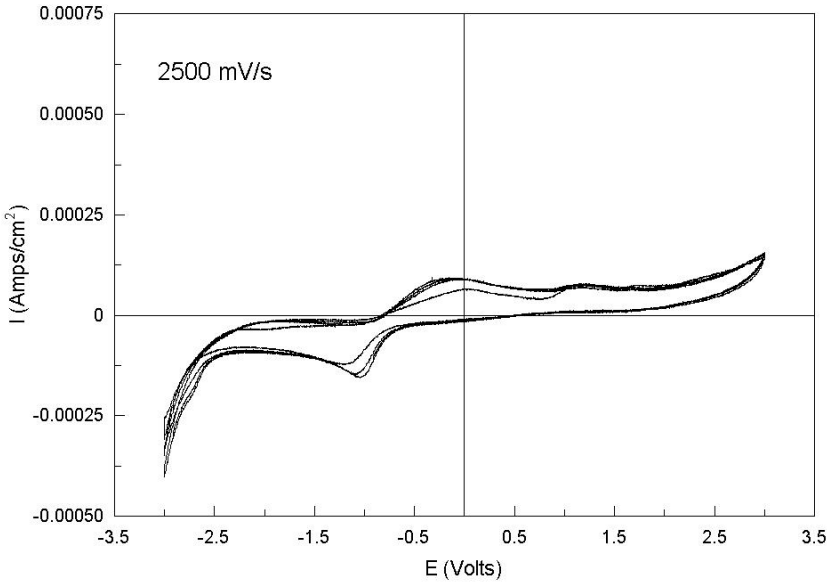

Figure 2.14: Cyclic voltammogram of 1 mM $[Et_3NH]_2B_{12}H_{12}$ in anhydrous acetonitrile with 0.1 M TBA-PF_6 supporting electrolyte. Scan rate = 2500 mV/s, WE = 0.5 mm Pt disk, CE = 2 mm Pt disk, RE = silver wire pseudo reference electrode.

In Figures 2.9 through 2.14, we notice that the potential sweep rate plays an important role in the electrochemical reactions that take place. For example, if the potential sweep rate was not varied while studying the polyboranes, then it would be possible to incorrectly assume that the samples were not electroactive – this is the case for extremely slow and extremely fast sweep rates (not shown) that are less than 50 mV/s or greater than 2500 mV/s. We can see through this series of experiments that the electroactivity increases as the sweep rate increases, but this trend only holds up to about 2000 mV/s after which it appears that the sweep rate is so fast that the electron transfer cannot proceed fast enough to oxidize the polyborane dianion. The reason for the large amount of electroactivity in Figure 2.13 is not known, but we hypothesize that the sweep rate of ~2000 mV/s is at a sufficient rate to activate certain oxidation reactions that are not seen at slower sweep rates. The complex electrochemical behavior as shown in Figures 2.9 through 2.14 has not been reported in the literature before and as such we must point out that our exploratory work indicates that the polyborane electrochemistry is not fully understood.

On the other hand, in Figures 2.15 through 2.20 we see the cyclic voltammograms of 1 mM $[Et_3NH]_2B_{12}H_{12}$ in acetonitrile with 0.1 M TBA-PF_6 supporting electrolyte as the potential sweep rate is varied; however, for these Figures the only difference is that the working electrode has been changed to a 0.5 mm gold disk rather than the platinum disk as before. The counter electrode is still a 2 mm Pt disk, and the reference electrode is once again a silver wire pseudo reference electrode. Note that in Figures 2.15 through 2.20 the current density axis scale and the potential axis scale are the same for each Figure (although they are different from Figures 2.9 through 2.14) so that the effect of sweep rate is more obvious.

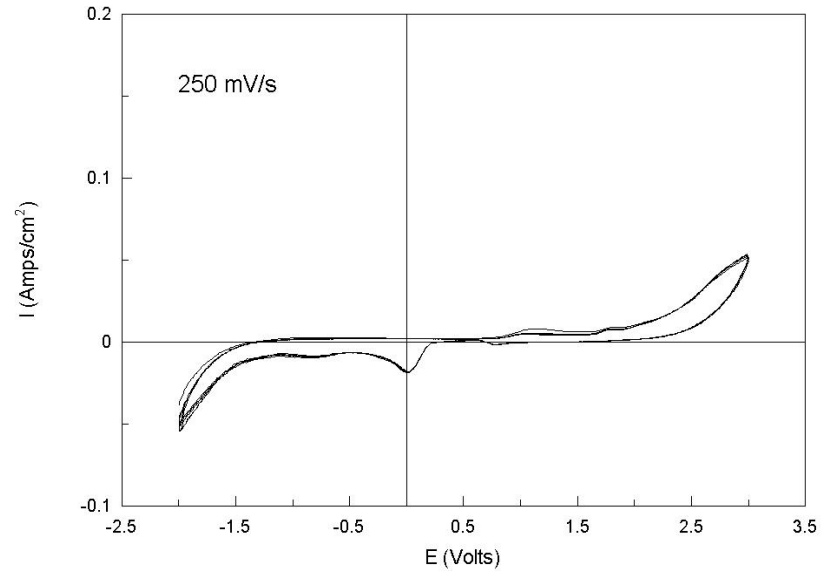

Figure 2.15: Cyclic voltammogram of 1 mM $[Et_3NH]_2B_{12}H_{12}$ in anhydrous acetonitrile with 0.1 M TBA-PF_6 supporting electrolyte. Scan rate = 250 mV/s, WE = 0.5 mm Au disk, CE = 2 mm Pt disk, RE = silver wire pseudo reference electrode.

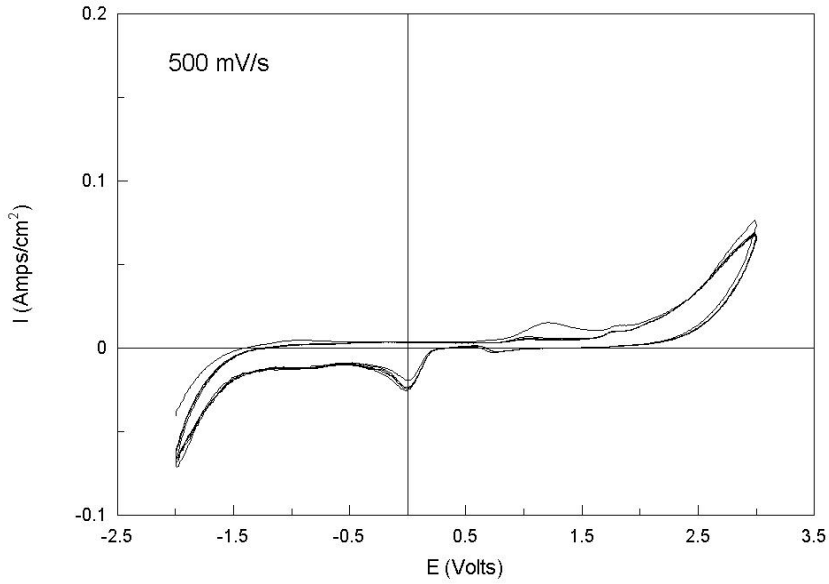

Figure 2.16: Cyclic voltammogram of 1 mM $[Et_3NH]_2B_{12}H_{12}$ in anhydrous acetonitrile with 0.1 M TBA-PF_6 supporting electrolyte. Scan rate = 500 mV/s, WE = 0.5 mm Au disk, CE = 2 mm Pt disk, RE = silver wire pseudo reference electrode.

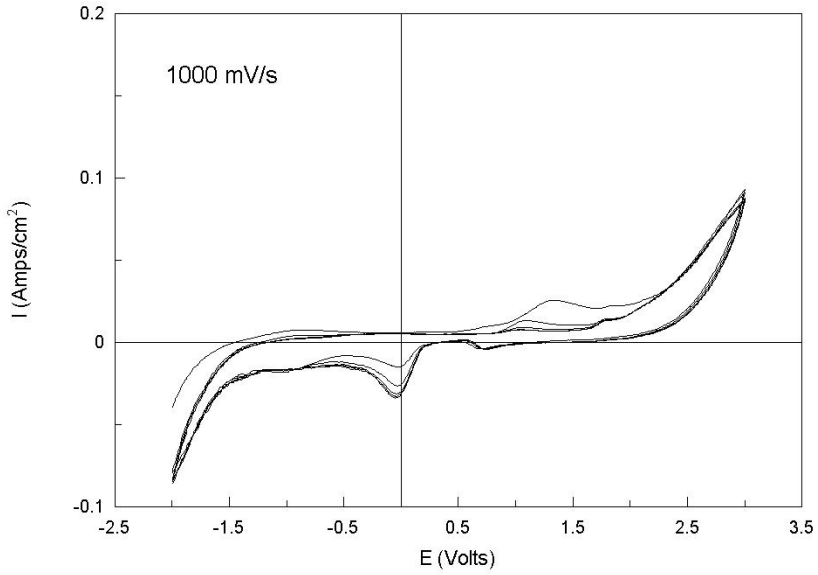

Figure 2.17: Cyclic voltammogram of 1 mM $[Et_3NH]_2B_{12}H_{12}$ in anhydrous acetonitrile with 0.1 M TBA-PF_6 supporting electrolyte. Scan rate = 1000 mV/s, WE = 0.5 mm Au disk, CE = 2 mm Pt disk, RE = silver wire pseudo reference electrode.

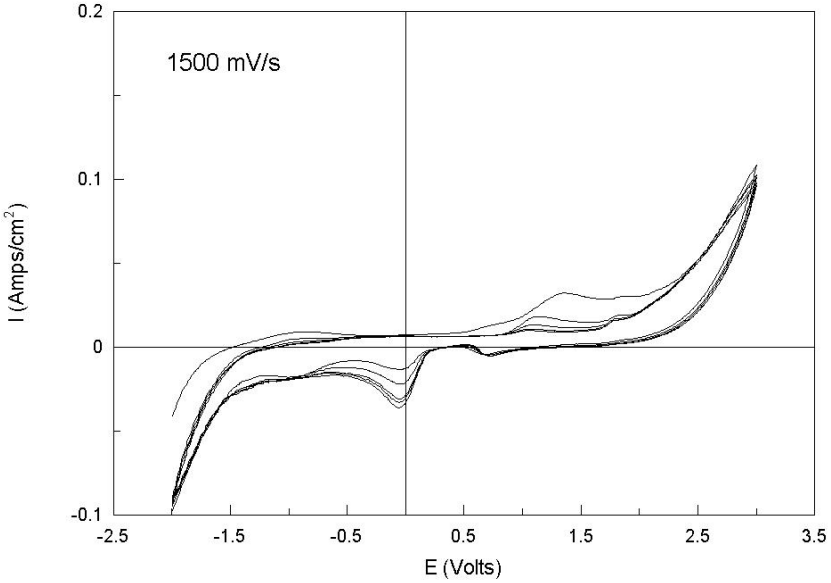

Figure 2.18: Cyclic voltammogram of 1 mM $[Et_3NH]_2B_{12}H_{12}$ in anhydrous acetonitrile with 0.1 M TBA-PF_6 supporting electrolyte. Scan rate = 1500 mV/s, WE = 0.5 mm Au disk, CE = 2 mm Pt disk, RE = silver wire pseudo reference electrode.

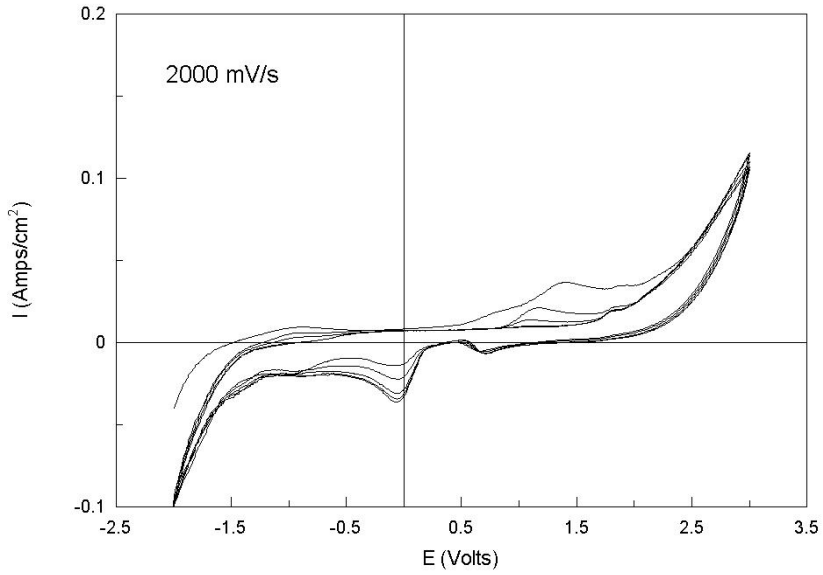

Figure 2.19: Cyclic voltammogram of 1 mM $[Et_3NH]_2B_{12}H_{12}$ in anhydrous acetonitrile with 0.1 M TBA-PF_6 supporting electrolyte. Scan rate = 2000 mV/s, WE = 0.5 mm Au disk, CE = 2 mm Pt disk, RE = silver wire pseudo reference electrode.

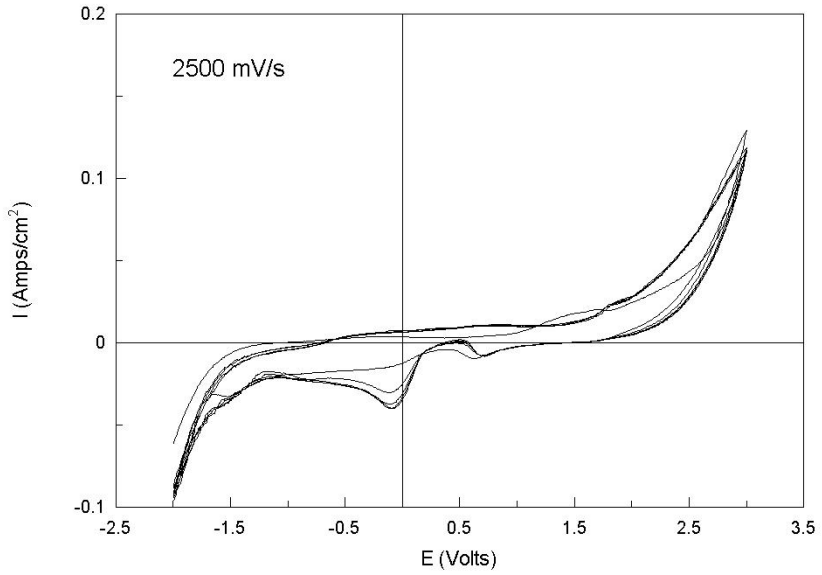

Figure 2.20: Cyclic voltammogram of 1 mM $[Et_3NH]_2B_{12}H_{12}$ in anhydrous acetonitrile with 0.1 M TBA-PF_6 supporting electrolyte. Scan rate = 2500 mV/s, WE = 0.5 mm Au disk, CE = 2 mm Pt disk, RE = silver wire pseudo reference electrode.

As seen in Figures 2.15 through 2.20, the electroactivity of the polyborane sample on the gold working electrode is much less than what was shown on a platinum working electrode in Figures 2.9 through 2.14. As a result of these experiments, we have shown that the complex electrochemical behavior of the polyboranes can also be attributed to the nature of the working electrode material.

2.5 Conclusions

The complex electrochemistry of the polyhedral borane dianions $B_{10}H_{10}^{2-}$ and $B_{12}H_{12}^{2-}$ has been investigated in depth for the first time in our laboratory and we proposed that these anions are potential hydrogen storage systems from both gravimetric and volumetric standpoints.

After verifying that 0.100 M TBA-PF_6 in acetonitrile is a suitable blank solution with a wide potential range available, we studied solutions with low concentrations of polyboranes. The cause of the oxidation wave moving toward higher potential and current density values for the solution of 1 mM triethylamine dodecahydrododecaborate ($[(CH_3CH_2)_3NH]_2B_{12}H_{12}$) is unknown at present, but it is possible that the potential moves to higher values because on each cycle another hydrogen is removed from the polyborane cage, thus making it more difficult on successive cycles to remove further hydrogen atoms from the cage.

Once the potassium cations of $K_2B_{12}H_{12}$•CH_3OH were exchanged to tetra-*n*-butylammonium, the resulting dodecahydrododecaborate salt (not containing methanol) exhibits approximately a 100-fold increase in solubility in acetonitrile, allowing for a wider range of concentrations to be studied. We notice that at low concentrations (1 mM in this case) the oxidation features are more wave-like, however at higher concentrations (such as 10 mM shown in Figure 2.4) the oxidation features become much more prevalent with a new peak present that was not noticed at lower concentrations. The entities that are oxidized within the 1 – 2 V region during the first cycle apparently inhibit further oxidation during subsequent cycles.

In addition, we have shown for the first time that the sweep rate and the working electrode material are important factors to consider when studying polyhedral boranes. The complex electrochemical reactions that occur are not fully understood, although as we have proposed it appears that the oxidation mechanism is a coupled ECE reaction path. In this ECE reaction, the first electrochemical step is the oxidation of the initial polyborane dianion, the product of this reaction is then able to dimerize in a chemical reaction step, and finally as the dimerized product is electrochemically oxidized we notice the second, more anodic oxidation peak.

The reduction peak that is observed throughout the cyclic voltammograms for the polyborane samples was shown to be present prior to any oxidation reactions, and therefore we conclude that it is due to an electroactive impurity in the samples. Because there are no conjugate

reduction features present for the polyboranes in our exploratory experiments we therefore report that the oxidation reaction products follow an irreversible mechanism. Finally, we conclude that the polyboranes are not desirable materials for hydrogen storage after all because no hydrogenation (reduction) takes place that would allow for a closed-loop for the fuel life cycle.

2.6 References

1. R. L. Middaugh and F. Farha, Jr., *J. Am. Chem. Soc.*, **88**, 4147 (1966).
2. R. J. Wiersema and R. L. Middaugh, *J. Am. Chem. Soc.*, **89**, 5078 (1967).
3. J. Q. Chambers et al, *J. Am. Chem. Soc.*, **90**, 6056 (1968).
4. R. J. Wiersema and R. L. Middaugh, *J. Am. Chem. Soc.*, **92**, 223 (1970).
5. R. L. Middaugh and R. J. Wiersema, *Inorg. Chem.*, **10**, 423 (1971).
6. A. P. Schmitt and R. L. Middaugh, *Inorg. Chem.*, **13**, 163, (1974).
7. H. Horáková, B. Grüner, and R. Vespalec, *J. Chromatogr. A*, **1051**, 227 (2004).
8. D. D. Macdonald, *Transient Techniques in Electrochemistry*, Plenum Press, NY (1977).
9. F. Li, K. Shelly, C. B. Knobler, and M. F. Hawthorne, *Angew. Chem. Int. Ed.*, **37**, 1868 (1998).
10. M. F. Hawthorne, R. L. Pilling, and P. F. Stokely, *J. Am. Chem. Soc.*, **87**, 1893 (1965).
11. A. R. Pitochelli, W. N. Lipscomb, and M. F. Hawthorne, *J. Am. Chem. Soc.*, **84**, 3026 (1962).
12. B. L. Chamberland and E. L. Muetterties, *Inorg. Chem.*, **3**, 1450 (1964).
13. K. Neigh, BASF Chemist – Boron Hydride Division, private communication.

3. Ammonia Borane and Organotin Hydrides

3.1 Introduction

The U.S. Department of Energy (DOE) has set a target gravimetric capacity of materials such that they must exceed 7 wt% with the potential to exceed 9 wt% to meet future storage targets. Because the polyborane salts were not promising to the DOE, another material was sought after that would meet the target requirements. One such material is ammonia borane (H_3BNH_3), which has been shown by our partners at the University of Pennsylvania [1] to be able to release between 7.2 - 10.2% hydrogen by weight even though it's theoretical limit for hydrogen release is 19.6 wt%. The reason that the current hydrogen release percent for ammonia borane (AB) is not pushed further toward its limit is because of the difficulty in regenerating the waste material back to a suitable fuel after dehydrogenation, which becomes more difficult as more hydrogen is released. The hydrogen release process below 100°C initially involves the formation of the diammoniate of diborane $[(NH_3)_2BH_2^+]BH_4^-$, then a mixture of linear, cyclic, and chain-branched polyamimoborane polymers $[-H_2NBH_2-]_n$ is formed, and upon further dehydrogenation, the unsaturated product boron nitride (BN) is expected to be formed [2].

There are two ways in which attempts were made to electrochemically recycle (hydrogenate) the spent ammonia borane waste back to the fuel, these will be discussed below.

3.2 Experimental Approach

In order to hydrogenate the spent ammonia borane fuel, we can either directly or indirectly reduce the material by electrochemical means. The direct path to electrochemical reduction depends upon the particular waste material, but to date we have not been supplied with any spent fuel materials from our project partners so we began by investigating the general electrochemical properties of ammonia borane.

Because ammonia borane is soluble in aqueous and nonaqueous solvents, we were able to exploit the ability of nonaqueous solvents to achieve a more cathodic potential limit than in aqueous solutions. The ability to reach lower cathodic limits enables us to detect reduction (hydrogenation) features that would not be possible in aqueous solutions. The only drawback to working in nonaqueous solvents, as mentioned before, is that the use of a common (store bought) reference electrode such as the saturated calomel electrode (SCE) is not possible because they are aqueous in nature and form an unknown liquid junction potential when used in nonaqueous solvents. To overcome this problem, we have developed a new reference electrode that can be used directly in nonaqueous solvents as described below.

3.3 Development of a Nonaqueous Reference Electrode

We first attempted to use a nonaqueous reference electrode based on the metal/polypyrrole quasi-reference electrode [3]. This electrode is suitable for cyclic voltammetry; however, it is not suitable for steady state techniques such as controlled potential electrolysis or electrochemical impedance spectroscopy in the same way as other pseudo reference electrodes behave. In addition, the metal/polypyrrole reference electrode is not suitable for strongly oxidizing or reducing media [3], and although ammonia borane is known to have slightly hydridic and slightly acidic hydrogen atoms we must address this issue after the electrode has been constructed to determine if this will be a problem.

Because we initially wanted to use cyclic voltammetry to study the electrochemistry of ammonia borane, we proceeded to build the metal/polypyrrole reference electrode as outlined in Reference 3 and summarized below.

The body of the metal/polypyrrole reference electrode can be made of any metal although it is recommended to use platinum or stainless steel [3]. For our electrode, we used a 5 cm length of type 316 stainless steel with a diameter of 1/16" and attached it to a length of copper rod to extend the overall length to 15 cm (the copper rod is the external electrical connection). The junction between the stainless steel and copper rods was insulated by PTFE shrink tube and the whole assembly was potted into chemically inert epoxy. The PTFE shrink tube was adjusted so that only 1 cm of the stainless steel rod was left exposed. After the epoxy for the electrode body was cured, the exposed portion of the stainless steel rod was immersed into a solution of 0.01 M pyrrole and 0.1 MTBA-PF_6 in acetonitrile. The polymerization of the pyrrole onto the stainless steel rod was performed in a three-electrode electrochemical cell with the stainless steel rod acting as the working electrode; a graphite rod was used as the counter electrode and a silver/silver ion reference electrode completed the cell. The electropolymerization occurs as the stainless steel working electrode is cycled 50 times through the redox region of pyrrole at a scan rate of 0.1 V/s. The polypyrrole (PPy) film grows thicker upon each cycle and the stainless steel rod is then removed on the final cycle so that the film is only partially oxidized so that the film is $PPy/PPy^{+}PF_6^{-}$ [3].

The newly fabricated metal/polypyrrole reference electrode was then characterized as outlined in [3] by examining a solution of ferrocenemethanol as a known redox couple and treating its oxidation peak potential on a gold working electrode as a standard for calibrating our metal/polypyrrole reference electrode. We found that the potential of the stainless steel/polypyrrole reference electrode was -0.208 V versus SHE.

As mentioned above, the metal/polypyrrole reference electrode is not suitable for controlled potential electrolysis or electrochemical impedance spectroscopy, so a different type of nonaqueous reference electrode based on the silver/silver chloride redox couple was designed for later use. This design was discussed in depth by McLafferty [4], but it will be summarized below. As a note to the reader, Jason McLafferty [4] was a fellow graduate student working on

the same project so this reference electrode was fabricated and characterized by McLafferty and the author simultaneously.

The construction of a nonaqueous silver/silver chloride reference electrode has been attempted with little success in the past [5]. The reason for this is because the silver chloride layer that is deposited onto a silver wire within the reference electrode body is known to dissolve in chloride-containing aprotic solvents, and the filling solution for the silver/silver chloride reference electrode by definition contains chloride so dissolution of silver chloride is inevitable. To get around the problem of silver chloride dissolution in the reference electrode filling solution [4], a sufficient amount of trimethylethylammonium chloride and silver chloride were added to obtain a saturated solution, which also contained 0.1 M TBA-PF_6 in acetonitrile. The addition of trimethylethylammonium chloride enables the formation of an equilibrium between the silver chloride layer on the silver wire and the free chloride ions in the filling solution.

In addition to the filling solution, we also needed to design the body of the nonaqueous silver/silver chloride reference electrode in such a way as to eliminate any leaking of the filling solution through the porous liquid junction. The primary reason why this is so important is to eliminate contamination of the test solution by the reference electrode filling solution, but it is also important because standard frit materials such as zirconia ceramic or porous Vycor glass have high leak rates and require frequent refilling of the reference electrode filling solution.

To address the problem of the porous liquid junction frit, we designed [4] our reference electrode body in such a way as to incorporate a layer of anion exchange polymer within the porous frit material, thereby allowing electronic conduction across the liquid junction and yet eliminating bulk flow of filling solution through the frit and into the test solution. For this task, we chose to use a cross-linked poly (4-vinylpyridine) polymer layer as described below [4]:

> "A 25% w/w solution of poly (4-vinylpyridine) (Sigma Aldrich, average molecular weight 60,000) in methanol was prepared. Two grams of this solution, containing 0.5 grams of poly (4-vinylpyridine) were stirred with 0.026g of 1,4-dichlorobutane [the cross-linking agent] for one hour in a closed glass vial. A 4 mm diameter zirconia frit was attached to a 5mm outer diameter glass tube with PTFE heat shrink tubing. The mixture of poly (4-vinylpyridine), methanol, and 1,4-dichlorobutane was applied over the frit using a Pasteur pipette; the thickness of the layer was about 5-6 mm. The tube was left open overnight on the bench top, to evaporate the methanol. The next day, the above assembly was heated at 110^{o}C in an oven for 5 hours, 20 minutes. After cooling, acetonitrile was placed in the tube and the open end of the tube was closed with parafilm to check for leaks. After leaving overnight, no leaks were found, and the tube was emptied of the acetonitrile. The assembly was then filled with a solution of 0.1M TBAPF_6 in acetonitrile saturated with silver chloride and tetramethylammonium chloride".

The next step after fabrication of the new nonaqueous silver/silver chloride reference electrode was to determine its stability and calibrate it, so that potentials measured on it are able to be adjusted to an accepted potential scale, such as the standard hydrogen scale (SHE). By examining cyclic voltammetry data for the oxidation of ferrocene on a platinum working electrode in acetonitrile with 0.1 M TBA-PF_6 as supporting electrolyte, we conclude that the nonaqueous silver/silver chloride reference electrode has a potential that is +345 mV above the standard hydrogen electrode (SHE) potential.

3.4 Results and Discussion

We studied ammonia borane by cyclic voltammetry in both aqueous and nonaqueous solvents as shown in Figures 3.1 and 3.2 below.

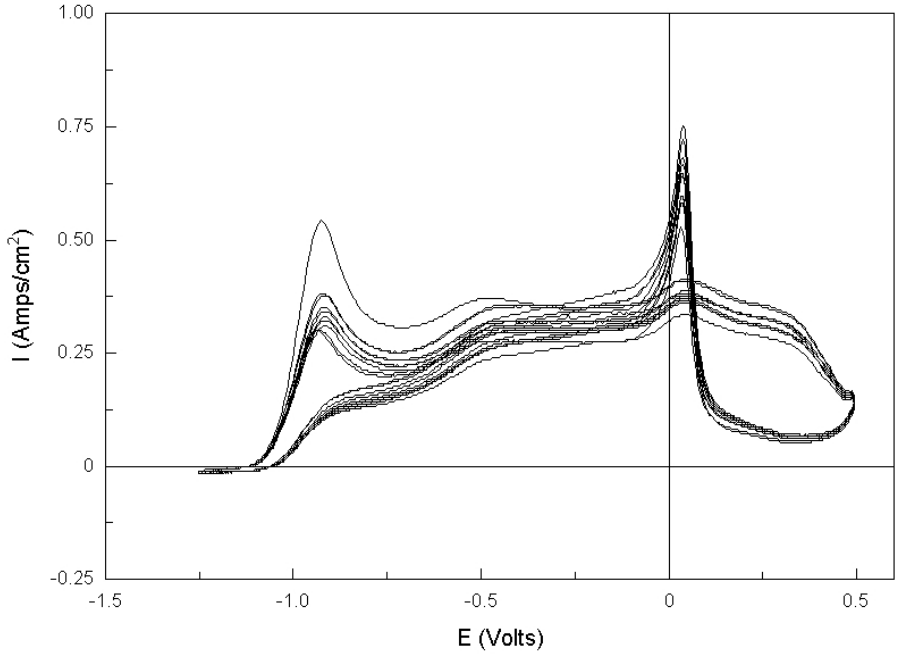

Figure 3.1: Electrochemical activity of 10 mM ammonia borane in aqueous 2 M sodium hydroxide. WE = 5 mm Au disk, CE = Pt mesh, RE = SCE. Scan rate = 50 mV/s. In this cyclic voltammogram the two peaks correspond oxidation reactions that take place on forward and reverse sweeps; no reduction peaks are observed that would indicate rehydrogenation of the newly created (oxidized) species. The oxidation peak near 0 Volts is because the gold working electrode becomes oxidized and it is then becoming active once again as the potential is swept toward more negative values.

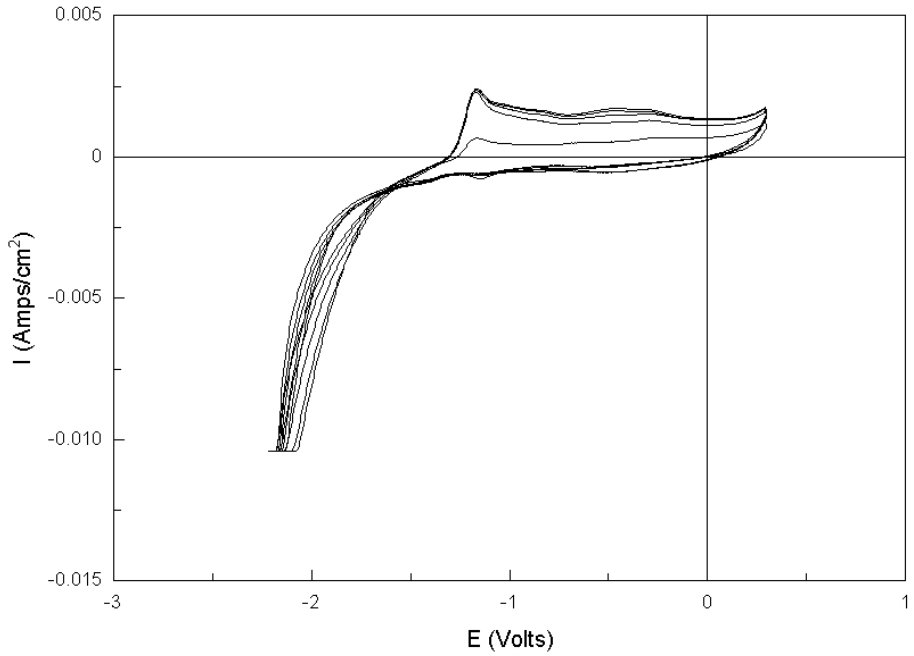

Figure 3.2: Electrochemical activity of 5 mM ammonia borane in 1:1 acetonitrile:dioxane with 0.1 M tetrabutylammonium hexafluorophosphate ($TBAPF_6$) as a supporting electrolyte. WE = 0.5 mm Pt disk, CE = 2 mm Pt disk, RE = Ag (pseudo). Scan rate = 100 mV/s. This cyclic voltammogram shows only one oxidation (dehydrogenation) peak without any subsequent reduction peaks. The feature near -2 volts is related to the discharge limit of the solvent and has nothing to do with the electrochemical behavior of the ammonia borane.

We can see from Figures 3.1 and 3.2 that ammonia borane exhibits oxidation peaks (removal of hydrogen), however we see no reduction peaks that would correspond to a direct path of hydrogenation. In Figure 3.1, the solvent is aqueous 2 M sodium hydroxide so if any reduction reactions were able to occur in the available potential window of the solvent, the solvent itself could act as the hydrogen source and donate the protons to the reduction reaction; however, the ammonia borane sample does not exhibit any reduction (hydrogenation) features.

Because of the limited cathodic potential limit that is available in aqueous solutions, we switched over to an organic solvent that allows for the cathodic potential limit to be extended at least one volt beyond that of aqueous solutions. The organic solvent that we chose to use was a 1:1 mixture of acetonitrile and dioxane; although the individual solvents are aprotic, this fact was taken into consideration by adding phenol (work done in conjunction with that of McLafferty in Reference 4) in some cases or by sparging hydrogen gas through the solution in other cases as a source of protons for any possible reduction reactions. Even though the cathodic limit was extended in the acetonitrile:dioxane mixture to nearly -2 volts, we still did not observe any reduction features indicative of a hydrogenation reaction.

Due to these results, the indirect reduction of spent ammonia borane back to a fuel has been looked upon by the DOE as the most likely reaction to succeed. The idea is to use a separate reducing agent to hydrogenate spent AB fuel at the cost of having to regenerate the auxiliary reducing agent. The reducing agent chosen by the DOE was an organotin hydride such as tributyltin hydride. Once the tributyltin hydride is used as a reducing agent to hydrogenate the ammonia borane spent fuel, it will be left as a tributyltin halide (most likely tributyltin chloride) so our task will then be to attempt to electrochemically reduce Bu_3SnCl back to Bu_3SnH. One possible reduction mechanism is as follows: $Bu_3SnCl + H + e^- \rightarrow Bu_3SnH + Cl^-$.

In order to accomplish this task, we used a Devanathan cell, because this provides a convenient source of hydrogen atoms on the surface of the working electrode. The Devanathan cell is shown below in Figure 3.3 where we can see the bi-polar membrane (Pd in the schematic) that is used as the working electrode for both sides of the cell; additionally we see two counter electrodes and the possibility to add a separator membrane on the reaction side, but the reference electrodes were omitted on each side for clarity.

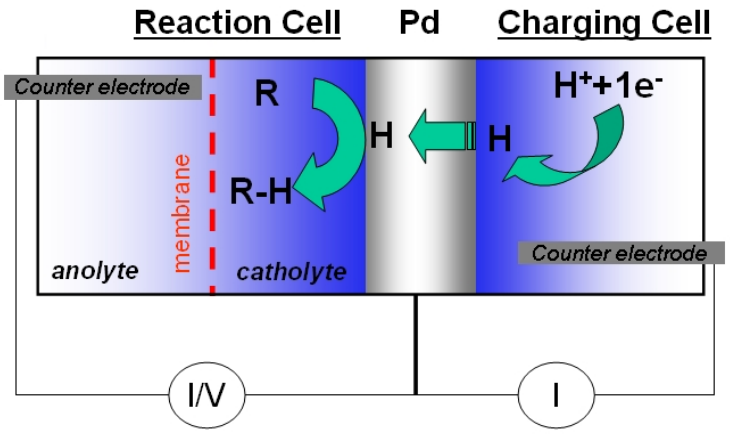

Figure 3.3: A schematic drawing of the Devanathan cell. The center membrane is a bi-polar electrode made from palladium or palladium:silver alloy. Counter electrodes complete the electrical circuits; however, the two reference electrodes have been omitted for clarity. A separator membrane can be added to the reaction side of the cell if the products are likely to be re-oxidized during the hydrogenation. The charging side is controlled galvanostatically (indicated by "I" in the circle) and the reaction side is controlled either potentiostatically or galvanostatically (indicated by "I/V" in the circle).

During the operation of the Devanathan cell, hydrogen atoms are produced in the charging side by the electrolysis of aqueous solutions (typically sulfuric acid or potassium hydroxide), the hydrogen then diffuses through the working electrode membrane, and it finally emerges on the other surface in the reaction side where it is used to reduce (hydrogenate) the species in solution on that side of the cell. Because the membrane for the working electrode is

made from palladium or palladium:silver alloy, the electrode surface is also catalytic so that chemical hydrogenation is possible along with electrochemical hydrogenation. The addition of palladium black to the palladium surface on the reaction side has been shown to increase the reactivity by up to 40 times [6] so that this was also used in these studies.

In order to test whether the Devanathan cell was operating properly, we attempted to hydrogenate styrene [7] as follows: $C_6H_5CH{=}CH_2 + 2H_{ads} \rightarrow C_6H_5CH_2CH_3$, in which styrene ($C_6H_5CH{=}CH_2$) reacts chemically with two adsorbed hydrogen atoms on the palladium/silver membrane to produce ethylbenzene ($C_6H_5CH_2CH_3$).

Each experiment began with a sample solution of styrene that was 50 mL in volume on the reaction (left) side of the Devanathan cell, and the charging side contained a solution of 6 M KOH that was approximately 100 mL in volume. Each solution was degassed with ultrahigh purity argon for 30 minutes prior to the start of the experiment, and the argon gas was allowed to remain flowing above the solutions so that evaporation was minimized and yet oxygen could be excluded continuously. Hydrogenation occurred after galvanostatic electrolysis of the KOH solution was started by applying a current density of -20 mA/cm^2 to the Pd:Ag membrane and using a platinum counter electrode to complete the circuit. The cell potential was monitored in time with a mercury/mercury oxide reference electrode.

The experiments were allowed to run for various times from one to six days. The results obtained by gas chromatography-mass spectrometry (GC-MS) indicate that the amount of ethylbenzene produced increases linearly with time and that the Coulombic efficiency is nearly constant for all experiments. The rate of ethylbenzene production is 2.90% per day and the Coulombic efficiency is ~79%. The results can be seen in Figure 3.4 below. These experiments clearly demonstrate the effectiveness of the Devanathan cell for hydrogenating unsaturated organic materials; the next task was to apply this technique to attempt the reduction of tributyltin chloride. Because tributyltin hydride might not be the only reaction product [8,9], we will identify the resulting species in the solution by cyclic voltammetry.

Although the reaction seems fairly straightforward for the reduction (hydrogenation) of tributyltin chloride, the results (not shown) indicate that the organotin halide cannot be directly hydrogenated in a common, undivided three-electrode electrochemical cell. We first determined whether cyclic voltammetry could distinguish the hydride apart from the halide form of the organotin compounds, and this is definitely the case as shown in Figure 3.5 where we see two oxidation peaks on the forward scan and one (larger peak current) oxidation feature on the reverse scan.

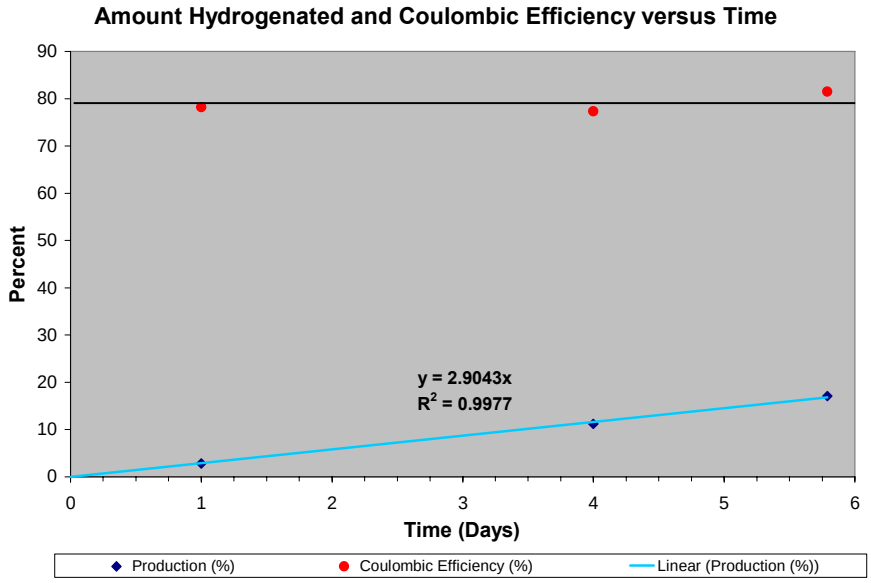

Figure 3.4: Experimental results for the hydrogenation of styrene using a Devanathan cell. The amount of ethylbenzene produced is shown in blue diamonds with a best-fit line shown in light blue indicating a rate of production of 2.90% per day. The Coulombic efficiency is shown in red dots with the average value (79%) shown as the black line.

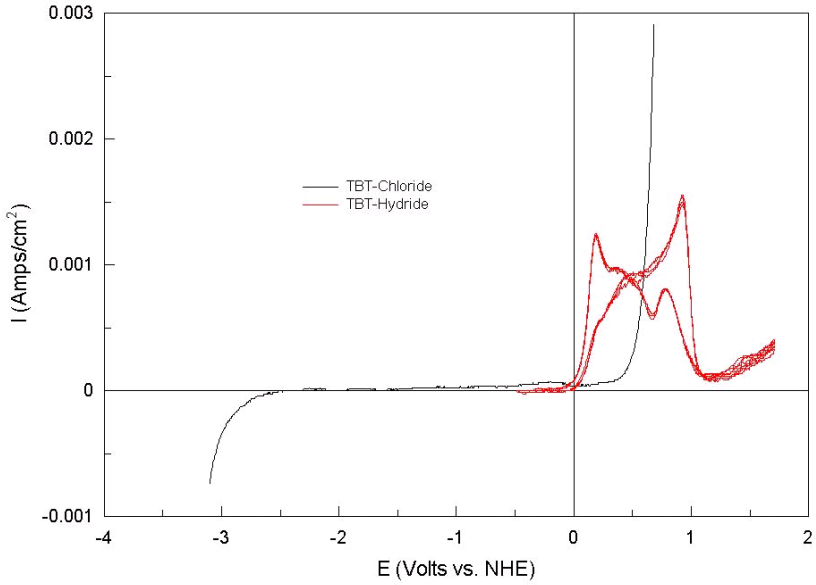

Figure 3.5: Cyclic voltammograms of tributyltin chloride (black line) and tributyltin hydride (red line) with 0.1 M TBA-PF_6 in acetonitrile. Working electrode = 5 mm gold disk, counter electrode = platinum wire (5 cm length), reference electrode = nonaqueous silver/silver chloride. Potential sweep rate = 50 mV/s.

The first oxidation peak near +0.18 V is attributed [8] to the oxidation of neutral tributyltin hydride to form the neutral radical species $Bu_3Sn^{\bullet}$. The radical species then has two options: (1) the radical can chemically dimerize to the hexabutylditin molecule, $Bu_3SnSnBu_3$, or (2) the radical can undergo an electrochemical oxidation at approximately +0.38 V to form the non-radical cation species, Bu_3Sn^+. The final oxidation around +0.78 V is due to the electrochemical oxidation of hexabutylditin, which forms the non-radical cation species, Bu_3Sn^+, once again. On the reverse sweep of the cyclic voltammogram in Figure 3.5 we see a single, larger oxidation peak. This peak is attributed to the reactivation of the gold working electrode, because as it is swept to the anodic limit the gold surface becomes oxidized and this peak simply indicates the removal of the surface oxide.

Now that we know that it is possible to differentiate between the tributyltin hydride and the tributyltin chloride, the next step was to attempt the electrochemical reduction (hydrogenation) process of the organotin halide in the Devanathan cell. The problem in this case is that the experiments take many hours to perform, and as such the applied potential to the Devanathan cell was found to drift in time due to a slightly unstable nonaqueous reference electrode in the reaction solution (its own potential drifts slowly with time so any applied potential will likewise drift in time). As a result, we were unable to conclusively determine whether the Devanathan cell is a viable option for the electrochemical hydrogenation of organotin halides.

An analysis of the solutions that were reacted in the Devanathan cell, even though the reference electrode was not fully stable in time, revealed that no organotin hydride was formed even for positive control solutions where an initial quantity of organotin hydride was spiked into the reaction solution (so at the very least we expect to see the initial quantity of organotin hydride after the Devanathan cell electrolysis). The results of a 24 hour electrochemical reduction at -2.3 V of a solution of 0.05 M tributyltin chloride, 1 mM tributyltin hydride (the initial spike), and 0.1 M TBA-PF_6 as the supporting electrolyte in acetonitrile are shown in Figure 3.6.

As we see in Figure 3.6, the results after 24 hours of electrolysis at -2.3 V in the Devanathan cell indicate that even the initial quantity of tributyltin hydride is absent. These results point toward two explanations: either (1) the applied potential of the working electrode has drifted far enough to oxidize any organotin hydride that is present, or (2) any organotin hydride that is formed is then consumed at the counter electrode of the Devanathan cell. The former issue could only be solved by the development of a more stable nonaqueous reference electrode. The latter issue could be addressed by utilizing a three-part Devanathan cell where the reaction side is separated into two parts rather than just one part as in our studies. The only downfall to this would be the additional potential loss across the separating membrane, which in the case of organic solutions that have poor conductivity could lead to potentials that might exceed the discharge potential of the solvent or the applied potential/current output of the potentiostat/galvanostat.

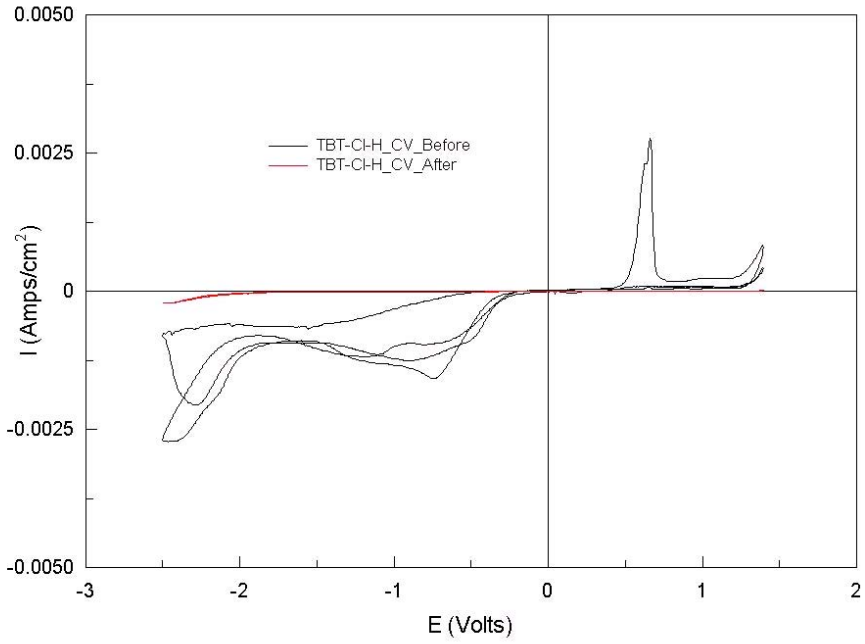

Figure 3.6: Cyclic voltammograms of 0.05 M tributyltin chloride, 1 mM tributyltin hydride (the initial spike), and 0.1 M TBA-PF_6 as the supporting electrolyte in acetonitrile before Devanathan cell electrolysis at -2.3 V (black line) and after 24 hours of electrolysis (red line). Working electrode = 5 mm gold disk, counter electrode = platinum wire (5 cm length), reference electrode = nonaqueous silver/silver chloride. Potential sweep rate = 50 mV/s.

3.5 Conclusions

Although ammonia borane is a very promising material for hydrogen storage, it has been shown in this work that it is not able to be directly electrochemically reduced (hydrogenated) in aqueous or nonaqueous solutions. The reduction of spent ammonia borane fuel is critical to the success of the overall fuel cycle; therefore, as an alternative approach, we investigated the feasibility of electrochemically reducing organotin halide back to organotin hydride for use as indirect hydrogenation materials.

The initial experiments revealed that the reduction of tributyltin chloride did not take place in an ordinary three-electrode undivided electrochemical cell, so we then explored the use of the bipolar Devanathan cell in order to electrochemically reduce the organotin halide species. We first began by testing the Devanathan cell using the chemical hydrogenation of styrene as a reaction that is known to occur. The results were very promising, so that we then moved on by attempting to electrochemically reduce tributyltin chloride to tributyltin hydride. Even though we built and characterized a nonaqueous reference electrode, the results of the Devanathan cell electrolysis indicated that no tributyltin hydride was formed after 24 hours even for positive control test solutions that contained an initial quantity of tributyltin hydride. We therefore

conclude that the Devanathan cell needs to be redesigned with a separating membrane and/or the choice of nonaqueous reference electrode is not the best suited one for this task.

3.6. References

1. L. G. Sneddon, *"Amineborane-Based Chemical Hydrogen Storage" U.S. Department of Energy 2008 Annual Progress Report*. Retrieved May 28, 2009 from http://www.hydrogen.energy.gov/pdfs/progress08/iv_b_1g_sneddon.pdf
2. M. E. Bluhm, M. G. Bradley, R. Butterick III, U. Kusari, and L. G. Sneddon, *J. Am. Chem. Soc.*, **128**, 7748 (2006).
3. J. Ghilane, P. Hapiot, and A. J. Bard, *Anal. Chem.*, **78**, 6868 (2006).
4. J. McLafferty. "Electrochemical Research in Chemical Hydrogen Storage Materials: Sodium Borohydride and Organotin Hydrides." PhD diss., The Pennsylvania State University, 2009.
5. A. I. Popov and D. H. Geske, *J. Am. Chem. Soc.*, **79**, 2074 (1957).
6. H. Inoue, Y. Yoshida, S. Ogata, T. Shimamune, and C. Iwakura, *J. Electrochem. Soc.*, **145**, 138 (1998).
7. C. Iwakura, T. Abe, and H. Inoue, *J. Electrochem. Soc.*, **143**, L71 (1996).
8. H. Tanaka, H. Ogawa, H. Suga, S. Torii, A. Jutand, S. Aziz, A. G. Suarez, and C. Amatore, *J. Org. Chem.*, **61**, 9402 (1996).
9. M. D. Booth and B. Fleet, *Anal. Chem.*, **42**, 825 (1970).

4. General Model of Electrochemical Impedance Spectroscopy

4.1 Introduction

The power of electrochemical impedance spectroscopy (EIS) cannot be overstated and it is clear that this technique has a profound impact in the electrochemical field as proof by the tens of thousands of publications in the open literature about this technique. Due to the vast amount of information obtained from an EIS data set, the application of this technique to study reaction mechanisms is very desirable. One of the main reasons for this applicability of using EIS for a mechanistic analysis of a reaction (or coupled reactions) is because the data span many orders in the time (or frequency) domain, thus allowing us to probe reactions steps of varying rates.

A brief summary of the electrochemical impedance spectroscopy technique is as follows: the system under study is first brought to a steady state by applying a fixed steady-state potential to the working electrode, next a small perturbing sinusoidal voltage amplitude (typically less than 20 mV) is superimposed over the steady-state potential as the frequency of the perturbing sinusoidal voltage wave is stepped from one value to the next, finally we measure how the current responds to the sum of the applied potentials. To keep this summary of the EIS technique brief, it will simply be mentioned that the measured current contains a phase shift relative to the applied potential and therefore we treat this by using complex numbers to describe the impedance; i.e. the impedance is $Z = E / I$, where E is the applied potential and I is the measured current, and this impedance is then treated as having real and imaginary components. For more information on the electrochemical impedance spectroscopy technique, see for instance Reference 1.

In order to use the EIS technique as a tool to study reaction mechanisms, it is very common in the literature to find discussions wherein the reaction mechanism is described by an analogous equivalent electronic circuit. Although it is possible to describe an electrochemical system as being analogous to an electronic circuit, it must be emphasized that when doing this the choice of equivalent circuit is quite ambiguous. The reason for the lack of a specific equivalent circuit that describes a true electrochemical system is because there is the possibility that any number of circuit elements can be added to the equivalent circuit analogue that allows for the impedance data to match the experimentally collected data, therefore the extraction of various parameters (resistances, capacitances, etc.) becomes impractical. In addition to this, even if an analogous equivalent circuit is found to describe the experimental data very well, the individual electronic components of the analogous circuit can sometimes be non-physical, which then leads us to question the validity of using equivalent circuit analysis for the study of reaction mechanisms.

The aim here is then to strictly avoid using equivalent circuit analogs and to describe the electrochemical impedance in a more classical mathematical manner. The idea of this approach is not new, however various attempts in the past have been found to have limitations that we wish to overcome in this model of electrochemical impedance spectroscopy. A short review of the previous work of others will be discussed below; the main contributions are from: D. A.

Harrington [2-6], B. Tribollet [7], S. K. Rangarajan [8-10], and H. Anderson [11-15]. It is not our goal to degrade the work of those mentioned above, because their contributions are significant to the science; however, we simply want to provide the proper motivation and justification as to why the model presented below is more applicable than the work of others that has been done in the past. In fact, the model described below contains some ideas from past work, in a classical mathematical approach, so not only does this model compliment previous work but it also extends it further.

The first contribution to be discussed, namely that of D. A. Harrington [2-6], shows a thorough analysis of electrochemical impedance for multistep reaction mechanisms including treatments for diffusing, static, and adsorbed species, as well as presenting a reduction of his model to equivalent circuit analogies [6]. However, the treatment of Harrington is limited to being able to handle only electrochemical reactions because he explicitly excludes from consideration any mechanisms that include homogeneous chemical reactions. Due to this restriction, the applicability of this model to actual reaction mechanisms (which can and do include coupled homogeneous chemical steps) is quite limited.

The work of Tribollet [7] is similar in restriction to that of Harrington in that Tribollet's model does not handle homogeneous chemical reaction steps either. In Tribollet's discussion, he says that his model "has [the] provision for an arbitrary number of simultaneous homogeneous and heterogeneous reactions," and yet his mathematical treatment does not have even the slightest treatment of coupled homogenous chemical reaction steps. Again, due to this restriction (similar to Harrington's model) we do not consider the model of Tribollet very practical.

One of the more elaborate treatments of coupled reaction mechanisms that include both electrochemical and chemical steps has been proposed by S. K. Rangarajan [8-10], wherein he describes his model as the "Scheme of Squares." Although his analysis of the problem is very sophisticated it still has its flaws. For example, even though the Scheme of Squares model can handle coupled reaction mechanisms with an arbitrary number of steps, we must emphasize that Rangarajan's treatment is restricted to handle a maximum of second order reactions, which cannot describe all of the possible reaction steps able to be written down.

It should be clear to the reader that even though the Scheme of Squares model by Rangarajan is quite powerful and capable of handling an arbitrary number of coupled reaction steps, it has a drawback in that the individual (elementary) chemical and electrochemical steps that it considers are not the most universal or applicable to all mechanisms that are able to be conceived. It is because of this drawback in Rangarajan's Scheme of Squares that we find it not applicable to all situations and find room to extend the theory in the model presented below to handle mechanisms that have been written with reaction steps that are higher than second order.

Finally, the work of Anderson in his thesis [11] and subsequent journal articles [12-15] are to be considered because the treatment within his model is of a similar nature as my model; however, it will be shown that his model is not without its drawbacks. The general idea of Anderson's work is that various mechanisms are chosen in advance, theoretical data are

calculated, and the experimental data are then compared manually (by eye) to choose which is the best model that describes the experimental data [11].

Regarding the applicability of Anderson's model, he considers coupled chemical steps in two cases: those with fast or slow rates; whereas in the new model described below we allow the chemical reactions rates to be of any value, not just fast or slow ones.

One last point to be made about Anderson's model is based upon his analysis of impedance spectra. Anderson has this to say about the two ways in which it is possible to analyze the impedance spectra [12]:

> The spectrum can be fitted by a least-squares method to some equations [equation numbers are omitted by this author to avoid confusion], which will give the corresponding parameters A, B, D, T [note that these parameters are not used in my model] … This is a non-linear problem which requires sophisticated mathematical tools and will not be treated here. The second and more common approach is to use <u>electrical equivalent circuits</u> [emphasis added by this author]… In order to obtain information about the kinetics for the electrochemical reaction the electric quantities associated with the [equivalent] circuit must be related to the parameters in the corresponding admittance equation.

The point being that Anderson eventually resorts to an equivalent circuit analog to analyze impedance data for some situations and this is also the case in Anderson's other work [14]. It is this point that once again shows how our model is an improvement over Anderson's model because we cannot emphasize enough that an equivalent circuit analog cannot fully describe true physical and chemical properties of an actual reaction mechanism.

Now with the proper motivation we present here the new model for electrochemical impedance spectroscopy, which has already been described in our publication by Tokash, Engelhardt, and Macdonald [16].

We begin by reminding the reader that since the amplitude of the perturbation to the system is quite small, we can assume that the corresponding mass transfer equation's relative perturbation concentrations are generally also in linear form even for the case of arbitrarily complicated (and nonlinear) systems. However, the solution of these equations also depends upon the steady-state concentrations of species, which in turn depend on the steady-state value of the applied potential. Thus, in order to calculate the impedance of a system and compare to experimental data we must solve steady-state mass transfer equations. In general, these transport equations are often nonlinear due to the presence of nonlinear electrochemical and chemical reactions, migration effects, concentration dependences of transport coefficients, and any other factors that cause the deviation of the system from dilute-solution behavior. As a result, a complete analysis of impedance data for nonlinear systems, as mentioned by Anderson [12], can only be accomplished by applying numerical methods because impedance is defined only for linear systems and numerical methods allow us to linearize a nonlinear system.

The model described below, and its associated computer code, generates theoretical electrochemical impedance spectroscopy (EIS) data for a one-dimensional system of heterogeneous and/or homogeneous reaction steps of arbitrary complexity (in terms of reactions and number of species) based on a small periodic (sine wave) perturbation of the potential, *E*, applied to this system. Our task is then to determine whether a certain mechanism is the appropriate choice for an unknown system under study by optimizing the theoretical model onto experimental EIS data with the determination being made by using "goodness of fit" criteria. Once a mechanism is deemed acceptable based upon the goodness of fit of the optimization process, we are presented with values for various model parameters that we desire to know (such as reaction rates or transfer coefficients).

As a final note on the mathematics that are presented below: the procedure that we follow is to solve equations that are nonlinear (the source of nonlinearity is mentioned above) by linearizing them and then we allow the numerical analysis method to determine whether the solutions are converging. The reason that we can trust the results of the optimization process is because we constrain the optimized parameters to a range of realistic values. Finally, the stability of this solution procedure is termed "asymptotically stable" because we limit the perturbations of the system to small amplitudes around the critical points. This can be explained in another way by an analogy to a simple pendulum under the force of gravity that has a damping force (be it mechanical friction or air resistance or both). We know from experience that one stable equilibrium point is gravitationally downward where the system will come to rest if we perturb it slightly. On the other hand, there exists a second equilibrium point for a pendulum, namely gravitationally upward. However, this second equilibrium point is unstable because slight perturbations from the equilibrium position do not bring it back to the same equilibrium point. So mathematically speaking, we need to assure we are near stable equilibrium points and as mentioned above we accomplish this by constraining the optimized values to those within a range of values that we know to exist in real life situations. Further, we assure that we do not go too far from the stable equilibrium point by restricting the system perturbation to a small-amplitude (as is the case for EIS experiments). By following this procedure, the solutions are "asymptotically stable," meaning that the system will eventually find a stable equilibrium solution.

The model that follows is exactly that which was presented in our publication [16] and it is written here in the same format as our publication with only minor changes being made.

4.2 Mathematical Model

We will describe both homogeneous and heterogeneous reactions by the single equation:

$$\sum_i \nu_{m,i} A_i^{z_i} \rightarrow \sum_i \mu_{m,i} A_i^{z_i} + n_m e^- , \qquad \text{m} = 1, 2, ... \tag{4.1}$$

Here $A_i^{z_i}$ is the chemical symbol of species i with charge z_i. For each reaction, m, the stoichiometric coefficients of species i in the left and right sides are $\nu_{m,i}$ and $\mu_{m,i}$, respectively. It is assumed that the change in valence, n_i, is positive if the electrochemical reaction is anodic (oxidation) and negative if this reaction is cathodic (reduction). For non-electrochemical, heterogeneous and homogeneous reactions we set $n_m = 0$.

The rate of production (depletion) of species i due to chemical reactions is expressed as:

$$R_i = \sum_m \mu_{m,i} V_m - \sum_m \nu_{m,i} V_m = \sum_m \lambda_{m,i} V_m \tag{4.2}$$

where $\lambda_{m,i} = \mu_{m,i} - \nu_{m,i}$ and V_m is the rate of reaction m. The summation in Equation 4.2 takes place for all chemical homogeneous or heterogeneous reactions depending on the type of reaction considered.

In general, the rates V_m and R_i are functions of concentrations, C_i, Kelvin temperature, T, and in the case of electrochemical reactions on the potential of the electrode, E. In our model, we assume that V_m can be presented in the form:

$$V_m = k_m \prod_i C_i^{\nu_{m,i}} \tag{4.3}$$

It is important to note that if some species is present in excess in the system its concentration is considered to be constant and included into the parameter k_m, which depends also on temperature and in the case of electrochemical reactions on the potential of the electrode. In this case, the rate expressions for second order reactions are conveniently reduced to linear form. Here we assume that the rate constant of an electrochemical reaction has the Tafel form:

$$k_m = k_m^0 \exp\left(\frac{\alpha_m F E}{RT}\right) \tag{4.4}$$

where, k_i^0 is the standard rate constant, R is the universal gas constant, F is the Faraday constant, and α_m is the transfer coefficient with α_m being positive for an anodic reaction and negative for cathodic one.

Here we will consider two hydrodynamic cases: Nernst diffusion layer and forced convection for the case of a rotating disk electrode (RDE). From mathematical point of view our task reduces to the solution of the following set of mass transfer equations:

$$\frac{\partial C_i}{\partial t} = D_i \frac{\partial^2 C_i}{\partial x^2} - V(x) \frac{\partial C_i}{\partial x} + R_i, \qquad i = 1,2,\ldots, N \tag{4.5}$$

where N is the total number species in the solution, whose concentrations have to be found, x is the distance from the electrode surface, t is the time, D_i is the diffusion coefficient, V is the

hydrodynamic velocity, and R_i is the source (sink) of species *i*. For the case of the Nernst diffusion layer $V = 0$ and for the case of RDE we have [17]:

$$V(x) = -0.51023 x^2 \Omega^{1.5} / \sqrt{\nu} \tag{4.6}$$

where Ω is the rotation speed of the disk (in rad/s) and *v* is the kinematic viscosity.

Two boundary conditions exist – one far from the electrode surface and the other at the electrode surface, and each one is of a different type. This case, in mathematics, is referred to as a mixed boundary condition, i.e. we have both a Dirichlet boundary condition (Equation 4.7) as well as a Neumann boundary condition (Equation 4.8).

Far from the metal we have all concentrations equal to their bulk solution values:

$$C_i = C_{i,\infty} \qquad \text{at } x = \Delta x, \quad \text{i} = 1,2,..,\text{N} \tag{4.7}$$

Here, $C_{i,\infty}$ is the bulk concentrations of species "*i*", which is assumed to be established by equilibrium with other components at a "sufficiently far" distance from the surface. In Equation 4.7, Δx is the width of the Nernst layer for quiescent solutions, but for the case of a RDE, we choose Δx = 2d, where $d = 1.61 D_{\max}^{1/3} \nu^{1/6} / \sqrt{\Omega}$ is the width of the Levich layer [17] and D_{max} is the maximum diffusion coefficient among all D_i.

On the metal surface we have:

$$-D_i \frac{\partial C_i}{\partial x} = J_i, \quad \text{i} = 1,2,...,\text{N}, \ \text{at } \text{x} = 0 \tag{4.8}$$

where flux densities of species, J_i, is considered to be the known function of surface concentrations and potential in accordance with Equations 4.6.

It should be mentioned here that the diffusion equations (Equations 4.5) are parabolic partial differential equations, but in Equations 4.9 below we have removed the time dependence in order to find the stationary solution, which results in elliptic equations. The nonlinear system of equations can be solved by usual linearization method using a Taylor series expansion. Let us denote $C_{old,i}^0$ as some guess for the solution C_i^0. On the fist step it can be simply assumed that $C_{old,i}^0 = C_{i,\infty}^0$. After expanding the expression for R_i as a Tailor series about the point $C_{old,i}^0$ and keeping only the linear terms ($R_i = a_i + \sum_{k=1}^{N} b_{i,k} C_k$), Equation 4.5 can be presented in linear form:

$$D_i \frac{d^2 C_i^0}{dx^2} - V(x) \frac{dC_i^0}{\partial x} + a_i + \sum_{k=1}^{N} b_{i,k} C_k = 0, \qquad i = 1,2,...,N \tag{4.9}$$

where

$$b_{i,k} = \frac{\partial R_i}{\partial C_k}\Big|_{old} \quad \text{and} \quad a_i = R_i\big|_{old} - \sum_{k=1}^{N} b_{i,k} C^0_{old,k} \tag{4.10}$$

By analogy, the boundary conditions to Equations 4.9 at $x = 0$, have the form:

$$-D_i \frac{dC_i^0}{dx} = \varsigma_i + \sum_{k=1}^{N} \xi_{i,k} C_k^0, \quad \text{i} = 1,2,...,\text{N}, \ \text{at} \ \text{x} = 0 \tag{4.11}$$

where

$$\xi_{i,k} = \frac{\partial J_i}{\partial C_k}\Big|_{old} \quad \text{and} \quad \varsigma_i = J_i\big|_{old} - \sum_{k=1}^{N} \xi_{i,k} C^0_{old,k} \tag{4.12}$$

and the boundary conditions to Equations 4.9 at $x = \Delta x$ are described by Equations 4.7.

The linear boundary value problem that is described by Equations 4.11, 4.12, and 4.7 can be solved by the finite difference method. It should be noted that (approximate) solutions obtained by the linearization of nonlinear differential equations are valid only under certain restricted conditions. One such valid scenario is when the perturbation to the system is of small amplitude, as is the case for this model. This treatment, by using small amplitude perturbations, is quite common in physics and mathematics for the analysis of the harmonic oscillator, for example.

Diffusion terms in the governing equations are approximated by the central scheme and the convective term is approximated by an up-wind scheme [18]. The obtained system of linear equations is solved by using Thomas algorithm for block tridiagonal matrixes [19,20]. After finding the solution C_i^0 it is declared to be $C^0_{old,i}$ and solution is continued until the convergence is achieved. In some cases, in order to insure convergence, it is necessary to use the method of lower relaxation, which means that after each solution of Equation 4.15 is found a new value of C_i^0 is recalculated via the relation:

$$C_i^0 = \alpha C_i^0 + (1-\alpha) C^0_{old,i} \tag{4.13}$$

where $\alpha < 1$ is the relaxation parameter(not to be confused with the transfer coefficient).

After obtaining the stationary solution, the transient perturbation solution can be obtained in the following way. We assume that $E = E_{dc}$ at $t < 0$ and that for $t > 0$ a sufficiently low amplitude sinusoidal perturbation, ΔE, is applied to the system, i.e.

$$E = E_{dc} + \Delta E \cos(\omega t) = E_{dc} + Re\left\{\Delta E e^{j\omega t}\right\} \quad \text{at } t > 0 \tag{4.14}$$

Here, ω is the modulation frequency, and ΔE is the real amplitude for the potential of the electrode. If the amplitude, ΔE, is sufficiently small, the dependence of electrochemical rate constants as a function of time can be presented as:

$$k_m = k_m\big|_0 + \frac{\partial k_m}{\partial E}\big|_0 \,\mathrm{Re}\{\Delta E e^{j\omega t}\} \tag{4.15}$$

and accordingly, the response of the system may be presented as:

$$C_i = C_i^0 + \mathrm{Re}\left\{\Delta C_i\, e^{j\omega t}\right\} \tag{4.16}$$

and

$$i = i^0 + \mathrm{Re}\left\{\Delta i e^{j\omega t}\right\} \tag{4.17}$$

where C_i^0 and i^0 are steady-state values and ΔC_i and Δi are the complex amplitudes for the concentrations and current density, correspondingly.

After substituting Equation 4.16 into Equations 4.5 we have:

$$j\omega\Delta C_i = D_i \frac{d^2\Delta C_i}{dx^2} - V(x)\frac{d\Delta C_i}{dx} + \sum_{k=1}^{N} b_{i,k}\Delta C_k, \qquad i = 1,2,...,N \tag{4.18}$$

where parameters $b_{i,k}$ are calculated by Equations 4.10 at point $C_k = C_k^0$.

The set of N complex equations (Equations 4.18) can be reduced to the set of 2N equations relative real and complex parts of the amplitude $\Delta C_i = \Delta C_{i,\mathrm{Re}} + j\Delta C_{i,\mathrm{Im}}$ [7], namely:

$$D_i \frac{d^2\Delta C_{i,\mathrm{Re}}}{dx^2} - V(x)\frac{d\Delta C_{i,\mathrm{Re}}}{dx} + \sum_{k=1}^{N} b_{i,k}\Delta C_{k,\mathrm{Re}} + \omega\Delta C_{i,\mathrm{Im}} = 0, \qquad i = 1,2,...,N \tag{4.19}$$

$$D_i \frac{d^2\Delta C_{i,\mathrm{Im}}}{dx^2} - V(x)\frac{d\Delta C_{i,\mathrm{Im}}}{dx} + \sum_{k=1}^{N} b_{i,j}\Delta C_{k,\mathrm{Im}} - \omega\Delta C_{i,\mathrm{Re}} = 0, \qquad i = 1,2,...,N \tag{4.20}$$

The boundary conditions are:

$$\Delta C_{i,\mathrm{Re}} = \Delta C_{i,\mathrm{Im}} = 0 \quad \text{at } \mathrm{x} = \Delta\mathrm{x},\ i = 1,2,...,N \tag{4.21}$$

$$-D_i \frac{d\Delta C_{i,\mathrm{Re}}}{dx} = \left(\frac{\partial J_i}{\partial E}\right)_{E=E^0} \Delta E + \sum_{j=1}^{N} \xi_{i,k}\Delta C_{k,\mathrm{Re}}, \quad \mathrm{i} = 1,2,...,\mathrm{N}, \ \text{at } \mathrm{x} = 0 \tag{4.22}$$

$$-D_i \frac{d\Delta C_{i,\mathrm{Im}}}{dx} = \sum_{k=1}^{N} \xi_{i,k} \Delta C_{k,\mathrm{Im}}, \quad \mathrm{i} = 1,2,...,\mathrm{N}, \ \text{at} \ \mathrm{x} = 0 \tag{4.23}$$

in which parameters $\xi_{i,k}$ are calculated by Equations 4.12 at the point $C_k = C_k^0$.

The solution of the formulated system of linear equations is performed by the same method that was described above for the steady-state case. After that, the real and imaginary components of the complex current amplitude $\Delta i = \Delta i_{\mathrm{Re}} + j\Delta i_{\mathrm{Im}}$ are determined via the relations:

$$\Delta i_{\mathrm{Re}} = -F \sum_{i=1}^{N} z_i D_i \left(\frac{d\Delta C_{i,\mathrm{Re}}}{dx} \right)_{x=0} \quad \text{and} \quad \Delta i_{\mathrm{Im}} = -F \sum_{i=1}^{N} z_i D_i \left(\frac{d\Delta C_{i,\mathrm{Im}}}{dx} \right)_{x=0} \tag{4.24}$$

Finally, the faradic admittance of the system is calculated as:

$$Y = \frac{\Delta i}{\Delta E} = \frac{\Delta i_{\mathrm{Re}}}{\Delta E} + j \frac{\Delta i_{\mathrm{Im}}}{\Delta E} \tag{4.25}$$

Accordingly, the faradic impedance of the system is:

$$Z_f = \frac{1}{Y} = \frac{\Delta i_{\mathrm{Re}} / \Delta E}{\sqrt{(\Delta i_{\mathrm{Re}} / \Delta E)^2 + (\Delta i_{\mathrm{Im}} / \Delta E)^2}} - j \frac{\Delta i_{\mathrm{Im}} / \Delta E}{\sqrt{(\Delta i_{\mathrm{Re}} / \Delta E)^2 + (\Delta i_{\mathrm{Im}} / \Delta E)^2}} \tag{4.26}$$

4.3 Example of Application

As an example we consider the application of the developed code to the case of electrochemical-chemical-electrochemical (ECE) mechanism [21]. We assume that the following reactions (in both directions) take place:

$$O + e^- \Leftrightarrow R \tag{4.27}$$

$$R \Leftrightarrow 2X \tag{4.28}$$

$$X + e^- \Leftrightarrow 2Y \tag{4.29}$$

This mechanism has been chosen, because it cannot be reduced in principle to linear mass transfer equations when species X and Y are not present in the bulk electrolyte, unless the pseudo first order approximation is adopted by utilizing large concentrations of X and Y in the solution such that these concentrations remain constant as the reactions proceed.

There are $N = 4$ species in this system, $M = 4$ electrochemical reactions and $L = 2$ chemical reactions First of all, we assign indexes to these species and describe their properties (see Table 4.1).

Table 4.1: Properties of species.

Index	**Species**	***D*, cm^2/s**	***z***	C_∞, **M**
1	*O*	10^{-5}	-1	0.01
2	*R*	10^{-5}	-2	0
3	*X*	10^{-5}	-1	0
4	*Y*	10^{-5}	-1	0

After that, we have to describe the properties of chemical and electrochemical reactions (see Table 4.2 and 4.3).

Table 4.2: Properties of electrochemical reactions.

Index	**Reaction**	**Non zero $\nu_{m,i}$**	$\mu_{m,i}$	α	k^0
1	$O + e^- \rightarrow R$	$\nu_{1,1}=1$	$\mu_{1,2}=1$	-0.5	1, cm/s
2	$R \rightarrow O + e^-$	$\nu_{2,2}=1$	$\mu_{2,1}=1$	0.5	0.1, cm/s
3	$X + e^- \rightarrow 2Y$	$\nu_{3,3}=1$	$\mu_{3,4}=2$	-0.5	$2\text{x}10^{-2}$, cm/s
4	$2Y \rightarrow X + e^-$	$\nu_{4,4}=2$	$\mu_{4,3}=1$	0.5	$3\text{x}10^{-3}$, cm^4/mol*s

Table 4.3: Properties of chemical reactions.

Index	**Reaction**	**Non zero $\nu_{m,i}$**	$\mu_{m,i}$	k
1	$R \rightarrow 2X$	$\nu_{1,2}=1$	$\mu_{1,3}=2$	2000, 1/s
2	$2X \rightarrow R$	$\nu_{2,3}=2$	$\mu_{2,3}=1$	1000, cm^3/mol* s

Some general properties of the system must be also defined: electrode potential, temperature and hydrodynamic conditions (see Table 4.4). Here the case of RDE is considered.

Table 4.4: General Properties of the system.

T, °C	E_{dc}, V (SHE)	Ω, rpm	v, cm^2/s
25	0.1	500	0.01

The calculated impedance data are presented in Figures 4.1 and 4.2.

As we can see from Figure 4.1 there are two well defined time constants for the chosen ECE mechanism and for the chosen set of parameters. For comparison purposes Figure 4.2 yields the corresponding Nyquist plot for the EC mechanism (described by Equations 4.27 and 4.28) and for the E mechanism (described by Equations 4.27) and for the same set of parameters.

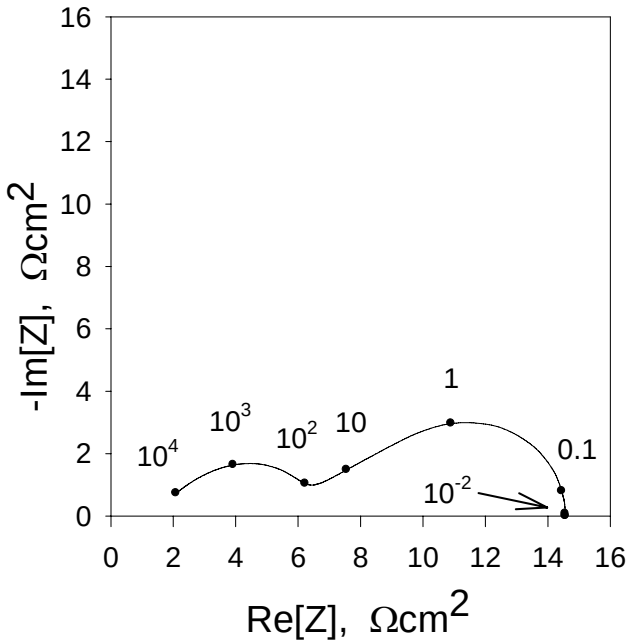

Figure 4.1: Nyquist plot for ECE mechanism (described by Equations 4.27-4.29). E_{dc} = 0.1V. Numbers denote some characteristic frequencies in Hz. Other parameters are defined in the Tables 4.1 through 4.4 above.

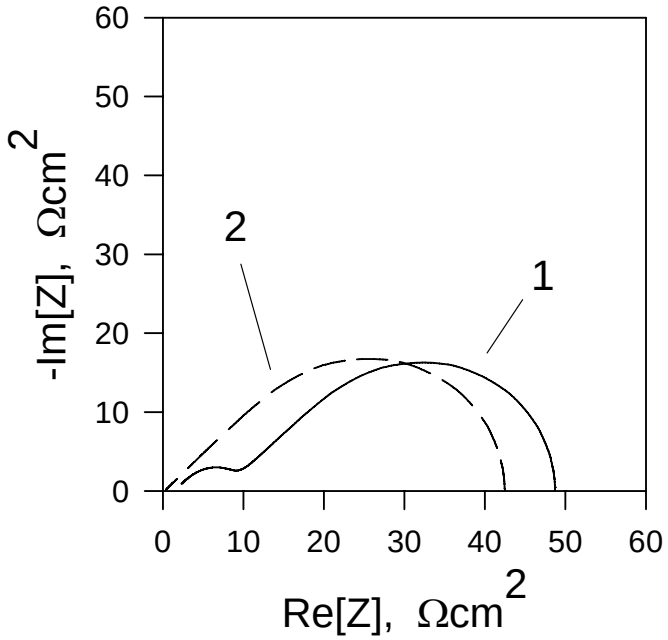

Figure 4.2: Nyquist plot for EC mechanism (described by Equations 4.27 and 4.28) is shown in curve 1 and the E mechanism (described by Equation 4.27) is shown in Curve 2. E_{dc} = 0.1V. Other parameters are defined in the Tables 4.1 through 4.4 above.

For the case of the EC mechanism, there are also two time visible constants, but for the case of a single electrochemical reaction we can see only one time constant, as expected.

Also for comparison purposes Figure 4.3 yields Bode plots for different values of initial constant potential, E_{dc}. We see in Figure 4.3, for example, that at low frequencies the impedance of the system reduces to the resistance component that does not depend on frequency. However, the value of this resistance component increases as E_{dc} is decreased. This fact is the result of the observed current approaching the limiting current value, which is determined by the transport of species X to the electrode surface.

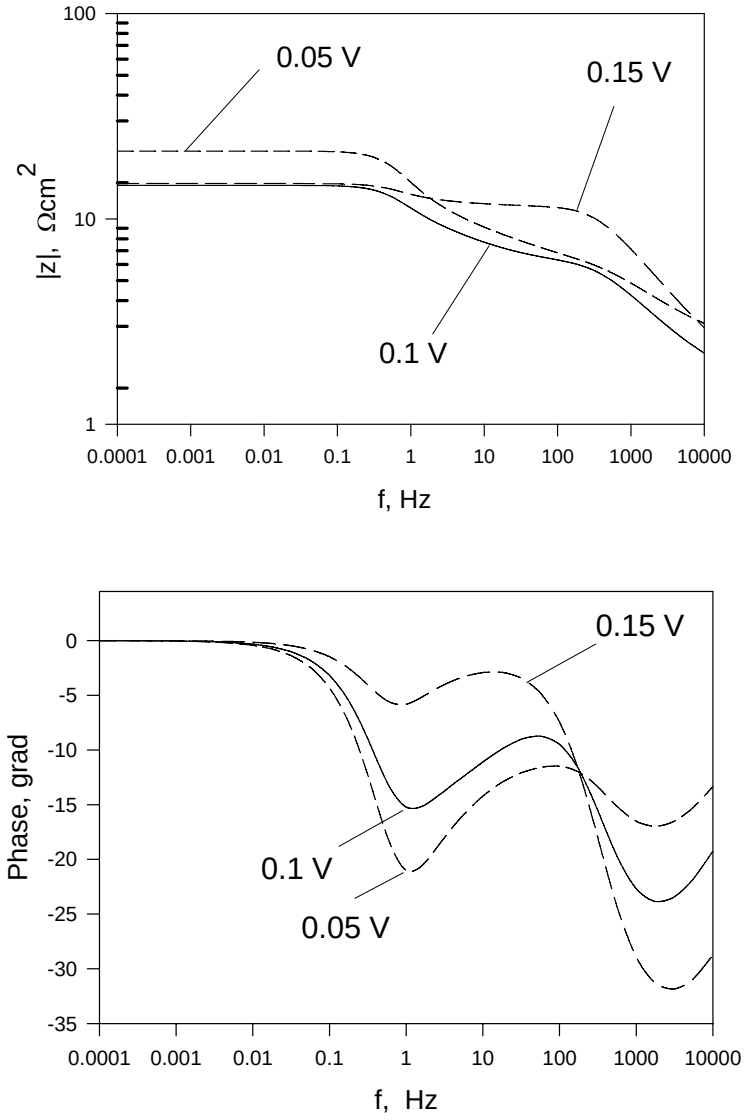

Figure 4.3: Bode plots for ECE mechanism and for different values of the initial constant potential, E_{dc}. Other parameters are defined in the Tables 4.1 through 4.4 above.

4.4 Evaluation of Unknown Parameters from Experimental Data

Each of the parameters that characterize a given species (e.g., the diffusion coefficient) or the kinetics of the chemical or electrochemical reactions (standard rate constant, transfer coefficient) can be considered as unknown values, which can be be determined by optimizing the model onto the experimental data. Practically, optimization reduces to the minimization of some value, S, which describes the discrepancy between calculated and experimentally measured values. In this study, we choose:

$$S = \sum_i \frac{\left| Z_{\mathrm{Re},i} - Z_{\mathrm{Re},i}^{\exp} \right|}{Z_{\mathrm{Re},i}^{\exp}} \tag{4.30}$$

where $Z_{\mathrm{Re},i}^{\exp}$ is the experimentally-measured real component of the impedance and index *i* numerates different frequencies. That is, we considered the minimization of the relative deviation of the real component of the impedance. If optimization is performed in the proper manner, satisfactory agreement between calculated and measured imaginary components must be also observed (or equivalently, amplitude of the impedance and phase angle).

It is important to note that the impedance of the experimental system, Z, is related with the faradic impedance, Z_f, that is described by Equation 4.26 by the relation:

$$Z = R_{el} + \frac{Z_c Z_f}{Z_c + Z_f} \tag{4.31}$$

where

$$Z_c = \frac{1}{j\omega C_d} \tag{4.32}$$

is the impedance of the double layer with the capacitance C_d and R_{el} is the resistance of the electrolyte between the metal surface and the tip of the Luggin probe.

Experimental impedance measurements were performed for 1 mM potassium ferricyanide + 1 mM potassium ferrocyanide + 2 M NaOH at a 5 mm diameter platinum RDE (1000 RPM) at 23°C. The frequency range was 100,000 Hz to 0.1 Hz and the perturbation potential amplitude was 20 mV peak-to-peak. A platinum wire counter electrode and Hg/HgO reference electrode were used.

The polarization behavior of this system is described by the Butler-Volmer equation:

$$i = Fk_R^0 C_{R,s}\, exp\left[\frac{(1-\beta)FE}{RT}\right] - Fk_O^0 C_{O,s}\, exp\left[-\frac{\beta FE}{RT}\right] \tag{4.33}$$

where index *O* denotes ferricyanide and index *R* denotes ferrocyanide, $C_{O,s}$ and $C_{R,s}$ are the surface concentrations of O and R, respectively, and β is the symmetry factor for the reaction. The parameters to be determined by optimization are: k_R^0, k_O^0, β, D_O, D_R, R_e, and C_d. The surface concentrations are readily calculated from the bulk concentrations and the limiting currents as [21]:

$$C_{O,s} = C_{O,b} \frac{i_{l,r} - i}{i_{l,r}} \tag{4.34}$$

and

$$C_{R,s} = C_{R,b} \frac{i_{l,f} - i}{i_{l,f}} \tag{4.35}$$

where $i_{l,f}$ and $i_{l,r}$ are the limiting current densities in the forward ($R \rightarrow O + ne^-$) and reverse directions ($O + ne^- \rightarrow R$), respectively and *i* is the current density.

The results of optimization that was performed by using the Monte Carlo method for the real part of impedance at E_{dc} = 304 mV vs. SHE (the equilibrium potential of the reaction is E^e = 0.379 V vs. SHE), yields: $k_R^0/k_O^0 = 3.55 \cdot 10^{-7}$, β = 0.5, $D_O = 4.06 \cdot 10^{-5}$ cm^2/s, $D_R = 4.66 \cdot 10^{-5}$ cm^2/s, R_e = 0.8 Ωcm^2 and C_{dl} = 43 μF/cm^2. Experimental measurements of the resistance of the electrolyte and the double layer capacitance in the absence of the redox couple yield results that are close to the fitted values, namely: R_e = 0.76 Ωcm^2 and C_{dl} = 46 μF/cm^2.

Figure 4.4 shows that the theoretical curve, which was calculated numerically (line) by using the values of the optimized parameters compares very well with the experimental data (dots) for real part of the impedance. The same values of the optimized parameters also yield excellent agreement between the calculated and experimental data for the imaginary part of the impedance (Figure 4.5).

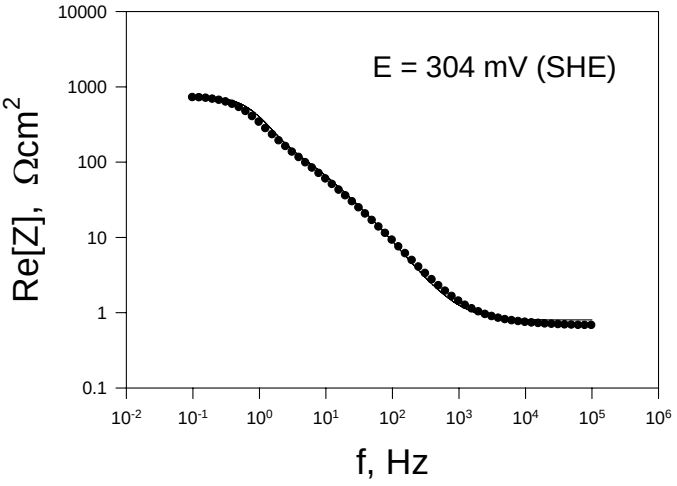

Figure 4.4: Comparison between experimental (dots) and calculated (line) values of real part of impedance at E_{dc} = 304 mV (SHE).

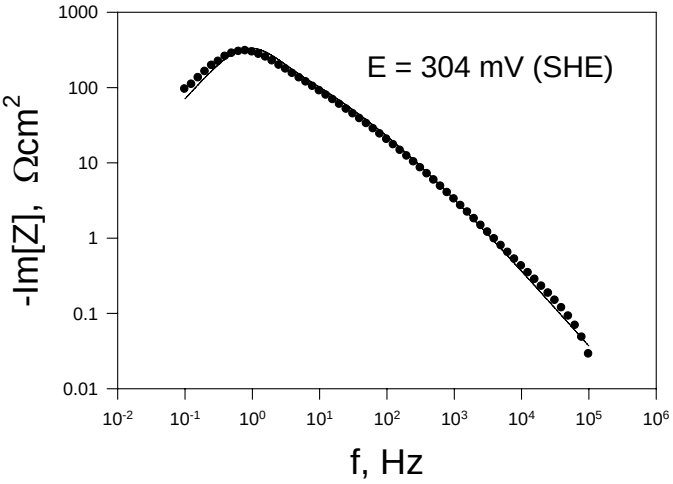

Figure 4.5: Comparison between experimental (dots) and calculated (line) values of imaginary part of impedance at E_{dc} = 304 mV (SHE).

Experimental measurements also were performed for E_{dc} = 329, 354, 379, 404, 429 and 454 mV vs. SHE. At all of these values of the steady-state potential of the electrode, except for 454 mV, excellent agreement has been observed between the calculated and measured real and imaginary parts of the impedance. Thus, for example, Figures 4.6 and 4.7 show comparison between calculated and measured values for E_{dc} = 429 mV vs. SHE.

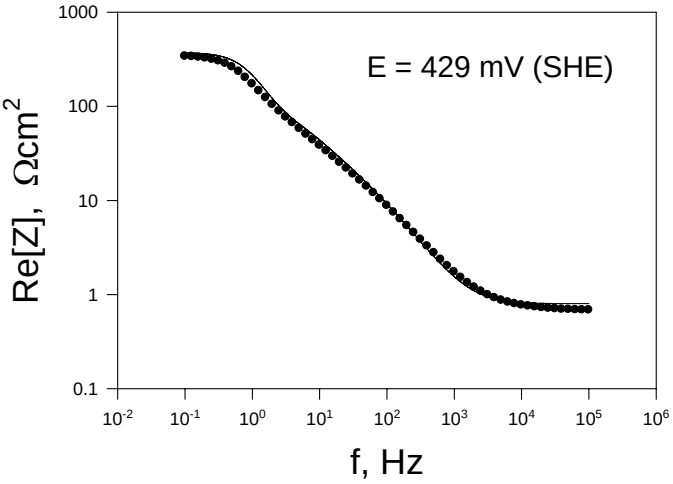

Figure 4.6: Comparison between experimental (dots) and calculated (line) values of real part of impedance at E_{dc} = 429 mV (SHE).

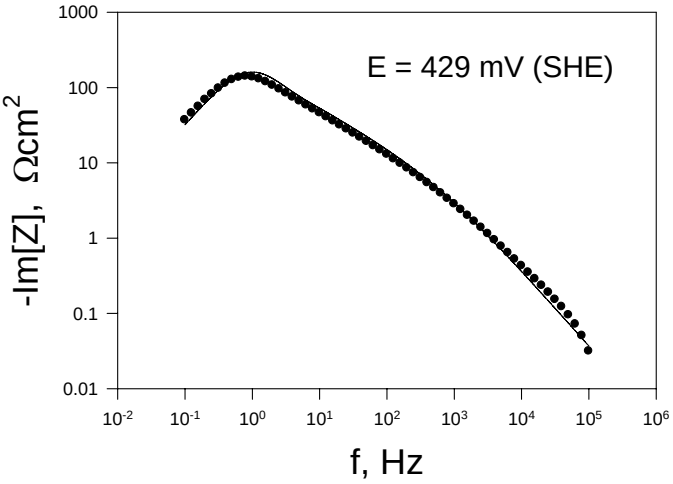

Figure 4.7: Comparison between experimental (dots) and calculated (line) values of imaginary part of impedance at E_{dc} = 429 mV (SHE).

However, for E_{dc} = 429mV (SHE), some discrepancy is observed (see Figures 4.8 and 4.9). The reason for the discrepancy is not clear at this time. However, we would like to remind the reader that only the experimental data for the real part of impedance at E_{dc} = 304 mV (SHE) was used for optimization. The fact that the impedance data that were calculated by using the optimized parameters at only one potential satisfactory coincides with the majority of the experimental data at different potentials confirms the adequacy of the fitted values.

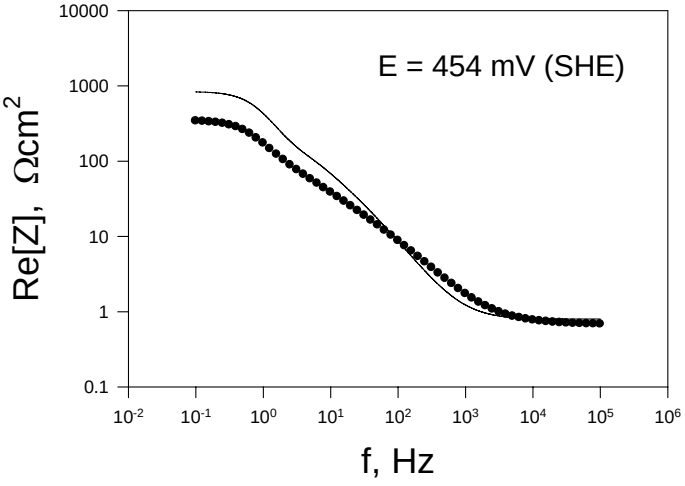

Figure 4.8: Comparison between experimental (dots) and calculated (line) values of real part of impedance at E_{dc} = 454 mV (SHE).

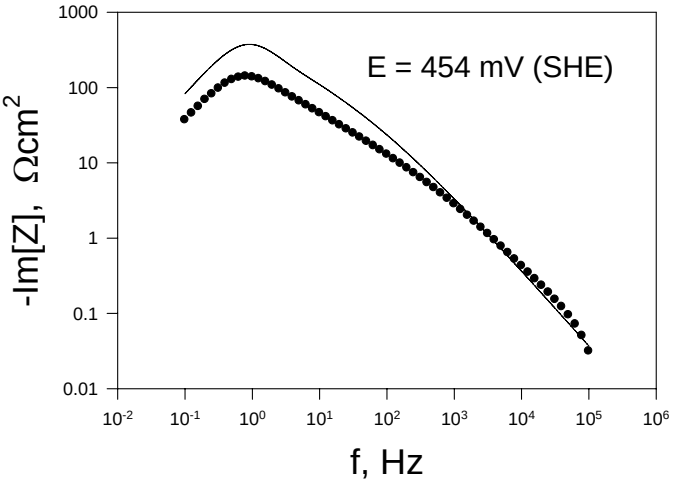

Figure 4.9: Comparison between experimental (dots) and calculated (line) values of imaginary part of impedance at E_{dc} = 454 mV (SHE).

It is important to note that the described procedure of optimization failed to determine the standard rate constants of the reactions, k_R^0 and k_O^0, separately (only their ratio could be obtained for the given system), because their values appear to be excessively high. Thus, the following approximate, but very accurate, analytical expression for the faradic impedance can be derived:

$$Z_f = \frac{\Delta i}{\Delta E} = \frac{1/k_O^0 + \dfrac{\exp\left[\dfrac{(1-\beta)F\bar{E}}{RT}\right]}{\sqrt{j\omega D_O}} th\left[\sqrt{\frac{j\omega}{D_O}}L_O\right] + \dfrac{(k_R^0/k_O^0)\exp\left[-\dfrac{\beta F\bar{E}}{RT}\right]}{\sqrt{j\omega D_R}} th\left[\sqrt{\frac{j\omega}{D_R}}L_R\right]}{C_{R,s}^0(1-\beta)\dfrac{F^2}{RT}\exp\left[\dfrac{(1-\beta)F\bar{E}}{RT}\right] + (k_R^0/k_O^0)C_{O,s}^0\beta\dfrac{F^2}{RT}\exp\left[-\dfrac{\beta F\bar{E}}{RT}\right]} \qquad (4.36)$$

Here $C_{R,s}^0$ and $C_{R,s}^0$ are steady surface concentration of ferricyanide and ferrocyanide, correspondingly and L_R and L_O are corresponding thicknesses of the Nernst diffusion layers. We see that as $k_O^0 \to \infty$, (practically for $k_O^0 >$ 100 cm/s) Z_f becomes independent of both k_O^0 and k_R^0, which is the case here. This example shows that, in some cases, not all unknown parameter values can be found by optimization, by using the impedance method.

Additionally, we wanted to test the new EIS model on a more complex, coupled reaction scheme to determine whether the model can fit the various reaction parameters for a more complicated case than the ferricyanide reduction discussed above. The two coupled reactions we studied were the reduction of nitromethane [22] and the reduction of ortho-bromonitrobenzene [23]. After verifying that the model works properly on one of these complex reaction

mechanisms, we intend to use it to discover the mechanisms and kinetic parameters for various boron hydride reactions as mentioned above.

The reduction of nitromethane has been explored by other groups and the original consensus among various researchers was that this reaction followed a coupled ECCE mechanism [24] as shown in Figure 4.10.

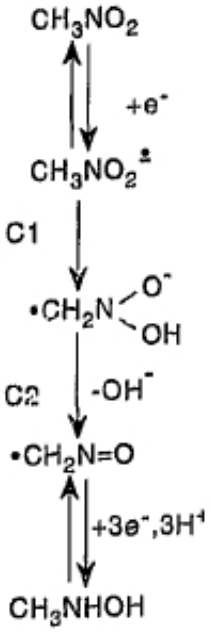

Figure 4.10: The proposed ECCE reaction mechanism for the electrochemical reduction of nitromethane, from [24].

During the electrochemical reduction of nitromethane, the blank solution is 1M NaCl + 0.15M NaH_2PO_4 + 0.05M citric acid. The sample of nitromethane is then made so that it contains 5mM nitromethane and the remainder is the same as the blank. At 23 degrees Celsius, the viscosity of the blank solution was 0.0010478 cm^2/s and the viscosity of the nitromethane sample solution was 0.0010631 cm^2/s.

Figure 4.11 displays cyclic voltammograms (collected at 0 RPM with a scan rate of 50 mV/s) and linear sweep voltammograms (collected at 1000 RPM and a scan rate of 5 mV/s) for the redox reactions of nitromethane, in 1M NaCl + 0.15M NaH_2PO_4 + 0.05M citric acid at 23 ^0C.

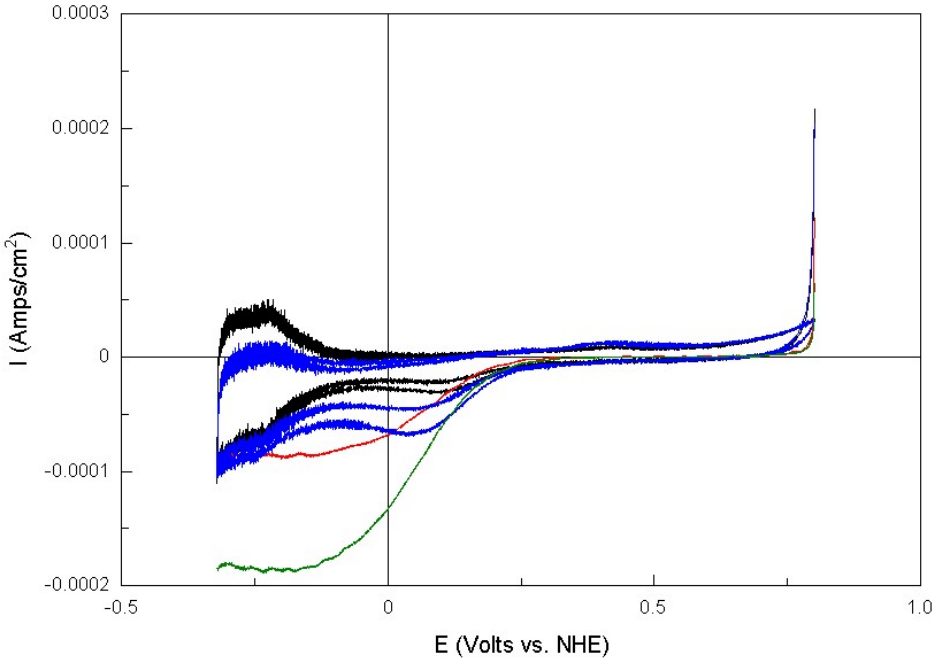

Figure 4.11: Black line is blank CV (0 RPM with a scan rate of 50 mV/s), blue line is nitromethane sample CV (0 RPM with a scan rate of 50 mV/s), red line is blank LSV (1000 RPM and a scan rate of 5 mV/s), and green line is nitromethane sample LSV (1000 RPM and a scan rate of 5 mV/s).

EIS data were collected at the following steady-state potentials versus SHE: 0.150V, 0.050V, -0.025V, and -0.100V. The peak-to-peak amplitude of the perturbing voltage signal was 20 mV. Table 4.5 presents the steady state current density, solution resistance, and double layer capacitance:

Table 4.5: Electrochemical properties during the reduction of nitromethane.

DC Potential (vs. SHE)	SS Current Density (A/cm^2)	R_s ($Ohm*cm^2$)	C_{dl} (F/cm^2)
0.150V	$-6.1131x10^{-6}$	2.312	$3.2594x10^{-5}$
0.050V	$-8.6602x10^{-6}$	2.321	$3.2871x10^{-5}$
-0.025V	$-9.1696x10^{-6}$	2.334	$3.4530x10^{-5}$
-0.100V	$-12.226x10^{-6}$	2.348	$3.8539x10^{-5}$

Figure 4.12 shows the Nyquist and Bode plots of the nitromethane solution:

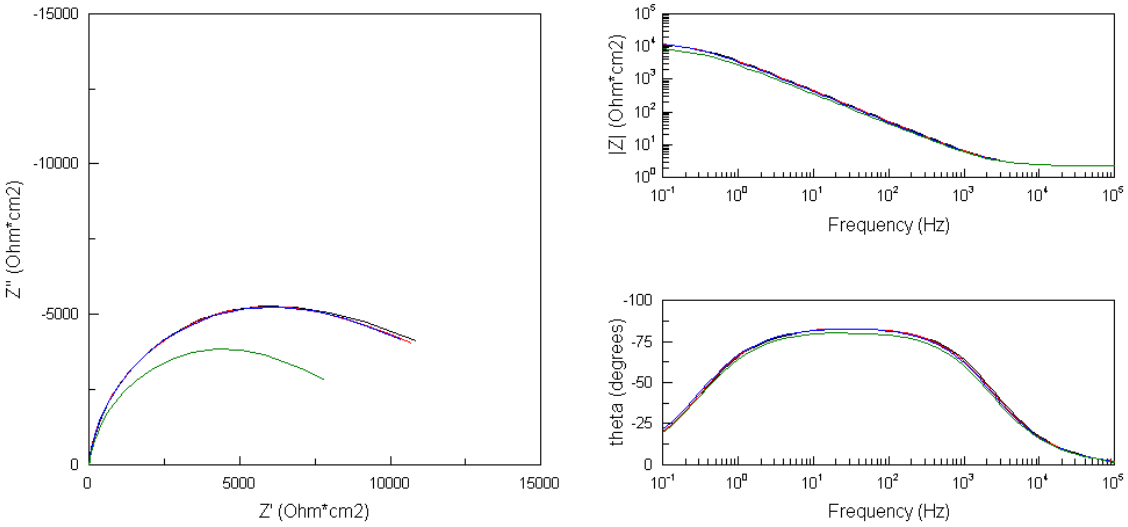

Figure 4.12: Nyquist and Bode plots for 5mM nitromethane in 1M NaCl + 0.150M NaH2PO4 + 0.05M citric acid. Frequency range was 100,000Hz to 0.1Hz. The green line corresponds to the DC potential of -0.100V (vs. SHE), all other potential values yield data that overlap one another.

When the collected EIS data were introduced into the computer code and a best-fit analysis was performed, we discovered that the real-value component results (Figure 4.13) were not suitable for extracting the necessary reaction parameters, with any degree of accuracy, even though the imaginary-value component results were fitted quite well (Figure 4.14).

Upon reviewing more literature on the subject or the electrochemical reduction of nitromethane, a paper was found [25] in which the reaction mechanism is not just a simple ECCE, but rather is as shown in Figure 4.15.

Due to the complexity of this reaction mechanism it was not explored any further and work was started on investigating the electrochemical reduction of ortho-bromonitrobenzene [23,26].

The proposed reaction mechanism from the literature is shown below in Figure 4.16.

EIS experimental data for the reduction of 2 mM ortho-bromonitrobenzene (o-BNB) with 100 mM tetrabutylammonium perchlorate (TBAP) as supporting electrolyte in acetonitrile were collected using a 5 mm gold RDE disk working electrode at 1000 RPM, a 1 mm platinum wire as the counter electrode with 5 cm length in solution, and a silver wire pseudo-reference electrode.

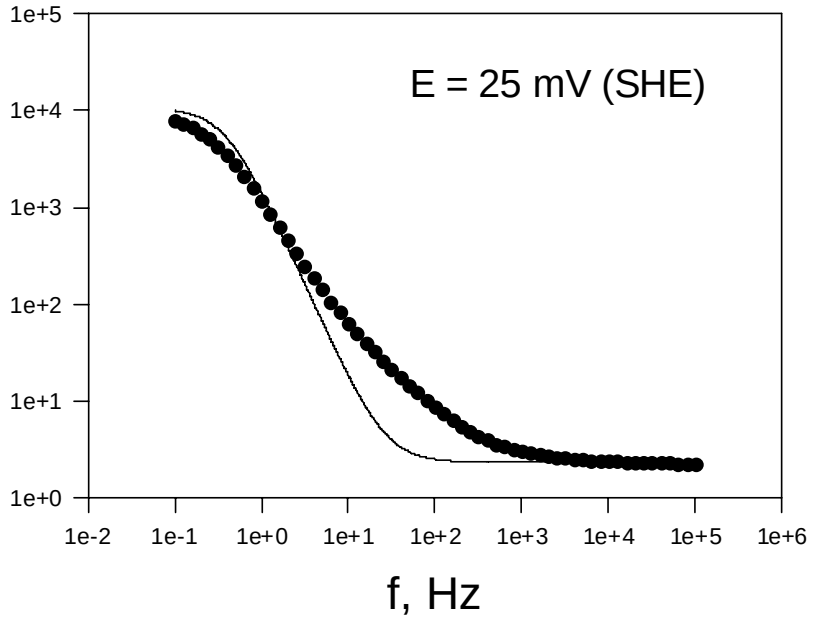

Figure 4.13: EIS fitting of reduction of nitromethane at 25 mV vs. SHE, real values shown.

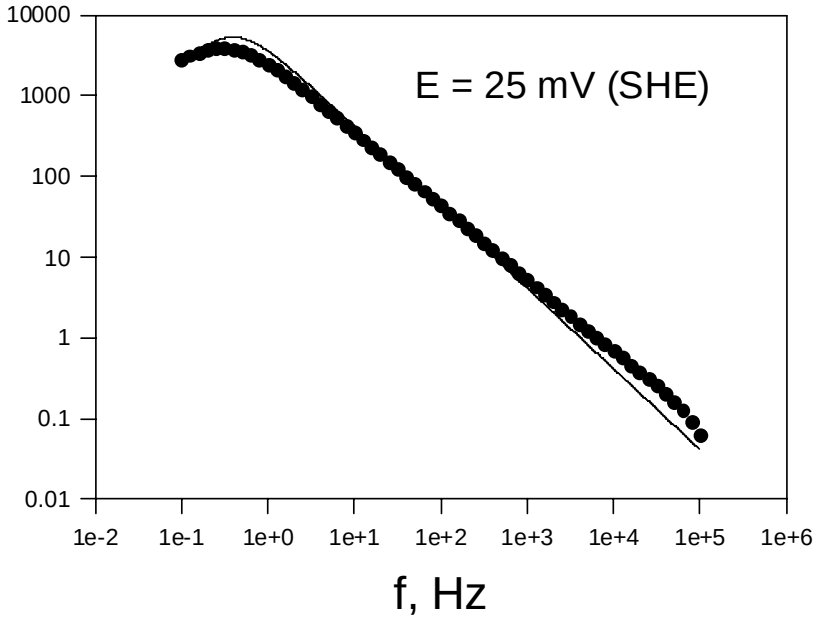

Figure 4.14: EIS fitting of reduction of nitromethane at 25 mV vs. SHE, imaginary values shown.

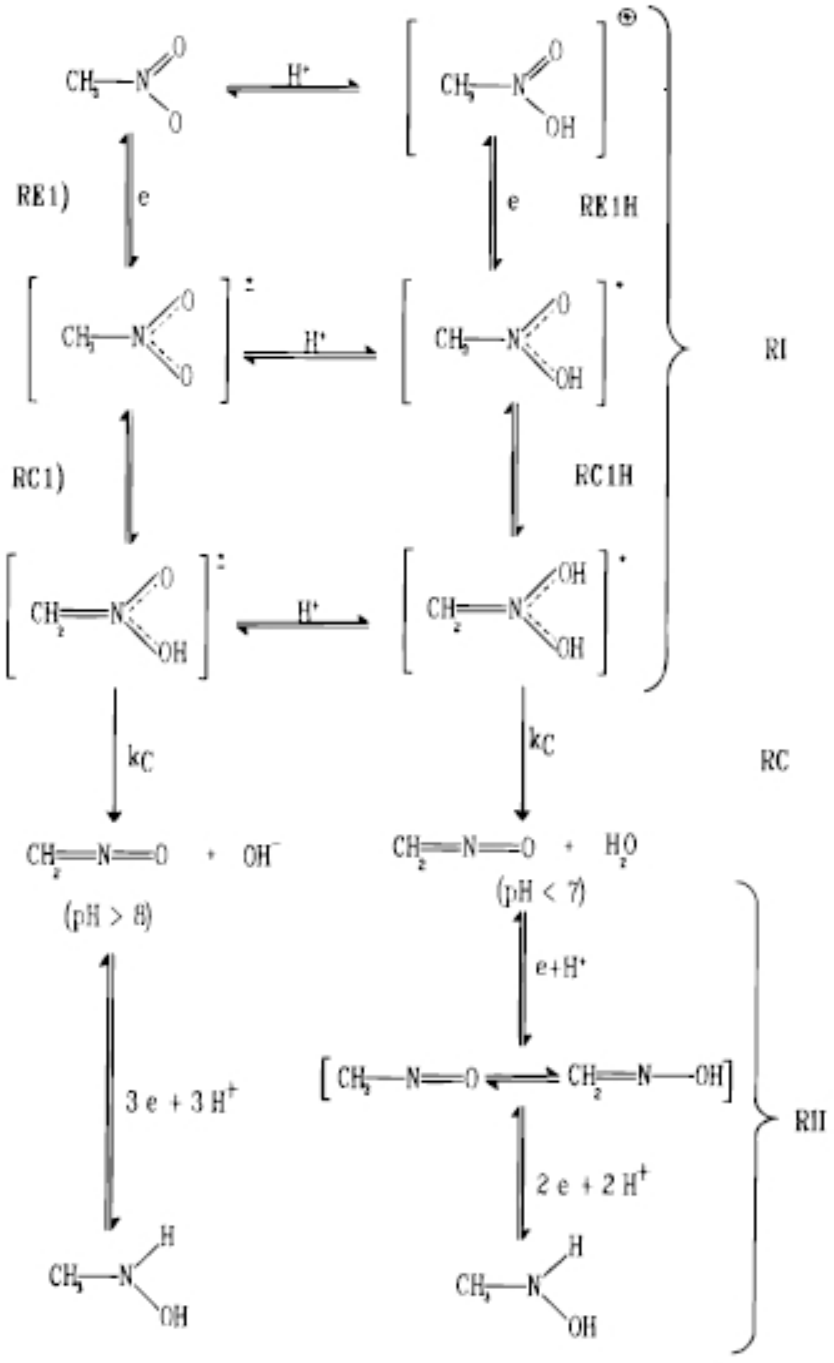

Figure 4.15: The proposed reaction mechanism for the electrochemical reduction of nitromethane, from [25].

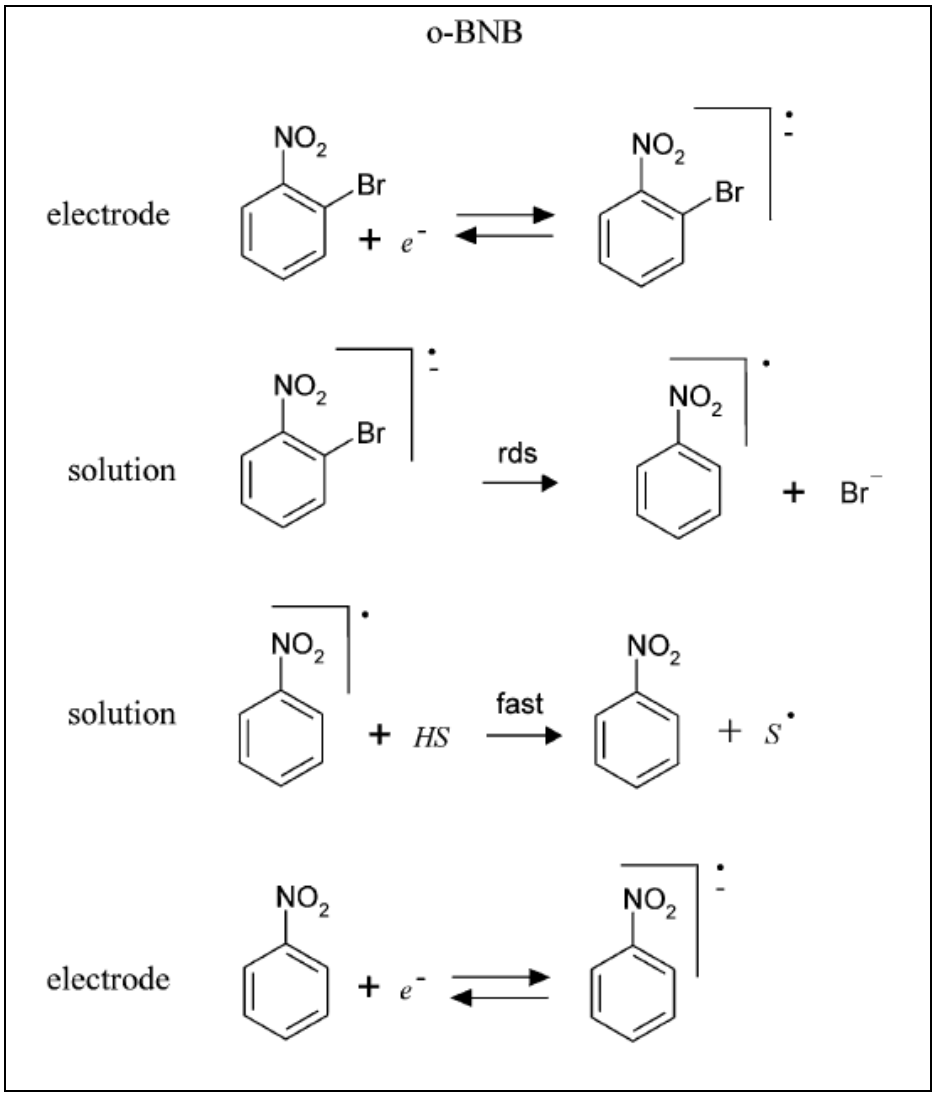

Figure 4.16: The proposed reaction mechanism for the reduction of ortho-bromonitrobenzene, from [26].

Within the filenames shown in Figures 4.17 through 4.20, the numbers at the end correspond to different steady-state potential values (all perturbation voltage amplitudes are 20 mV): 01 = -0.900 V; 02 = -0.945 V; 03 = -0.990 V; 04 = -1.035 V; 05 = -1.080 V; 06 = -1.125 V, all potentials are measured versus silver wire pseudo-reference electrode. The frequency range for each data set is from 65535 Hz down to 0.1 Hz.

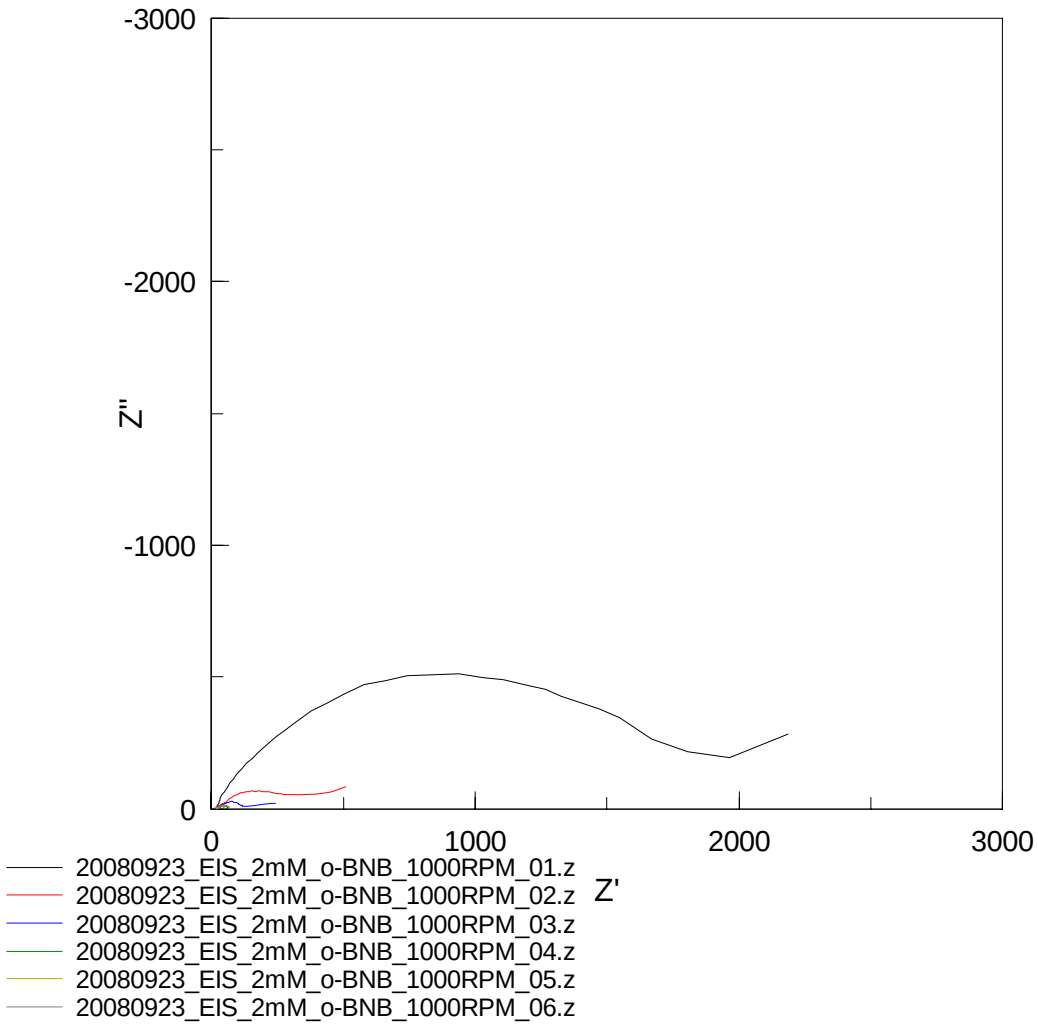

Figure 4.17: Nyquist plot for the reduction of 2 mM o-BNB in 100 mM TBAP in acetonitrile measured by EIS. Experimental parameters defined in the text above.

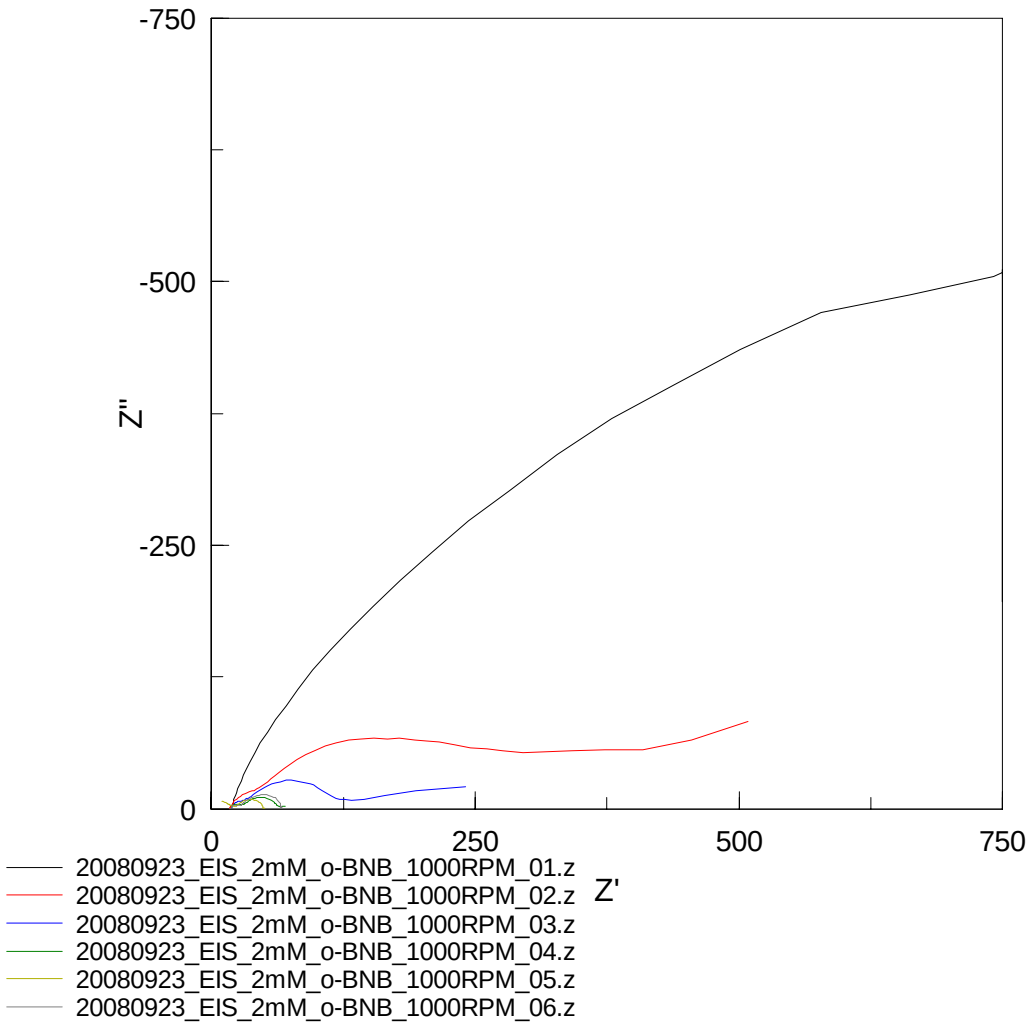

Figure 4.18: Same as Figure 4.17, just a different scale.

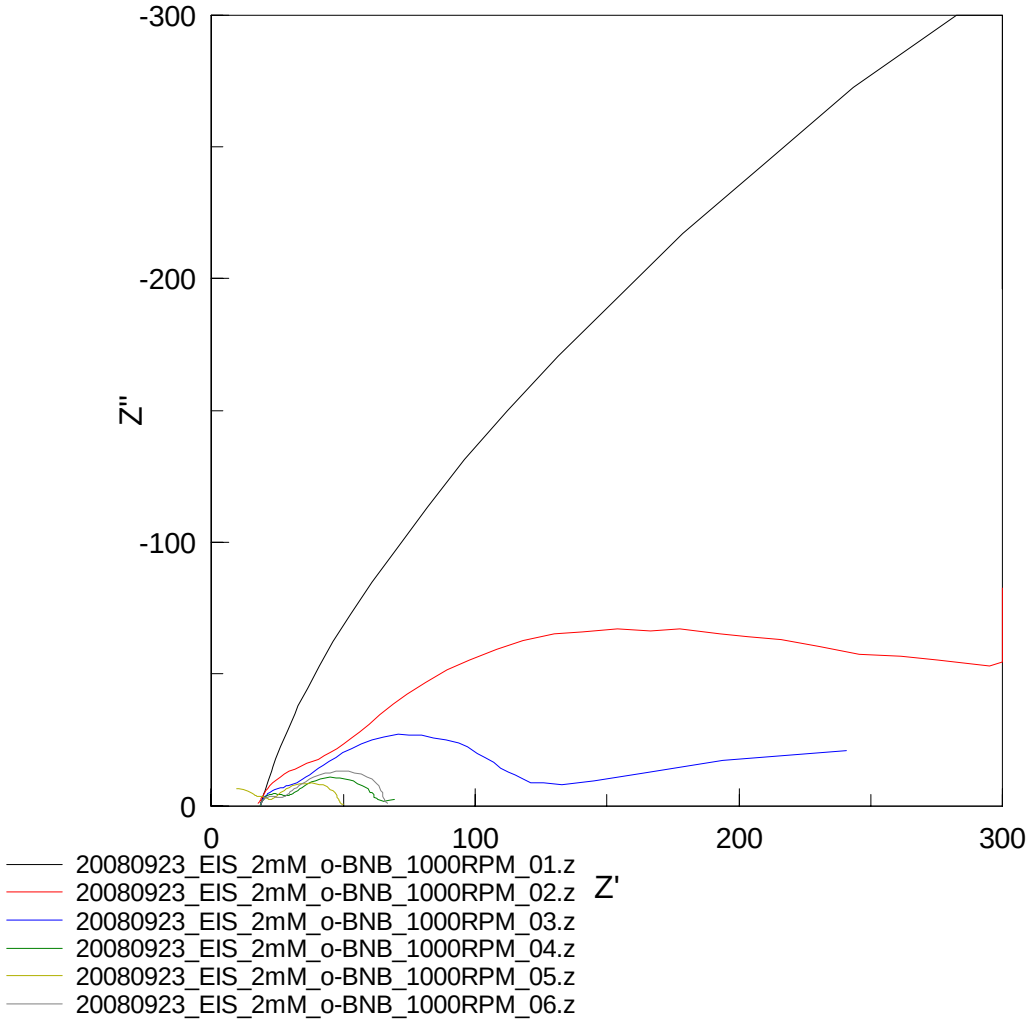

Figure 4.19: Same as Figures 4.17 and 4.18, just a different scale.

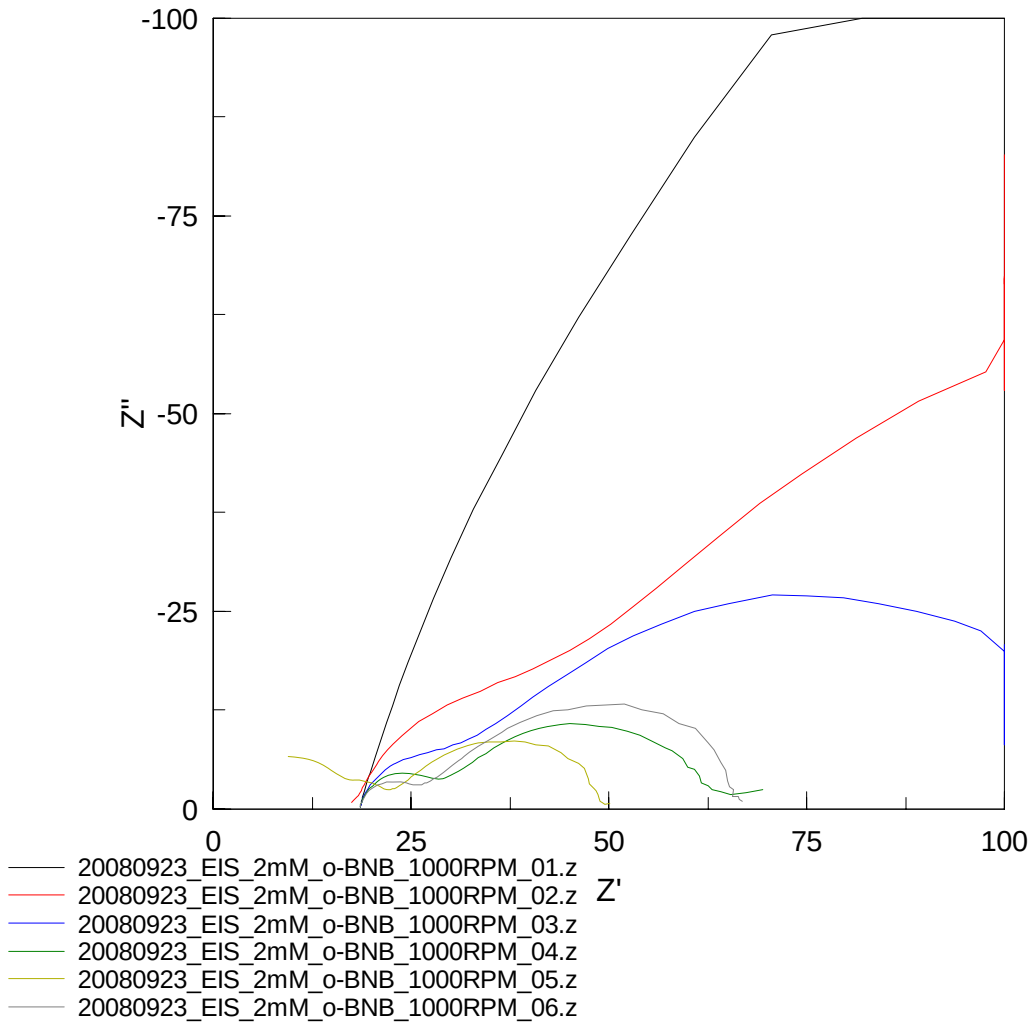

Figure 4.20: Same as Figures 4.17 through 4.19, just a different scale.

Figure 4.21 shows the cyclic voltammogram of 2 mM o-BNB when the working electrode is stationary (0 RPM) and when it is rotated at 1000 RPM.

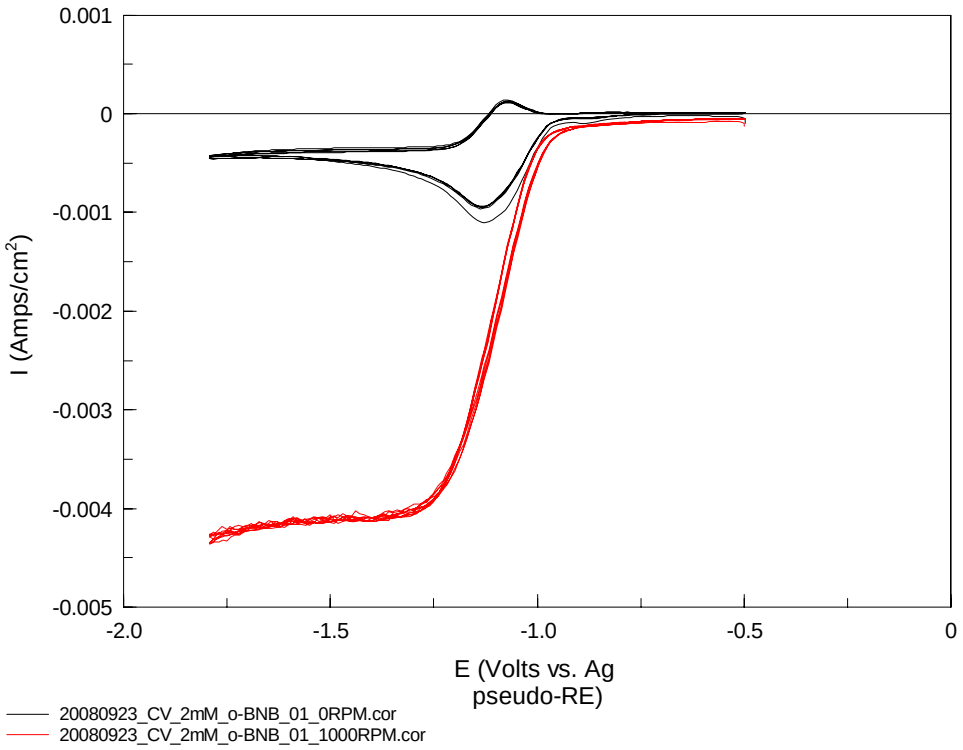

Figure 4.21: CV of 2 mM o-BNB with 100 mM TBAP in acetonitrile. Same experimental setup as for EIS experiments above. Black line is for 0 RPM of the 5 mm gold working electrode, while the red line is for 1000 RPM.

Results from other experiments (not shown) revealed that, even though the purity of the ortho-bromonitrobenzene we purchased was stated to be greater than 99%, there was a sufficient amount of its isomer, para-bromonitrobenzene, to interfere with the EIS analysis because the para- isomer undergoes a competing electron transfer process at virtually the exact same potential value. As a result of the chemical contamination (from the source) and lack of a higher purity sample of ortho-bromonitrobenzene, these results could not be used to validate this model on a more complex, yet known, reaction mechanism.

4.5 Summary and Conclusions

A general model and computer code have been developed for writing down by inspection the impedance of one-dimensional systems involving arbitrary numbers of coupled electrochemical and chemical processes under activation or mass transport control. This code is

based on the direct solution of the mass transport equations by using the finite difference up-wind scheme. In the first step, the steady-state distributions of concentration, C_i, and potential, E, are found and in the second step the periodic reaction of the concentrations, electric potential in the solution, and current density to the small periodic perturbation of E are determined. In this last step, the number of unknown values is doubled (we have to find the real and imaginary components of the perturbation and responses) and, accordingly, the number of governing equations is also doubled. The current version of the code is able to handle any arbitrary number (and complexity) of homogeneous and heterogeneous reactions in the frame of dilute solution theory. However, it can be easily generalized to the case of concentrated electrolytes. This code simulates, and can be used for optimization, coupled chemical/electrochemical reaction mechanisms at rotating disk electrode (RDE) or by using the Nernst diffusion layer approximation. The code executes rapidly and the output is formatted for easy comparison with experimental impedance measurements. On the other hand, the models are presented in a form that allows them to be readily optimized on experimental EIS data, in order to determine values for various model parameters (rate constants, transfer coefficients, diffusivities, etc). The application of the code was illustrated with "synthetic" EIS data and with the experimental data obtained on the RDE.

4.7 References

1. M. E. Orazem and Bernard Tribollet, *Electrochemical Impedance Spectroscopy*, John Wiley and Sons, Inc., Hoboken, NJ (2008).
2. D. A. Harrington, *J. Electroanal. Chem.,* **403**, 11 (1996).
3. D. A. Harrington, *J. Electroanal. Chem.,* **449**, 9 (1998).
4. D. A. Harrington, *J. Electroanal. Chem.,* **449**, 29 (1998).
5. D. A. Harrington and P. van den Driessche, *J. Electroanal. Chem.,* **501**, 222 (2001).
6. D. A. Harrington and P. van den Driessche, *J. Electroanal. Chem.,* **567**, 153 (2004).
7. B. Tribollet and J. Newman, *J. Electrochem. Soc*., **131**, 2780 (1984).
8. M. Seralathan and S. K. Rangarajan, *J. Electroanal. Chem.,* **191**, 209 (1985).
9. M. Seralathan and S. K. Rangarajan, *J. Electroanal. Chem.,* **191**, 229 (1985).
10. M. Seralathan and S. K. Rangarajan, *J. Electroanal. Chem.,* **191**, 237 (1985).
11. H. Anderson. "The Impedance of Metal Dissolution Reactions." PhD diss., University of Gothenburg, 1993.
12. E. Ahlberg and H. Anderson, *Acta Chem. Scand.*, **46**, 1 (1992).
13. E. Ahlberg and H. Anderson, *Acta Chem. Scand.*, **46**, 15 (1992).
14. E. Ahlberg and H. Anderson, *Acta Chem. Scand.*, **47**, 1063 (1993).
15. E. Ahlberg and H. Anderson, *Acta Chem. Scand.*, **47**, 1162 (1993).
16. J. C. Tokash, G. R. Engelhardt, and D. D. Macdonald, *ECS Trans.*, **19**, 13 (2009).
17. V. Pleskov and V. Yu. Filinovskii, *The Rotating Disc Electrode*, Consultants Bureau, New York (1976).

18. S. V. Patancar, *Numerical Heat Transfer and Fluid Flow*, McGraw-Hill, New York (1980).
19. S. D. Conte and C. deBoor, *Elementary Numerical Analysis*. McGraw-Hill, New York (1972).
20. J. Newman and K. E. Thomas-Alea, *Electrochemical Systems*, Prentice Hall, Inc. Englewood Cliffs, NJ (2004).
21. D. D. Macdonald, *Transient Techniques in Electrochemistry*, Plenum Press, New York (1977).
22. F. Prieto et al., *J. Electroanal. Chem.*, **437**, 183 (1997).
23. A. J. Wain and R. G. Compton, *J. Electroanal. Chem.*, **587**, 203 (2006).
24. M. Rueda, *J. Electroanal. Chem.*, **261**, 23 (1989).
25. F. Prieto, *J. Phys. Chem.*, **100**, 16346 (1996).
26. I. Svir, *J. Electroanal. Chem.*, **578**, 289 (2005).

PART III

Hydrogenation Research

1. Hydrogenation Research

In the first phase of this project, the electrochemical conversion of BO_2^- to BH_4^- was explored. Cyclic voltammetry was demonstrated as a quantitative analytical method for BH_4^- in aqueous solution. Experiments for electrochemical production of BH_4^- from BO_2^- reported by a partner institute (Rohm and Haas) were repeated. Finally, novel concepts proposed by Penn State, emphasizing overcoming of electrostatic repulsion of BO_2^- from cathodes in electrochemical experiments, were explored. None of the electrochemical reduction experiments produced detectable quantities of BH_4^- products.

Since the no-go decision for $NaBH_4$ work, Penn State has been investigating other hydride materials important to the Center's work on ammonia borane (NH_3BH_3; AB). Currently, regeneration of organotin hydrides (e.g. tributyltin hydride) is being explored, as this reagent is critical in schemes for regeneration of AB.

Also being investigated is the direct reduction of spent AB fuel without the use of intermediate species. To this end, we first wish to understand the oxidation mechanism of the aminoborane fuel so that the reduction of the spent fuel back to a hydride (or higher hydride) may be carried out in the most efficient way possible. To aide us in this process, we have created a general model of chemical and electrochemical reaction mechanisms (coupled or uncoupled) as well as a computer code that was designed for use with electrochemical impedance spectroscopy (EIS); much of this work was already accomplished in the first phase of this project. With our model and code, we are looking to identify the reaction mechanism and the important parameters so that they can be understood in terms of improving the reduction reaction.

1.1 Background

Current regeneration schemes for AB require organotin hydrides to reduce B-X bonds (X = O, S, halogen ligands) to B-H bonds. A classic route to organotin hydrides involves decarboxylation of organotin formates, i.e. heating of organotin formates under reduced pressure to drive off CO_2. Energy and efficiency computations performed by Argonne National Laboratory indicated an efficiency problem in this method related to compression of CO_2. Electrochemical routes to organotin hydrides are being explored by PSU to assess the feasibility of this alternative.

The direct reduction of AB spent fuel has not been considered as feasible because of the relative difficulty of exchanging B-X bonds to B-H bonds without an intermediate species. We feel that with a better understanding of the forward reaction mechanism (hydrogen release) we can take steps to reverse the reaction (hydrogen uptake) with success. We plan to use our EIS reaction model and computer code to achieve this goal.

Status: In this quarter, experimental and theoretical work has continued along three paths:

- Organotin halide/hydride electrochemistry in acetonitrile.
- Formulating thermodynamic phase stability diagrams for selective electrocatalysis.
- Direct hydrogenation using ionic liquids.

The achievements made during the last quarter in each of these areas are summarized below.

1.2 Organotin electrochemistry

The work performed recently for the organotin halide regeneration was focused on electrochemical reduction using the Devanathan cell. We previously reported that the Devanathan cell was successful at hydrogenating styrene at high efficiency, so we moved forward by attempting the hydrogenation of tributyltin chloride. In our last report, we showed that the cyclic voltammetery (CV) technique is suitable at identifying tributyltin hydride, so our procedure was to allow a sufficient time for hydrogenation to take place in the Devanathan cell and then use CV to determine if any hydride was formed. Multiple runs of this experiment resulted in no detectable amount of tributyltin hydride, even in positive control experiments where we spiked the reaction side with a small amount of tributyltin hydride in addition to the large amount of tributyltin chloride. Therefore, we conclude that the existing tributyltin hydride and any quantity that might be formed by hydrogenation of tributyltin chloride are being consumed in the Devanathan cell. It is possible that due to the cell design the tributyltin hydride is being consumed (oxidized) by the counter electrode, and thus we expect that future experiments will require the use of a separating membrane to isolate the working electrode (where hydrogenation is expected to occur) from the counter electrode (where re-oxidation might occur).

1.3 Formulating thermodynamic phase stability diagrams for selective electrocatalysis

In addition, another approach we are taking toward this task is to formulate thermodynamic phase stability diagrams for selective electrocatalysis using the Devanathan cell.

One of the issues encountered when attempting to hydrogenate a specific organic molecule is avoiding the waste of both electricity and hydrogen expended when erroneously hydrogenating the organic solvent containing the target molecule, or un-targeted sites.

A mechanism has been proposed (Figure 1.1) for electrocatalysis for triphenyltin chloride which involves electrocatalysis on a metal catalyst surface of a hydrogen permeation membrane, which filters ultra-pure hydrogen generated on the opposite side, in the style of Devanathan and Stachurski [1].

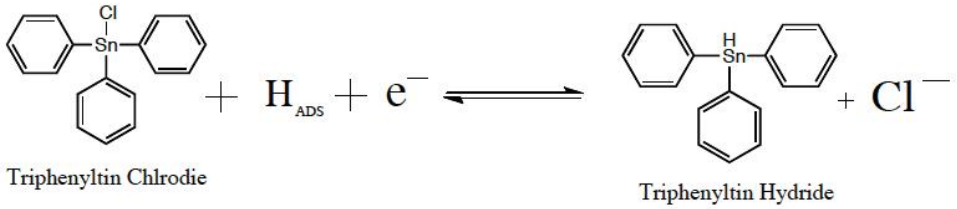

Figure 1.1: Hydrogenation scheme for triphenyltin chloride.

In the Devanathan cell (Figure 1.2), hydrogen is generated via electrolysis of water under galvanostatic conditions on the entrance side of a metallic membrane electrode, where it absorbs and then transports through the metal down a diffusion gradient until it emerges from the other (exit) side. Metal is a perfect filter for hydrogen (Figure 1.3), that is, no other element is small enough to diffuse within a metallic crystal, making the membrane permeable to hydrogen, but remarkably impermeable to any other contaminant.

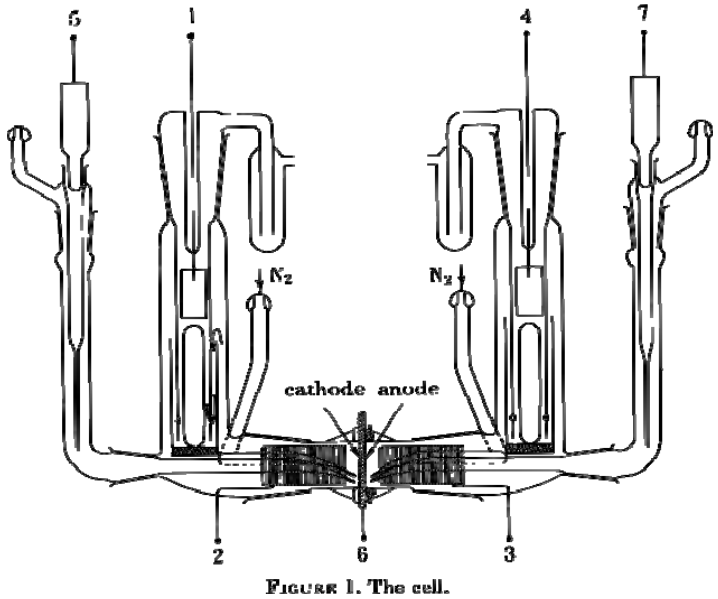

Figure 1.2: A schematic drawing of the original Devanathan cell.

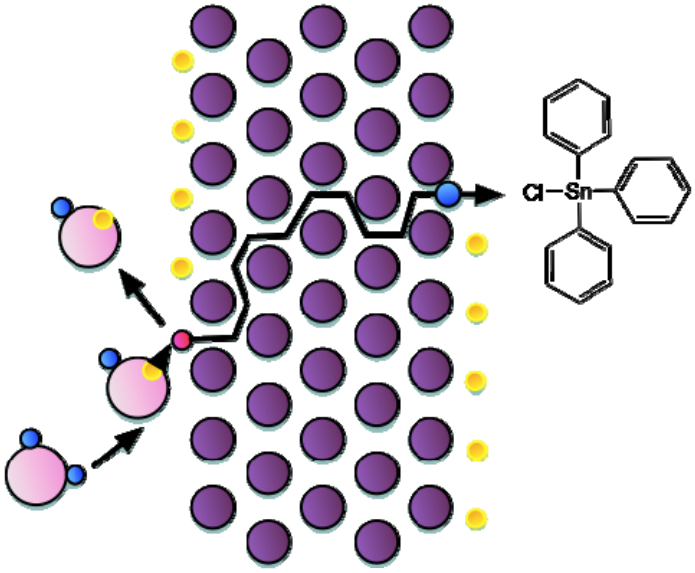

Figure 1.3: Hydrogen permeation through a metal membrane, for example the membrane used in a Devanathan cell.

The supply of ultra-pure hydrogen is critical to high quality hydrogenation, and the avoidance of waste products. Using a potentiostat, a bias may be applied to the exit face. In the past, such a positive bias is used to electrically detect the flux of hydrogen across the membrane's surface by oxidizing the hydrogen to a proton, and sending the electron through an ammeter counting circuit. In the case of electrocatalysis, a negative bias will be applied, in order to supply the required electrons for the electrocatalysis reaction. The effective hydrogen exit flux for a given galvanostatic hydrogen generation current will be characterized and tailored to the availability of electrons on the surface. The use of electrons to hydrogen in the electrocatalysis reaction is in a known ratio of 1:1, and therefore the efficiency can be readily calculated, not only for the electrocatalysis reaction, but also for the generation of hydrogen.One challenge of this electrocatalysis is to replace the chlorine atom, without hydrogenating the double bonds on the benzene rings. It would be useful, therefore, to identify the thermodynamically dominant species in the hydrogenation process.

A thermodynamic approach is proposed whereby a slight modification of the Nernst equation [2] relates the activity of hydrogen to the potential applied to the electrode for electrocatalysis. The Nernst equation will be applied to each possible reaction in the system, determining the equilibrium species in the system. The Nernst equation may be used in this manner, due to the electron transfer required for an electrocatalysis mechanism.

This is the same treatment masterfully enacted by Marcel Pourbaix [3] to describe the relationship between pH and electrode potential (Figure 1.4), mapping out the stable phases relevant to aqueous corrosion, Bailey applied this technique to organic reduction/oxidation

reactions in 1983 [4] in aqueous solutions (Figure 1.5). We propose to use the technique where pH is not easily regulated or measured. For instance, triphenyltin will be acted upon in the pure liquid state, in which the activity of hydrogen ion is poorly defined.

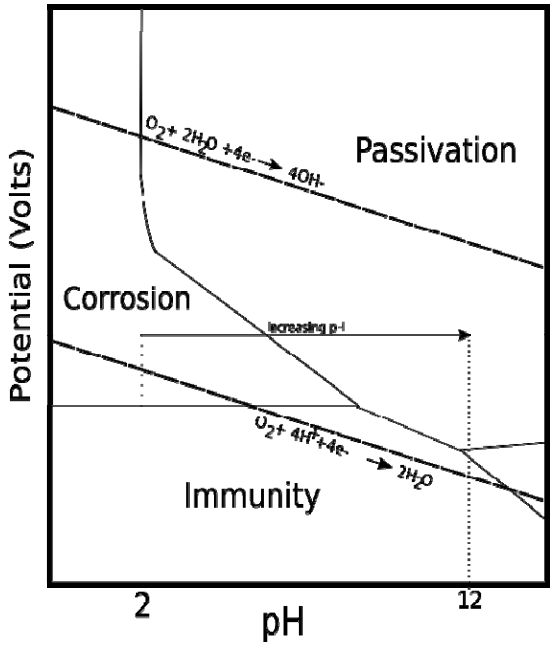

Figure 1.4: A simplified Pourbaix diagram for pure iron in water [3].

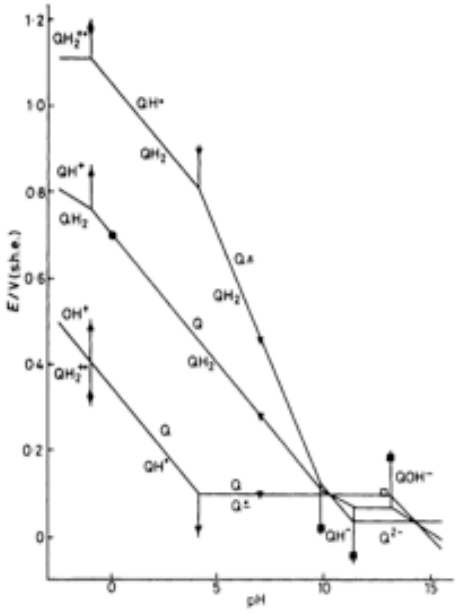

Figure 1.5: Bailey's diagram of organic redox equilibria.

With the Devanathan apparatus, the activity of adsorbed hydrogen exposed to the system can be controlled directly by controlling the galvanostatic current on the entrance face of the hydrogen permeation membrane. In palladium, for instance, hydrogen transport follows Fick's second law, that is, diffusion down a concentration gradient. Setting the ingress hydrogen activity will dictate the non-equilibrium egress hydrogen flux, and hence, the adsorbed hydrogen activity. Because hydrogen is being consumed in the electrocatalysis reaction, this demand on the activity must be considered when preparing a commercial apparatus.

1.4 Conceptual Construction of the Diagram

The construction of equilibrium redox diagrams follows the same general principles that are employed in devising potential-pH (Pourbaix) diagrams for corrosion systems. Thus, the steps are as follows:

Step 1: Write down all possible species in the system and note the standard Gibbs energy of formation, ΔG_f^o for each.

Step 2: Write down all possible equilibrium reactions between said species which include H, e-, or both H and e-.

Step 3: Apply the modified Nernst equation to each equilibrium reaction to obtain functions of E and a_H

Step 4: Plot the resulting lines of equilibria, on a Cartesian field of potential (E) on the Y axis, and activity of hydrogen, a_H on the horizontal axis. Note that reactions containing both e- and H will appear as sloped lines, while reactions containing only e- will appear as vertical lines and reactions containing only H will appear as horizontal lines. Resolve conflicts where these lines cross.

In much the same way that the product molecules have been studied, it is important to define the range of stability of the membrane. For a pure palladium membrane, for instance, there is a limit of dissolved hydrogen whereby breakdown of the membrane occurs. A similar overlay diagram shall be constructed for the membrane in question, analogous to the lines demarcating the zone on the Pourbaix diagram where water is stable, and hence, of interest to the corrosion scientist.

1.5 Direct Hydrogenation using Ionic Liquids

Prior to working with ammonia borane (or triphenyltin chloride), a test hydrogenation process needed to be used to verify that the technique works. As such, we chose to use the hydrogenation of CO_2 to methanol in ionic liquid (IL) as our test system.

The present investigation involves conversion of CO_2 to methanol via electrochemical hydrogenation in ionic liquid (1-butyl 3-methyl Immidazolium Hexafluorophosphate [BMIM-PF_6)]. The structural formula of BMIM-PF_6 is:

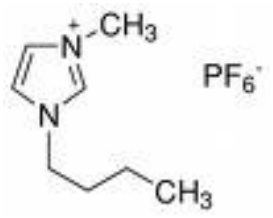

Figure 1.6: structural formula of BMIM-PF_6.

The electrochemical hydrogenation process has a key problem that focuses on the appropriate selection of an electrochemical mediator. Ionic liquids are characterized by a wide electrochemical window of stability, a reasonable ionic conductivity, and very low vapor pressure [2,3]. CO_2 has high solubility in ionic liquids, which makes the electrochemical hydrogenation of CO_2 more prospective in ionic liquid than in an aqueous medium. Ionic liquids that possess the bis-trifluoromethanesulphonyl-imide anion have a strong affinity for carbon dioxide and, hence, they are considered to be ideal solvents for the present study. However, they are very costly, so that our initial work has been carried out in the much less expensive Immidazolium Hexafluorophosphate (BMIM-PF_6))

The technique used to induce hydrogenation of CO_2 has been potentiostatic polarization, augmented with cyclic voltammetry; this was carried out with a computerized electrochemical workstation (Gamry Instrument). To analyze for the reaction product, Fourier Transform Infrared - Attenuated Total Reflectance (FTIR-ATR) spectroscopy has been employed.

Initial experiments were carried out in 0.01M 1-butyl 3-methyl Immidazolium Hexafluorophosphate aqueous solution. In some experiments, a platinum metal plate (99.9% metal basis) was employed as the working electrode. The surface of the electrode was etched by hot concentrated sulfuric acid. The electrode potential of the cathode was measured with respect to Ag/AgCl (sat. KCl) reference electrode. A platinum wire was used as the counter electrode. Pure N_2 gas was bubbled into the solution for an hour to remove dissolved oxygen. The electrolysis was carried out in a closed U-cell and the solvent was saturated with CO_2 for 120

minutes. The cell was usually operated at room temperature under a H_2 atmosphere, with H_2 being the source of hydrogen for the reduction (note that the ionic liquid is an aprotic solvent).

Experiments were also carried out using a copper mesh electrode, since copper has been previously noted to be a superior surface upon which to reduce CO_2, at least in aqueous solutions. A copper mesh (99.9% metal basis) was employed as a working electrode. The surface of the electrode was etched by nitric acid. The electrode potential of the cathode was measured with respect to Ag/AgCl (sat. KCl) reference electrode. A copper mesh was used as counter electrode. Pure N_2 gas was bubbled into the solution for an hour to remove dissolved oxygen. The electrolysis was carried out in a closed cell and the solvent was saturated with CO_2 for 120 minutes. The electrode was held at -0.2 V (Ag/AgCl) for 3 hrs, shown in Figure 1.7 and the current was recorded. The cell was usually operated at room temperature under H_2 atmosphere. The reader will note that the current decreases (becomes less negative) with time in a manner that suggests a loss in catalytic activity or passivation. Both possible mechanisms of deactivation may reflect the formation of a passivating film of a hydride (e.g., CuH) on the working electrode surface [3].

The cyclic voltammetry responses for platinum plate in CO_2-saturated ionic liquid solution are shown in Figure 1.8, Curve (b) and N_2 saturated solution are shown in Figure 1.8, Curve (a). The cyclic voltammetry response in CO_2-saturated solution is featureless over the potential region between 0.5 V to -0.3 V. In Curve (b) the reduction current starts at more positive potential (-0.1 V) compared to that shown by Curve (a) and the current gradually increases as potential goes to more negative values. It has been assumed that this reduction response is due either to CO_2 reduction or the hydrogen evolution reaction.

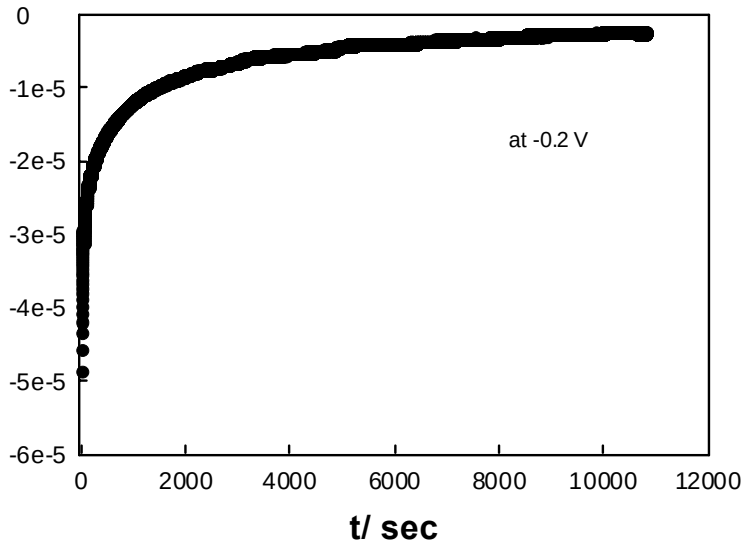

Figure 1.7: Potentiostatic transient for a Cu mesh working electrode in ionic liquid at -0.2V (Ag/AgCl), at room temperature.

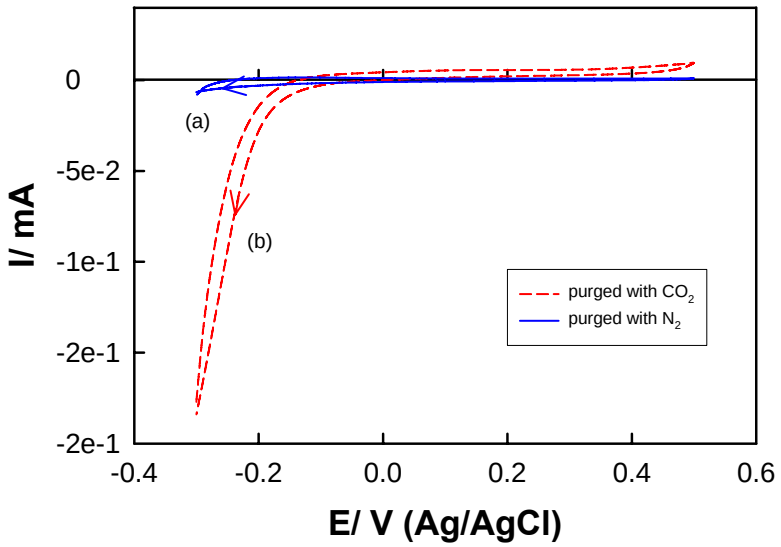

Figure 1.8: Cyclic voltammetry responses for Pt electrode (0.50 to -0.30 V, 10 mV s^{-1}) in ionic liquid aqueous solution at room temperature; (a) solvent saturated with nitrogen and (b) saturated with CO_2.

In the case of copper electrodes, the electrolysis was carried out in a closed cell and the solvent was saturated with CO_2 for 120 minutes. The electrode was held at -0.2 V (Ag/AgCl) for 3 hrs, shown in Figure 1.7. The cell was usually operated at room temperature under H_2 atmosphere. The current was found to become less negative with increasing time and to approach zero asymptotically. As noted above, this behavior can be accounted for by the electrode losing its catalytic activity or by passivation of the surface, possibly via the formation of copper hydride. Regardless, maintaining catalytic activity would appear to be a significant problem, at least in ionic liquids.

Similar observations were reported by Y. Tomita and Y. Hori in earlier work [5]. They noted that the reduction current in CO_2-saturated solution starts at a more positive potential than it does in an argon saturated solution. In their work, they used argon instead of nitrogen gas to deoxygenate the solution.

Some other experiments were carried out in an aqueous solution of the ionic liquid, in order to take advantage of the best features of both media. As noted above, cyclic voltammetry was used as an *in situ* probe for determining CO_2 reduction, because it is relatively an inexpensive and easily implemented method. Infrared spectroscopy has also been employed, in order to analyze for the presence of reaction product in solvent. Figure 8 shows the FTIR-ATR spectra for ionic liquid solvents for both prior and post experimental conditions. It was shown that both the pre-(red) and post-(blue) reduction samples appeared similar to that which would be expected for water. The possible reasons for this infrared spectrum result are either (1) no

methanol was produced or (2) due to the low concentration of ionic liquid the product concentration was below the detection limit.

It is noticeable from Figure 1.9 and 1.10 that the peak areas for both methyl alcohol and acetaldehyde are higher for the EGDE sample. Upon adding the sample to EGDE, the areas noticeably decreased. Since the peak areas for methyl alcohol and acetaldehyde are lower in the bubbled sample than the solvent blank, it appears that the MeOH and CH_3CHO etc are being blown out of the solvent while transferring to a closed vial of EGDE. This analysis is therefore ill-defined with respect to whether the reaction product was methanol or not. To overcome this interference, a new setup is being assembled that will allow for online-GC analysis. It should be noted that on-line gas chromatography-mass spectrometry commonly uses solvent-free samples.

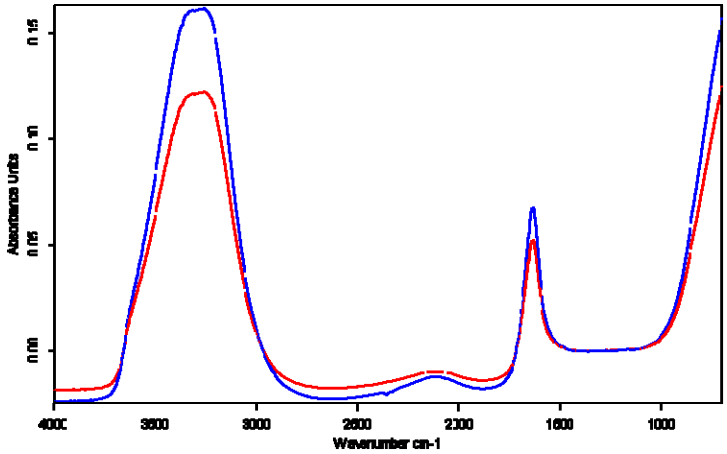

Figure 1.9: Fourier Transform Infrared - Attenuated Total Reflectance spectra for ionic liquid aqueous solution. Red line for prior-to-experiment and blue line for post-experiment.

Figure 1.10 shows the GC/MS for EGDE and sample. The methyl alcohol and acetaldehyde peaks are coincident and lie between 1:50 to 1:60. To resolve these peaks, this region was explored to higher sensitive scale which is shown in Figure 1.11.

In a new set-up of experiment, a 1:1 CO_2:H_2 (15 cm) mixture was used as the purge gas. The gas outlet was sampled using a syringe, which was then used to inject a 10 uL sample into the GC column. The gas components were separated on 30 m x 0.25 mm Supelco SB5-ms column with 1 um film. The GC/MS results from the injected sample are similar to those shown in Figures 1.12 and 1.13, but with one important difference. Thus, a formaldehyde peak was found in this analysis; this is one of the intermediate products of the reduction of CO_2 to methanol. More experiments are now being carried out in an attempt to obtain methanol as the final product.

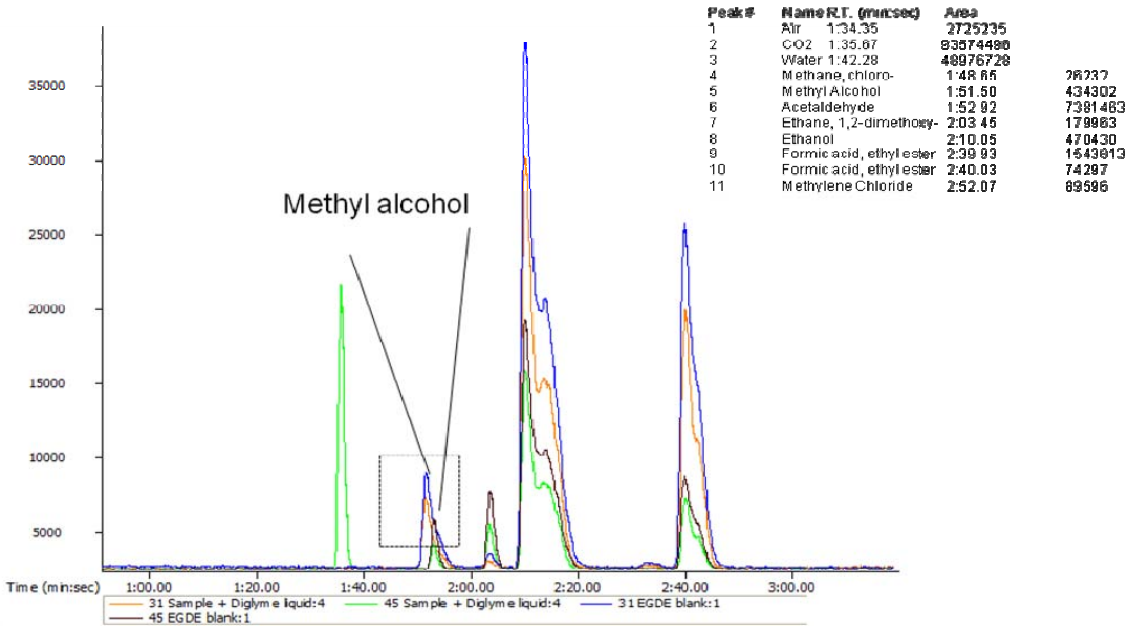

Figure 1.10: GC/MS results of collected sample and EFDE.

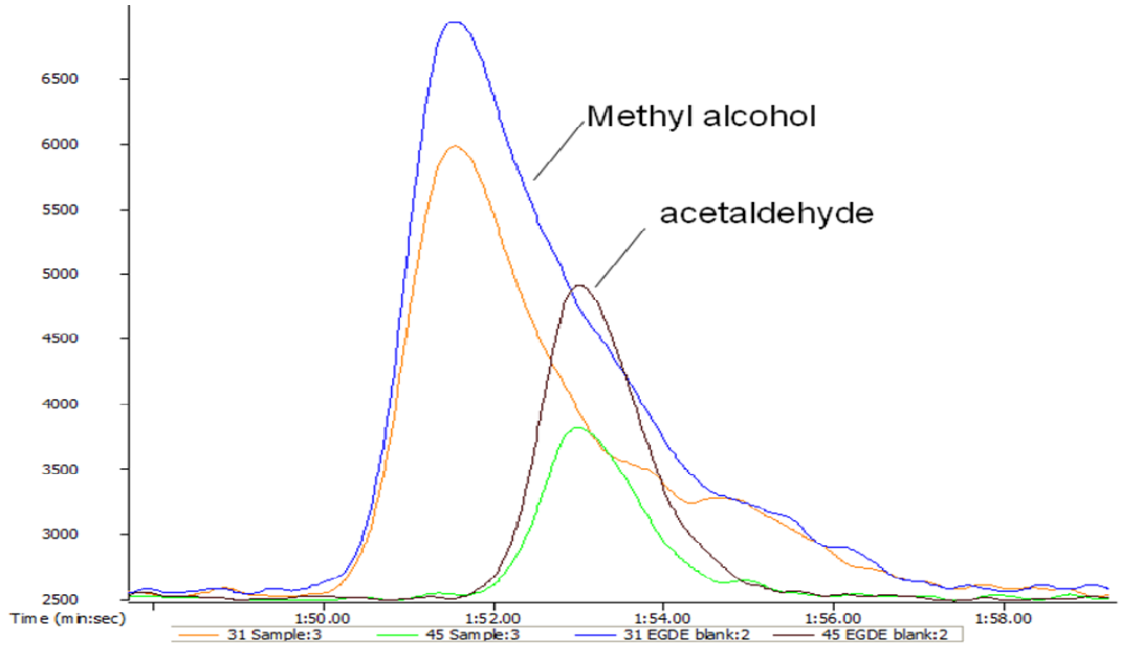

Figure 1.11: GC/MS results of collected sample and EFDE. Exploded view between mass numbers 31 and 45 shown in Figure 1.10.

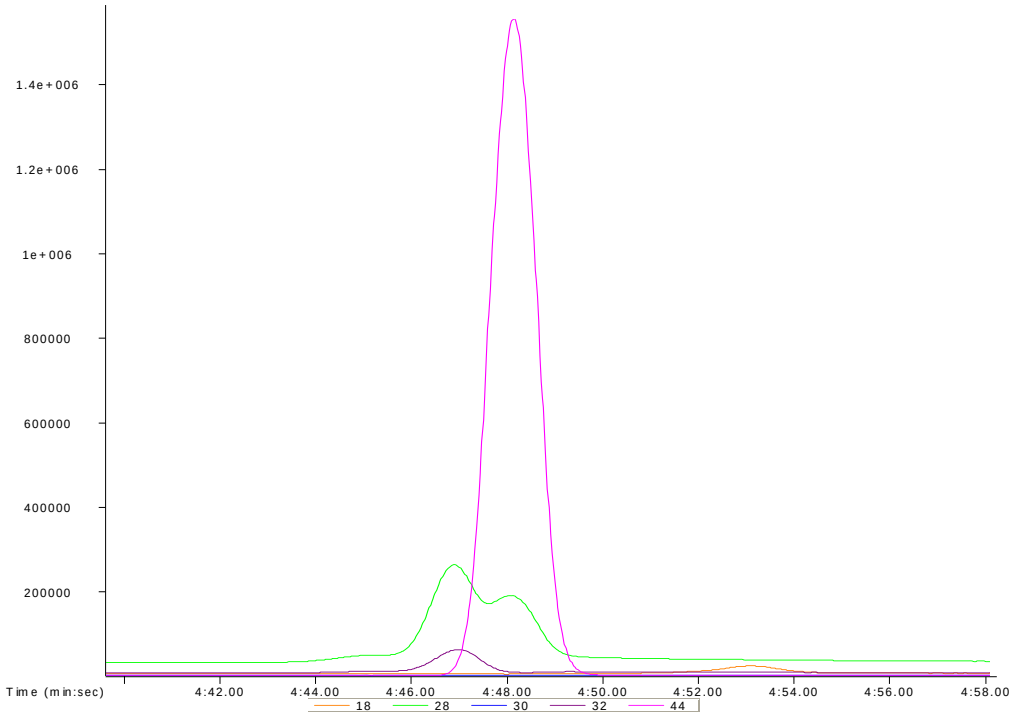

Figure 1.12: GC/MS results of injected sample.

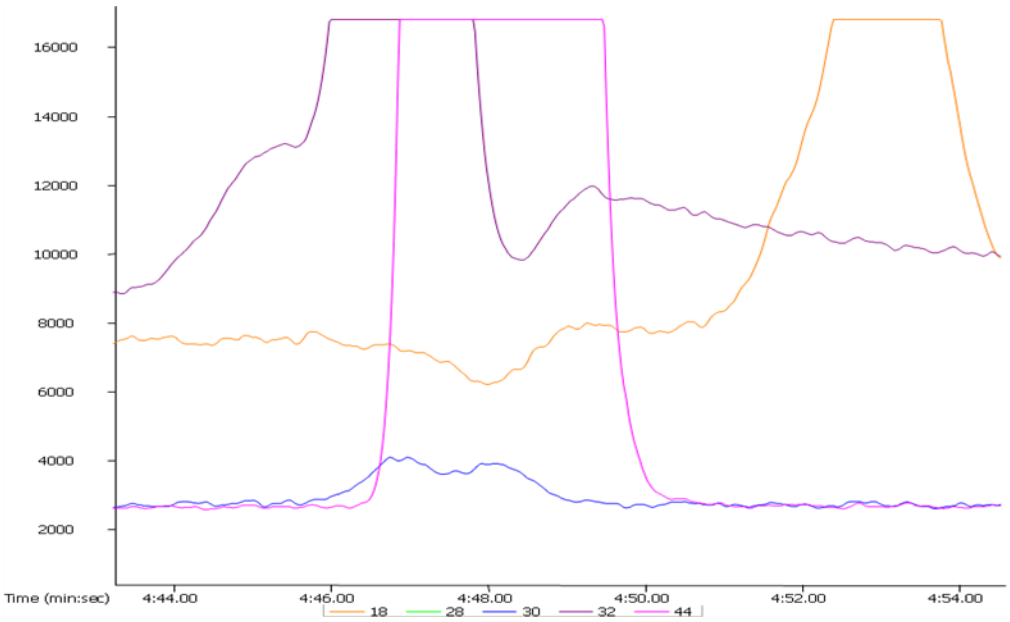

Figure 1.13: GC/MS results of injected sample. Exploded view around mass number 30 (Formaldehyde) shown in Figure 1.12.

1.6 References

1. M. Devanathan, Z. Stachurski, *Proceedings of the Royal Society of London. Series A, Mathematical and Physical Sciences (1934-1990)* **270**, 90 (1962).
2. W. Nernst, *Experimental and theoretical applications of thermodynamics to chemistry* (1907),
3. M. Pourbaix, *Atlas of electrochemical equilibria in aqueous solutions* 1974), pp. 644.
4. S. Bailey, I. Ritchie, F. Hewgill, *Journal of the Chemical Society, Perkin Transactions 2* **1983**, 645 (1983).
5. Y. Tomita and Y. Hori. In "*Advances in Chemical Conversions for Mitigating Carbon Dioxide: Studies in Surface Science and Catalysis*," edited by T. Inui, M. Anpo, K. Izui, S. Yanagida, and T. Yamaguchi, Vol. 114, pp 581.

Part IV

Overal Summary and Conclusion

1.1 Summary and Conclusions

This project began based on requirements from the US Department of Energy for researching chemical hydrides that were likely candidates to meet their ultimate goals (high storage capacity, good safety qualities, and ability to be regenerated). The first chemical hydrides that were proposed to be studied by our group were the polyborane salts. Although they were shown to be electroactive, we discovered that the oxidation was irreversible and no hydrogenation could take place. This generality of the polyboranes' lack of electrochemical reversibility is found in the decahydrodecaborate and dodecahydrododecaborate salts with various cations in the salts.

As a result of the less than favorable outcome of the polyboranes, the DOE then requested that we study ammonia borane in the same manner. Once again, we found that the electrochemical oxidation for ammonia borane was irreversible. In order to take a second attempt at the hydrogenation of ammonia borane, we looked into using the Devanathan cell as a tool for indirect hydrogenation using organotin hydrides. Unfortunately, the organotin halides were not able to be hydrogenated, thus a closed-loop cycle could not take place.

In parallel with the work on chemical hydrogen storage, we developed a new model of electrochemical impedance spectroscopy. The new model was originally supposed to be used to determine the reaction mechanism(s) within the chemical hydrogen storage materials (though it applies to any reaction mechanism and not just chemical hydrogen materials), however we ran out of time to validate the model and collect EIS data from the chemical hydrogen storage materials. The new model of EIS was shown to extract accurate kinetic information from various sets of experimental data based on the ferricyanide/ferrocyanide anion redox couple. We attempted to find a more complex (and yet known) reaction mechanism that we could use as a standard for validating the model, but the two compounds that we chose were found later to be not well suited for the task at hand.

In the future, the greatest benefit would be found in researching the nonaqueous silver/silver chloride reference electrode in more depth. Having this electrode available to the investigator would provide the means to perform long-term electrolyses and electrochemical impedance spectroscopy measurements. In order to make this reference electrode a reality, a new junction mater is needed that allows for good electronic conductivity but at the same time it should limit the bulk flow of filling solution into the test cell, which thereby contaminates the working solution.

1.2 Patents

None, two Invention Disclosures:

1. J. McLafferty and D. D. Macdonald, "Novel Modified Electrodes for the Electrochemical Reduction of Born-Oxygen Entities to Boron-Hydrogen Species", Invention Disclosure, Pennsylvania State University, April 20, 2006.
2. J. McLafferty and D. D. Macdonald, "Novel Modified Electrodes for the Electrochemical Reduction of Born-Oxygen Entities to Boron-Hydrogen Species", Invention Disclosure, Pennsylvania State University, April 20, 2006.

1.2 Publications / Presentations

1. D.D. Macdonald, J.C. Tokash, and J.B. McLafferty, "Electrochemical Hydrogen Storage," US Department of Energy's Chemical Hydrogen Storage Center of Excellence Center Meeting, University Park, PA, March 2005.
2. D.D. Macdonald, J.C. Tokash, and J.B. McLafferty, "Electrochemical Hydrogen Storage Systems," U.S. Department of Energy 2005 Hydrogen Program Review, Washington, D.C., May 2005.
3. D.D. Macdonald, W.J. Coulson, Y-C. Zhang, J.B. McLafferty, and J.C. Tokash, "Electrochemical Hydrogen Storage," Penn State University, September 2005.
4. D.D. Macdonald, W.J. Coulson, Y-C. Zhang, J.B. McLafferty, and J.C. Tokash, "Electrochemical Hydrogen Storage," CHSCoE Center Meeting, Salt Lake City, UT, October 2005.
5. D.D. Macdonald and J.B. McLafferty, "Conversion of Oxides into Hydrides Using a Hydrogen Plasma," Invention Disclosure, Pennsylvania State University, February 2006.
6. J.B. McLafferty, J.C. Tokash, Y-C. Zhang, W.J. Coulson, and D.D. Macdonald, "Electrochemical Hydrogen Storage," CHSCoE Center Meeting, Los Alamos, NM, March 2006.
7. J.B. McLafferty and D.D. Macdonald, "Novel Modified Electrodes for the Electrochemical Reduction of Born-Oxygen Entities to Boron-Hydrogen Species," Invention Disclosure, Pennsylvania State University, April 2006.
8. J.B. McLafferty, J.C. Tokash, Y-C. Zhang, W.J. Coulson, and D.D. Macdonald, "Electroanalysis of Borohydride Ion," Electrochemical Society Spring Meeting, Denver, CO, May 2006.
9. J.C. Tokash, J.B. McLafferty, Y-C. Zhang, W.J. Coulson, and D.D. Macdonald, "Polyhedral Boranes as Electrochemical Hydrogen Storage Materials," Electrochemical Society Spring Meeting, Denver, CO, May 2006.
10. D.D. Macdonald, J.C. Tokash, J.B. McLafferty, and Y-C. Zhang, "Electrochemical Hydrogen Storage Systems," U.S. Department of Energy 2006 Hydrogen Program Review, Washington, D.C., May 2006.
11. J.B. McLafferty, J. Tokash, D.D. Macdonald, Y-Z. Zhang, and J-E. Bao, "B-O to B-H Conversion Activities at Penn State University," Meeting at Penn State University, August 2006.
12. J.B. McLafferty, J.C. Tokash, J. Nollinger, J-E. Bao, Y. Chen, S. Colominas, M. Urquidi-Macdonald and D.D. Macdonald, "Boron Compounds for Chemical Hydrogen Storage," Penn State Hydrogen Day, University Park, PA, November 2006.

13. J.C. Tokash, J.B. McLafferty, J. Nollinger, J-E. Bao, Y. Chen, S. Colominas and D.D. Macdonald, "Chemical Hydrogen Storage Activities at Penn State," US Department of Energy's Chemical Hydrogen Storage Center of Excellence Center Meeting, Denver, CO, November 2006.
14. D. D. Macdonald, S. Colominas, J.C. Tokash, J.B. McLafferty, J-E. Bao, and J. Nollinger, "Hydrogen Storage Tech Team Meeting," Meeting at PNNL, March 2007.
15. D.D. Macdonald, S. Colominas, J.C. Tokash, J.B. McLafferty, J-E. Bao, J. Nollinger and G.R. Engelhardt, "Electrochemical Hydrogen Storage Systems," U.S. Department of Energy 2007 Hydrogen Program Review, Washington, D.C., May 2007.
16. D.D. Macdonald, S. Colominas, J.C. Tokash, J.B. McLafferty and J. Nollinger, "DOE Go/No-Go Meeting," Meeting at ANL, September 2007.
17. J.B. McLafferty, S. Colominas, and D.D. Macdonald, "Stability of Aqueous Borohydride Solutions in Contact With Cu, Ag, Au, and Hg," Electrochemical Society Fall Conference, Washington D.C., October 2007.
18. D.D. Macdonald, S. Colominas, J.C. Tokash, J.B. McLafferty, J-E. Bao, and J. Nollinger, "Chemical Hydrogen Storage Activities at Penn State University," Denver, CO, November 2007.
19. D.D. Macdonald, S. Colominas, J.C. Tokash, J.B. McLafferty, J. Nollinger and G.R. Engelhardt, "Electrochemical Hydrogen Storage Systems," U.S. Department of Energy 2008 Hydrogen Program Review, Washington, D.C., May 2008.
20. J.B. McLafferty, J.C. Tokash, S. Colominas, and D.D. Macdonald, "PSU Group Activity Summary," Meeting at Rohm & Haas, Philadelphia, PA, August 2008.
21. S. Colominas, J.B. McLafferty, and D.D. Macdonald, "Electrochemical Studies of Sodium Borohydride in Alkaline Aqueous Solutions Using a Gold Electrode," Electrochim. Acta, in press (2009).
22. J.B. McLafferty, S. Colominas, and D. D. Macdonald, "Attempts to Cathodically Reduce Boron Oxides to Borohydride in Aqueous Solution," Electrochim. Acta, in preparation, (2009).
23. J.C. Tokash, G.R. Engelhardt, and D.D. Macdonald, "On the Development of a General Electrochemical Impedance Model," 215th Meeting of The Electrochemical Society, San Francisco, CA, May 2009.
24. D.D. Macdonald, J.C. Tokash, J.B. McLafferty, A. Saleh, R. Sharna, and G.R. Engelhardt, "Electrochemical Hydrogen Storage Systems," U.S. Department of Energy 2009 Hydrogen Program Review, Washington, D.C., May 2009.
25. J.C. Tokash, G.R. Engelhardt, and D.D. Macdonald, "On the Development of a General Impedance Model", *Trans. Electrochem. Soc.*, **19**(20), 13 (2009).

Task Schedule

Task Number	Project Milestones	Task Completion Date				Progress Notes
		Original Planned	Revised Planned	Actual	Percent Complete	
1	Preliminary demonstration of electrochemical transformations in the B/O and B/H systems, in particular B-O to B-H	4/06		3/08	100%	Completed
2	Demonstration of practically useful oxidation state changes (go/no go decision)	4/08			100%	Completed
3	Definition of reaction kinetics and mechanisms	4/09			100%	Completed
4	Demonstration of reversible hydrogen storage	4/09			100%	Completed
5	Specification of optimal system	4/09			100%	Not applicable, because reactions are not reversible.
6	Task completion	4/09			80%	Completed